ROBERT C. NELSON

FLIGHT STABILITY AND AUTOMATIC CONTROL

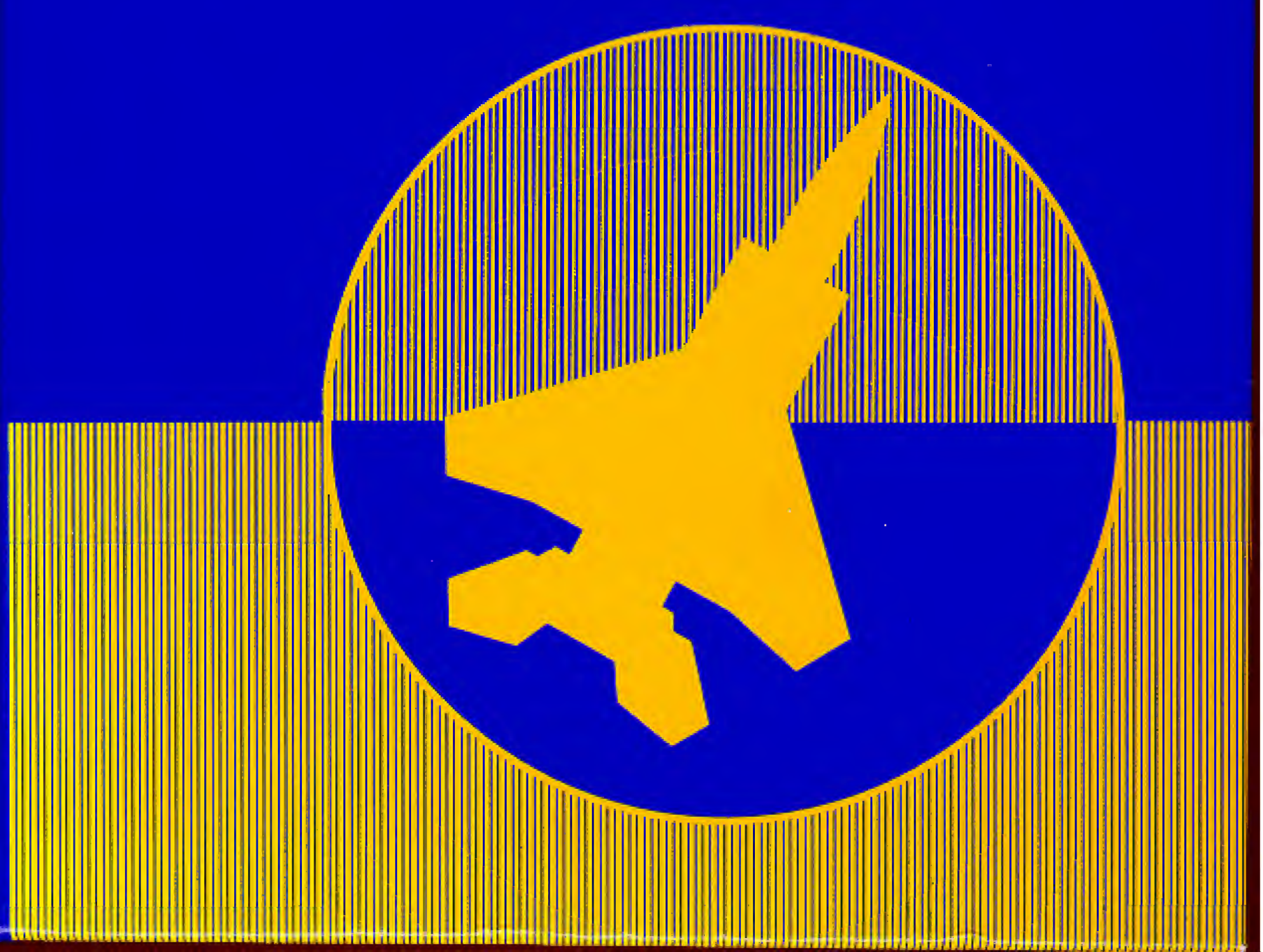

FLIGHT STABILITY AND AUTOMATIC CONTROL

FLIGHT STABILITY AND AUTOMATIC CONTROL

Dr. Robert C. Nelson

Aerospace and Mechanical Engineering Department
University of Notre Dame

McGraw-Hill Book Company

New York St. Louis San Francisco Auckland Bogotá Caracas Colorado Springs Hamburg
Lisbon London Madrid Mexico Milan Montreal New Delhi Oklahoma City
Panama Paris San Juan São Paulo Singapore Sydney Tokyo Toronto

This book was set in Times Roman.
The editors were Anne T. Brown and John M. Morriss;
the designer was Amy Becker
the production supervisor was Leroy A. Young.
Project supervision was done by The Universities Press.
R. R. Donnelley & Sons Company was printer and binder.

FLIGHT STABILITY AND AUTOMATIC CONTROL

Printed 34567890DOCDOC8932109

ISBN 0-07-046218-6

Nelson, Robert C., (date).
Flight stability and automatic control.

Includes bibliographies and index.
1. Stability of airplanes. 2. Airplanes—Control systems. I. Title.
TL574.S7N45 1989 629.132'36 87-32481
ISBN 0-07-046218-6

ABOUT THE AUTHOR

Dr. Nelson received his B.S. and M.S. degrees in Aerospace Engineering from the University of Notre Dame and his Ph.D. in Aerospace Engineering from the Pennsylvania State University. Prior to joining Notre Dame, Dr. Nelson was an instructor of Aerospace Engineering at the Pennsylvania State University and an engineer for the Air Force Flight Dynamics Laboratory at Wright Patterson Air Force Base, Ohio. While employed by AFFDL, he worked on an advanced development program to develop the technology for an air to air short range bomber defense missile. For his contribution to this effort he received a Technical Achievement award from the Air Force Systems Command.

In 1975, Dr. Nelson joined the faculty at Notre Dame and has been active in research dealing with the aerodynamics and flight dynamics of both aircraft and missiles. His present research interests include the aerodynamics of slender bodies at large angles of attack, flow visualization techniques and delta wing aerodynamics. He has published over forty articles and papers on his research. Dr. Nelson has also contributed a chapter to the AIAA Progress Series book *Missile Aerodynamics* entitled, "The Role of Flow Visualization in the Study of High Angle of Attack Aerodynamics," which was published by the AIAA in 1986.

Dr. Nelson has also been active as a consultant to government and industrial organizations. He is a Registered Professional Engineer and Associate Fellow of the American Institute of Aeronautics and Astronautics (AIAA). He served as the General Chairman of the AIAA Atmospheric Flight Mechanics Conference in 1982 and was the Chairman of the AIAA Atmospheric Flight Mechanics Technical Committee from May 1983 to 1985.

CONTENTS

	Preface	xi
1	**Introduction**	1
1.1	Atmospheric Flight Mechanics	1
1.2	Basic Definitions	2
	1.2.1 Fluid	2
	1.2.2 Pressure	4
	1.2.3 Temperature	4
	1.2.4 Density	5
	1.2.5 Viscosity	5
	1.2.6 Mach Number and the Speed of Sound	6
1.3	Aerostatics	7
	1.3.1 Variation of Pressure in a Static Fluid	7
1.4	Development of Bernoulli's Equation	9
	1.4.1 Incompressible Bernoulli Equation	10
	1.4.2 Bernoulli's Equation for a Compressible Fluid	11
1.5	The Atmosphere	12
	1.5.1 Example Problem 1.1	18
1.6	Aerodynamic Nomenclature	19
1.7	Aircraft Instruments	22
	1.7.1 Air Data Systems	23
	1.7.2 Airspeed Indicator	23
	1.7.3 Altimeter	26
	1.7.4 Rate of Climb Indicator	27
	1.7.5 Machmeter	28
	1.7.6 Angle of Attack Indicators	29
	1.7.7 Example Problem 1.2	29
1.8	Summary	31
	Problems	32
	References	33
2	**Static Stability and Control**	34
2.1	Historical Perspective	34
2.2	Introduction	39

2.2.1 Static Stability 39
2.2.2 Dynamic Stability 40
2.3 Static Stability and Control 42
2.3.1 Definition of Longitudinal Static Stability 42
2.3.2 Contribution of Aircraft Components 43
2.3.3 Wing Contribution 44
2.3.4 Tail Contribution—Aft Tail 45
2.3.5 Canard—Forward Tail Surface 49
2.3.6 Fuselage Contribution 49
2.3.7 Power Effects 51
2.3.8 Stick Fixed Neutral Point 52
2.3.9 Example Problem 2.1 53
2.4 Longitudinal Control 58
2.4.1 Elevator Effectiveness 59
2.4.2 Elevator Angle to Trim 61
2.4.3 Flight Measurement of X_{NP} 61
2.4.4 Elevator Hinge Moment 62
2.5 Stick Forces 64
2.5.1 Trim Tabs 66
2.5.2 Stick Force Gradients 66
2.6 Definition of Directional Stability 67
2.6.1 Contribution of Aircraft Components 68
2.7 Directional Control 71
2.8 Roll Stability 73
2.9 Roll Control 75
2.10 Summary 77
Problems 78
References 81

3 Aircraft Equations of Motion 83
3.1 Introduction 83
3.2 Derivation of Rigid Body Equations of Motion 84
3.3 Orientation and Position of the Airplane 88
3.4 Gravitational and Thrust Forces 90
3.5 Small Disturbance Theory 92
3.6 Aircraft Transfer Functions 95
3.6.1 Longitudinal Transfer Function 96
3.6.2 Lateral Transfer Functions 97
3.7 Aerodynamic Force and Moment Representation 100
3.7.1 Derivatives Due to the Change in Forward Speed 102
3.7.2 Derivatives Due to Pitching Velocity q 103
3.7.3 Derivatives Due to the Time Rate of Change of the Angle of Attack 105
3.8 Summary 106
Problems 109
References 111

4 Longitudinal Motion (Stick Fixed) 112
4.1 Historical Perspective 112
4.2 Second Order Differential Equations 114

4.3 Pure Pitching Motion 120
4.4 Stick Fixed Longitudinal Motion 124
4.4.1 State Variable Representation of the Equations of Motion 125
4.5 Longitudinal Approximations 128
4.5.1 Short Period Approximation 130
4.5.2 Example Problem 4.1 131
4.5.3 Solution 131
4.5.4 Short Period Approximation 135
4.6 The Influence of Stability Derivatives on the Longitudinal Modes of Motion 138
4.7 Flying Qualities 139
Example Problem 4.2 142
Solution 143
4.8 Flight Simulation 144
4.9 Summary 144
Problems 148
References 151

5 Lateral Motion (Stick Fixed) 152
5.1 Introduction 152
5.2 Pure Rolling Motion 153
5.2.1 Example Problem 5.1 155
5.2.2 Roll Control Reversal 156
5.3 Pure Yawing Motion 158
5.4 Lateral-Directional Equations of Motion 160
5.4.1 Spiral Approximation 163
5.4.2 Roll Approximation 164
5.4.3 Dutch Roll Approximation 164
5.4.4 Example Problem 5.2 165
5.5 Lateral Flying Qualities 169
5.4.5 Example Problem 5.3 170
5.6 Inertial Coupling 172
5.7 Summary 172
Problems 173
References 175

6 Aircraft Response to Control or Atmospheric Inputs 176
6.1 Introduction 176
6.2 Equations of Motion in a Nonuniform Atmosphere 180
6.3 Pure Vertical or Plunging Motion 183
6.4 Atmospheric Turbulence 189
6.5 Harmonic Analysis 190
6.5.1 Turbulence Models 192
6.6 Wind Shear 193
6.6.1 Example Problem 6.1 195
6.7 Summary 196
Problems 196
References 197

7 Automatic Control—Application of Conventional Control Theory 198
7.1 Introduction 198
7.2 Routh's Criterion 201
7.2.1 Example Problem 7.1 203
7.3 Root Locus Technique 204
7.4 Frequency Domain Techniques 206
7.5 Time and Frequency Domain Specifications 207
7.5.1 Higher Order Systems 210
7.6 The Displacement Autopilot 211
7.6.1 Pitch Displacement Autopilot 211
7.6.2 Example Problem 7.2 213
7.7 Stability Augmentation 215
7.7.1 Example Problem 7.3 215
7.8 Instrument Landing 217
7.9 Summary 220
Problems 222
References 223

8 Automatic Control, Application of Modern Control Theory 224
8.1 Introduction 224
8.2 State Space Modeling 225
8.2.1 State Transition Matrix 228
8.2.2 Example Problem 8.1 229
8.2.3 Controllability and Observability 231
8.3 State Feedback Design 232
8.3.1 Longitudinal Stability Augmentation 232
8.3.2 Example Problem 8.2 234
8.3.3 Lateral Stability Augmentation 236
8.3.4 Example Problem 8.3 237
8.4 State Variable Reconstruction—The State Observer 238
8.5 Optimal State Space Control System Design 240
Example Problem 8.4 241
8.6 Summary 243
Problems 243
References 244

Appendices 246
Atmospheric Table 246
Geometric, Mass and Aerodynamic Characteristics of Selected Airplanes 250
Mathematical Review Laplace Transforms Matrix Algebra 261
Review of Control System Analysis Techniques 270

Index 279

PREFACE

The goal of this book is to present an integrated treatment of the basic elements of aircraft stability, flight control, and autopilot design. An understanding of flight stability and control played an important role in the ultimate success of the earliest aircraft designs. In later years the design of automatic controls ushered in the rapid development of the commercial and military aircraft. Today, both military and civilian aircraft rely heavily on automatic control systems to provide artifical stabilization and autopilots to aid pilots in navigating and landing their aircraft in adverse weather conditions.

This book is intended as a textbook for a course in aircraft flight dynamics for senior undergraduate or first year graduate students. The material presented includes static stability, aircraft equations of motion, dynamic stability, flying or handling qualities, and automatic control. Chapter 1 reviews some basic concepts of aerodynamics, properties of the atmosphere, several of the primary flight instruments and nomenclature. In Chapter 2 the concepts of airplane static stability and control are presented. The design features that can be incorporated into an aircraft design to provide static stability and sufficient control power are discussed. The rigid body aircraft equations of motion are developed along with techniques to model the aerodynamic forces and moments acting on the airplane in Chapter 3. The dynamic characteristics of an airplane for free and forced response are presented in Chapters 4 and 5. Chapter 4 discusses the longitudinal dynamics while Chapter 5 presents the lateral dynamics. In both chapters the relationship between the rigid body motions and the pilot's opinion of the ease or difficulty of flying the airplane is explained. Handling or flying qualities are those control and dynamic characteristics that govern how well a pilot can fly a particular control task. Chapter 6 discusses the solution of the equations of motion for either arbitrary control input or atmospheric disturbances. The last two chapters, 7 and 8, deal with the application of control theory to airplane stabilization and control. Autopilot design concepts are presented for control-

ling aircraft attitude, flight speed as well as conceptual designs for an automatic landing systems. Both classical root locus and modern matrix control analysis techniques are used to design simple autopilots.

To help in understanding the concepts presented in the text I have included a number of worked-out example problems throughout the book, and at the end of each chapter one will find a problem set. A major feature of the textbook is that the material is introduced by way of simple exercises. For example, dynamic stability is presented first by restricted single degree of freedom motions. This approach permits the reader to gain some experience in the mathematical representation and physical understanding or aircraft response before the more complicated multiple degree of freedom motions are analysized. Several appendices have also been included to provide additional data on airplane aerodynamic, mass, and geometric characteristics as well as review material of some of the mathematical and analysis techniques used in the text.

I am indebted to all the students who used the early drafts of this book. Their many suggestions and patience as the book evolved is greatly appreciated. In addition, I would like to acknowledge the support of Dr. Albin A. Szewczyk, Chairman of the Department of Aerospace and Mechanical at the University of Notre Dame, for making department resources available to me. As in any large undertaking one needs encouragement from time to time and I am greatful for the support from my wife, Julie, and my colleagues Stephen M. Batill and Thomas J. Mueller. I would like to express my thanks for the many useful comments and suggestions provided by colleagues who reviewed this text during the course of its development, especially to John Anderson, University of Maryland; Richard Duprey, United States Air Force Academy; Paul J. Hermann, Iowa State University; Ira D. Jacobson, University of Virginia; James F. Marchman III, Virginia Polytechnic Institute and N. X. Vinh, University of Michigan.

Finally, I would like to express my appreciation to Marilyn Walker for her patience in typing the many versions of this manuscript and to Cecilia Brendel for providing quality figures and artwork from my rough sketches.

Robert C. Nelson

CHAPTER 1

INTRODUCTION

"For some years I have been afflicted with the belief that flight is possible to man."
Wilbur Wright, May 13, 1900

1.1 ATMOSPHERIC FLIGHT MECHANICS

Atmospheric flight mechanics is a broad heading that encompasses three major disciplines, namely, performance, flight dynamics and aeroelasticity. In the past, each of these subjects was treated independently of the other. However, because of the structural flexibility of modern airplanes, the interplay between the disciplines can no longer be ignored. For example, if the flight loads cause significant structural deformation of the aircraft, one can expect changes in the airplane's aerodynamic and stability characteristics which in turn will influence its performance and dynamic behavior.

Airplane performance deals with the determination of performance indices such as range, endurance, rate of climb, and take off and landing distance as well as flight path optimization. To evaluate these indices, one normally treats the airplane as a point mass that is acted on by gravity, lift, drag and thrust. The accuracy of the performance calculations depends upon how accurately the lift, drag and thrust can be determined.

Flight dynamics is concerned with the motion of an airplane due to internally or externally generated disturbances. We are particularly interested in the vehicle's stability and control capabilities. To describe adequately the

rigid-body motion of an airplane one needs to consider the complete equations of motion with six degrees of freedom. Again, this will require accurate estimates of the aerodynamic forces and moments acting on the airplane.

The final subject included under the heading of atmospheric flight mechanics is aeroelasticity. Aeroelasticity deals with both static and dynamic aeroelastic phenomena. Basically, aeroelasticity is concerned with phenomena associated with interactions between inertial, elastic and aerodynamic forces. Problems that arise for a flexible aircraft include control reversal, wing divergence, and control surface flutter, to name just a few.

This book is divided into three sections; the first section deals with the properties of the atmosphere, static stability and control concepts, development of aircraft equations of motion and aerodynamic modeling of the airplane; the second part examines aircraft motions due to control inputs or atmospheric disturbances; and the third portion is devoted to aircraft autopilots. Although no specific chapters are devoted entirely to performance or aeroelasticity, an effort is made to show the reader, at least in a qualitative way, how performance specifications and aeroelastic phenomena influence aircraft stability and control characteristics.

The interplay between the three disciplines that make up atmospheric flight mechanics is best illustrated by the experimental high-performance airplane shown in Fig. 1.1. The X-29A aircraft incorporates the latest in advanced technologies in controls, structures, and aerodynamics. These technologies will provide substantial performance improvements over more conventional fighter designs. Such a design could not be developed without paying close attention to the interplay between performance, aeroelasticity, stability and control. In fact, the evolution of this radical design was developed using tradeoff studies between the various disciplines to justify the expected performance improvements.

The forces and moments acting on an airplane depend upon the properties of the atmosphere through which it is flying. In the following sections we will review some basic concepts of fluid mechanics that will help us develop an appreciation of the atmospheric properties essential to our understanding of airplane flight mechanics. In addition we will discuss some of the important aircraft instruments that provide flight information to the pilot.

Not needed 1.2 → 1.6

1.2 BASIC DEFINITIONS

The aerodynamic forces and moments generated on an airplane are due to its geometric shape, attitude to the flow, airspeed, and to the properties of the ambient air mass through which it is flying. Air is a fluid and, as such, possesses certain fluid properties. The properties that we are interested in are the pressure, temperature, density, viscosity and speed of sound of air at the flight altitude.

FLUID. A fluid can be thought of as any substance that flows. To have such a property, the fluid must deform continuously when acted on by a shearing

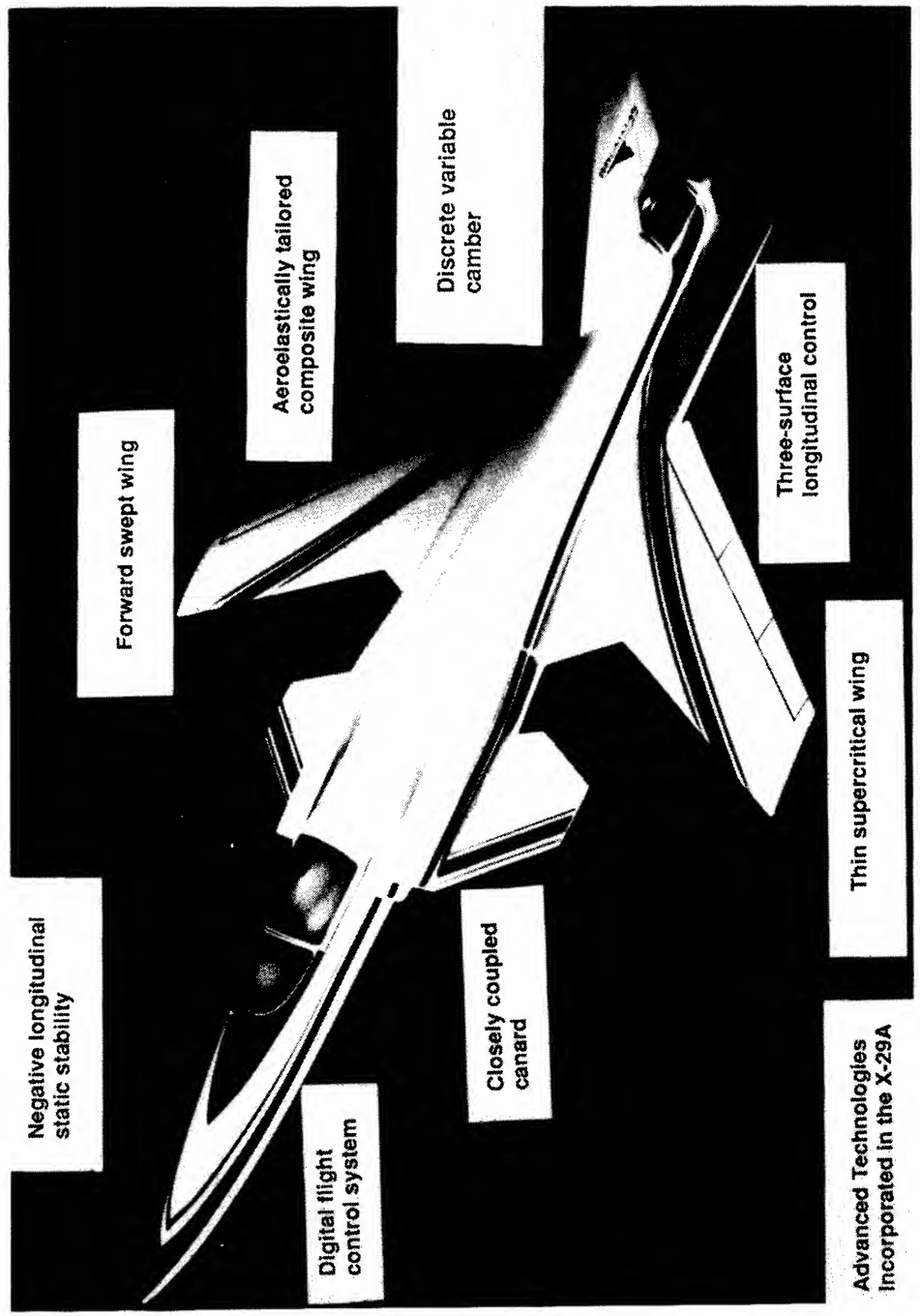

FIGURE 1.1
Advanced technologies incorporated on the X-29A aircraft.

force. A shear force is a force tangent to the surface of the fluid element. There are no shear stresses present in the fluid when it is at rest. A fluid can transmit forces normal to any chosen direction. The normal force and the normal stress are the pressure force and pressure, respectively.

Both liquids and gases can be considered to be fluids. Liquids under most conditions do not change their weight per unit volume appreciably and can be considered to be incompressible for most engineering applications. Gases, on the other hand, do change their weight or mass per unit volume appreciably under the influences of pressure or temperature and, therefore, must be considered to be compressible.

PRESSURE. Pressure is the normal force per unit area acting on the fluid. The average pressure is calculated by dividing the normal force to the surface by the surface area:

$$P = \frac{F}{A} \tag{1.1}$$

The static pressure in the atmosphere is nothing more than the weight per unit area of the air above the elevation being considered. The ratio of the pressure P at altitude to sea-level standard pressure P_0 is given the symbol δ:

$$\delta = \frac{P}{P_0} \tag{1.2}$$

The relationship between pressure, density ρ, and temperature T is given by the equation of state,

$$P = \rho RT \tag{1.3}$$

where R is a constant, the magnitude depending on the gas being considered. For air, R has a value 287 J/(kg K) or 1716 $ft^2/(sec^2\,°R)$. Atmospheric air follows the equation of state provided that the temperature is not too high and that air can be treated as a continuum.

TEMPERATURE. In aeronautics the temperature of air is an extremely important parameter, in that it affects the properties of air such as density and viscosity. Temperature is an abstract concept but can be thought of as a measure of the motion of molecular particles within a substance. The concept of temperature also serves as a means of determining the direction in which heat energy will flow when two objects of different temperatures come into contact. Heat energy will flow from the higher temperature object to that at lower temperature.

As we will show later, the temperature of the atmosphere varies significantly with altitude. The ratio of the ambient temperature at altitude, T, to a sea-level standard value, T_0 is denoted by the symbol θ:

$$\theta = \frac{T}{T_0} \tag{1.4}$$

where the temperatures are measured using the absolute Kelvin or Rankine scales.

DENSITY. The density of a substance is defined as the mass per unit volume:

$$\rho = \frac{\text{Mass}}{\text{Unit volume}} \tag{1.5}$$

From the equation of state, it can be seen that the density of a gas is directly proportional to the pressure and inversely proportional to the absolute temperature. The ratio of ambient air density ρ to standard sea level air density ρ_0 occurs in many aeronautical formulas and is given the designation σ.

$$\sigma = \rho/\rho_0 \tag{1.6}$$

VISCOSITY. Viscosity can be thought of as the internal friction of a fluid. Both liquids and gases possess the property of viscosity, with liquids being much more viscous than gases. As an aid in visualizing the concept of viscosity, consider the following simple experiment. Consider the motion of the fluid between two parallel plates separated by the distance h. If one plate is held fixed while the other plate is being pulled with a constant velocity u, then the velocity distribution of the fluid between the plates will be linear as shown in Fig. 1.2.

To produce the constant velocity motion of the upper plate, a tangential force must be applied to the plate. The magnitude of the force must be equal to the friction forces in the fluid. It has been established from experiments that the force per unit area of the plate is proportional to the velocity of the moving plate and inversely proportional to the distance between the plates. Expressed mathematically we have

$$\tau \propto \frac{u}{h} \tag{1.7}$$

where τ is the force per unit area, which is called the shear stress.

A more general form of Eq. (1.7) can be written by replacing u/h with the derivative du/dy. The proportionality factor is denoted by μ, the coefficient of absolute viscosity, which is obtained experimentally.

$$\tau = \mu \frac{du}{dy} \tag{1.8}$$

Equation (1.8) is known as Newton's law of friction.

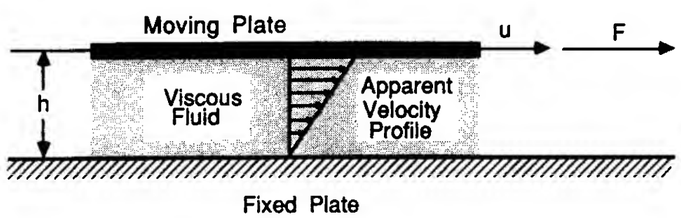

FIGURE 1.2
Shear stress between two plates.

For gases, the absolute viscosity depends only on temperature, with increasing temperature causing an increase in viscosity. To estimate the change in viscosity with temperature, several empirical formulations are commonly used. The simplest formula is Rayleigh's, which is

$$\frac{\mu_1}{\mu_0} = \left(\frac{T_1}{T_0}\right)^{3/4} \tag{1.9}$$

where the temperatures are on the absolute scale and the subscript zero denotes the reference condition.

An alternate expression for calculating the variation of absolute viscosity with temperature was developed by Sutherland. The empirical formula developed by Sutherland is valid provided the pressure is greater than 0.1 atmosphere, and is

$$\frac{\mu_1}{\mu_0} = \left(\frac{T_1}{T_0}\right)^{3/2} \frac{T_0 + S_1}{T_1 + S_1} \tag{1.10}$$

where S_1 is a constant. When the temperatures are expressed in the Rankine scale, $S_1 = 198°\text{R}$; when the temperatures are expressed in the Kelvin scale, $S_1 = 110\ \text{K}$.

The ratio of the absolute viscosity to the density of the fluid is a parameter that appears frequently and has been identified with the symbol ν; it is called the kinematic viscosity:

$$\nu = \frac{\mu}{\rho} \tag{1.11}$$

An important dimensionless quantity known as the Reynolds number is defined as

$$R = \frac{\rho V l}{\mu} = \frac{V l}{\nu} \tag{1.12}$$

and can be thought of as the ratio of the inertial to viscous forces of the fluid.

MACH NUMBER AND THE SPEED OF SOUND. The ratio of an airplane's speed V to the local speed of sound a is an extremely important parameter, called Mach number after the Austrian physicist Ernst Mach. The mathematical definition of Mach number is

$$M = \frac{V}{a} \tag{1.13}$$

As an airplane moves through the air, it creates pressure disturbances that propagate away from the airplane in all directions with the speed of sound. If the airplane is flying at a Mach number less than 1, the pressure disturbances travel faster than the airplane and influence the air ahead of the airplane. An example of this phenomenon is the upwash field created in front of a wing.

However, for flight at Mach numbers greater than 1 the pressure disturbances are moving more slowly than the airplane and, therefore, the flow ahead of the airplane has no warning of the oncoming aircraft.

The aerodynamic characteristics of an airplane depend upon the flow regime existing around the airplane. As the flight Mach number is increased, the flow around the airplane can be completely subsonic, a mixture of subsonic and supersonic flow, or completely supersonic. The flight Mach number is used to classify the various flow regimes. An approximate classification of the flow regimes is given below.

Incompressible subsonic flow	$0 < M < 0.5$
Compressible subsonic flow	$0.5 < M < 0.8$
Transonic flow	$0.8 < M < 1.2$
Supersonic flow	$1.2 < M < 5$
Hypersonic flow	$5 < M$

In order to have accurate aerodynamic predictions at $M > 0.5$ compressibility effects must be included.

The local speed of sound must be known to determine the Mach number. The speed of sound can be shown to be related to the absolute ambient temperature by the following expression:

$$a = (\gamma R T)^{1/2} \tag{1.14}$$

where γ is the ratio of specific heats and R is the gas constant. The ambient temperature will be shown in a later section to be a function of altitude.

1.3 AEROSTATICS

Aerostatics deals with the state of a gas at rest. It follows from the definition given for a fluid that all forces acting on the fluid must be normal to any cross-section within the fluid. Unlike a solid, a fluid at rest cannot support a shearing force. A consequence of this is that the pressure in a fluid at rest is independent of direction. That is to say that, at any point, the pressure is the same in all directions. This fundamental concept owes its origin to Pascal, a French scientist (1623–1662).

VARIATION OF PRESSURE IN A STATIC FLUID. Consider the small vertical column of fluid shown in Fig. 1.3. Because the fluid is at rest, the forces in both the vertical and horizontal directions must sum to zero. The forces in the vertical direction are due to the pressure forces and the weight of the fluid column. The force balance in the vertical direction is given by

$$PA = (P + dP)A + \rho g A\, dh \tag{1.15}$$

or

$$dP = -\rho g\, dh \tag{1.16}$$

Equation (1.16) tells us how the pressure varies with elevation above some

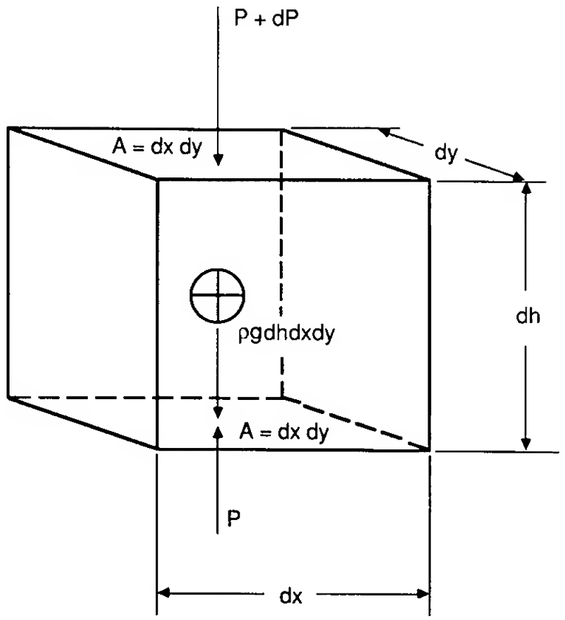

FIGURE 1.3
Element of fluid at rest.

reference level in a fluid. As the elevation is increased, the pressure will decrease. Therefore, the pressure in a static fluid is equal to the weight of the column of fluid above the point of interest.

One of the simplest means of measuring pressure is by way of a fluid manometer. Figure 1.4 shows two types of manometers. The first manometer consists of a U-shaped tube containing a liquid. When pressures of different magnitudes are applied across the manometer the fluid will rise on the side of the lower pressure and fall on the side of the higher pressure. By writing a force balance for each side, one can show that

$$P_1A + \rho gxA = P_2A + \rho g(x + h)A \tag{1.17}$$

which yields a relationship for the pressure difference in terms of the change in

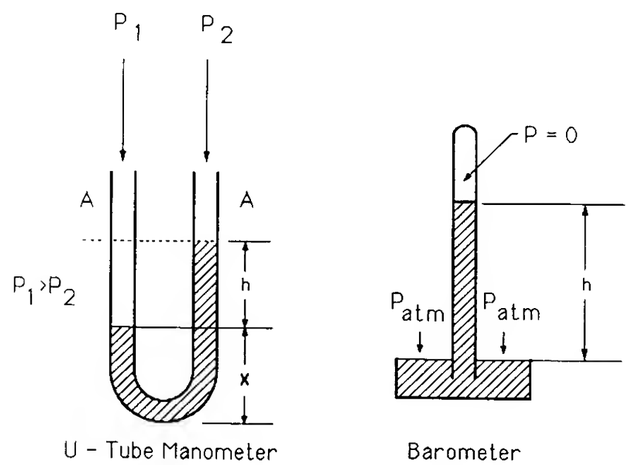

FIGURE 1.4
Sketch of U-tube manometer and barometer.

height of the liquid column:

$$P_1 - P_2 = \rho gh \tag{1.18}$$

The second sketch shows a simple mercury barometer. The barometer can be thought of as a modified U-tube manometer. One leg of the tube is closed off and evacuated. The pressure at the top of this leg is zero and atmospheric pressure acts on the open leg. The atmospheric pressure is therefore equal to the height of the mercury column, i.e.

$$P_{atm} = \rho gh \tag{1.19}$$

In practice the atmospheric pressure is commonly expressed as so many inches or millimeters of mercury. Remember, however, that neither inches nor millimeters of mercury are units of pressure.

1.4 DEVELOPMENT OF BERNOULLI'S EQUATION

Bernoulli's equation establishes the relationship between pressure, elevation, and velocity of the flow along a stream tube. For this analysis, the fluid is assumed to be a perfect fluid, i.e. we will ignore viscous effects. Consider the element of fluid in the stream tube shown in Fig. 1.5. The forces acting on the differential element of fluid are due to pressure and gravitational forces. The pressure force acting in the direction of the motion is given by

$$F_{pressure} = P\,dA - \left(P + \frac{\partial P}{\partial s}ds\right)dA \tag{1.20}$$

or

$$= dP\,dA \tag{1.21}$$

The gravitational force can be expressed as

$$F_{gravitational} = -g\,dm\sin\alpha \tag{1.22}$$

$$= g\,dm\frac{dz}{ds} \tag{1.23}$$

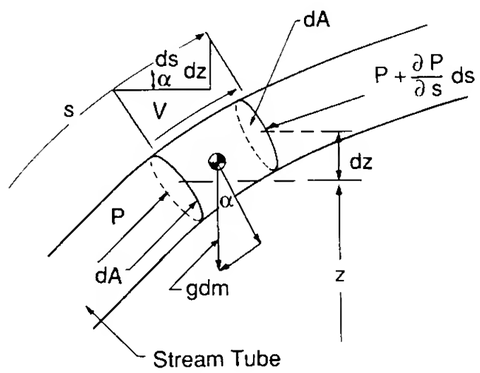

FIGURE 1.5
Forces acting on an element of flow in a stream tube.

Applying Newton's second law yields

$$-dP\,dA - g\,dm\frac{dz}{ds} = dm\frac{dV}{dt} \tag{1.24}$$

The differential mass dm can be expressed in terms of the mass density of the fluid element times its respective volume, i.e.

$$dm = \rho\,dA\,ds \tag{1.25}$$

Inserting the expression for the differential mass, the acceleration of the fluid can be expressed as

$$\frac{dV}{dt} = -\frac{1}{\rho}\frac{dP}{ds} - g\frac{dz}{ds} \tag{1.26}$$

The acceleration can be expressed as

$$\frac{dV}{dt} = \frac{\partial V}{\partial t} + \frac{\partial V}{\partial s}\frac{ds}{dt} \tag{1.27}$$

The first term on the right-hand side, $\partial V/\partial t$, denotes the change in velocity as a function of time for the entire flow field. The second term denotes the acceleration due to a change in location. If the flow field is steady, the term $\partial V/\partial t = 0$ and Eq. (1.27) reduces to

$$\frac{\partial V}{\partial s}\frac{ds}{dt} = -\frac{1}{\rho}\frac{dP}{ds} - g\frac{dz}{ds} \tag{1.28}$$

The changes of pressure as a function of time cannot accelerate a fluid particle. This is because the same pressure would be acting at every instant on all sides of the fluid particles. Therefore, the partial differential can be replaced by the total derivative in Eq. (1.28):

$$V\frac{dV}{ds} = -\frac{1}{\rho}\frac{dP}{ds} - g\frac{dz}{ds} \tag{1.29}$$

Integrating Eq. (1.29) along a streamline yields

$$\int_1^2 V\,dV = -\int_1^2 \frac{dP}{\rho} - g\int_1^2 dz \tag{1.30}$$

which is known as Bernoulli's equation. Bernoulli's equation establishes the relationship between pressure, elevation, and velocity along a stream tube.

INCOMPRESSIBLE BERNOULLI EQUATION. If the fluid is considered to be incompressible, Eq. (1.29) readily can be integrated to yield the incompressible Bernoulli equation:

$$P_1 + \tfrac{1}{2}\rho V_1^2 + \rho g z_1 = P_2 + \tfrac{1}{2}\rho V_2^2 + \rho g z_2 \tag{1.31}$$

The differences in elevation can usually be ignored when dealing with the flow

of gases such as air. An important application of Bernoulli's equation is the determination of the so-called stagnation pressure of a moving body or a body exposed to a flow. The stagnation point is defined as that point on the body at which the flow comes to rest. At that point the pressure is

$$P_0 = P_\infty + \tfrac{1}{2}\rho V_\infty^2 \tag{1.32}$$

where P_∞ and V_∞ are the static pressure and velocity far away from the body, that is the pressures and velocities that would exist if the body were not present. In the case of a moving body, V_∞ is equal to the velocity of the body itself and P_∞ is the static pressure of the medium through which the body is moving.

BERNOULLI'S EQUATION FOR A COMPRESSIBLE FLUID. At higher speeds (of the order of 100 m/s), the assumption that the fluid density of gases is constant, becomes invalid. As speed is increased, the air undergoes a compression and, therefore, the density cannot be treated as a constant. If the flow can be assumed to be isentropic, the relationship between pressure and density can be expressed as

$$P = c\rho^\gamma \tag{1.33}$$

where γ is the ratio of specific heats for the gas. For air, γ is approximately 1.4.

Substituting Eq. (1.33) into Eq. (1.30) and performing the indicated integrations yields the compressible form of Bernoulli's equation:

$$\frac{\gamma}{\gamma - 1}\frac{P}{\rho} + \tfrac{1}{2}V^2 + gz = \text{constant}. \tag{1.34}$$

As noted earlier, the elevation term is usually quite small for most aeronautical applications and, therefore, can be ignored. The stagnation pressure can be found by letting $V = 0$, in Eq. (1.34).

$$\frac{\gamma}{\gamma - 1}\frac{P}{\rho} + \tfrac{1}{2}V^2 = \frac{\gamma}{\gamma - 1}\frac{P_0}{\rho_0} \tag{1.35}$$

If we divide Eq. (1.35) by the term P/ρ, we obtain

$$1 + \frac{\gamma - 1}{2}\frac{1}{\gamma P/\rho}V^2 = \frac{P_0/P}{\rho_0/\rho} \tag{1.36}$$

Equation (1.36) can be solved for the velocity by substituting the following expressions,

$$a^2 = \gamma RT = \gamma P/\rho \tag{1.37}$$

and

$$\frac{P_0}{P} = \left(\frac{\rho_0}{\rho}\right)^\gamma \tag{1.38}$$

into Eq. (1.36) and rearranging to yield a relationship for the velocity and Mach number as follows.

$$V = \left[\frac{2a^2}{\gamma - 1}\left[\left(\frac{P_0}{P}\right)^{(\gamma-1)/\gamma} - 1\right]\right]^{1/2} \tag{1.39}$$

$$M = \left[\frac{2}{\gamma - 1}\left[\left(\frac{P_0}{P}\right)^{(\gamma-1)/\gamma} - 1\right]\right]^{1/2} \tag{1.40}$$

Equations (1.39) and (1.40) can be used to find the velocity and Mach number provided the flow regime is below $M = 1$.

1.5 THE ATMOSPHERE

The performance characteristics of an airplane depend on the properties of the atmosphere through which it flies. Because the atmosphere is continuously changing with time, it is impossible to determine airplane performance parameters precisely without first defining the state of the atmosphere.

The earth's atmosphere is a gaseous envelope surrounding the planet. The gas which we call air is actually a composition of numerous gases. The composition of dry air at sea level is shown in Table 1.1. The relative percentages of the constituents remains essentially the same up to an altitude of 90 km or 300 000 ft owing primarily to atmospheric mixing caused by winds and turbulence. At altitudes above 90 km the gases begin to settle or separate. The variability of water vapor in the atmosphere must be taken into account by the performance analyst. Water vapor can comprise up to 4 percent by volume of atmospheric air. When the relative humidity is high, the air density is lower than that for dry air for the same conditions of pressure and temperature. Under these conditions the density may be reduced by as much as 3 percent. A change in air density will cause a change in the aerodynamic forces acting on the airplane and therefore influence its performance capabilities. Furthermore, changes in air density created by water vapor will affect engine performance, which again influences the performance of the airplane.

TABLE 1.1
Composition of atmospheric air

	Density		Percentage by volume	Percentage by weight
	kg/m^3	slugs/ft^3		
Air	1.2250	2.3769×10^{-3}	100	100
Nitrogen			78.03	75.48
Oxygen			20.99	23.18
Argon			0.94	1.29

The remaining small portion of the composition of air is made up of neon, helium, krypton, xenon, CO_2 and water vapor

The atmosphere can be thought of as being composed of various layers, with each layer of the atmosphere having its own distinct characteristics. For the purpose of this discussion we will divide the atmosphere into four regions. In ascending order the layers are the troposphere, stratosphere, ionosphere and exosphere. The four layers are illustrated in Fig. 1.6. The troposphere and stratosphere are extremely important to aerospace engineers since most aircraft fly in these regions. The troposphere extends from the earth's surface to an altitude of approximately 6–13 miles or 10–20 km. The air masses in the troposphere are in constant motion and the region is characterized by unsteady or gusting winds and turbulence. The influence of turbulence and wind shear on aircraft structural integrity and flight behavior continues to be an important area of research for the aeronautical community. The structural loads imposed on an aircraft during an encounter with turbulent air can reduce the structural life of the airframe or, in an encounter with severe turbulence, can cause structural damage to the airframe.

Wind shear is an important atmospheric phenomenon that can be hazardous to aircraft during take-off or landing. Wind shear is the variation of the wind vector in both magnitude and direction. In vertical wind shear, the wind speed and direction change with altitude. An airplane landing in such a

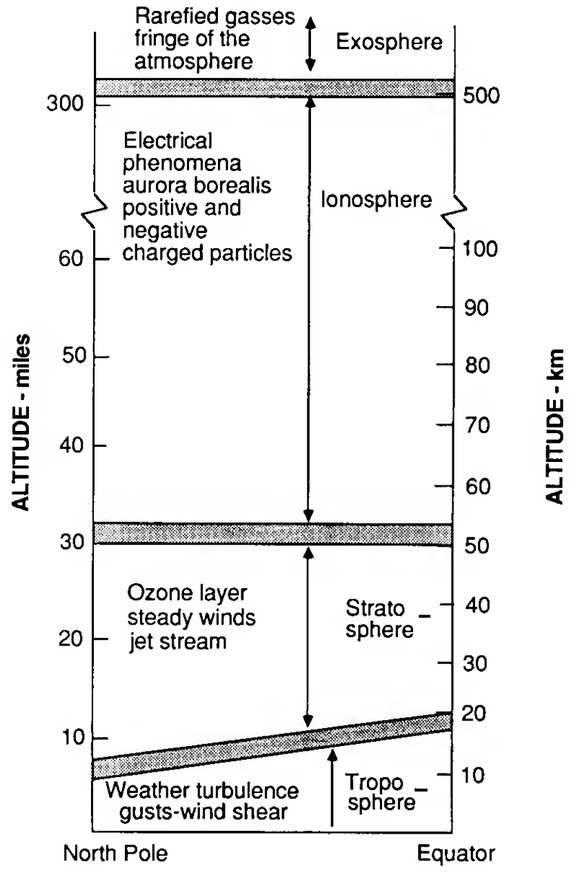

FIGURE 1.6
Layers of earth's atmosphere.

wind shear may be difficult to control; this can cause deviations from the intended touchdown point. Wind shears are created by the movement of air masses relative to one another or to the earth's surface. Thunderstorms, frontal systems, and the earth's boundary layer all produce wind shear profiles, that at times are severe enough to be hazardous to aircraft flying at low altitude.

The next layer above the troposphere is called the stratosphere. The stratosphere extends up to 50–70 miles, or 80–113 km, above the earth's surface. Unlike the troposphere, the stratosphere is a relatively tranquil region, free of gusts and turbulence, but it is characterized by high, steady winds. Wind speeds of the order of 37 m/s or 120 ft/s have been measured in the stratosphere.

The ionosphere extends from the upper edge of the stratosphere to an altitude of 200–300 miles, or 124–186 km (The name is derived from the word "ion", which describes a particle which has either a positive or negative electric charge.) This is the region where the air molecules undergo dissociation and many electrical phenomena occur. The aurora borealis is a visible electrical display that occurs in the ionosphere.

The last layer of the atmosphere is called the exosphere. The exosphere is the outermost region of the atmosphere and is made up of rarefied gas. In effect this is a transition zone between the earth's atmosphere and interplanetary space. For many applications we can consider air resistance to cease in the exosphere.

As stated previously, the properties of the atmosphere change with time and location on the earth. In order to compare the flight performance characteristics of airplanes and flight instruments, a standard atmosphere was needed. The modern standard atmosphere was first developed in the 1920s, independently in the United States and in Europe. The National Advisory Committee for Aeronautics (NACA) generated the American Standard Atmosphere. The European standard was developed by the International Commission for Aerial Navigation (ICAN). The two standard atmospheres were essentially the same except for some slight differences. These differences were resolved by an international committee and an international standard atmosphere was adopted by the International Civil Aviation Organization (ICAO) in 1952.

The standard atmosphere assumes a unique temperature profile which was determined by an extensive observation program. The temperature profile consists of regions of linear variations of temperature with altitude, and regions of constant temperature (isothermal regions). Figure 1.7 shows the temperature profile through the standard atmosphere. The standard sea-level properties of air are listed in Table 1.2.

The properties of the atmosphere can be expressed analytically as a function of altitude. However, before proceeding with the development of the analytical model of the atmosphere, we must define what we mean by altitude. For the present we will be concerned with three different definitions of

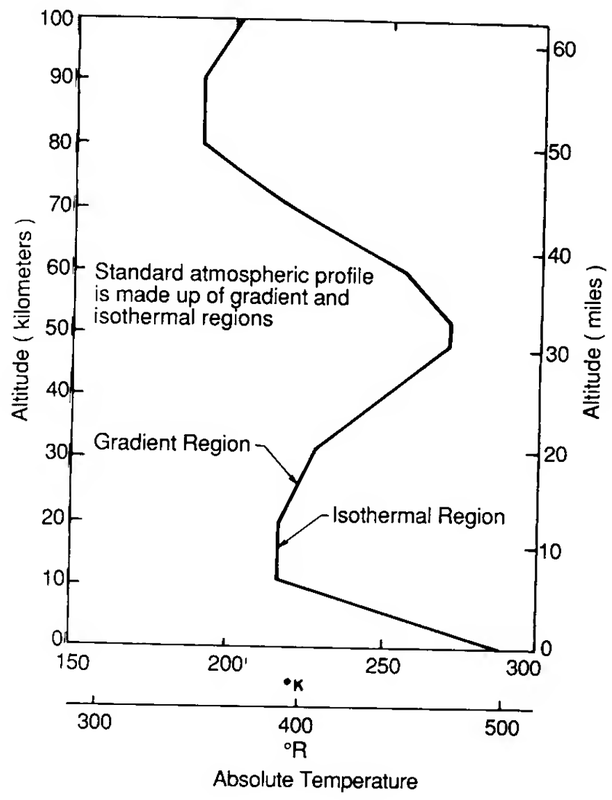

FIGURE 1.7
Temperature profile in the standard atmosphere.

altitude; absolute, geometric, and geopotential. Figure 1.8 shows the relationship between absolute and geometric altitude. Absolute altitude is the distance from the center of the Earth to the point in question, whereas the geometric altitude is the height of the point above sea level. The absolute and geometric altitudes are related to each other in the following manner:

$$h_a = h_G + R_0 \tag{1.41}$$

where h_a, h_G, and R_0 are the absolute altitude, geometric altitude, and radius of the Earth, respectively.

TABLE 1.2
Properties of air at sea level in the standard atmosphere

	English units	SI units
Gas constant, R	1716 ft·lb/(slug·°R)	287 $m^2/(K \cdot s^2)$
Pressure, P	2116.2 lb/ft^2	1.012×10^5 N/m^2
	29.92 in Hg	760 mm Hg
Density, ρ	(2.377×10^{-3}) $slug/ft^3$	1.225 kg/m^3
Temperature	518.69°R	288.16 K
Absolute viscosity, μ	3.737×10^{-7} lb·s/ft^2	1.789×10^{-3} N·s/m^2
Kinematic viscosity, ν	1.572×10^{-4} ft^{-2}/s	1.460×10^{-3} m^{-2}/s
Speed of sound, a	1116.4 ft/s	340.3 m/s

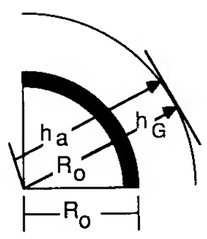

FIGURE 1.8
Definition of geometric and absolute altitude.

Historically, measurements of atmospheric properties have been based upon the assumption that the acceleration due to gravity is constant. This assumption leads to a fictitious altitude called the geopotential altitude. The relationship between the geometric and geopotential altitudes can be determined from an examination of the hydrostatic equation (Eq. (1.16)). Rewriting the hydrostatic equation,

$$dP = -\rho g\, dh \tag{1.42}$$

we see that the change in pressure is a function of the fluid density, and if we employ the acceleration due to gravity at sea level then h is the geopotential altitude. Therefore, we have

$$dP = -\rho g_0\, dh \tag{1.43}$$

when h is the geopotential height, and

$$dP = -\rho g\, dh_G \tag{1.44}$$

when h_G is the geometric height.

Equations (1.43) and (1.44) can be used to establish the relationship between the geometric and geopotential altitude. Upon comparing these equations we see that

$$dh = \frac{g}{g_0}\, dh_G \tag{1.45}$$

Further, it can be shown that

$$g = g_0\left(\frac{R_0}{R_0 + h_G}\right)^2 \tag{1.46}$$

which, when substituted into Eq. (1.45) yields

$$dh = \frac{R_0^2\, dh_G}{(R_0 + h_G)^2} \tag{1.47}$$

Equation (1.47) can be integrated to give an expression relating the two altitudes:

$$h = \frac{R_0}{R_0 + h_G} h_G \tag{1.48}$$

or

$$h_G = \frac{R_0}{R_0 - h} h \tag{1.49}$$

In practice, the difference between the geometric and geopotential altitudes is quite small for altitudes below 15.2 km or 50 000 ft. However, for the higher altitudes the difference must be taken into account for accurate performance calculations.

Starting with the relationship for the change in pressure with altitude and the equations of state

$$dP = -\rho g_0\, dh \tag{1.50}$$

and

$$P = \rho R T \tag{1.51}$$

we can obtain the following expression by dividing Eq. (1.50) by (1.51):

$$\frac{dP}{P} = -\frac{g_0}{R}\frac{dh}{T} \tag{1.52}$$

If the temperature varies with altitude in a linear manner, Eq. (1.52) yields

$$\int_{P_1}^{P} \frac{dP}{P} = -\frac{g_0}{R}\int_{h_1}^{h} \frac{dh}{T_1 + \lambda(h - h_1)} \tag{1.53}$$

which, upon integration, gives

$$\ln\frac{P}{P_1} = -\frac{g_0}{R\lambda}\ln\frac{T_1 + \lambda(h - h_1)}{T_1} \tag{1.54}$$

where P_1, T_1, and h_1, are the pressure, temperature and altitude at the start of the linear region and λ is the rate of temperature change with altitude, which is called the lapse rate. Equation (1.54) can be rewritten in a more convenient form as

$$\frac{P}{P_1} = \left(\frac{T}{T_1}\right)^{-g_0/(R\lambda)} \tag{1.55}$$

Equation (1.55) can be used to calculate the pressure at various altitudes in any one of the linear temperature profile regions, provided the appropriate constants P_1, T_1, h_1 and λ are used.

The density variation can be easily determined as follows:

$$\frac{P}{P_1} = \frac{\rho T}{\rho_1 T_1} \tag{1.56}$$

and therefore

$$\frac{\rho}{\rho_1} = \left(\frac{T}{T_1}\right)^{-(1+g_0/(R\lambda))} \tag{1.57}$$

In the isothermal regions, the temperature remains constant as altitude varies. Starting again with equation (1.52), we obtain

$$\ln \frac{P}{P_1} = -\frac{g_0}{RT_1}(h - h_1) \tag{1.58}$$

or

$$\frac{P}{P_1} = e^{-g_0(h-h_1)/(RT_1)} \tag{1.59}$$

where P_1, T_1, and h_1 are the values of pressure, temperature and altitude at the start of the isothermal region. The density variation in the isothermal regions can be obtained as

$$\frac{\rho}{\rho_1} = e^{-g_0(h-h_1)/(RT_1)} \tag{1.60}$$

Equations (1.55), (1.57), (1.59) and (1.60) can be used to predict accurately the pressure and density variation in the standard atmosphere up to approximately 57 miles, or 91 km. Table 1.3 gives the values of temperature pressure and density at the boundaries between the various temperature segments. The properties of the standard atmosphere as a function of altitude are presented in tabular form in the Appendix.

Example Problem 1.1. The temperature from sea level to 30 000 ft is found to decrease in a linear manner. The temperature and pressure at sea level are measured to be 40°F and 2050 lb/ft^2, respectively. If the temperature at 30 000 ft is −60°F, find the pressure and density at 20 000 ft.

Solution. The temperature can be represented by the linear equation

$$T = T_1 + \lambda h \qquad \text{where} \qquad T_1 = 499.6°\text{R} \qquad \text{and} \qquad \lambda = \frac{T - T_1}{h} = -0.00333°\text{R/ft}$$

TABLE 1.3
Properties of the atmosphere at the isothermal gradient boundaries

Geopotential altitude, H, km	Geometric altitude, Z, km	T_0, K	P, N/m^2	ρ, kg/m^3	dT/dH, K/km
0	0	288.15	1.01325×10^5	1.225	−6.5
11	11.019	216.65	2.2636×10^4	3.639×10^{-1}	0
20	20.063	216.65	5.474×10^3	8.803×10^{-2}	1
32	32.162	228.65	8.6805×10^2	1.332×10^{-2}	1
47	47.350	270.65	1.1095×10^2	1.427×10^{-3}	2.8
52	52.429	270.65	5.9002×10^1	7.594×10^{-4}	0
61	61.591	252.65	1.8208×10^1	2.511×10^{-4}	−2
79	79.994	180.65	1.03757	2.001×10^{-5}	−4
88.74	90.0	180.65	0.16435	3.170×10^{-5}	0

The temperature at 20 000 ft can be obtained as

$$T = 499.6 - (0.00333°\text{R/ft})h$$

When $h = 20\,000$ ft, $T = 432.9°$R. The pressure can be calculated from Eq. (1.54), i.e.

$$\frac{P}{P_1} = \left(\frac{T}{T_1}\right)^{-g_0/R\lambda} \qquad P = P_1\left(\frac{T}{T_1}\right)^{-g_0/R\lambda} = (2050\ \text{lb/ft}^2)\left(\frac{432.9°\text{R}}{499.6°\text{R}}\right)^{5.63} = 915\ \text{lb/ft}^2$$

The density can be found from either Eq. (1.3) or (1.56). Using the equation of state,

$$P = \rho RT \qquad \rho = \frac{P}{RT}$$

$$\rho = \frac{915\ \text{lb/ft}^2}{(1718\ \text{ft}^2/(\text{s}^2\cdot°\text{R}))(432.9°\text{R})}\, 0.00123\ \text{slug/ft}^3$$

1.6 AERODYNAMIC NOMENCLATURE

To describe the motion of an airplane it is necessary to define a suitable coordinate system for formulation of the equations of motion. For most problems dealing with aircraft motion, two coordinate systems are used. One coordinate system is fixed to the earth and may be considered for the purpose of aircraft motion analysis to be an inertial coordinate system. The other coordinate system is fixed to the airplane and is referred to as a body coordinate system. Figure 1.9 shows the two right-handed coordinate systems.

The forces acting on an airplane in flight consist of aerodynamic, thrust and gravitational forces. These forces can be resolved along an axis system fixed to the airplane's center of gravity, as illustrated in Fig. 1.10. The force components are denoted X, Y and Z, T_x, T_y and T_z and W_x, W_y and W_z for the

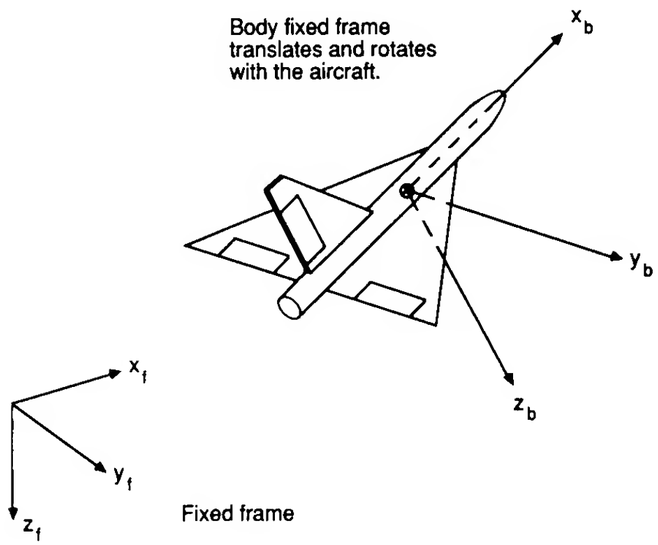

FIGURE 1.9
Body axes coordinate system.

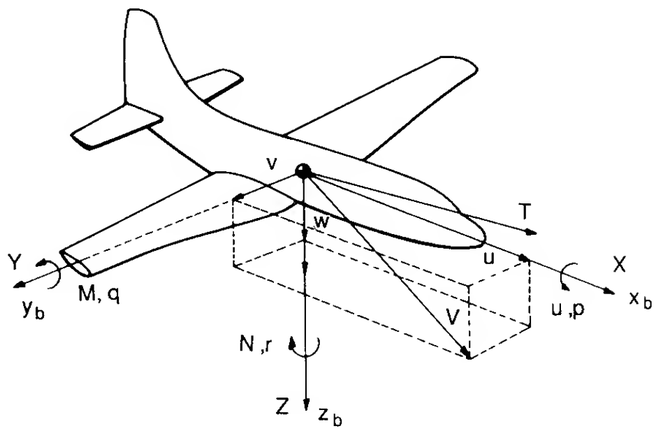

	Roll Axis x_b	Pitch Axis y_b	Yaw Axis z_b
Angular rates	p	q	r
Velocity components	u	v	w
Aerodynamic force components	X	Y	Z
Aerodynamic moment components	L	M	N
Moment of inertia about each axis	I_x	I_y	I_z
Products of inertia	I_{yz}	I_{xz}	I_{xy}

FIGURE 1.10
Definition of forces, moments and velocity components in a body fixed coordinate frame.

aerodynamic, thrust and gravitational force components along the x, y and z axes, respectively. The aerodynamic forces are defined in terms of dimensionless coefficients, the flight dynamic pressure and a reference area as follows:

$$X = C_x QS \quad \text{axial force} \tag{1.61}$$

$$Y = C_y QS \quad \text{side force} \tag{1.62}$$

$$Z = C_z QS \quad \text{normal force} \tag{1.63}$$

In a similar manner, the moments on the airplane can be divided into moments created by the aerodynamic load distribution and the thrust force not acting through the center of gravity. The components of the aerodynamic moment are also expressed in terms of dimensionless coefficients, flight dynamc pressure, reference area and a characteristic length as follows:

$$L = C_l QSl \quad \text{rolling moment} \tag{1.64}$$

$$M = C_m QSl \quad \text{pitching moment} \tag{1.65}$$

$$N = C_n QSl \quad \text{yawing moment} \tag{1.66}$$

For airplanes, the reference area S is taken as the wing platform area and the characteristic length l is taken as the wing span for the rolling and yawing moment and the mean chord for the pitching moment. For rockets and

missiles, the reference area is usually taken as the maximum cross-sectional area, and the characteristic length is taken as the maximum diameter.

The aerodynamic coefficients C_x, C_y, C_z, C_l, C_m, and C_n are primarily a function of Mach number, Reynolds number, angle of attack and sideslip angle, and are secondary functions of the time rate of change of angle of attack and sideslip, and the angular velocity of the airplane.

The aerodynamic force and moment acting on the airplane and its angular and translational velocity are illustrated in Fig. 1.10. The x and z axes are in the plane of symmetry with the x axis pointing along the fuselage and the positive y axis along the right wing. The resultant force and moment, as well as the airplane's velocity, can be resolved along these axes.

The angle of attack and sideslip can be defined in terms of the velocity components as illustrated in Fig. 1.11. The equations for α and β are given below.

$$\alpha = \tan^{-1}\frac{w}{u} \tag{1.67}$$

and

$$\beta = \sin^{-1}\frac{v}{V} \tag{1.68}$$

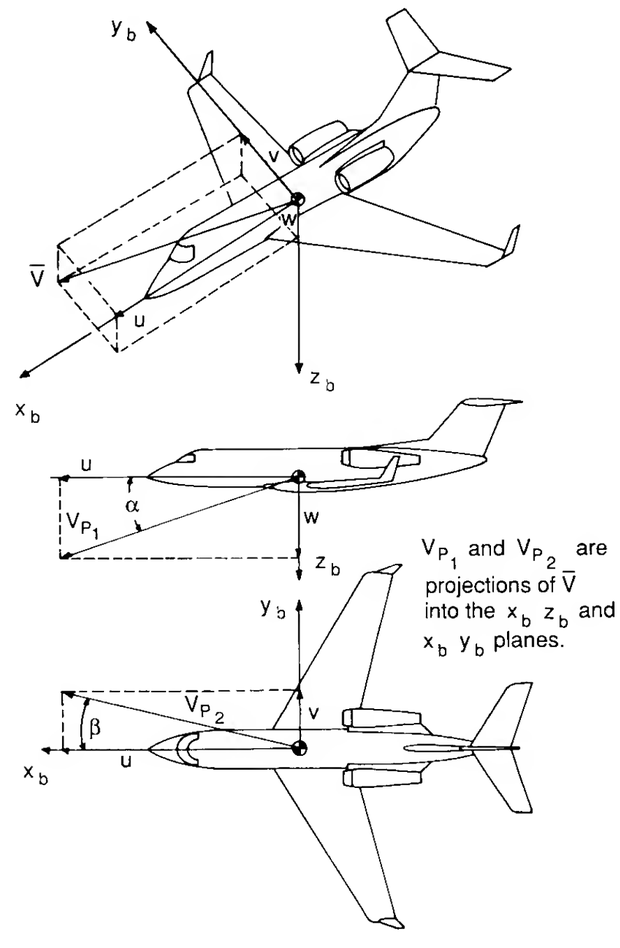

FIGURE 1.11
Definition of angle of attack and sideslip.

where

$$V = (u^2 + v^2 + w^2)^{1/2} \tag{1.69}$$

If the angle of attack and sideslip are small, i.e. <15°, then Eq. (1.67) and (1.68) can be approximated by

$$\alpha = \frac{w}{u} \tag{1.70}$$

and

$$\beta = \frac{v}{u} \tag{1.71}$$

where α and β are in radians.

1.7 AIRCRAFT INSTRUMENTS

The earliest successful airplanes were generally flown without the aid of aircraft instruments.[1] The pilots of these early vehicles were primarily preoccupied with maneuvering and controlling their sometimes temperamental aircraft. However, as new designs were developed, the performance, stability, and control steadily improved to the point where the pilot needed more information about the airplane's flight conditions to fly the airplane safely. One of the major changes in aircraft design that lead to improved performance was the evolution of the open air cockpit. Prior to this development, pilots flew their airplanes in either a crouched or inclined position, exposed to the oncoming airstream. Besides providing the pilot with shelter from the airstream, the cockpit also provided a convenient place for the location of aircraft instruments. The early open-cockpit pilots were hesitant to fly from a closed cockpit because this eliminated their ability to judge sideslip (or skid) by the wind blowing on one side of their face. They also used the sound of the slipstream to provide an indication of the airspeed.

The actual chronological development of aircraft instruments is not readily available; however, one can safely guess that some of the earliest instruments to appear on the cockpit instrument panel were a magnetic compass for navigation, airspeed and altitude indicators for flight information, and engine instruments such as rpm and fuel gauges. The flight decks of modern airplanes are equipped with a multitude of instruments that provide the flight crew with information they need to fly their aircraft. The instruments can be categorized according to their primary use as flight, navigation, power plant, environmental, and electrical systems instruments.

Several of the instruments that compose the flight instrument group will be discussed in the following sections. The instruments include the airspeed

[1] The Wright brothers used several instruments on their historic flight. They had a tachometer to measure engine rpm, an anemometer to measure air speed, and a stop watch.

indicator, altimeter, rate of climb indicator, and Mach meter. These four instruments, along with angle of attack and sideslip indicators, are extremely important for flight test measurement of performance and stability data.

AIR DATA SYSTEMS. The Pitot static system of an airplane is used to measure the total pressure created by the forward motion of the airplane and the static pressure of the ambient atmosphere. The difference between total and static pressures is used to measure airspeed and Mach number and the static pressure is used for measurement of altitude and rate of climb. The Pitot static system is illustrated in Fig. 1.12. The Pitot static probe normally consists of two concentric tubes; the inner tube is used to determine the total pressure and the outer tube is used to determine the static pressure of the surrounding air.

AIRSPEED INDICATOR. The pressures measured by the Pitot static probe can be used to determine the airspeed of the airplane. For low flight speeds, when compressibility effects can be safely ignored, we can use the incompressible form of Bernoulli's equation to show that the difference between the total and the static pressure is the dynamic pressure:

$$P_0 = P + \tfrac{1}{2}\rho V_\infty^2 \tag{1.72}$$

$$\tfrac{1}{2}\rho V_\infty^2 = P_0 - P \tag{1.73}$$

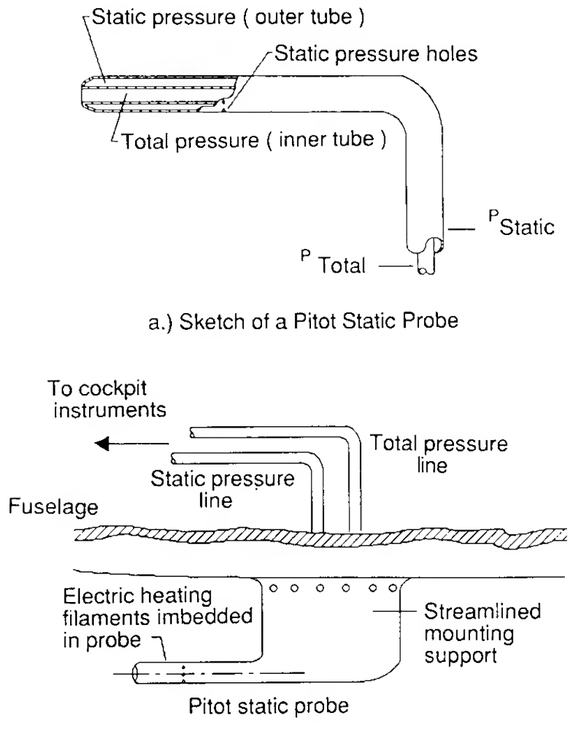

FIGURE 1.12
Pitot static system.

or

$$V_\infty = \left(\frac{2(P_0 - P)}{\rho}\right)^{1/2} \tag{1.74}$$

The airspeed indicator in the cockpit consists of a differential pressure gauge that measures the dynamic pressure and deflects an indicator hand proportionally to the pressure difference. As indicated by Eq. (1.74), the airspeed is both a function of the measured pressure difference and the air density ρ. As was shown earlier, air density is a function of altitude and atmospheric conditions. To obtain the true airspeed, the airspeed indicator would be required to measure the change in both pressure and air density. This is not feasible for a simple instrument and therefore the scale on the airspeed indicator is calibrated using standard sea-level air. The speed measured by the indicator is called the indicated airspeed (IAS).

The speed measured by an airspeed indicator can be used to determine the true flight speed provided that the indicated airspeed is corrected for instrument error, position error, compressibility effects, and density corrections for altitude variations. Instrument error includes those errors inherent to the instrument itself, for example, pressure losses or mechanical inaccuracies in the system. Position error has to do with the location of the Pitot static probe on the airplane. Ideally, the probe should be located so that it is in the undisturbed freestream; in general this is not possible and thus the probe is affected by flow distortion due to the fuselage and/or wing. The total pressure measured by a Pitot static probe is relatively insensitive to flow inclination. Unfortunately, this is not the case for the static measurement and care must be used to position the probe so as to minimize the error in the static measurement. If one knows the instrument and position errors, one can correct the indicated airspeed to give what is referred to as the calibrated airspeed (CAS).

At high speeds, the Pitot static probe must be corrected for compressibility effects. This can be demonstrated by examining the compressible form of the Bernoulli equation:

$$\frac{V^2}{2} + \frac{\gamma}{\gamma - 1}\frac{P}{\rho} = \frac{\gamma}{\gamma - 1}\frac{P_0}{\rho_0} \tag{1.75}$$

Equation (1.75) can be expressed in terms of Mach number as follows:

$$P_0 = P\left(1 + \frac{\gamma - 1}{2}M^2\right)^{\gamma/(\gamma-1)} \tag{1.76}$$

Recall that the airspeed indicator measures the difference between the total and static pressure. Equation (1.76) can be rewritten as

$$q_c = P_0 - P = P\left[\left(1 + \frac{\gamma - 1}{2}M^2\right)^{\gamma/(\gamma-1)} - 1\right] \tag{1.77}$$

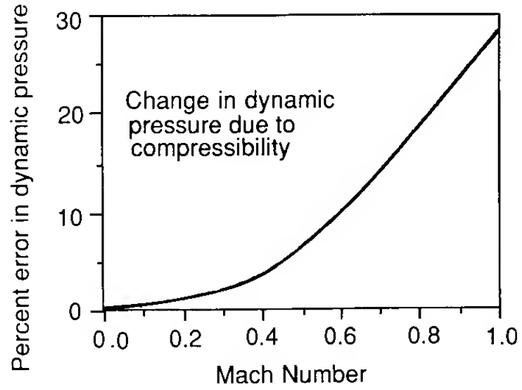

FIGURE 1.13
Percent error in dynamic pressure if compressibility is neglected.

where q_c is the compressible equivalent to the dynamic pressure. Figure 1.13 shows the percentage error in dynamic pressure if compressibility is ignored.

The equivalent airspeed (EAS) can be thought of as the flight speed in the standard sea-level air mass which produces the same dynamic pressure as the actual flight speed. To obtain the actual, or true, airspeed, (TAS) the equivalent airspeed must be corrected for density variations. Using the fact that the dynamic pressures are the same, one can develop a relationship between the true and equivalent airspeeds as follows:

$$\tfrac{1}{2}\rho_0 V_{\text{EAS}}^2 = \tfrac{1}{2}\rho V_{\text{TAS}}^2 \tag{1.78}$$

$$V_{\text{TAS}} = \frac{V_{\text{EAS}}}{\sqrt{\sigma}} \tag{1.79}$$

where $\sigma = \rho/\rho_0$.

The definitions for the various airspeed designations are summarized in Table 1.4.

TABLE 1.4
Airspeed designations

Airspeed*	Definition
V_{IAS} Indicated airspeed	Airspeed indicated by the airspeed instrument The indicated airspeed is affected by altitude, compressibility, instrument and position error.
V_{CAS} Calibrated airspeed	Indicated airspeed corrected for instrument and position errors.
V_{EAS} Equivalent airspeed	Calibrated airspeed corrected for compressibility.
V_{TAS} True airspeed	Equivalent airspeed corrected for density altitude.

* When the prefix K is used, the airspeed is in knots.

ALTIMETER. An altimeter is a device used to measure the altitude of an airplane. The control of an airplane's altitude is very important for safe operation of an aircraft. Pilots use an altimeter to maintain adequate vertical spacing between their aircraft and other airplanes operating in the same area and to establish sufficient distance between the airplane and the ground.

Earlier in this chapter we briefly discussed the mercury barometer. A barometer can be used to measure the atmospheric pressure. As we have shown, the static pressure in the atmosphere varies with altitude, so that if we use a device similar to a barometer we can measure the static pressure outside the airplane, and then relate that pressure to a corresponding altitude in the standard atmosphere. This is the basic idea behind a pressure altimeter.

The mercury barometer would of course be impractical for application in aircraft, because it is both fragile and sensitive to the motion of the airplane. To avoid this difficulty, the pressure altimeter uses the same principle as an aneroid[2] barometer. This type of barometer measures the pressure by magnifying small deflections of an elastic element that deforms as pressure acts upon it.

The altimeter is a sensitive pressure transducer that measures the ambient static pressure and displays an altitude value on the instrument dial. The altimeter is calibrated using the standard atmosphere and the altitude indicated by the instrument is referred to as the pressure altitude. The *pressure altitude* is the altitude in the standard atmosphere corresponding to the measured pressure. The pressure altitude and actual or geometric altitude will be the same only when the atmosphere through which the airplane is flying is identical to the standard atmosphere.

In addition to pressure altitude, there are two other altitudes that are important for performance analysis. They are the density and temperature altitudes. The *density altitude* is the altitude in the standard atmosphere corresponding to the ambient density. In general, the ambient density is not measured, but rather is calculated from the pressure altitude given by the altimeter and the ambient temperature measured by a temperature probe. The *temperature altitude* is, as you might guess, the altitude in the standard atmosphere corresponding to the measured ambient temperature.

As noted earlier, the atmosphere is continuously changing; therefore, to compare performance data for an airplane from one test to another, or for comparison of different airplanes, the data must be referred to a common atmospheric reference. The density altitude is used for airplane performance data comparisons.

An altimeter is an extremely sophisticated instrument, as illustrated by the drawing in Fig. 1.14. This particular altimeter uses two aneroid capsules to increase the sensitivity of the instrument. The deflections of the capsules are magnified and represented by the movement of the pointer with respect to a scale on the surface plate of the meter and a counter. This altimeter is

[2] Aneroid is derived from the Greek word aneros which means "not wet."

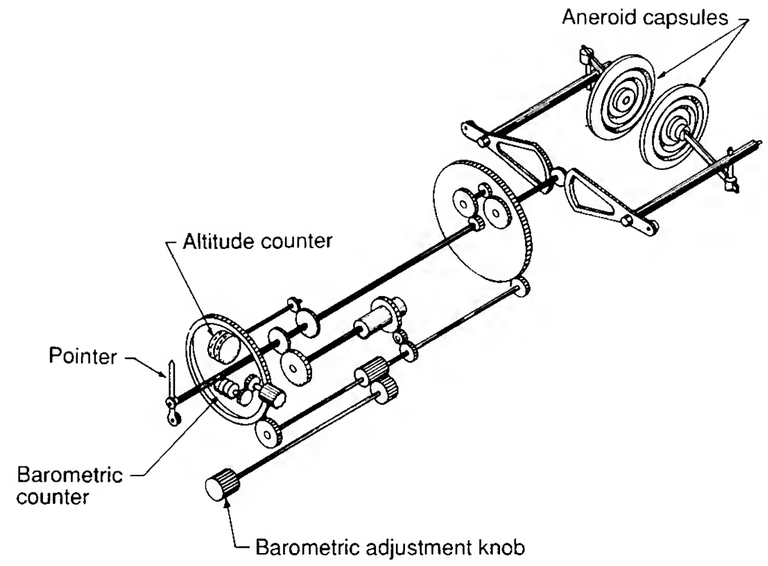

FIGURE 1.14
Cutaway drawing of an altimeter.

equipped with a barometric pressure setting mechanism. The adjusting mechanism allows the pilot manually to correct the altimeter for variations in sea-level barometric pressure. With such adjustments, the altimeter will indicate an altitude that closely approaches the true altitude above sea level.

RATE OF CLIMB INDICATOR. One of the earliest instruments used to measure rate of climb was called a statoscope. This instrument was used by balloonists to detect variation from a desired altitude. The instrument consisted of a closed atmospheric chamber connected by a tube containing a small quantity of liquid to an outer chamber vented to the atmosphere. As the altitude changed, air would flow from one chamber to the other to equalize the pressure. Air passing through the liquid would create bubbles and the direction of the flow of bubbles indicated whether the balloon was ascending or descending. A crude indication of the rate of climb was obtained by observing the frequency of the bubbles passing through the liquid.

Although the statoscope provided the balloonist with a means of detecting departure from a constant altitude, it was difficult to use as a rate of climb indicator. A new instrument called the balloon variometer was developed for rate of climb measurements. The variometer was similar to the statoscope; however, the flow into the chamber took place through a capillary leak. The pressure difference across the leak was measured with a sensitive liquid manometer that was calibrated to indicate the rate of climb.

Present-day rate of climb indicators are similar to the variometer. An example of a leak type rate of climb indicator is shown in Fig. 1.15. This instrument consists of an insulated chamber, a diaphragm, a calibrated leak,

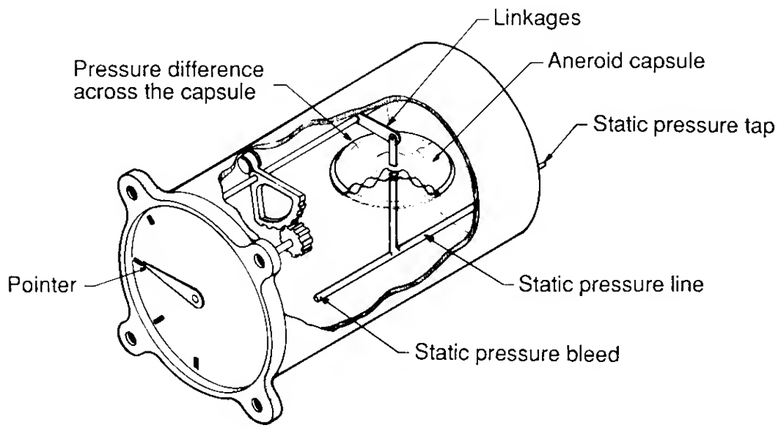

FIGURE 1.15
Sketch of the basic components of a rate of climb indicator.

and an appropriate mechanical linkage to measure the deflection of the diaphragm. The static pressure is applied to the interior of the diaphragm and is also allowed to leak into the chamber by way of a capillary or orifice opening. The diaphragm measures the differential pressure across the leak and the deflection of the diaphragm is transmitted to the indicator dial by a mechanical linkage, as illustrated in the sketch in Fig. 1.15.

MACHMETER. The Pitot static tube can be used to determine the Mach number of an airplane from the measured stagnation and static pressure. If the Mach number is less than 1, Eq. (1.40) can be used to find the Mach number of the airplane:

$$\frac{P_0}{P} = \left(1 + \frac{\gamma - 1}{2} M^2\right)^{\gamma/(\gamma-1)} \tag{1.80}$$

However, when the Mach number is greater than unity, a bow wave forms ahead of the Pitot probe, as illustrated in Fig. 1.16. The bow wave is a curved

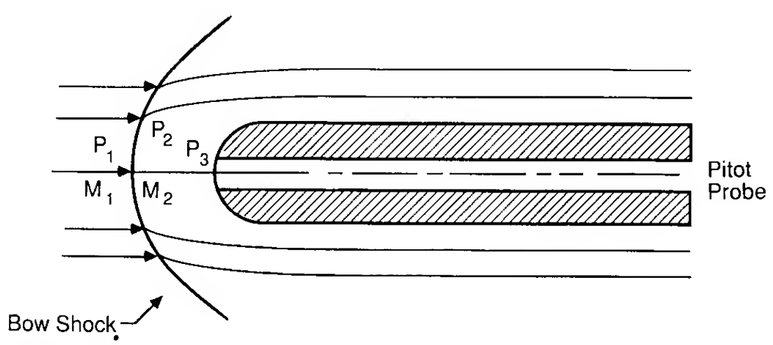

FIGURE 1.16
Detached shock wave ahead of a Pitot static probe.

detached shock wave. In the immediate vicinity of the Pitot orifice, the shock wave can be approximated as a normal shock wave. Using the normal shock relationships, the pressure ratio across the shock can be written as

$$\frac{P_2}{P_1} = \left(\frac{2\gamma}{\gamma - 1}\right) M_1^2 - \left(\frac{\gamma - 1}{\gamma + 1}\right) \tag{1.81}$$

where M_1 is the Mach number ahead of the shock wave. The relationship between the Mach number M_1 ahead of the normal shock and the Mach number M_2 behind the shock is given by Eq. (1.82):

$$M_2^2 = \frac{\frac{1}{2}(\gamma - 1)M_1^2 + 1}{\gamma M_1^2 - \frac{1}{2}(\gamma - 1)} \tag{1.82}$$

After passing through the shock wave, the air is slowed down adiabatically to zero velocity at the total pressure orifice of the Pitot probe. The pressure ratio behind the shock can be expressed as

$$\frac{P_3}{P_2} = \left(1 + \frac{\gamma - 1}{2} M_2^2\right)^{\gamma/(\gamma-1)} \tag{1.83}$$

Upon combining the previous equations, the ratio of stagnation pressure to static pressure in terms of the flight Mach number can be written.

$$\frac{P_3}{P_1} = \left[\left(\frac{2\gamma}{\gamma + 1}\right) M_1^2 - \left(\frac{\gamma - 1}{\gamma + 1}\right)\right]\left[1 + \frac{\gamma - 1}{2}\left[\left(\frac{\frac{1}{2}(\gamma - 1)M_1^2 + 1}{\gamma M_1^2 - \frac{1}{2}(\gamma - 1)}\right)\right]\right]^{\gamma/(\gamma-1)} \tag{1.84}$$

The above expression is known as the Rayleigh Pitot tube formula, named after Lord Rayleigh who first developed this equation in 1910. If we assume that the ratio γ of specific heats for air is 1.4, the above expression can be rewritten as

$$\frac{P_3}{P_1} = \frac{7M_1^2 - 1}{6}\left[1 + 0.2\left(\frac{M_1^2 + 5}{7M_1^2 - 1}\right)\right]^{3.5} \tag{1.85}$$

The preceding equations can be used to design a Mach meter.

The use of Rayleigh's formula is invalid for very high Mach numbers or altitudes. When the Mach number is high, there will be appreciable heat exchange, which violates the assumption of adiabatic flow used in the development of the equation. At very high altitude, air cannot be considered as a continuous medium and again the analysis breaks down.

ANGLE OF ATTACK INDICATORS. The measurement of angle of attack is important for cruise control and stall warning. There are several devices that can be used to measure the angle of attack of an airplane, two of which are the vane and pressure-sensor type indicator. The pivot vane sensor is a mass-balanced wind vane that is free to align itself with the oncoming flow. The vane type angle of attack sensor has been used extensively in airplane flight test programs. For flight test applications the sensor is usually mounted on a nose

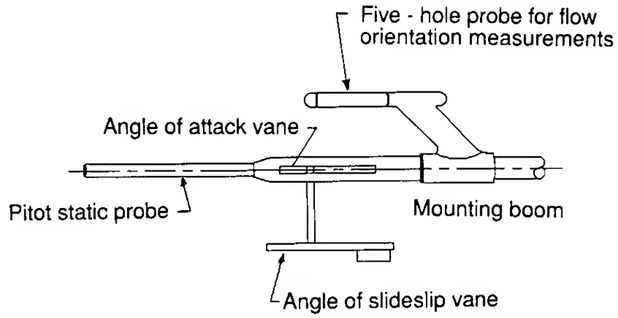

FIGURE 1.17
Flight test instrumentation, Pitot static probe, angle of attack and sideslip varies, five-hole probe mounted on a nose or wing boom.

boom or a boom mounted to the wing tips along with a Pitot static probe, as illustrated in Fig. 1.17. Note that a second vane system is mounted on the boom to measure the side-slip angle.

The angle measured by the vane is influenced by the distortion of the flow field created by the airplane. Actually, the sensor only measures the local angle of attack. The difference between the measured and actual angle of attack is called the position error. Position error can be minimized by mounting the sensor on the fuselage, where the flow distortion is small. The deflection of the vane is recorded by means of a potentiometer.

A null-seeking pressure sensor can also be used to measure the angle of attack. Figure 1.18 is a schematic of a null-seeking pressure sensor. The sensor consists of the following components; a rotatable tube containing two orifices spaced at equal angles to the tube axis; a pressure transducer to detect the difference in pressure between the two orifices; a mechanism for rotating the probe until the pressure differential is zero; and a device for measuring the rotation or angle of attack. The device shown in Fig. 1.18 consists of a rotatable probe that protrudes through the fuselage and an air chamber that is

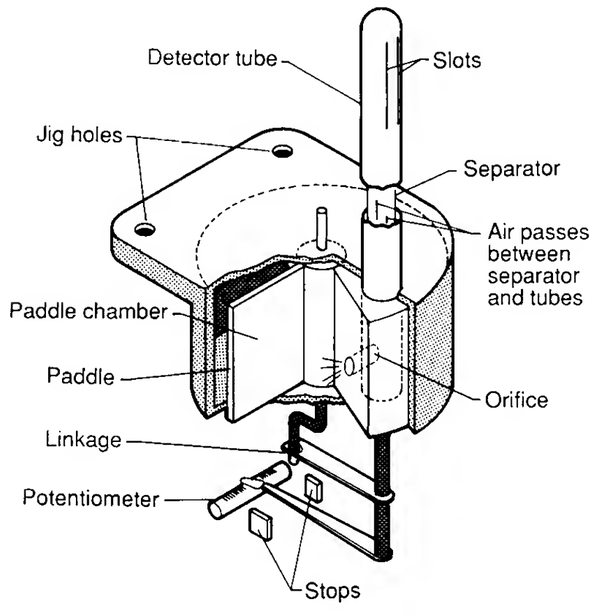

FIGURE 1.18
Null sensing pressure probe for measuring angle of attack.

mounted inside the fuselage. The pressures from the two slits are vented to air chambers by a swivel paddle. If a pressure difference exists at the two slots, the swivel paddle rotates. The paddle is connected by way of linkages so that as the paddle moves the pressure tube is rotated until the pressures are equalized. The angular position of the probe is recorded by a potentiometer.

Example Problem 1.2. An aircraft altimeter calibrated to the standard atmosphere reads 10 000 ft. The airspeed indicator has been calibrated for both instrument and position errors and reads a velocity of 120 knots. If the outside air temperature is 20°F, determine the true airspeed.

Solution. The altimeter is a pressure gauge calibrated to the standard atmosphere. If the altimeter reads 10 000 ft, the static pressure it senses must correspond to the static pressure at 10 000 ft in the standard atmosphere. Using the standard atmospheric table in the Appendix, the static pressure at 10 000 ft is given as

$$P = 1455.6\ \text{lb/ft}^2$$

The ambient density can be calculated using the equation of state:

$$\rho = \frac{P}{RT}$$

$$\rho = \frac{1455.6\ \text{lb/ft}^2}{(1716\ \text{ft}^2/(\text{s}^2\cdot{}^\circ\text{R}))(479.7^\circ\text{R})}$$

$$\rho = 0.001768\ \text{slug/ft}^3$$

A low-speed airspeed indicator corrected for instrument and position error reads the equivalent airspeed. The true speed and equivalent airspeed are related by

$$V_{\text{TAS}} = \frac{V_{\text{EAS}}}{\sqrt{\sigma}}$$

where σ is the ratio of the density at altitude to the standard sea level value of density:

$$\sigma = \rho/\rho_0 = (0.001768/0.002739) = 0.7432$$

Now, solving for the true airspeed:

$$V_{\text{KTAS}} = \frac{V_{\text{KEAS}}}{\sqrt{\sigma}} = \frac{120\ \text{knots}}{\sqrt{0.7432}}$$

$$= 139\ \text{knots}$$

1.8 SUMMARY

In this chapter we have examined the properties of air and how those properties vary with altitude. For the comparison of flight test data and for calibrating aircraft instruments, a standard atmosphere is a necessity: the 1962 U.S. Standard Atmosphere provides the needed reference for the aerospace

community. The standard atmosphere was shown to be made up of gradient and isothermal regions.

Finally, we discussed the basic concepts behind several basic flight instruments that play an important role in flight test measurements of aircraft performance, stability and control. In principle these instruments seem to be quite simple: they are, in fact, extremely complicated mechanical devices. Although we have discussed several mechanical instruments, most of the information presented to the flight crew on the newest aircraft designs comes from multifunctional electronic displays. Color cathode ray tubes are used to display air data such as attitude, speed and altitude. Additional displays include navigation, weather, and engine performance information, to name just a few items. The improvements offered by this new technology can be used to reduce the workload of the flight crew and improve the flight safety of the next generation of airplane designs.

1.9 PROBLEMS

1.1. An altimeter set for sea-level standard pressure indicates an altitude of 20 000 ft. If the outside ambient temperature is −15°F, find the air density and the density altitude.

1.2. An airplane is flying at an altitude of 5000 m as indicated by the altimeter, and the outside air temperature is −20°C. If the airplane is flying at a true airspeed of 300 m/s, determine the indicated airspeed.

1.3. A high-altitude remotely piloted communications platform is flying at a pressure altitude of 60 000 ft and an indicated airspeed of 160 ft/s. The outside ambient temperature is −75°F. Estimate the Reynolds number of the wing based on a mean chord of 3.5 ft.

1.4. An airplane is flying at a pressure altitude of 10 000 ft and the airspeed indicator reads 100 knots. If there is no instrument error and the position error is given by Fig. P1.4, find the true airspeed of the airplane.

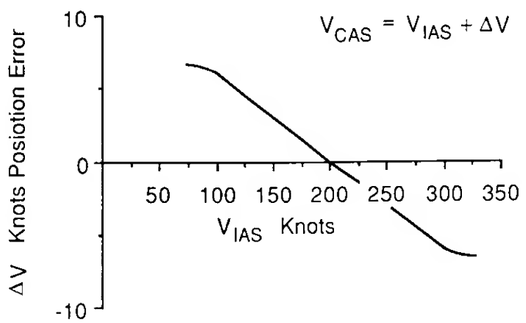

FIGURE P1.4
Position error versus indicated airspeed.

1.5. Under what conditions are the following relationships valid?

$$V_{CAS} = V_{EAS} = V_{TAS}$$

$$V_{CAS} = V_{EAS} \neq V_{TAS}$$

$$V_{CAS} \neq V_{EAS} = V_{TAS}$$

1.6. A small right circular cylinder is used to measure the angle of attack of an airplane by measuring the difference in pressure at two port locations which are located at $\theta = \pm 20°$. Assuming that the flow on the forward face of the cylinder can be accurately modeled as an inviscid flow, the velocity along the cylinder surface can be expressed as

$$V_\theta = 2V_\infty \sin \theta$$

If, while flying at 200 ft/s under sea-level standard conditions, the pressure difference is 32.5 lb/ft^2, what is the angle of the airplane?

REFERENCES

1.1. Anderson, J. D.: *Introduction to Flight,* McGraw-Hill, New York, 1978.
1.2. Domnasch, D. O., S. S. Sherby, and T. F. Connolly: *Airplane Aerodynamics,* Pitman, New York, 1967.
1.3. Pallett, E. H. J.: *Aircraft Instruments* Pitman, London, England, 1982.
1.4. *U.S. Standard Atmosphere, 1962,* prepared under sponsorship of the National Aeronautics and Space Administration, United States Air Force, and United States Weather Bureau, Washington, D.C., December 1962.
1.5. Putnam, T. W.: "The X-29 Flight-Research Program," *AIAA Student Journal,* Fall, 1984.

CHAPTER 2

STATIC STABILITY AND CONTROL

"Isn't it astonishing that all these secrets have been preserved for so many years just so that we could discover them!"
Orville Wright/June 7, 1903

2.1 HISTORICAL PERSPECTIVE

By the start of the twentieth century, the aeronautical community had solved many of the technical problems necessary for achieving powered flight of a heavier-than-air aircraft. One of the problems still beyond the grasp of these early investigators was a lack of understanding of the relationship between stability and control, as well as the influence of the pilot on the pilot–machine system. Most of the ideas regarding stability and control came from experiments with uncontrolled hand-launched gliders. Through such experiments, it was quickly discovered that for a successful flight, the glider had to be inherently stable. Earlier aviation pioneers such as Albert Zahm in the United States, Alphonse Penaud in France, and Frederick Lanchester in England, all contributed to the notion of stability. Zahm, however, was the first to correctly outline the requirements for static stability in a paper he presented in 1893. In his paper, he analyzed the conditions necessary for obtaining a stable equilibrium for an airplane descending at a constant speed. Figure 2.1 shows a sketch of a glider from Zahm's paper. Zahm concluded that the center of gravity had to be in front of the aerodynamic force and the vehicle would require what he referred to as "longitudinal dihedral" to have a stable equilibrium point. In the terminology of today, he showed that if the

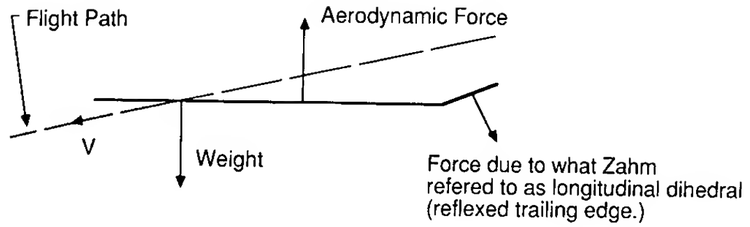

FIGURE 2.1
Zahm's description of longitudinal stability.

center of gravity was ahead of the wing aerodynamic center, then one would need a reflexed airfoil in order to be stable at a positive angle of attack.

In the twenty years prior to the Wright brothers' successful flight, there were many individuals in the United States and Europe working with gliders and unmanned powered models. These investigators were constantly trying to improve their vehicles, with the ultimate goal of achieving powered flight of a airplane under human control. Three men who would leave lasting impressions on the Wright brothers were Otto Lilienthal of Germany and Octave Chanute and Samuel Pierpont Langley of the United States.

Lilienthal made a significant contribution to aeronautics by his work with model and man-carrying gliders. His experiments included the determination of the properties of curved or cambered wings. He carefully recorded the details of over 2000 glider flights. The information in his journal includes data on materials, construction techniques, handling characteristics of his gliders, and aerodynamics. His successful flights and recorded data inspired and aided many other aviation pioneers. Lilienthal's glider designs were statically stable but had very little control capability. For control, Lilienthal would shift his weight to maintain equilibrium flight, much as hang-glider pilots do today. The lack of suitable control proved to be a fatal flaw for Lilienthal. In 1896, he lost control of his glider; the glider stalled and plunged to earth from an altitude of 50 ft. Lilienthal died a day later from the injuries incurred in the accident.

In the United States, Octave Chanute became interested in gliding flight in the mid 1890s. Initially, he built gliders patterned after Lilienthal's designs. After experimenting with modified versions of Lilienthal's gliders, he developed his own designs. His gliders incorporated biplane and multiplane wings, controls to adjust the wings to maintain equilibrium, and a vertical tail for steering. These design changes represented substantial improvements over Lilienthal's monoplane gliders. Many of Chanute's innovations would be incorporated in the Wright brothers' designs. In addition to corresponding with the Wright brothers, Chanute visited their camp at Kitty Hawk to lend his experience and advice to their efforts.

Another individual who helped the Wright brothers was Samuel Pierpont Langley, secretary of the Smithsonian Institution. The Wright brothers knew of Langley's work and wrote to the Smithsonian asking for the available aeronautical literature. The Smithsonian informed the Wright brothers of the

activities of many of the leading aviation pioneers and this information was, no doubt, very helpful to them.

Around 1890, Langley became interested in problems of flight. Initially, his work consisted of collecting and examining all the available aerodynamic data. From the study of these data and his own experiments, he concluded that heavier-than-air powered flight was possible. Langley then turned his attention to designing and perfecting unmanned powered models. On May 6, 1896, his powered model flew for one and one-half minutes and covered a distance of three-quarters of a mile. Langley's success with powered models pioneered the practicality of mechanical flight.

After his successful model flights, Langley was engaged by the War Department to develop a man-carrying airplane. Congress appropriated $50 000 for the project. Langley and his engineering assistant, Charles Manley, started work on their own design in 1899. For the next four years, they were busy designing, fabricating and testing the full-size airplane which was to be launched by a catapult fixed to the top of a houseboat. The first trial was conducted on September 7, 1903, in the middle of the Potomac River near Tidewater, Virginia. The first attempt ended in failure as the airplane pitched down into the river at the end of the launch rails. A second attempt was made on December 8, 1903; this time, the airplane pitched up and fell back into the river. In both trails, the launching system prevented the possibility of a successful flight. For Langley, it was a bitter disappointment, and the criticism he received from the press deeply troubled him. He was, however, one of the pioneering geniuses of early aviation and it is a shame that he went to his grave still smarting from the ridicule. Some twenty years later his airplane was modified, a new engine was installed, and the airplane flew successfully.

The time had come for someone to design a powered airplane capable of carrying a man aloft. As we all know, the Wright brothers made their historic first flight on a powered airplane at Kitty Hawk, North Carolina, on December 17, 1903. Orville Wright made the initial flight which lasted only 12 seconds and covered approximately 125 feet. Taking turns operating the aircraft, Orville and Wilbur made three more flights that day. The final flight lasted 59 seconds and covered a distance of 852 feet while flying into a 20 mph headwind. The airplane tended to fly in a porpoising fashion, with each flight ending abruptly as the vehicle's landing skids struck the ground. The Wright brothers found their powered airplane to be much more responsive than their earlier gliders and, as a result, had difficulty controlling their airplane.

Figure 2.2 shows two photographs of the Kitty Hawk Flyer. The first photograph shows Orville Wright making the historical initial flight and the second shows the airplane after the fourth and last flight of the day. Notice the damaged horizontal rudder (the term used by the Wright brothers). Today we use the term canard to describe a forward control surface. The word canard comes to us from the French word that means "duck." The French used the term canard to describe an early French airplane that had its horizontal tail located far forward of the wing. They thought this airplane looked like a duck with its neck stretched out in flight.

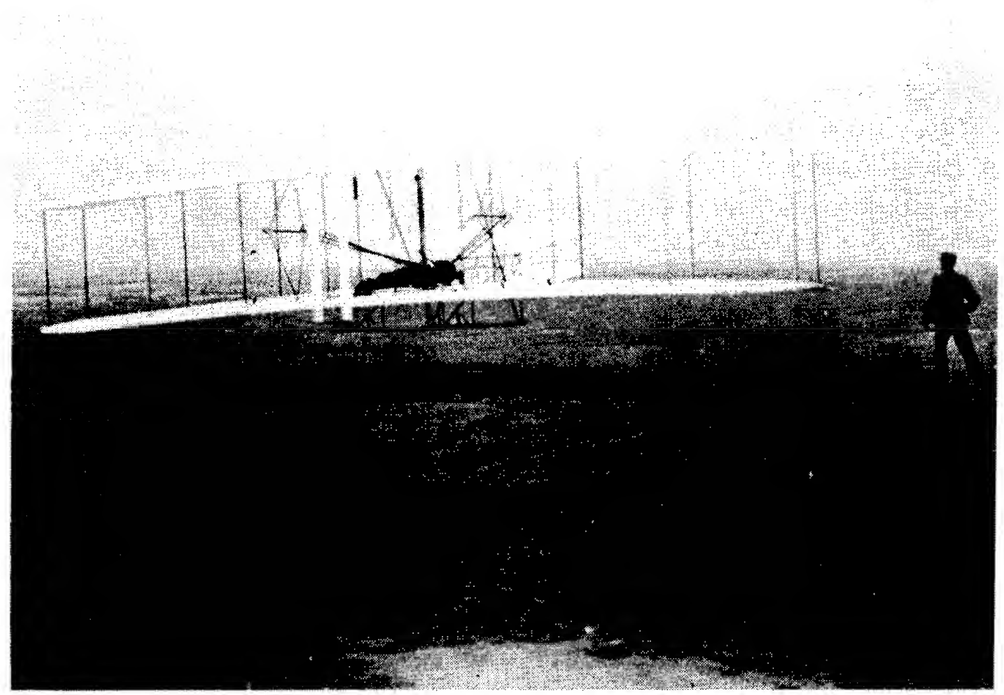

The first flight of a powered heavier - than - air airplane

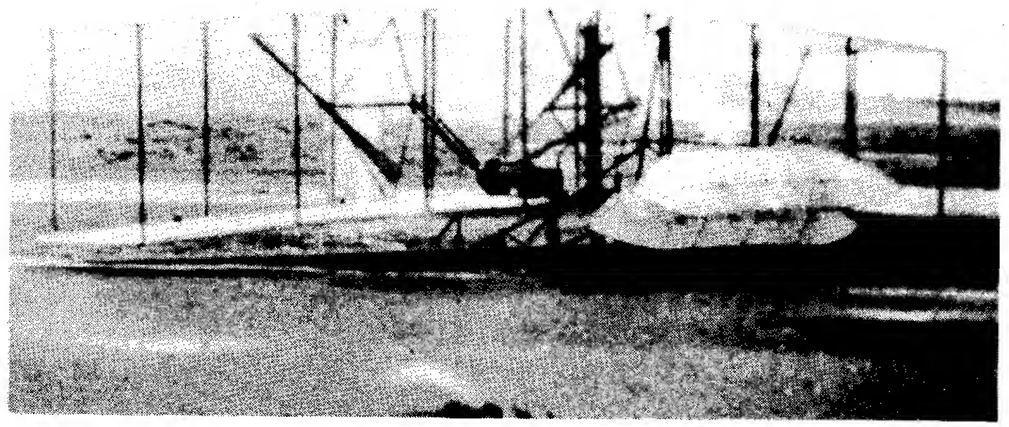

On the fourth flight the horizontal rudder (canard) was broken during the landing

FIGURE 2.2
Photographs of the Wright brothers' airplane, December 17, 1903, Kitty Hawk, North Carolina.

From this very primitive beginning, we have witnessed a remarkable revolution in aircraft development. In a matter of decades, airplanes have evolved into an essential part of our national defense and commercial transportation system. The success of the Wright brothers can be attributed to their step-by-step experimental approach. After reviewing the experimental data of their contemporaries, the Wright brothers were convinced that additional information was necessary before a successful airplane could be designed. They embarked upon an experimental program which included wind-tunnel and flight-test experiments. The Wright brothers designed and constructed a small wind tunnel and made thousands of model tests to determine the aerodynamic characteristics of curved airfoils. They also conducted thousands of glider experiments in developing their airplane. Through their study of the works of others and their own experimental investigations, the Wright brothers were convinced that the major obstacle to achieving powered flight was the lack of sufficient control. Therefore, much of their work was directed towards improving the control capabilities of their gliders. They felt strongly that powerful controls were essential for the pilot to maintain equilibrium and to prevent accidents such as the ones that caused the tragic deaths of Lilienthal and other glider enthusiasts.

This approach represented a radical break with the design philosophy of the day. The gliders and airplanes designed by Lilenthal, Chanute, Langley and other aviation pioneers were designed to be inherently stable. In these designs, the pilot's only function was to steer the vehicle. Although such vehicles were statically stable, they lacked maneuverability and were susceptible to upset by atmospheric disturbances. The Wright brothers' airplane was statically unstable but quite maneuverable. The lack of stability made their work as pilots very difficult. However, through their glider experiments they were able to teach themselves to fly their unstable airplane.

The Wright brothers succeeded where others failed because of their dedicated scientific and engineering efforts. Their accomplishments were the foundation on which others could build. Some of the major accomplishments are listed below.

1. They designed and built a wind tunnel and balance system to conduct aerodynamic tests. With their tunnel they developed a systematic airfoil aerodynamic data base.
2. They developed a complete flight control system with adequate control capability.
3. They designed a lightweight engine and an efficient propeller.
4. Finally, they designed an airplane with a sufficient strength-to-weight ratio, capable of sustaining powered flight.

These early pioneers provided much of the understanding that we have today regarding static stability, maneuverability, and control. However, it is not clear whether any of these men truly comprehended the relationship between these topics.

2.2 INTRODUCTION

How well an airplane flies and how easily it can be controlled are subjects studied in aircraft stability and control. By stability we mean the tendency of the airplane to return to its equilibrium position after it has been disturbed. The disturbance may be generated by the pilot's control actions or by atmospheric phenomena. The atmospheric disturbances can be wind gusts, wind gradients, or turbulent air. An airplane must have sufficient stability that the pilot does not become fatigued by constantly having to control the airplane owing to external disturbances. Although airplanes with little or no inherent aerodynamic stability can be flown, they are unsafe to fly, unless they are provided artificial stability by way of an electromechanical device called a stability augmentation system (SAS).

Two flight conditions are necessary for an airplane to fly its mission successfully. The airplane must be able to achieve equilibrium flight and it must have the capability to maneuver for a wide range of flight velocities and altitudes. To achieve equilibrium or to perform maneuvers, the airplane must be equipped with aerodynamic and propulsive controls. The design and performance of control systems is an integral part of airplane stability and control.

The stability and control characteristics of an airplane are referred to as the vehicle's handling or flying qualities. It is important to the pilot that the airplane possesses satisfactory handling qualities. Airplanes with poor handling qualities will be difficult to fly and could be potentially dangerous. Pilots form their opinions of the airplane on the basis of its handling characteristics. An airplane will be considered to be of poor design if it lacks adequate handling qualities, regardless of how outstanding the airplane's performance might be. In the study of airplane stability and control, we are interested in what makes an airplane stable, how to design the control systems, and what conditions are necessary for good handling qualities. In the following chapters we will discuss each of these topics from the point of view of how they influence the design of the airplane.

STATIC STABILITY. Stability is a property of an equilibrium state. To discuss stability we must first define what is meant by equilibrium. If an airplane is to remain in steady uniform flight, the resultant force as well as the resultant moment about the center of gravity must both be equal to zero. An airplane satisfying this requirement is said to be in a state of equilibrium or flying at a trim condition. On the other hand, if the forces and moments do not sum to zero, the airplane will be subjected to translational and rotational accelerations.

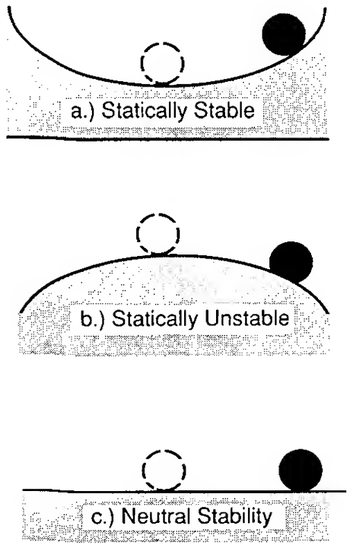

FIGURE 2.3
Sketches illustrating various conditions of static stability.

The subject of airplane stability is generally divided into static and dynamic stability. Static stability is the initial tendency of the vehicle to return to its equilibrium state after a disturbance. An example of the various types of static stability that can exist are illustrated in Fig. 2.3. If the ball were to be displaced from the bottom of the bowl (Fig. 2.3(a)), the ball would, by virtue of the gravitational attraction, roll back to the bottom of the bowl (i.e. the force and moment would tend to restore the ball to its equilibrium point). Such a situation would be referred to as a stable equilibrium point. On the other hand, if we were able to balance a ball on the bowl shown in Fig. 2.3(b), then any displacement from the equilibrium point would cause the ball to roll off the bowl. In this case, the equilibrium point would be classified as an unstable equilibrium point. The last example is shown in Fig. 2.3(c), where the ball is placed on a flat surface. Now, if the wall were to be displaced from its initial equilibrium point to another position, the ball would remain at the new position. This example would be classified as a neutrally stable equilibrium point and represents the limiting (or boundary) between static stability and static instability. The important point in this simple example is that if we are to have a stable equilibrium point, the vehicle must develop a restoring force and/or moment which tends to bring the vehicle back to the equilibrium condition.

DYNAMIC STABILITY. In the study of dynamic stability we are concerned with the time history of the motion of the vehicle after it is disturbed from its equilibrium point. Figure 2.4 shows several possible airplane motions that could occur if the airplane were disturbed from its equilibrium conditions. Note that the vehicle can be statically stable but dynamically unstable. Static stability, therefore, does not guarantee the existence of dynamic stability. However, if the vehicle is dynamically stable it must be statically stable.

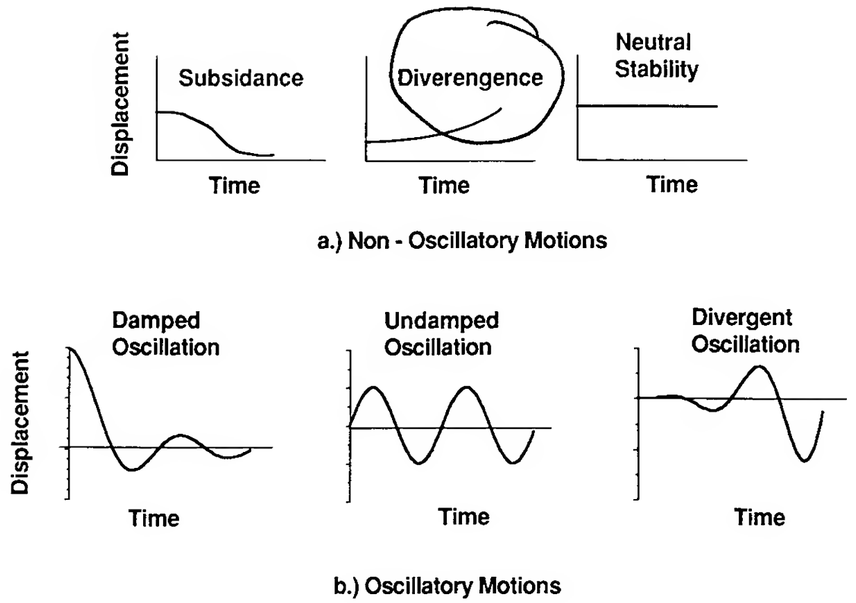

FIGURE 2.4
Examples of stable and unstable dynamic motions.

The reduction of the disturbance with time indicates that there is resistance to the motion and, therefore, that energy is being dissipated. The dissipation of energy is called positive damping. If energy is being added to the system, then we have a negative damping. Positive damping for an airplane is provided by forces and moments which arise owing to the airplanes motion. In the case of positive damping, these forces and moments will oppose the motion of the airplane and cause the disturbance to damp out with time. An airplane that has negative aerodynamic damping will be dynamically unstable; to fly such an airplane, artificial damping must be designed into the vehicle. The artificial damping is provided by a Stability Augmentation System (SAS). Basically, a Stability Augmentation System is an electromechanical device which senses the undesirable motion and then moves the appropriate controls to damp out the motion. This is usually accomplished with small control movements and, therefore, the pilot's control actions are not influenced by the system.

Of particular interest to the pilot and designer is the degree of dynamic stability. Dynamic stability is usually specified by the time it takes a disturbance to be damped to half of its initial amplitude or, in the case of an unstable motion, the time it takes for the initial amplitude of the disturbance to double. In the case of an oscillatory motion, the frequency and period of the motion are extremely important.

So far, we have been discussing the response of an airplane to external disturbances while the controls are held fixed. When we add the pilot to the system, additional complications can arise. For example, an airplane that is dynamically stable to external disturbances with the controls fixed can become

unstable by the pilot's control actions. If the pilot attempts to correct for a disturbance and his or her control input is out of phase with the oscillatory motion of the airplane, the control actions would increase the motion rather than correct it. This type of pilot/vehicle response is called Pilot-Induced-Oscillation (PIO). There are many factors which contribute to the PIO tendency of an airplane. A few of the major contributions are insufficient aerodynamic damping, insufficient control system damping, and pilot reaction time.

2.3 STATIC STABILITY AND CONTROL

DEFINITION OF LONGITUDINAL STATIC STABILITY. In the first example we showed that, to have static stability, we need to develop a restoring moment on the ball when it is displaced from its equilibrium point. The same requirement exists for an airplane. Let us consider the two airplanes and their respective pitching moment curves shown in Fig. 2.5. The pitching moment curves have been assumed to be linear until the wing is close to stalling.

In Fig. 2.5, both airplanes are flying at the trim point denoted by B, i.e. $C_{m_{cg}} = 0$. Suppose the airplanes suddenly encounter an upward gust such that the angle of attack is increased to point C. At the angle of attack denoted by C, airplane 1 develops a negative (nose-down) pitching moment which tends to rotate the airplane back towards it equilibrium point. However, for the same disturbance, airplane 2 develops a positive (nose-up) pitching moment which tends to rotate the aircraft away from the equilibrium point. If we were to encounter a disturbance which reduced the angle of attack, e.g to point A, we would find that the airplane 1 develops a nose-up moment which rotates the aircraft back toward the equilibrium point. On the other hand, airplane 2 is found to develop a nose-down moment which rotates the aircraft away from the equilibrium point. On the basis of this simple analysis, we can conclude that to have static longitudinal stability the aircraft pitching moment curve

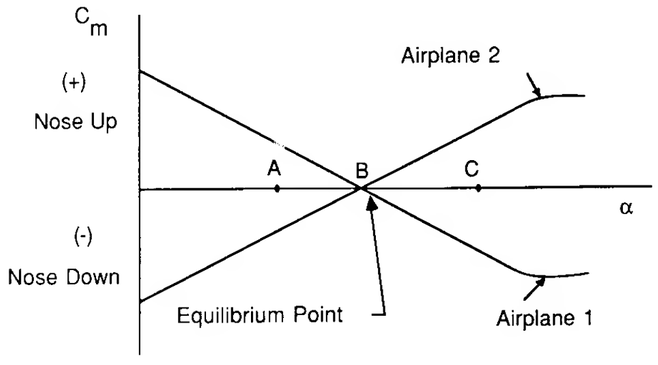

FIGURE 2.5
Pitching moment coefficient versus angle of attack.

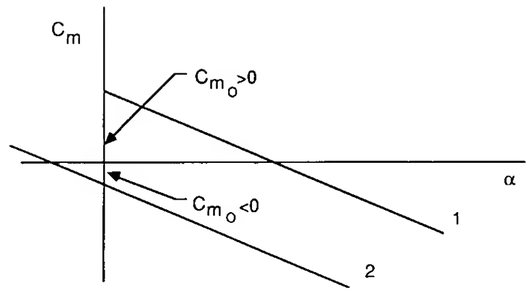

FIGURE 2.6
Pitching moment coefficient versus angle of attack for a stable airplane.

must have a negative slope. i.e.

$$\frac{dC_m}{d\alpha} < 0 \tag{2.1}$$

through the equilibrium point.

Another point that we must make is illustrated in Fig. 2.6. Here we see two pitching moment curves which both satisfy the condition for static stability. However, only curve 1 can be trimmed at a positive angle of attack. Therefore, in addition to having static stability, we must also have a positive intercept, i.e. $C_{m_0} > 0$ in order to trim at positive angles of attack. Although we developed the criterion for static stability from the C_m versus α curve, we could have just as easily accomplished the same result by working with a C_m versus C_L curve. In this case, the requirement for static stability would be as follows:

$$\frac{dC_m}{dC_L} < 0 \tag{2.2}$$

The two conditions are related by the following expression:

$$C_{m_\alpha} = \frac{dC_m}{d\alpha} = \frac{dC_m}{dC_L}\frac{dC_L}{d\alpha} \tag{2.3}$$

which shows that the derivatives differ only by the slope of the lift curve.

CONTRIBUTION OF AIRCRAFT COMPONENTS. In discussing the requirements for static stability, we have so far only considered the total airplane pitching moment curve. However, it is of interest (particularly to airplane designers) to know the contribution of the wing, fuselage, tail, propulsion system, etc., to the pitching moment and static stability characteristics of the airplane. In the following sections, each of the components will be considered separately. We will start by breaking the airplane down into its basic components such as the wing, fuselage, horizontal tail, and propulsion unit. Detailed methods for estimating the aerodynamic stability coefficients can be found in the United States Air Force Stability and Control Datcom [2.7]. The

Datcom, short for Data Compendium, is a collection of methods for estimating the basic stability and control coefficients for flight regimes of subsonic, transonic, supersonic, and hypersonic speeds. Methods are presented in a systematic body build-up fashion, e.g. wing alone, body alone, wing–body and wing–body–tail techniques. The methods range from techniques that are based upon simple expressions developed from theory to correlations obtained from experimental data. In the following sections, as well as in later chapters, we shall develop simple methods for computing the aerodynamic stability and control coefficients. Our emphasis will be for the most part on methods that can be derived from simple theoretical considerations. These methods are in general accurate for preliminary design purposes and show the relationship between the stability coefficients and the geometric and aerodynamic characteristics of the airplane. Furthermore, the methods are generally only valid for the subsonic flight regime. A complete discussion of how to extend these methods to higher speed flight regimes is beyond the scope of this book and the reader is referred to Ref. 2.7 for the high-speed methods.

WING CONTRIBUTION. The contribution of the wing to an airplane's static stability can be examined with aid of Fig. 2.7. In this sketch we have replaced the wing by its mean aerodynamic chord $\bar{c}$. The distances from the wing leading edge to the aerodynamic center and the center of gravity are denoted by X_{ac} and X_{cg}, respectively. The vertical displacement of the center of gravity is denoted by Z_{cg}. The angle the wing chord line makes with the fuselage reference line is denoted as i_w. This is the angle at which the wing is mounted onto the fuselage.

If we sum the moments about the center of gravity, the following equation is obtained:

$$\sum \text{Moments} = M_{cg_w}$$

$$M_{cg_w} = L_w \cos(\alpha_w - i_w)[X_{cg} - X_{ac}] + D_w \sin(\alpha_w - i_w)[X_{cg} - X_{ac}]$$
$$+ L_w \sin(\alpha_w - i_w)[Z_{cg}] - D_w \cos(\alpha_w - i_w)[Z_{cg}] + M_{ac_w} \qquad (2.4)$$

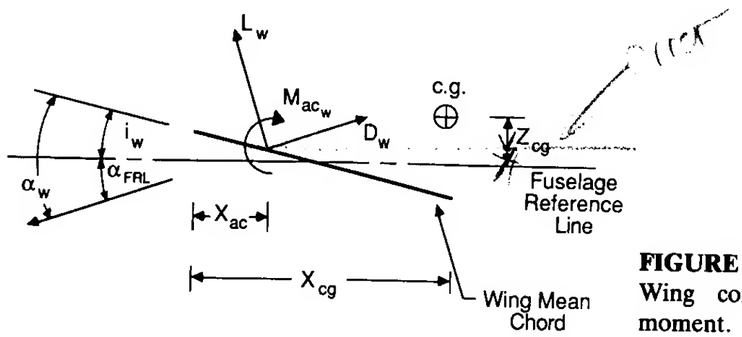

FIGURE 2.7
Wing contribution to the pitching moment.

Dividing by $\frac{1}{2}\rho V^2 S\bar{c}$ yields

$$C_{m_{cg_w}} = C_{L_w}\left(\frac{X_{cg}}{\bar{c}} - \frac{X_{ac}}{\bar{c}}\right)\cos(\alpha_w - i_w) + C_{Dw}\left(\frac{X_{cg}}{\bar{c}} - \frac{X_{ac}}{\bar{c}}\right)\sin(\alpha_w - i_w)$$
$$+ C_{L_w}\frac{(Z_{cg})}{\bar{c}}\sin(\alpha_w - i_w) - C_{D_w}\frac{(Z_{cg})}{\bar{c}}\cos(\alpha_w - i_w) + C_{m_{ac_w}} \qquad (2.5)$$

Equation (2.5) can be simplified by assuming that the angle of attack is small. With this assumption the following approximations can be made.

$$\cos(\alpha_w - i_w) = 1, \qquad \sin(\alpha_w - i_w) = \alpha_w - i_w, \qquad C_L \gg C_D$$

If we further assume that the vertical contribution is negligible, then Eq. (2.5) reduces to:

$$C_{m_{cg_w}} = C_{m_{ac_w}} + C_{L_w}\left(\frac{X_{cg}}{\bar{c}} - \frac{X_{ac}}{\bar{c}}\right) \qquad (2.6)$$

or

$$C_{m_{cg_w}} = C_{m_{ac_w}} + (C_{L_{0_w}} + C_{L_{\alpha_w}}\alpha_w)\left(\frac{X_{cg}}{\bar{c}} - \frac{X_{ac}}{\bar{c}}\right) \qquad (2.7)$$

where $C_{L_w} = C_{L_{0_w}} + C_{L_{\alpha_w}}\alpha_w$. Applying the condition for static stability yields:

$$C_{m_{0_w}} = C_{m_{ac_w}} + C_{L_{0_w}}\left(\frac{X_{cg}}{\bar{c}} - \frac{X_{ac}}{\bar{c}}\right) \qquad (2.9)$$

$$C_{m_{\alpha_w}} = C_{L_{\alpha_w}}\left(\frac{X_{cg}}{\bar{c}} - \frac{X_{ac}}{\bar{c}}\right) \qquad (2.10)$$

For a wing-alone design to be statically stable, Eq. (2.10) tells us that the aerodynamic center must lie aft of the center of gravity to make $C_{m_\alpha} < 0$. Since we also want to be able to trim the aircraft at a positive angle of attack, the pitching moment coefficient at zero angle of attack, C_{m_0}, must be greater than zero. A positive pitching moment about the aerodynamic center can be achieved by using a negative-cambered airfoil section or an airfoil section that has a reflexed trailing edge. For many airplanes, the center of gravity position is located slightly aft of the aerodynamic center (see data in the Appendix). Also, the wing is normally constructed of airfoil profiles having positive camber. Therefore, the wing contribution to static longitudinal stability is usually destabilizing for most conventional airplanes.

TAIL CONTRIBUTION—AFT TAIL. The horizontal tail surface can be located either forward or aft of the wing. When the surface is located forward of the wing, the surface is called a canard. Both surfaces are influenced by the flow field created by the wing. The canard surface is affected by the upwash flow from the wing, whereas the aft tail is subjected to the downwash flow. Figure 2.8 is a sketch of the flow field surrounding a lifting wing. The wing flow field

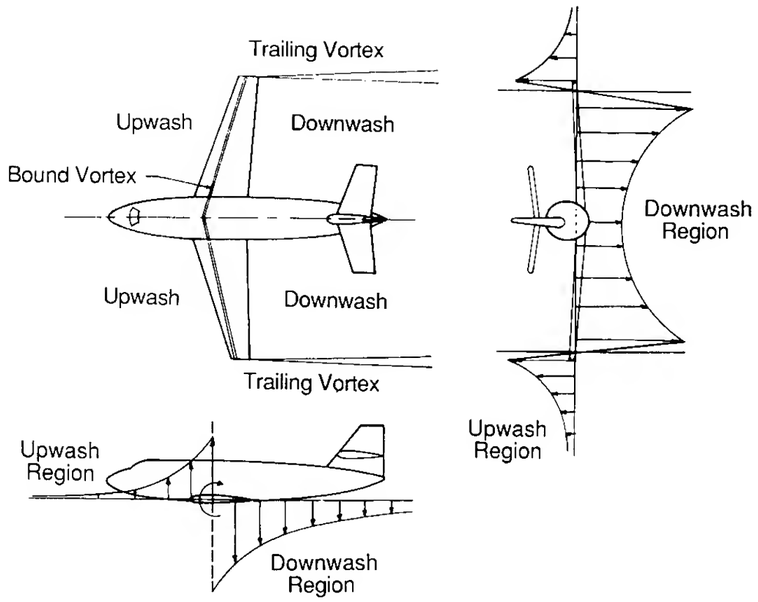

FIGURE 2.8
Flow field around an airplane created by the wing.

is due, primarily, to the bound and trailing vortices. The magnitude of the upwash or downwash depends upon the location of the tail surface with respect to the wing.

The contribution that a tail surface located aft of the wing makes to the airplane's lift and pitching moment can be developed with the aid of Fig. 2.9. In this sketch, the tail surface has been replaced by its mean aerodynamic chord. The angle of attack at the tail can be expressed as

$$\alpha_t = \alpha_w - i_w - \varepsilon + i_t \tag{2.11}$$

where ε and i_t are the downwash and tail incidence angles, respectively. If we assume small angles and neglect the drag contribution of the tail, the total lift

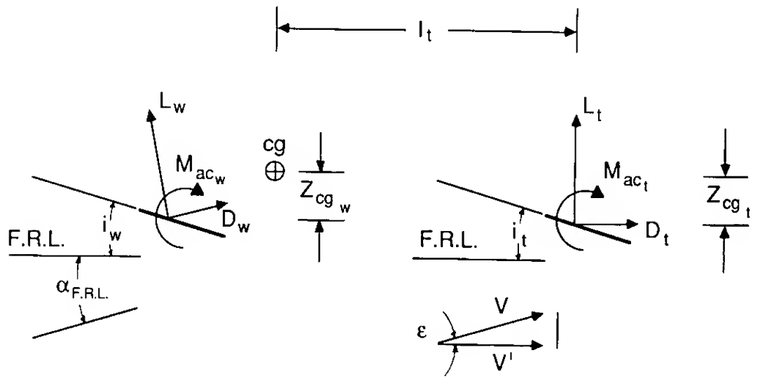

FIGURE 2.9
Aft tail contribution to the pitching moment.

of the wing and tail can be expressed as

$$L = L_w + L_t \tag{2.12}$$

or

$$C_L = C_{L_w} + \eta \frac{S_t}{S} C_{L_t} \tag{2.13}$$

where

$$\eta = \frac{\frac{1}{2}\rho V_t^2}{\frac{1}{2}\rho V_w^2} \tag{2.14}$$

The ratio of the dynamic pressures is called the tail efficiency and can have values in the range 0.8–1.2. The magnitude of η depends upon the location of the tail surface. If the tail is located in the wake region of the wing or fuselage, η will be less than unity because $Q_t < Q_w$ due to the momentum loss in the wake. On the other hand, if the tail is located in a region where $Q_t > Q_w$, then η will be greater than unity. Such a situation could exist if the tail were located in either the slip stream of the propeller or in the exhaust wake of a jet engine.

The pitching moment due to the tail can be obtained by summing the moments about the center of gravity:

$$M_t = -l_t[L_t \cos(\alpha_{\text{FRL}} - \varepsilon) + D_t \sin(\alpha_{\text{FRL}} - \varepsilon)] - Z_{cg_t}[D_t \cos(\alpha_{\text{FRL}} - \varepsilon) - L_t \sin(\alpha_{\text{FRL}} - \varepsilon)] + M_{ac_t} \tag{2.15}$$

Usually only the first term of the preceding equation is retained; the other terms are generally small in comparison to the first term. If we again use the small-angle assumption and that $C_{L_t} \gg C_{D_t}$, then Eq. (2.15) reduces to

$$M_t = -l_t L_t = -l_t C_{L_t} \tfrac{1}{2}\rho V_t^2 S_t \tag{2.16}$$

$$C_{m_t} = \frac{M_t}{\frac{1}{2}\rho V^2 S\bar{c}} = -\frac{l_t S_t}{S\bar{c}} \eta C_{L_t} \tag{2.17}$$

or

$$C_{m_t} = -V_H \eta C_{L_t} \tag{2.18}$$

where $V_H = l_t S_t / S\bar{c}$ and is called the horizontal tail volume ratio.

From Fig. 2.9, the angle of attack of the tail is seen to be

$$\alpha_t = \alpha_w - i_w - \varepsilon + i_t \tag{2.19}$$

The coefficient C_{L_t} can be written as

$$C_{L_t} = C_{L_{\alpha_t}} \alpha_t = C_{L_{\alpha_t}}(\alpha_w - i_w - \varepsilon + i_t) \tag{2.20}$$

where $C_{L_{\alpha_t}}$ is the slope of the tail lift curve. The downwash angle ε can be expressed as

$$\varepsilon = \varepsilon_0 + \frac{d\varepsilon}{d\alpha} \alpha_w \tag{2.21}$$

where ε_0 is the downwash at zero angle of attack.

The downwash behind a wing with an elliptic lift distribution can be derived from finite-wing theory and can be shown to be related to the wing lift coefficient and aspect ratio:

$$\varepsilon = \frac{2C_{L_w}}{\pi A R_w} \tag{2.22}$$

where the downwash angle is in radians. The rate of change of downwash angle with angle of attack is determined by taking the derivative of Eq. (2.22).

$$\frac{d\varepsilon}{d\alpha} = \frac{2C_{L_{\alpha_w}}}{\pi A R_w} \tag{2.23}$$

where $C_{L_{\alpha_w}}$ is per radian. The above expressions do not take into account the position of the tail plane relative to the wing, i.e. its vertical and longitudinal spacing. More accurate methods for estimating the downwash at the tailplane can be found in Ref. 2.7. An experimental technique for determining the downwash using wind tunnel force and moment measurements will be presented by way of a problem assignment at the end of this chapter.

Rewriting the tail contribution to the pitching moment yields

$$C_{m_{cg_t}} = -V_H \eta C_{L_t} \tag{2.24}$$

$$C_{m_{cg_t}} = \eta V_H C_{L_{\alpha_t}}(\varepsilon_0 + i_w - i_t) - \eta V_H C_{L_{\alpha_t}} \alpha \left(1 - \frac{d\varepsilon}{d\alpha}\right) \tag{2.25}$$

Comparing Eq. (2.25) with the linear expression for the pitching moment given as

$$C_{m_{cg_t}} = C_{m_0} + C_{m_\alpha}\alpha \tag{2.26}$$

yields expressions for the intercept and slope:

$$C_{m_{0_t}} = \eta V_H C_{L_{\alpha_t}}(\varepsilon_0 + i_w - i_t) \tag{2.27}$$

$$C_{m_{\alpha_t}} = -\eta V_H C_{L_{\alpha_t}} \left(1 - \frac{d\varepsilon}{d\alpha}\right) \tag{2.28}$$

Recall that earlier we showed that the wing contribution to C_{m_0} was negative for an airfoil having positive camber. The tail contribution to C_{m_0} can be used to ensure that C_{m_0} for the complete airplane is positive. This can be accomplished by adjusting the tail incidence angle i_t. Note that we would want to mount the tail plane at a negative angle of incidence to the fuselage reference line to increase C_{m_0} due to the tail.

The tail contribution to the static stability of the airplane ($C_{m_{\alpha_t}} < 0$) can be

controlled by proper selection of V_H and $C_{L_{\alpha_t}}$. The contribution of $C_{m_{\alpha_t}}$ will become more negative by increasing the tail moment arm l_t or tail surface area S_t and by increasing $C_{L_{\alpha_t}}$. The tail lift curve slope $C_{L_{\alpha_t}}$ can be increased most easily by increasing the aspect ratio of the tail planform. The designer can adjust anyone of these parameters to achieve the desired slope. As noted here, a tail surface located aft of the wing can be used to ensure that the airplane has a positive C_{m_0} and a negative C_{m_α}.

CANARD—FORWARD TAIL SURFACE. A canard is a tail surface located ahead of the wing. There are several attractive features of the canard surface. The canard, if properly positioned, can be relatively free from wing or propulsive flow interference. Canard control is more attractive for trimming the large nose-down moment produced by high-lift devices. To counteract the nose-down pitching moment, the canard must produce lift which will add to the lift being produced by the wing. An aft tail must produce a down load to counteract the pitching moment and thus reduce the airplane's overall lift force. The major disadvantage of the canard is that it produces a destabilizing contribution to the aircraft's static stability. However, this is not a severe limitation. By proper location of the center of gravity, one can ensure the airplane is statically stable.

FUSELAGE CONTRIBUTION. The primary function of the fuselage is to provide room for the flight crew and payload such as passengers and cargo. The optimum shape for the internal volume at minimum drag is a body for which the length is larger that the width or height. For most fuselage shapes used in airplane designs, the width and height are of the same order of magnitude and for many designs a circular cross-section is used.

The aerodynamic characteristics of long, slender bodies were studied by Max Munk [2.8] in the earlier 1920s. Munk was interested in the pitching moment characteristics of airship hulls. In his analysis, he neglected viscosity and treated the flow around the body as an ideal fluid. Using momentum and energy relationships, he showed that the rate of change of the pitching moment with angle of attack (per radian) for a body of revolution is proportional to the body volume and dynamic pressure:

$$\frac{dM}{d\alpha} = \text{fn}(\text{volume}, \tfrac{1}{2}\rho V^2) \tag{2.29}$$

Multhopp [2.9] extended this analysis to account for the induced flow along the fuselage due to the wings for bodies of arbitrary cross-section. A summary of Multhopp's method for C_{m_0} and C_{m_α} due to the fuselage is presented as follows:

$$C_{m_{0_f}} = \frac{k_2 - k_1}{36.5 S \bar{c}} \int_0^{l_f} w_f^2(\alpha_{0w} + i_f)\, dx \tag{2.30}$$

which can be approximated as

$$C_{m_{0_f}} = \frac{k_2 - k_1}{36.5S\bar{c}} \sum_{x=0}^{x=l_f} w_f^2(\alpha_{0w} + i_f)\,\Delta x \tag{2.31}$$

where $k_2 - k_1$ = correction factor for body fineness ratio
S = the wing reference area
$\bar{c}$ = the wing mean aerodynamic cord
w_f = the average width of the fuselage sections
α_{0w} = the wing zero-lift angle relative to the fuselage reference line
i_f = the incidence of the fuselage camber line relative to the fuselage reference line at the center of each fuselage increment. The incidence angle is defined as negative for nose droop and aft upsweep.
Δx = the length of the fuselage increments

Figure 2.10 illustrates how the fuselage can be divided into segments for the calculation of C_{m_0} and also defines the body width w_f for various body cross-sectional shapes. The correction factor $(k_2 - k_1)$ is given in Fig. 2.11.

The local angle of attack along the fuselage is greatly affected by the flow field created by the wing, as was illustrated in Fig. 2.8. The portion of the fuselage ahead of the wing is in the wing upwash, while the aft portion is in the wing downwash flow. The change in pitching moment with angle of attack is given by

$$C_{m_{\alpha_f}} = \frac{1}{36.5S\bar{c}} \int_0^{l_f} w_f^2 \frac{\partial \varepsilon_u}{\partial \alpha}\,dx \qquad (\text{deg}^{-1}) \tag{2.32}$$

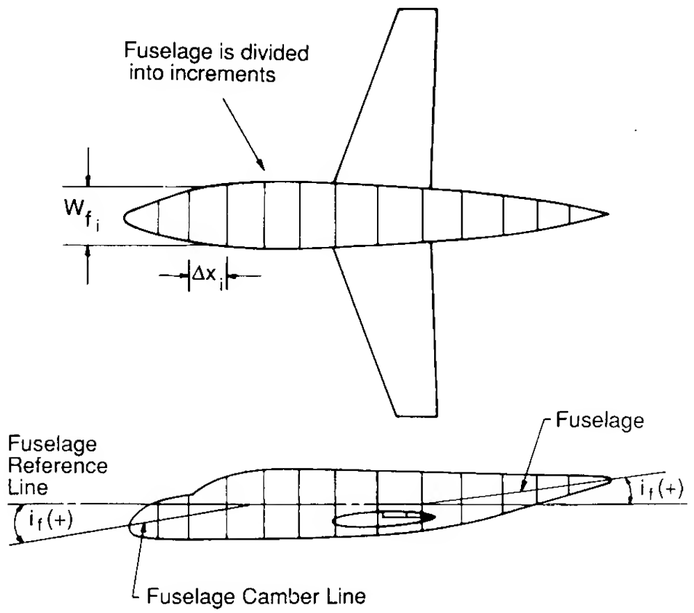

FIGURE 2.10
Procedure for calculating C_{m0} due to the fuselage.

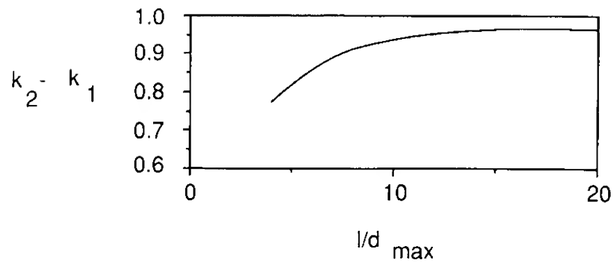

FIGURE 2.11
$k_2 - k_1$ vs $1/d$.

which can be approximated by

$$C_{m_{\alpha_f}} = \frac{1}{36.5S\bar{c}} \sum_{x=0}^{x=l_f} w_f^2 \frac{\partial \varepsilon_u}{\partial \alpha}\,\Delta x \tag{2.33}$$

where S = the wing reference area, and $\bar{c}$ = the wing mean aerodynamic chord.

The fuselage can again be divided into segments and the local angle of attack of each section, which is composed of the geometric angle of attack of the section plus the local induced angle due to the wing upwash or downwash for each segment, can be estimated. The change in local flow angle with angle of attack, $\partial \varepsilon_u / \partial \alpha$, varies along the fuselage and can be estimated from Fig. 2.12. For locations ahead of the wing, the upwash field creates large local angles of attack, therefore $\partial \varepsilon_u / \partial \alpha > 1$. On the other hand, a station behind the wing is in the downwash region of the wing vortex system and the local angle of attack is reduced. For the region behind the wing, $\partial \varepsilon_u / \partial \alpha$ is assumed to vary linearly from zero to $(1 - \partial \varepsilon / \partial \alpha)$ at the tail. The region between the wing leading edge and trailing edge is assumed to be unaffected by the wing flow field, $\partial \varepsilon_u / \partial \alpha = 0$. Figure 2.13 is a sketch showing the application of Eq. (2.33)

POWER EFFECTS. The propulsion unit can have a significant effect on both the longitudinal trim and static stability of the airplane. If the thrust line is offset from the center of gravity, the propulsive force will create a pitching moment that must be counteracted by the aerodynamic control surface.

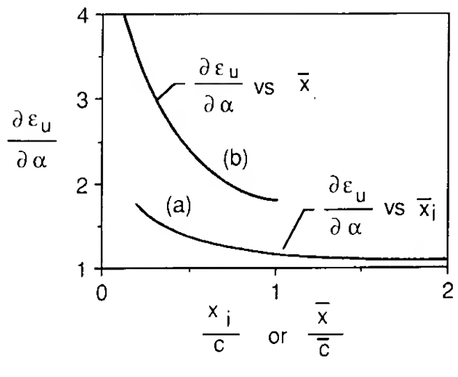

FIGURE 2.12
Variation of local flow angle along the fuselage.

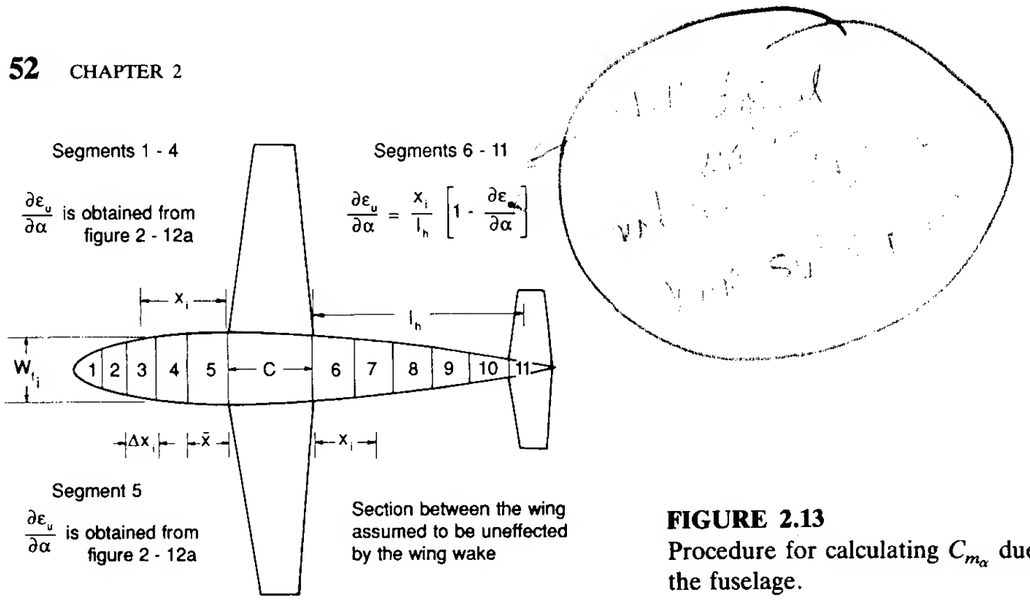

FIGURE 2.13
Procedure for calculating C_{m_α} due to the fuselage.

The static stability of the airplane is also influenced by the propulsion system. For a propeller driven airplane the propeller will develop a normal force in its plane of rotation when the propeller is at an angle of attack. The propeller normal force will create a pitching moment about the center of gravity thus producing a propulsion contribution to C_{m_α}. Although one can derive a simple expression for C_{m_α} due to the propeller, the actual contribution of the propulsion system to the static stability is much more difficult to estimate. This is due to the indirect effects that the propulsion system has on the airplanes characteristics. For example, the propeller slipstream can have an effect on the tail efficiency η and the downwash field. Because of these complicated interactions the propulsive effects on airplane stability are commonly estimated from powered wind tunnel models.

A normal force will be created on the inlet of a jet engine when it is at an angle of attack. As in the case of the propeller powered airplane, the normal force will produce a contribution to C_{m_α}.

STICK FIXED NEUTRAL POINT. The total pitching moment for the airplane can now be obtained by summing the wing, fuselage, and tail contributions.

$$C_{m_{cg}} = C_{m_0} + C_{m_\alpha}\alpha \tag{2.34}$$

where

$$C_{m_0} = C_{m_{0_w}} + C_{m_{0_f}} + \eta V_H C_{L_{\alpha_t}}(\varepsilon_0 + i_w - i_t) \tag{2.35}$$

$$C_{m_\alpha} = C_{L_{\alpha_w}}\left(\frac{X_{cg}}{\bar{c}} - \frac{X_{ac}}{\bar{c}}\right) + C_{m_{\alpha_f}} - \eta V_H C_{L_{\alpha_t}}\left(1 - \frac{d\varepsilon}{d\alpha}\right) \tag{2.36}$$

Notice that the expression for C_{m_α} depends upon the center of gravity position as well as the aerodynamic characteristics of the airplane. The center of gravity

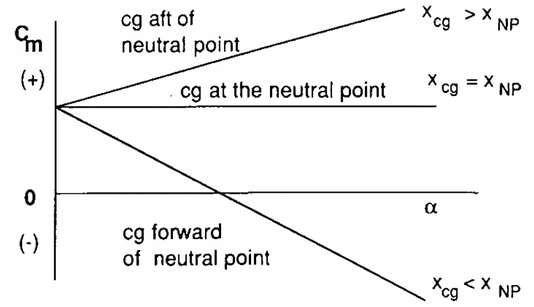

FIGURE 2.14
The influence of center of gravity position on longitudinal static stability.

of an airplane varies during the course of its operation and, therefore, it is important to know if there are any limits to the center of gravity travel. To ensure that the airplane possesses static longitudinal stability, we would like to know at what point $C_{m_\alpha} = 0$. Setting C_{m_α} equal to zero and solving for the center of gravity position yields

$$\frac{X_{NP}}{\bar{c}} = \frac{X_{ac}}{\bar{c}} - \frac{C_{m_{\alpha_f}}}{C_{L_{\alpha_w}}} + \eta V_H \frac{C_{L_{\alpha_t}}}{C_{L_{\alpha_w}}}\left(1 - \frac{d\varepsilon}{d\alpha}\right) \tag{2.37}$$

We call this location the stick fixed neutral point. If the airplane's center of gravity ever reaches this point, the airplane will be neutrally stable. Movement of the center of gravity beyond the neutral point causes the airplane to be statically unstable. The influence of center of gravity position on static stabililty is shown in Fig. 2.14.

Example Problem 2.1. Given the general aviation airplane shown in Fig. 2.15, determine the contribution of the wing, tail and fuselage to the C_m versus α curve. Also determine the stick fixed neutral point. For this problem, assume standard sea-level atmospheric conditions.

Solution. The lift curve slopes for the two-dimensional sections making up the wing and tail must be corrected for a finite aspect ratio. This is accomplished by using the formula

$$C_{L_\alpha} = \frac{C_{l_\alpha}}{1 + C_{l_\alpha}/(\pi AR)}$$

Substituting the two-dimensional lift curve slope and the appropriate aspect ratio yields

$$C_{L_{\alpha_w}} = \frac{C_{l_{\alpha_w}}}{1 + C_{l_{\alpha_w}}/(\pi AR_w)} = \frac{(0.097/\text{deg})(57.3\ \text{deg/rad})}{1 + (0.097/\text{deg})(57.3\ \text{deg/rad})/(\pi(6.06))} = 4.3\ \text{rad}^{-1}$$

In a similar manner the lift curve slope for the tail can be found:

$$C_{L_{\alpha_t}} = 3.91\ \text{rad}^{-1}$$

General Aviation Airplane

Flight Condition

W = 2750
V = 176 ft/sec

Wing Airfoil Characteristics

$C_{m_{ac}} = -0.116$
$C_{l_\alpha} = 0.097$/deg
$\alpha_{o_L} = -5°$
$X_{ac} = 0.25\bar{c}$
No twist
$i_w = 1.0°$

Tail Airfoil Section

$C_{l_\alpha} = 0.01$/deg
$C_{m_{ac}} = 0.0$
$i_t = -1.0°$

Reference Geometry

$S = 184\ ft^2$ $S_H = 43\ ft^2$
$b = 33.4$ ft $l_t = 16$ ft
$\bar{c} = 5.7$ ft

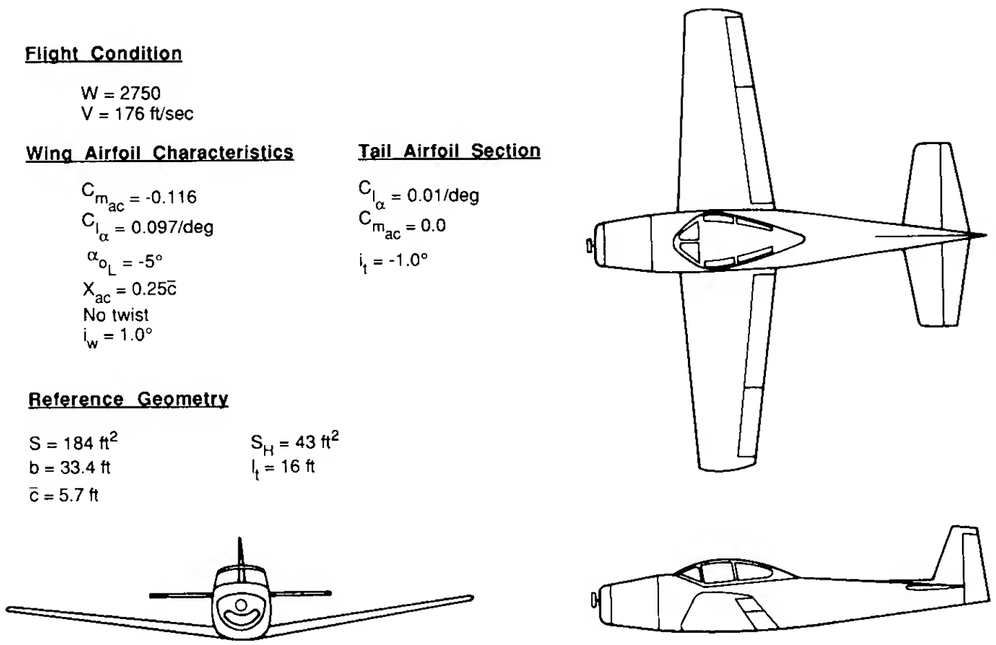

FIGURE 2.15
General Aviation airplane.

The wing contribution to C_{m_0} and C_{m_α} is found from Eq. (2.9) and (2.10):

$$C_{m_{0_w}} = C_{m_{ac_w}} + C_{L_{0_w}}\left(\frac{X_{cg}}{\bar{c}} - \frac{X_{ac}}{\bar{c}}\right)$$

and

$$C_{m_{\alpha_w}} = C_{L_{\alpha_w}}\left(\frac{X_{cg}}{\bar{c}} - \frac{X_{ac}}{\bar{c}}\right)$$

The lift coefficient at zero angle of attack is obtained by multiplying the absolute value of the zero lift angle of attack by the lift curve slope:

$$\begin{aligned} C_{L_{0_w}} &= C_{L_{\alpha_w}}|\alpha_0| \\ &= (4.3\ \text{rad}^{-1})(5\ \text{deg})/(57.3\ \text{deg/rad}) \\ &= 0.375 \end{aligned}$$

Substituting the approximate information into the equations for $C_{m_{0_w}}$ and $C_{m_{\alpha_w}}$ yields

$$\begin{aligned} C_{m_{0_w}} &= C_{m_{ac_w}} + C_{L_{0_w}}\left(\frac{X_{cg}}{\bar{c}} - \frac{X_{ac}}{\bar{c}}\right) \\ &= -0.116 + (0.375)(0.295 - 0.250) \\ &= -0.099 \end{aligned}$$

$$\begin{aligned} C_{m_{\alpha_w}} &= C_{L_{\alpha_w}}\left(\frac{X_{cg}}{\bar{c}} - \frac{X_{ac}}{\bar{c}}\right) \\ &= (4.3\ \text{rad}^{-1})(0.295 - 0.250) \\ &= 0.1935\ \text{rad}^{-1} \end{aligned}$$

For this particular airplane, the wing contribution to C_{m_α} is destabilizing.

The tail contribution to the intercept and slope can be estimated from Eqs (2.27) and (2.28):

$$C_{m_{0_t}} = \eta V_H C_{L_{\alpha_t}}(\varepsilon_0 + i_w - i_t)$$

$$C_{m_{\alpha_t}} = -\eta V_H C_{L_{\alpha_t}}\left(1 - \frac{d\varepsilon}{d\alpha}\right)$$

The tail volume ratio V_H is given by

$$V_H = \frac{l_t S_t}{S\bar{c}}$$

or

$$V_H = \frac{(16\ \text{ft})(43\ \text{ft}^2)}{(184\ \text{ft}^2)(5.7\ \text{ft})} = 0.66$$

The downwash term is estimated using the expression

$$\varepsilon = \frac{2C_{L_w}}{\pi AR}$$

where ε is the downwash angle in radians:

$$\begin{aligned} \varepsilon_0 &= \frac{2C_{L_{w_0}}}{\pi AR} \\ &= \frac{2(0.375)(57.3\ \text{deg/rad})}{\pi(6.06)} = 0.04\ \text{rad} = 2.3° \end{aligned}$$

and

$$\frac{d\varepsilon}{d\alpha} = \frac{2C_{L_{\alpha_w}}}{\pi AR}$$

where $C_{L_{\alpha_w}}$ is per radians:

$$\frac{d\varepsilon}{d\alpha} = \frac{2(4.3)}{\pi(6.06)} = 0.45$$

Substituting the preceding information into the formulas for the intercept and slope yields

$$\begin{aligned} C_{m_{0_t}} &= \eta V_H C_{L_{\alpha_t}}(\varepsilon_0 + i_w - i_t) \\ &= (0.66)(3.91)[2.3° + 1.0° - (-1.0°)]/57.2\ \text{deg/rad} \\ &= 0.194 \end{aligned}$$

and

$$\begin{aligned} C_{m_{\alpha_t}} &= -\eta V_H C_{L_{\alpha_t}}\left(1 - \frac{d\varepsilon}{d\alpha}\right) \\ &= -(0.66)(3.91)(1 - 0.45) \\ &= -1.42\ \text{rad}^{-1} \end{aligned}$$

In this example, the ratio η of tail to wing dynamic pressure was assumed to be unity.

The fuselage contribution to C_{m_0} and C_{m_α} can be estimated from Eqs (2.29) and (2.31) respectively. To use these equations, we must divide the fuselage into segments, as indicated in Fig. 2.16. The summation in Eq. (2.31) can easily be

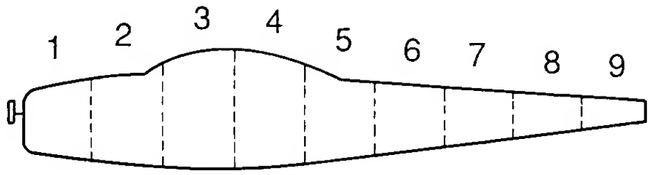

Station	Δx ft	w_f ft	$\alpha_{o_w} + i_f$	$w_f^2 [\alpha_{o_w} + i_f] \Delta x$
1	3.0	3.6	-1.5	-58.3
2	3.0	4.6	-1.5	-95.2
3	3.0	4.6	-1.5	-95.2
4	3.0	4.6	-1.5	-95.2
5	3.0	4.1	-1.5	-75.6
6	3.0	3.1	-1.5	-43.2
7	3.0	2.3	-1.5	-23.8
8	3.0	1.5	-1.5	-10.1
9	3.0	0.8	-1.5	-2.9
				Sum = -499.5

FIGURE 2.16
Sketch of segmented fuselage for calculating $C_{m\alpha}$ for the example problem.

estimated from the geometry and is found by summing the individual contributions as illustrated by the table in Fig. 2.16.

$$\sum_{x=0}^{l_B} w_f^2(\alpha_{0w} + i_f)\,\Delta x = -500$$

The body fineness ratio is estimated from the geometrical data given in Fig. 2.15:

$$\frac{l_f}{d_{\max}} = 6.2$$

and the correction factor $k_2 - k_1$ is found from Fig. 2.11, $k_2 - k_1 = 0.86$. Substituting these values into Eq. (2.31) yields

$$C_{m_{0_f}} = -0.010$$

In a similar manner C_{m_α} can be estimated. A table is included in Fig. 2.16 that shows the estimate of the summation. $C_{m_{\alpha_f}}$ was estimated to be

$$C_{m_{\alpha_f}} = 0.12 \text{ rad}^{-1}$$

The individual contributions and the total pitching moment curve are shown in Fig. 2.17.

The stick fixed neutral point can be estimated from Eq. (2.37):

$$\frac{X_{\text{NP}}}{\bar{c}} = \frac{X_{\text{ac}}}{\bar{c}} - \frac{C_{m_{\alpha_f}}}{C_{L_{\alpha_w}}} + \eta V_{\text{H}} \frac{C_{L_{\alpha_t}}}{C_{L_{\alpha_w}}} \left(1 - \frac{d\varepsilon}{d\alpha}\right)$$
$$= 0.37$$

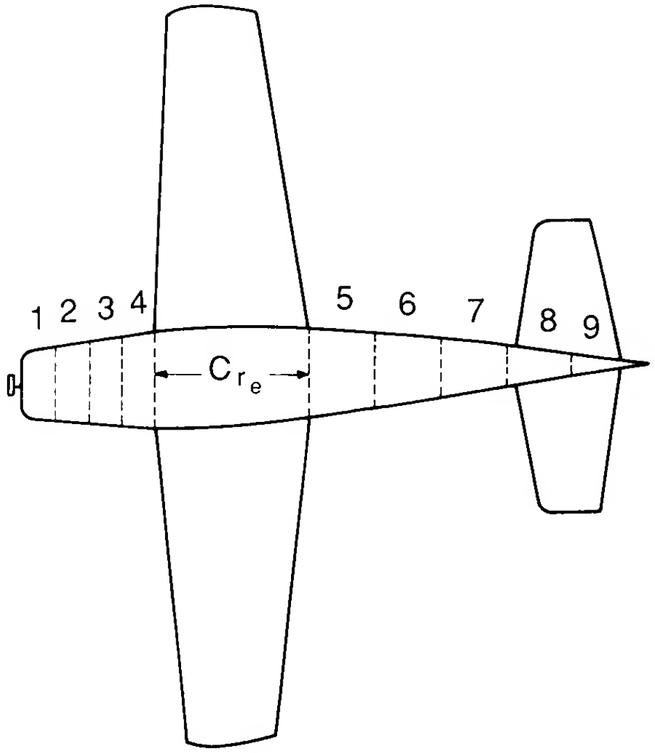

Station	Δx ft	w_f ft	x	$\frac{\partial \varepsilon_\mu}{\partial \alpha}$	$w_f^2 \frac{\partial \varepsilon_\mu}{\partial \alpha} \Delta x$
1	1.5	3.0	5.25	1.2	16.2
2	1.5	3.4	4.5	1.3	22.5
3	1.5	3.8	3.75	1.4	30.3
4	1.5	4.2	1.5	3.2	84.7
5	2.9	3.8	1.45	0.06	2.5
6	2.9	3.1	4.35	0.18	5.0
7	2.9	2.3	7.25	0.31	4.8
8	2.9	1.5	10.15	0.43	2.8
9	2.9	0.8	13.05	0.55	1.0

$C_{r_e} = 6.5$ ft $l_h = 13$ ft Sum = 85.1

FIGURE 2.16 (*contd.*)

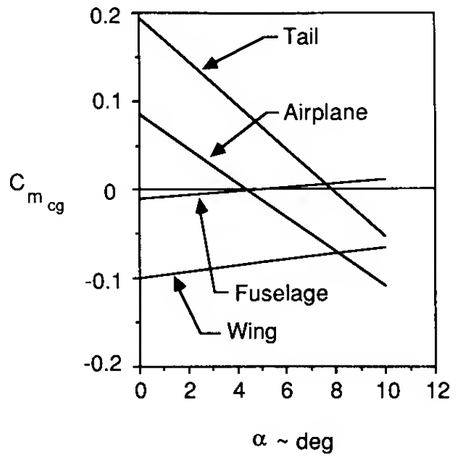

FIGURE 2.17
Component contributions to pitching moment for example problem.

2.4 LONGITUDINAL CONTROL

Control of an airplane can be achieved by providing an incremental lift force on one or more of the airplane's lifting surfaces. The incremental lift force can be produced by deflecting the entire lifting surface or by deflecting a flap incorporated in the lifting surface. Owing to the fact that the control flaps or movable lifting surfaces are located at some distance from the center of gravity, the incremental lift force creates a moment about the airplane's center of gravity. Figure 2.18 shows the three primary aerodynamic controls. Pitch control can be achieved by changing the lift on either a forward or aft control surface. If a flap is used, the flapped portion of the tail surface is called an elevator. Yaw control is achieved by deflecting a flap on the vertical tail called the rudder and roll control can be achieved by deflecting small flaps located outboard toward the wing tips in a differential manner. These flaps are called ailerons. A roll moment can also be produced by deflecting a wing spoiler. As the name implies a spoiler disrupts the lift. This is accomplished by deflecting a section of the upper wing surface so that the flow separates behind the spoiler

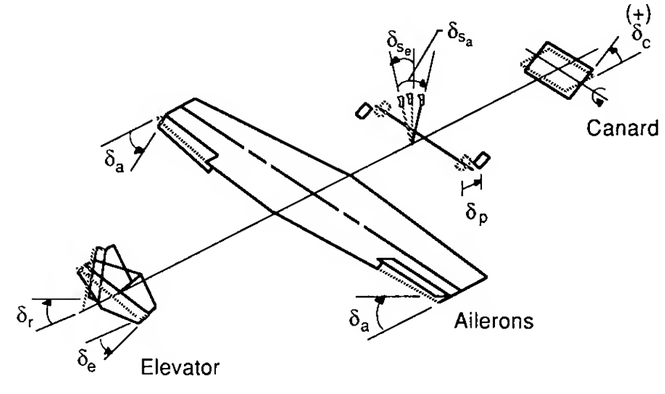

FIGURE 2.18
Primary aerodynamic controls.

which causes a reduction in the lifting force. To achieve a roll moment, only one spoiler needs to be deflected.

In this section we shall be concerned with longitudinal control. Control of the pitch attitude of an airplane can be achieved by deflecting all or a portion of either a forward or an aft tail surface. Factors affecting the design of a control surface are control effectiveness, hinge moments, and aerodynamic and mass balancing. Control effectiveness is a measure of how effective the control deflection is in producing the desired control moment. As we shall show shortly, control effectiveness is a function of the size of the flap and tail volume ratio. Hinge moments are also important because they are the aerodynamic moments that must be overcome to rotate the control surface. The hinge moment governs the magnitude of force required of the pilot to move the control surface. Therefore, great care must be used in designing a control surface so that the control forces are within acceptable limits for the pilots. Finally, aerodynamic and mass balancing deal with techniques to vary the hinge moments so that the control stick forces stay within an acceptable range.

ELEVATOR EFFECTIVENESS. We need some form of longitudinal control to fly at various trim conditions. As shown earlier, the pitch attitude can be controlled by either an aft tail or forward tail (canard). We shall examine how an elevator on an aft tail provides the required control moments. Although we are restricting our discussion to an elevator on an aft tail, the same arguments could be made with regard to a canard surface. In Fig. 2.19 we see a sketch of the horizontal tail as well as the influence of the elevator on the pitching moment curve. Notice that the elevator does not change the slope of the pitching moment curves, but only shifts them so that different trim angles can be achieved.

When the elevator is deflected, it changes the lift and pitching moment of the airplane. The change in lift for the airplane can be expressed as follows:

$$\Delta C_L = C_{L_{\delta_e}} \delta_e \qquad \text{where} \qquad C_{L_{\delta_e}} = \frac{dC_L}{d\delta_e} \tag{2.38}$$

$$C_L = C_{L_\alpha} \alpha + C_{L_{\delta_e}} \delta_e \tag{2.39}$$

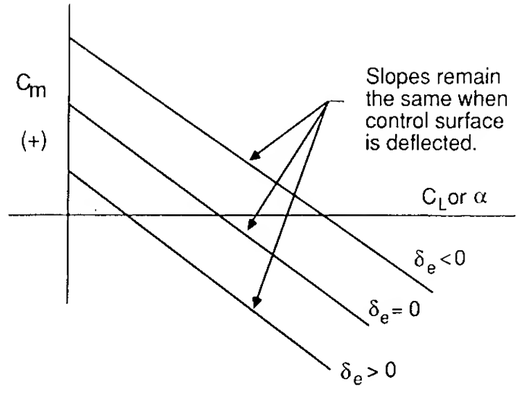

FIGURE 2.19
The influence of the elevator on the C_m vs α curve.

On the other hand, the change in pitching moment acting on the airplane can be written as

$$\Delta C_m = C_{m_{\delta_e}} \delta_e \qquad \text{where} \qquad C_{m_{\delta_e}} = \frac{dC_m}{d\delta_e} \tag{2.40}$$

The stability derivative $C_{m_{\delta_e}}$ is called the elevator control power. The larger the value of $C_{m_{\delta_e}}$ the more effective the control is in creating the control moment.

Adding ΔC_m to the pitching moment equation yields

$$C_m = C_{m_0} + C_{m_\alpha}\alpha + C_{m_{\delta_e}}\delta_e \tag{2.41}$$

The derivatives $C_{L_{\delta_e}}$ and $C_{m_{\delta_e}}$ can be related to the aerodynamic and geometric characteristics of the horizontal tail in the following manner. The change in lift of the airplane due to deflecting the elevator is equal to the change in lift force acting on the tail:

$$\Delta L = \Delta L_t \tag{2.42}$$

$$\Delta C_L = \frac{S_t}{S}\eta\, \Delta C_{L_t} = \frac{S_t}{S}\eta \frac{dC_{L_t}}{d\delta_e}\delta_e \tag{2.43}$$

where $dC_{L_t}/d\delta_e$ is the elevator effectiveness. The elevator effectiveness is proportional to the size of the flap being used as an elevator and can be estimated from the equation

$$\frac{dC_{L_t}}{d\delta_e} = \frac{dC_{L_t}}{d\alpha_t}\frac{d\alpha_t}{d\delta_e} = C_{L_{\alpha_t}}\tau \tag{2.44}$$

The parameter τ can be determined from Fig. 2.20:

$$C_{L_{\delta_e}} = \frac{S_t}{S}\eta \frac{dC_{L_t}}{d\delta_e} \tag{2.45}$$

The increment in airplane pitching moment is

$$\Delta C_m = -V_H \eta\, \Delta C_{L_t} = -V_H \eta \frac{dC_{L_t}}{d\delta_e}\delta_e \tag{2.46}$$

or

$$C_{m_{\delta_e}} = -V_H \eta \frac{dC_{L_t}}{d\delta_e} \tag{2.47}$$

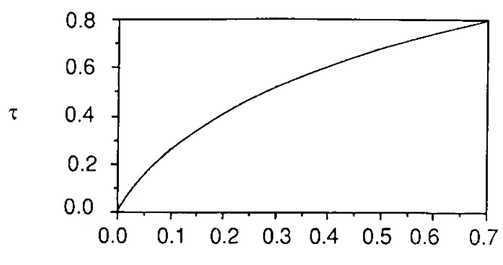

FIGURE 2.20
Flap effectiveness parameter.

The designer can control the magnitude of the elevator control effectiveness by proper selection of the volume ratio and flap size.

ELEVATOR ANGLE TO TRIM. Now let us consider the trim requirements. An airplane is said to be trimmed if the forces and moments acting on the airplane are in equilibrium. Setting the pitching moment of equation equal to zero (definition of trim) we can solve for the elevator angle required to trim the airplane:

$$C_m = 0 = C_{m_0} + C_{m_\alpha}\alpha + C_{m_{\delta_e}}\delta_e \tag{2.48}$$

or

$$\delta_{\text{trim}} = -\frac{C_{m_0} + C_{m_\alpha}\alpha_{\text{trim}}}{C_{m_{\delta_e}}} \tag{2.49}$$

The lift coefficient to trim is

$$C_{L\text{trim}} = C_{L_\alpha}\alpha_{\text{trim}} + C_{L_{\delta_e}}\delta_{\text{trim}} \tag{2.50}$$

We can use the above equation to obtain the trim angle of attack.

$$\alpha_{\text{trim}} = \frac{C_{L\text{trim}} - C_{L_{\delta_e}}\delta_{\text{trim}}}{C_{L_\alpha}} \tag{2.51}$$

If we substitute this equation back into Eq. (2.49) we get the following equation for the elevator angle to trim:

$$\delta_{\text{trim}} = -\frac{C_{m_0}C_{L_\alpha} + C_{m_\alpha}C_{L\text{trim}}}{C_{m_{\delta_e}}C_{L_\alpha} - C_{m_\alpha}C_{L_{\delta_e}}} \tag{2.52}$$

The elevator angle to trim can also be obtained directly from the pitching moment curves shown in Fig. 2.19.

FLIGHT MEASUREMENT OF X_{NP}. The equation developed for estimating the elevator angle to trim the airplane can be used to determine the stick fixed neutral point from flight test data. Suppose we conducted a flight test experiment in which we measured the elevator angle of trim at various air speeds for different positions of the center of gravity. If we did this, we could develop curves as shown in Fig. 2.21.

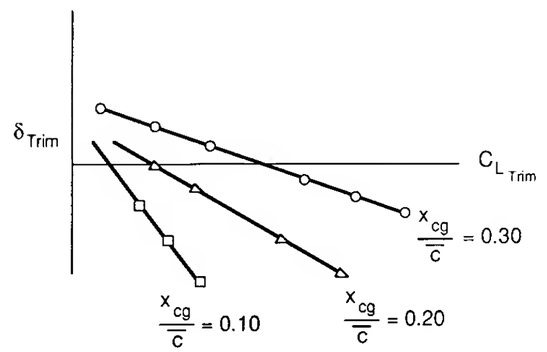

FIGURE 2.21
δ_{etrim} vs C_{Ltrim}.

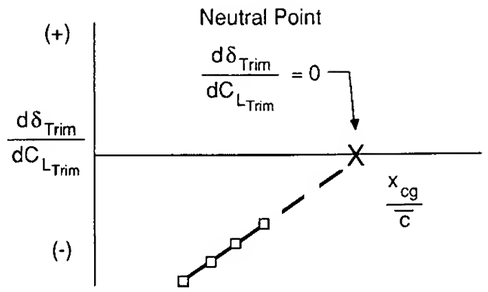

FIGURE 2.22
$d\delta_{etrim}/dC_{Ltrim}$ vs C.G.

Now, differentiating Eq. (2.52) with respect to $C_{L_{trim}}$ yields

$$\frac{d\delta_{trim}}{dC_{L_{trim}}} = -\frac{C_{m_\alpha}}{C_{m_{\delta_e}}C_{L_\alpha} - C_{m_\alpha}C_{L_{\delta_e}}} \tag{2.53}$$

Note that when $C_{m_\alpha} = 0$ (i.e. the center of gravity is at the neutral point) Eq. (2.53) equals zero. Therefore, if we measure the slopes of the curves in Fig. 2.21 and plot them as a function of center of gravity location, we can estimate the stick fixed neutral point as illustrated in Fig. 2.22 by extrapolating to find the center of gravity position that makes $d\delta_{trim}/dC_{L_{trim}}$ equal to zero.

ELEVATOR HINGE MOMENT. It is important to know the moment acting at the hinge line of the elevator (or other type of control surface). The hinge moment is, of course, the moment the pilot must overcome by exerting a force on the control stick. Therefore, to design the control system properly we must know the hinge moment characteristics. The hinge moment is defined as shown below in Fig. 2.23. If we assume that the hinge moment can be expressed as the addition of the effects of angle of attack, elevator deflection angle, and tab angle taken separately, then we can express the hinge moment coefficient in the following manner:

$$C_{h_e} = C_{h_0} + C_{h_{\alpha_t}}\alpha_t + C_{h_{\delta_e}}\delta_e + C_{h_{\delta_t}}\delta_t \tag{2.54}$$

$H_e = C_{h_e} 1/2\ \rho V^2\ S_e c_e$

S_e = Area aft of the hinge line

c_e = Chord measured from hinge line to trailing edge of the flap

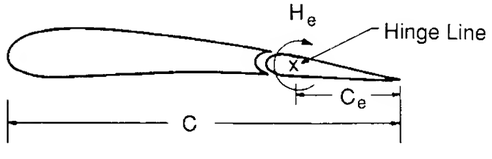

FIGURE 2.23
Definition of hinge moments.

where C_{h_0} is the residual moment, and

$$C_{h_{\alpha_t}} = \frac{dC_h}{d\alpha_t} \qquad C_{h_{\delta_e}} = \frac{dC_h}{d\delta_e} \qquad C_{h_{\delta_t}} = \frac{dC_h}{d\delta_t} \tag{2.55}$$

The hinge moment parameters defined above are very difficult to predict analytically with great precision. Wind tunnel tests are usually required to provide the control system designer with the information needed to design the control system properly.

When the elevator is set free, i.e. the control stick is released the stability and control characteristics of the airplane are affected. For simplicity, we shall assume that both δ_t and C_{h_0} are equal to zero. Then, for the case when the elevator is allowed to be free,

$$C_{h_e} = 0 = C_{h_{\alpha_t}}\alpha_t + C_{h_{\delta_e}}\delta_e \tag{2.56}$$

Solving for δ_e yields

$$(\delta_e)_{free} = -\frac{C_{h_{\alpha_t}}}{C_{h_{\delta_e}}}\alpha_t \tag{2.57}$$

Usually, the coefficients $C_{h_{\alpha_t}}$ and $C_{h_{\delta_e}}$ are negative. If this is indeed the case, then Eq. (2.57) tells us that the elevator will float upwards as the angle of attack is increased. The lift coefficient for a tail with a free elevator is given by

$$C_{L_t} = C_{L_{\alpha_t}}\alpha_t + C_{L_{\delta_e}}\delta_{efree} \tag{2.58}$$

$$C_{L_t} = C_{L_{\alpha_t}}\alpha_t - C_{L_{\delta_e}}\frac{C_{h_{\alpha_t}}}{C_{h_{\delta_e}}}\alpha_t \tag{2.59}$$

which simplifies to

$$C_{L_t} = C_{L_{\alpha_t}}\alpha_t\left(1 - \frac{C_{L_{\delta_e}}}{C_{L_{\alpha_t}}}\frac{C_{h_{\alpha_t}}}{C_{h_{\delta_e}}}\right) = C'_{L_{\alpha_t}}\alpha_t \tag{2.60}$$

where

$$C'_{L_{\alpha_t}} = C_{L_{\alpha_t}}\left(1 - \frac{C_{L_{\delta_e}}}{C_{L_{\alpha_t}}}\frac{C_{h_{\alpha_t}}}{C_{h_{\delta_e}}}\right) = C_{L_{\alpha_t}}f \tag{2.61}$$

The slope of the tail lift curve is modified by the term in the parentheses. The factor f can be greater than or less than unity depending on the sign of the hinge parameters $C_{h_{\alpha_t}}$ and $C_{h_{\delta_e}}$. Now, if we were to develop the equations for the total pitching moment for the free elevator case, we would obtain an equation similar to Eqs (2.35)–(2.36). The only difference would be that the term $C_{L_{\alpha_t}}$ would be replaced by $C'_{L_{\alpha_t}}$. Substituting $C'_{L_{\alpha_t}}$ into Eqs (2.35) and

(2.36) yields

$$C'_{m_0} = C_{m_{0_w}} + C_{m_{0_f}} + C'_{L_{\alpha_t}} \eta V_H (\varepsilon_0 + i_w - i_t) \tag{2.62}$$

$$C'_{m_\alpha} = C_{L_{\alpha_w}} \left(\frac{X_{cg}}{\bar{c}} - \frac{X_{ac}}{\bar{c}} \right) + C_{m_{\alpha_f}} - C'_{L_{\alpha_t}} \eta V_H \left(1 - \frac{\partial \varepsilon}{\partial \alpha} \right) \tag{2.63}$$

where the prime indicates elevator free values. To determine the influence of a free elevator on the static longitudinal stability, we again examine the condition in which $C_{m_\alpha} = 0$. Setting C'_{m_α} equal to zero in Eq. (2.63) and solving for $x/\bar{c}$ yields the stick free neutral point:

$$\frac{X'_{NP}}{\bar{c}} = \frac{X_{ac}}{\bar{c}} + V_H \eta \frac{C'_{L_{\alpha_t}}}{C_{L_{\alpha_w}}} \left(1 - \frac{d\varepsilon}{d\alpha} \right) - \frac{C_{m_{\alpha_f}}}{C_{L_{\alpha_w}}} \tag{2.64}$$

The difference between the stick fixed neutral point and the stick free neutral point can be expressed as follows:

$$\frac{X_{NP}}{\bar{c}} - \frac{X'_{NP}}{\bar{c}} = (1 - f) V_H \eta \frac{C_{L_{\alpha_t}}}{C_{L_{\alpha_w}}} \left(1 - \frac{d\varepsilon}{d\alpha} \right) \tag{2.65}$$

The factor f determines whether the stick free neutral point lies forward or aft of the stick fixed neutral point.

A term which appears frequently in the literature is static margin. The static margin is simply the distance between the neutral point and the actual center of gravity position.

$$\text{Stick fixed static margin} = \frac{X_{NP}}{\bar{c}} - \frac{X_{cg}}{\bar{c}} \tag{2.66}$$

$$\text{Stick free static margin} = \frac{X'_{NP}}{\bar{c}} - \frac{X_{cg}}{\bar{c}} \tag{2.67}$$

For most aircraft designs, it is desirable to have a stick fixed static margin of approximately 5 percent of the mean chord. The stick fixed or stick free static neutral points represent an aft limit on the center of gravity travel for the airplane.

2.5 STICK FORCES

In order to deflect a control surface, the pilot must move the control stick or rudder pedals. The forces exerted by the pilot to move the control surface is called the stick force or pedal force, depending upon which control is being used. The stick force is proportional to the hinge moment acting on the control surface:

$$F = \text{fn}(H_e) \tag{2.68}$$

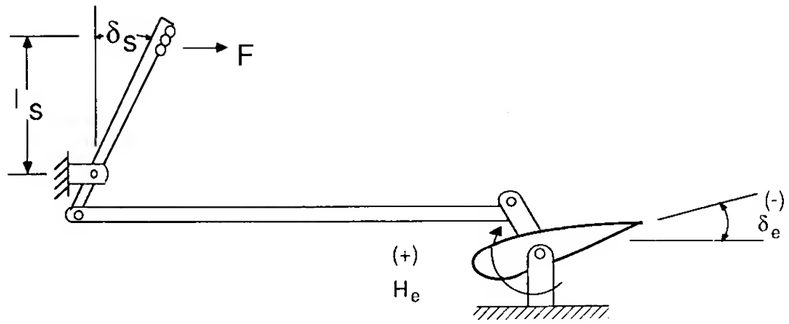

FIGURE 2.24
Relationship between stick force and hinge moment.

Figure 2.24 is a sketch of a simple mechanical system used for deflecting the elevator. The work of displacing the control stick is equal to the work done in moving the control surface to the desired deflection angle. From Fig. 2.24 we can write the expressions for the work performed at the stick and elevator:

$$F l_s \delta_s = H_e \delta_e \tag{2.69}$$

or

$$F = \frac{\delta_e}{l_s \delta_s} H_e \tag{2.70}$$

or

$$F = G H_e \tag{2.71}$$

where $G = \delta_e / l_s \delta_s$ is called the gearing ratio and is a measure of the mechanical advantage provided by the control system.

Substituting the expression for the hinge moment defined earlier into the stick force equation yields

$$F = G C_{h_e} \tfrac{1}{2} \rho V^2 S_e \bar{c}_e \tag{2.72}$$

From this expression we see that the magnitude of the stick force increases with the size of the airplane and with the square of the airplane's speed. Similar expressions can be obtained for the rudder pedal force and aileron stick force.

The control system is designed to convert the stick and pedal movements into control surface deflections. Although this may seem to be a relatively easy task, it is in fact quite complicated. The control system must be designed so that the control forces are within acceptable limits. On the other hand, the control forces required in normal maneuvers must not be too small, otherwise it might be possible to overstress the airplane. Proper control system design will provide the pilot with stick force magnitudes that give the pilot a feel for

the commanded maneuver. The magnitude of the stick force provides the pilot with an indication of the severity of the motion that will result from the stick movement.

The convention for longitudinal control is that a pull force should always rotate the nose upward which causes the airplane to slow down. A push force will have the opposite effect, i.e. the nose will rotate downward and the airplane will speed up. The control system designer must also be sure that the airplane does not experience control reversals due to aerodynamic or aeroelastic phenomena.

TRIM TABS. In addition to making sure that the stick and rudder pedal forces required to maneuver or trim the airplane are within acceptable limits, it is important that some means be provided to zero out the stick force at the trimmed flight speed. If such a provision is not made, the pilot will become fatigued by trying to maintain the necessary stick force. The stick force at trim can be made zero by incorporating a tab on either the elevator or the rudder. The tab is a small flap located at the trailing edge of the control surface. The trim tab can be used to zero out the hinge moment and thereby eliminate the stick or pedal forces. Figure 2.25 is a sketch illustrating the concept of a trim tab. Although the trim tab has a great influence over the hinge moment, it has only a slight effect on the lift produced by the control surface.

STICK FORCE GRADIENTS. Another important parameter in the design of a control system is called the stick force gradient. Figure 2.26 shows the variation of the stick force with speed. The stick force gradient is a measure of the change in stick force needed to change the speed of the airplane. To provide the airplane with speed stability, the stick force gradient must be

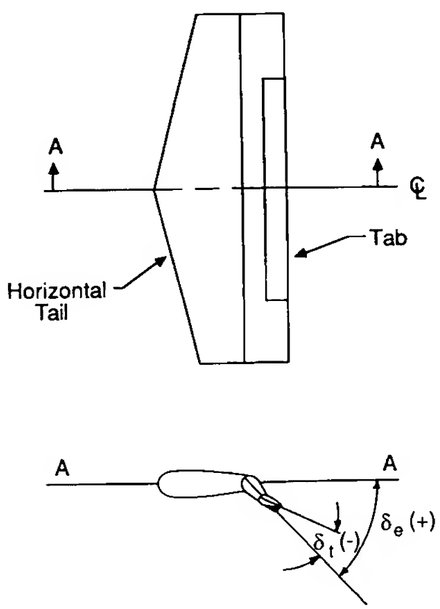

FIGURE 2.25
Trim tabs.

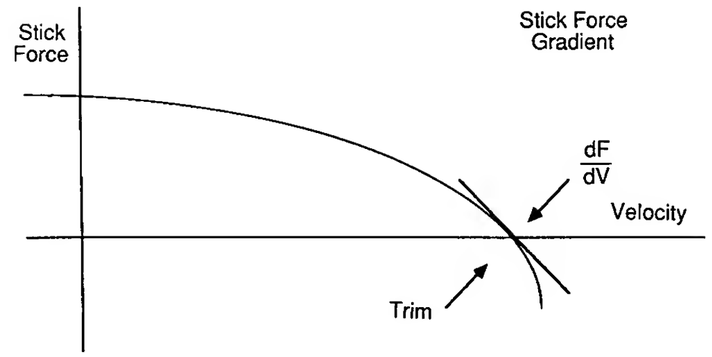

FIGURE 2.26
Stick force versus velocity.

negative, i.e.

$$\frac{dF}{dV} < 0 \tag{2.73}$$

The need for a negative stick force gradient can be appreciated by examining Fig. 2.26. If the airplane slows down, a positive stick force occurs which rotates the nose of the airplane downwards, which causes the airplane to increase its speed back towards the trim velocity. For the case in which the airplane exceeds the trim velocity, a negative (pull) stick force causes the airplane's nose to pitch up, which causes the airplane to slow down. The negative stick force gradient provides the pilot and airplane with speed stability. The larger the gradient, the more resistant the airplane will be to disturbances in the flight speed. If an airplane did not have speed stability the pilot would have to continuously monitor and control the airplane's speed. This would be highly undesirable from the pilot's point of view.

2.6 DEFINITION OF DIRECTIONAL STABILITY

Directional, or weathercock, stability is concerned with the static stability of the airplane about the z axis. Just as in the case of longitudinal static stability, it is desirable that the airplane should tend to return to an equilibrium condition when subjected to some form of yawing disturbance. Figure 2.27 shows the yawing moment coefficient versus sideslip angle β for two airplane configurations. To have static directional stability, the airplane must develop a yawing moment which will restore the airplane to its equilibrium state. Assume that both airplanes are disturbed from their equilibrium conditions, so that the airplanes are flying with a positive sideslip angle β. Airplane 1 will develop a restoring moment which will tend to rotate the airplane back to its equilibrium condition, i.e. zero sideslip angle. Airplane 2 will develop a yawing moment that will tend to increase the sideslip angle. Examining these curves, we see that to have static directional stability the slope of the yawing moment curve must be positive ($C_{n_\beta} > 0$). Note that an airplane possessing static directional

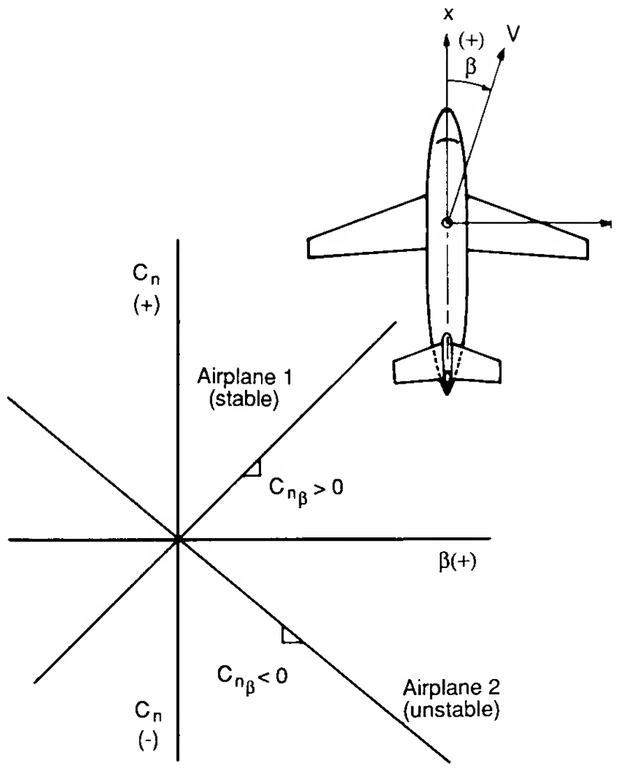

FIGURE 2.27
Static directional stability.

stability will always point into the relative wind, thus the name "weathercock stability."

CONTRIBUTION OF AIRCRAFT COMPONENTS. The contribution of the wing to directional stability is usually quite small in comparison to the fuselage, provided the angle of attack is not large. The fuselage and engine nacelles, in general, create a destabilizing contribution to directional stability. The wing fuselage contribution can be calculated from the following empirical expression taken from Ref. 2.7.

$$C_{n_{\beta_{wf}}} = -k_n k_{Rl} \frac{S_{fs}}{S_w} \frac{l_f}{b} \quad \text{(per deg)} \tag{2.74}$$

where k_n = an empirical wing–body interference factor that is a function of the fuselage geometry
k_{Rl} = an empirical correction factor that is a function of the fuselage Reynolds number
S_{fs} = the projected side area of the fuselage
l_f = the length of the fuselage

The empirical factors k_n and k_{Rl} are determined from Figs 2.28 and 2.29, respectively.

Since the wing–fuselage contribution to directional stability is destabilizing, the vertical tail must be properly sized to ensure that the airplane has

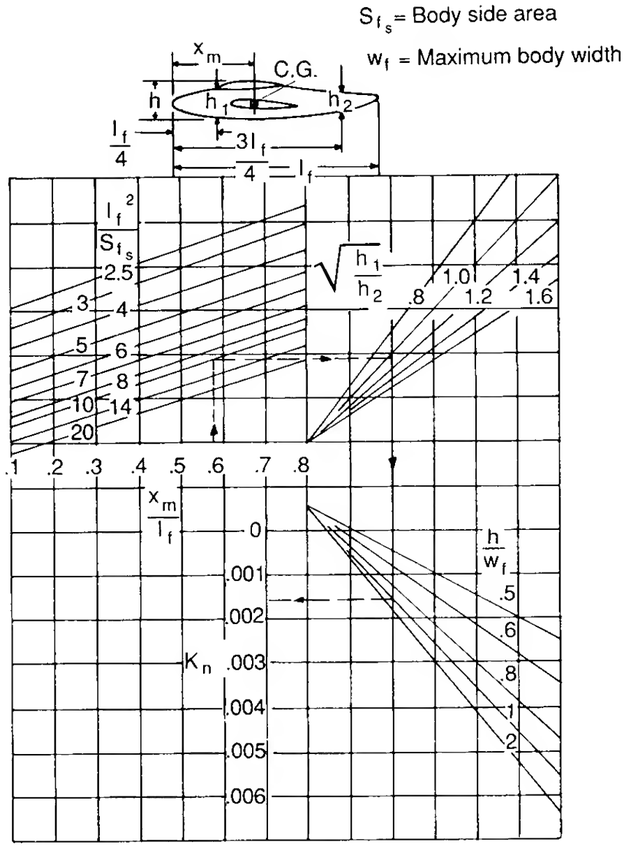

FIGURE 2.28
Wing body interference factor.

directional stability. The mechanism by which the vertical tail produces directional stability is shown in Fig. 2.30. If we consider the vertical tail surface in Fig. 2.30, we see that when the airplane is flying at a positive sideslip angle, the vertical tail produces a side force (lift force in xy plane) which tends to rotate the airplane about its center of gravity. The moment produced is a restoring moment. The side force acting on the vertical tail can be expressed as

$$Y_v = -C_{L_{\alpha_v}} \alpha_v Q_v S_v \tag{2.75}$$

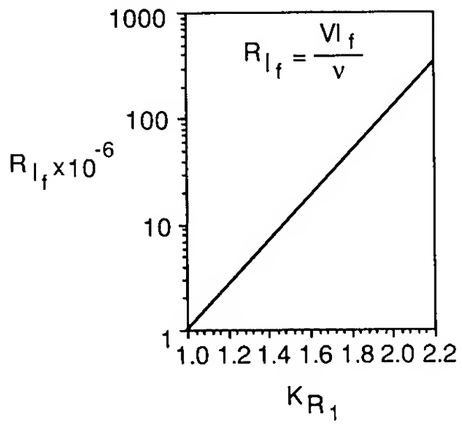

FIGURE 2.29
Reynolds number correction factor.

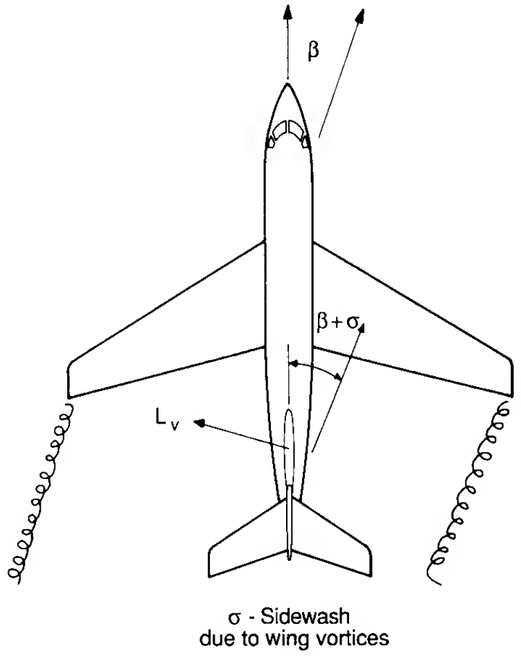

FIGURE 2.30
Vertical tail contribution to directional stability.

where the subscript v refers to properties of the vertical tail. The angle of attack α_v that the vertical tail plane will experience can be written as

$$\alpha_v = \beta + \sigma \tag{2.76}$$

where σ is the sidewash angle. The sidewash angle is analogous to the downwash angle ε for the horizontal tail plane. The sidewash is caused by the flow field distortion due to the wings and fuselage. The moment produced by the vertical tail can be written as a function of the side force acting on it:

$$N_v = l_v Y_v = l_v C_{L_{\alpha_v}}(\beta + \sigma) Q_v S_v \tag{2.77}$$

or in coefficient form:

$$C_n = \frac{N_v}{Q_w S b} = \frac{l_v S_v}{S b}\frac{Q_v}{Q_w} C_{L_{\alpha_v}}(\beta + \sigma) \tag{2.78}$$

$$= V_v \eta_v C_{L_{\alpha_v}}(\beta + \sigma) \tag{2.79}$$

where V_v is the vertical tail volume ratio and η_v is the ratio of the dynamic pressure at the vertical tail to the dynamic pressure at the wing.

The contribution of the vertical tail to directional stability can now be obtained by taking the derivative of Eq. (2.77) with respect to β:

$$C_{n_{\beta_v}} = V_v \eta_v C_{L_{\alpha_v}}\left(1 + \frac{d\sigma}{d\beta}\right) \tag{2.80}$$

A simple algebraic equation for estimating the combined sidewash and tail

efficiency factor η_v is presented in Ref. 2.7 and is reproduced below.

$$\eta_v\left(1 + \frac{d\sigma}{d\beta}\right) = 0.724 + 3.06\frac{S_v/S}{1 + \cos\Lambda_{c/4w}} + 0.4\frac{z_w}{d} + 0.009AR_w \tag{2.81}$$

where S = the wing area
S_v = the vertical tail area, including the submerged area to the fuselage centerline
z_w = is the distance, parallel to the z axis, from wing root quarter chord point to fuselage centerline
d = is the maximum fuselage depth
AR_w = is the aspect ratio of the wing
$\Lambda_{c/4w}$ = sweep of wing quarter chord.

2.7 DIRECTIONAL CONTROL

Directional control is achieved by a control surface called a rudder which is located on the vertical tail, as shown in Fig. 2.31. The rudder is a hinged flap which forms the aft portion of the vertical tail. By rotating the flap, the lift force (side force) on the fixed vertical surface can be varied to create a yawing moment about the center of gravity. The size of the rudder is determined by the directional control requirements. The rudder control power must be sufficient to accomplish the requirements listed in Table 2.1.

The yawing moment produced by the rudder depends upon the change in lift on the vertical tail due to the deflection of the rudder times its distance from the center of gravity. For a positive rudder deflection, a positive side force is created on the vertical tail. A positive side force will produce a negative yawing moment:

$$N = -l_v Y_v \tag{2.82}$$

where the side force is given by

$$Y_v = C_{L_v} Q_v S_v$$

Rewriting this equation in terms of a yawing moment coefficient yields

$$C_n = \frac{N}{Q_w S b} = -\frac{Q_v}{Q_w}\frac{l_v S_v}{S b}\frac{dC_{L_v}}{d\delta_r}\delta_r \tag{2.83}$$

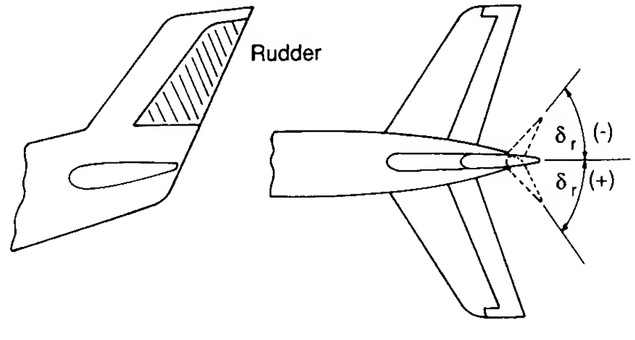

FIGURE 2.31
Directional control by means of the rudder.

TABLE 2.1
Requirements for directional control

Rudder requirements	Implication for rudder design
Adverse yaw	When an airplane is banked, in order to execute a turning maneuver, the ailerons may create a yawing moment that opposes the turn (i.e. adverse yaw). The rudder must be able to overcome the adverse yaw so that a coordinated turn can be achieved. The critical condition for adverse yaw occurs when the airplane is flying slow (i.e. high C_L).
Cross-wind landings	To maintain alignment with the runway during a cross-wind landing requires the pilot to fly the airplane at a sideslip angle. The rudder must be powerful enough to permit the pilot to trim the airplane for the specified cross-winds. For transport airplanes, landing may be carried out for cross-winds up to 15.5 m/s or 51 ft/s.
Asymmetric power condition	The critical asymmetric power condition occurs for a multi-engine airplane when one engine fails at low flight speeds. The rudder must be able to overcome the yawing moment produced by the asymmetric thrust arrangement.
Spin recovery	The primary control for spin recovery in many airplanes is a powerful rudder. The rudder must be powerful enough to oppose the spin rotation.

or

$$C_n = -\eta_v V_v \frac{dC_{L_v}}{d\delta_r}\delta_r \tag{2.84}$$

The rudder control effectiveness is the rate of change of yawing moment with rudder deflection angle:

$$C_n = C_{n_{\delta_r}}\delta_r = -\eta_v V_v \frac{dC_{L_v}}{d\delta_r}\delta_r \tag{2.85}$$

or

$$C_{n_{\delta_r}} = -\eta V_v \frac{dC_{L_v}}{d\delta_r} \tag{2.86}$$

where

$$\frac{dC_{L_v}}{d\delta_r} = \frac{dC_{L_v}}{d\alpha_v}\frac{d\alpha_v}{d\delta_r} = C_{L_{\alpha_v}}\tau \tag{2.87}$$

and the factor τ can be estimated from Fig. 2.20.

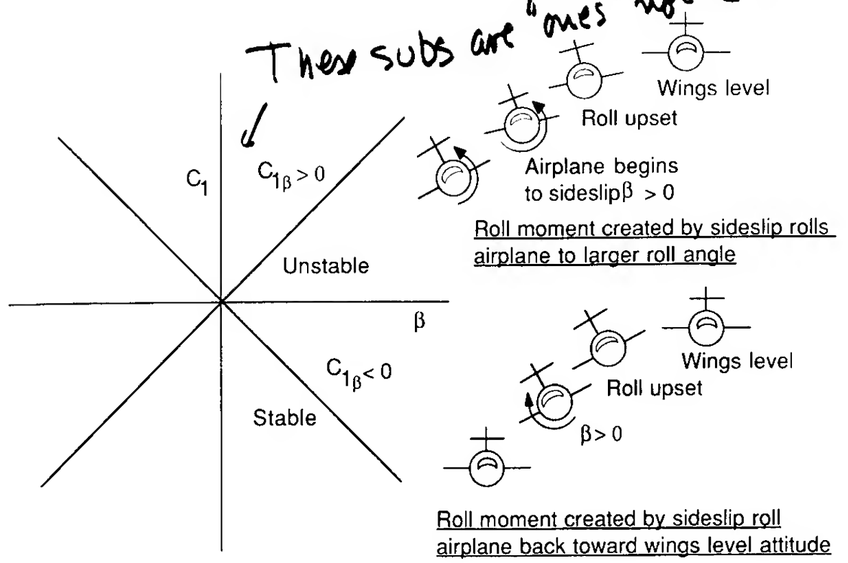

FIGURE 2.32
Static roll stability.

2.8 ROLL STABILITY

An airplane possesses static roll stability if, when it is disturbed from a wings-level attitude, a restoring moment is developed. The restoring rolling moment can be shown to be a function of the sideslip angle β as illustrated in Fig. 2.32. The requirement for stability is that $C_{l_\beta} < 0$. The roll moment created on an airplane when it starts to sideslip depends upon wing dihedral, wing sweep, position of the wing on the fuselage, and the vertical tail. Each of these contributions will be discussed qualitatively in the following paragraphs.

The major contributor to C_{l_β} is the wing dihedral angle Γ. The dihedral angle is defined as the spanwise inclination of the wing with respect to the horizontal. If the wing tip is higher than the root section, then the dihedral angle is positive; if the wing tip is lower than the root section, then the dihedral angle is negative. A negative dihedral angle is commonly called anhedral.

When an airplane is disturbed from a wings-level attitude, it will begin to sideslip as shown in Fig. 2.32. Once the airplane starts to sideslip a component of the relative wind is directed toward the side of the airplane. The leading wing experiences an increased angle of attack and consequently an increase in lift. The trailing wing experiences the opposite effect. The net result is a rolling moment that tries to bring the wing back to a wings-level attitude. This restoring moment is often referred to as the "dihedral effect".

The additional lift created on the downward-moving wing is created by the change in angle of attack produced by the sideslipping motion. If we resolve the sideward velocity component into components along and normal to

the wing span the local change in angle of attack can be estimated as

$$\Delta\alpha = \frac{v_n}{u} \tag{2.88}$$

where

$$v_n = V \sin \Gamma \tag{2.89}$$

By approximating the sideslip angle as

$$\beta = \frac{v}{u} \tag{2.90}$$

and assuming that Γ is a small angle, then the change in angle of attack can be written as

$$\Delta\alpha \cong \beta\Gamma \tag{2.91}$$

The angle of attack on the upward-moving wing will be decreased by the same amount. Methods for estimating the wing contribution to C_{l_β} can again be found in Ref. 2.7.

Wing sweep also contributes to the dihedral effect. In the case of a sweptback wing, the windward wing has an effective decrease in sweep angle while the trailing wing experiences an effective increase in sweep angle. For a given angle of attack, a decrease in sweepback angle will result in a higher lift coefficient. Therefore, the windward wing (less effective sweep) will experience more lift than the trailing wing. It can be concluded that sweepback adds to the dihedral effect. On the other hand, sweepforward will decrease the effective dihedral effect.

The fuselage contribution to dihedral effect is illustrated in Fig. 2.33. The

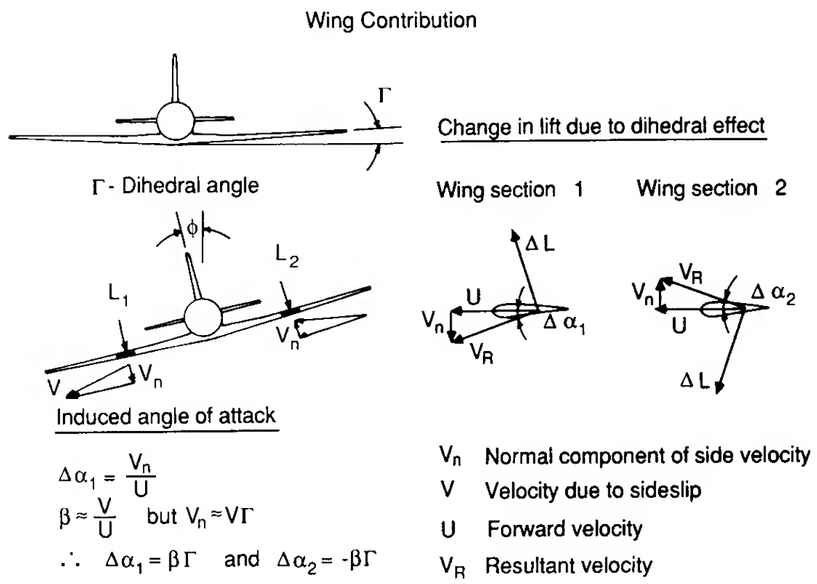

FIGURE 2.33
Wing and fuselage contribution to the dihedral effect.

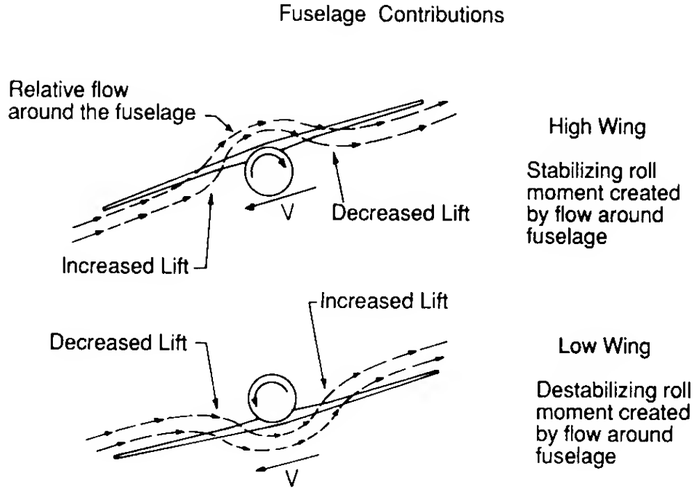

FIGURE 2.33 (*contd.*)

sideward flow turns in the vicinity of the fuselage and creates a local change in wing angle of attack at the inboard wing stations. For a low wing position, the fuselage contributes a negative dihedral effect; the high wing produces a positive dihedral effect. In order to maintain the same C_{l_β}, a low-wing aircraft will require a considerably greater wing dihedral angle than a high-wing configuration.

The horizontal tail can also contribute to the dihedral effect in a manner similar to the wing. However, owing to the size of the horizontal tail with respect to the wing, its contribution is usually small. The contribution to dihedral effect from the vertical tail is produced by the side force on the tail due to sideslip. The side force on the vertical tail produces both a yawing and a rolling moment. The rolling moment occurs because the center of pressure for the vertical tail is located above the aircraft's center of gravity. The rolling moment produced by the vertical tail tends to bring the aircraft back to a wings-level attitude.

2.9 ROLL CONTROL

Roll control is achieved by the differential deflection of small flaps called ailerons which are located outboard on the wings, or by the use of spoilers. Figure 2.34 is a sketch showing both types of roll control devices. The basic principle behind these devices is to modify the spanwise lift distribution so that a moment is created about the x axis. An estimate of the roll control power for an aileron can be obtained by a simple strip integration method as illustrated in Fig. 2.35 and the equations that follow. The incremental change in roll moment due to a change in aileron angle can be expressed as

$$\Delta L = (\Delta \text{ Lift})y \tag{2.92}$$

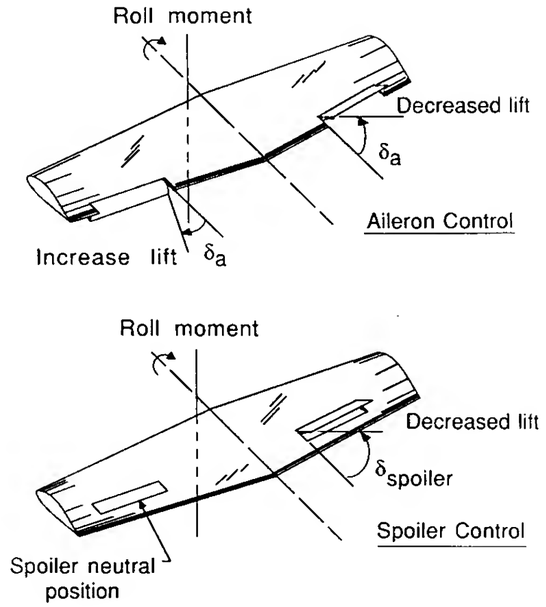

FIGURE 2.34
Aileron and spoilers for roll control.

which can be written in coefficient form as

$$\Delta C_l = \frac{\Delta L}{QSb} = \frac{C_L Q c y \, dy}{QSb} \tag{2.93}$$

$$= \frac{C_L c y \, dy}{Sb} \tag{2.94}$$

The lift coefficient on the stations containing the aileron can be written as

$$C_l = C_{L_\alpha} \frac{d\alpha}{d\delta_a} \delta_a = C_{L_\alpha} \tau \delta_a \tag{2.95}$$

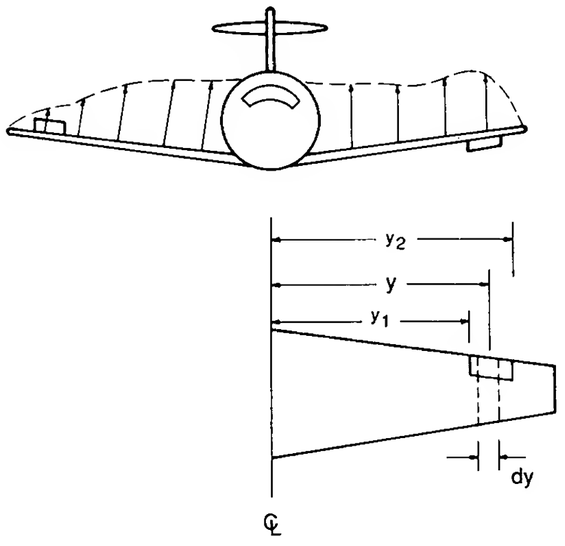

FIGURE 2.35
Strip theory approximation of roll control effectiveness.

which is similar to the technique used to estimate the control effectiveness of an elevator and rudder. Substituting Eq. (2.94) into Eq. (2.95) and integrating over the region containing the aileron yields

$$C_l = \frac{2C_{L_{\alpha_w}} \tau \delta_a}{Sb} \int_{y_1}^{y_2} c y \, dy \tag{2.96}$$

where $C_{L_{\alpha_w}}$ and τ have been corrected for three-dimensional flow and the factor of 2 has been introduced to account for the other aileron. The control power $C_{l_{\delta_a}}$ can be obtained by taking the derivative with respect to δ_a:

$$C_{l_{\delta_a}} = \frac{2C_{L_{\alpha_w}} \tau}{Sb} \int_{y_1}^{y_2} c y \, dy \tag{2.97}$$

2.10 SUMMARY

The requirements for static stability were developed for longitudinal, lateral directional and rolling motions. It is easy to see why a pilot would require the airplane that he or she is flying to possess some degree of static stability. Without static stability the pilot would have to continuously control the airplane to maintain a desired flight path. This would be quite fatiguing for the pilot. The degree of static stability desired by the pilot has been determined through flying quality studies and will be discussed in a later chapter. The important point at this time is to recognize that the airplane must be made statically stable, either because of the inherent aerodynamic characteristics or by artificial means through the use of an automatic control system, for the pilot to find the airplane acceptable for flying.

The inherent static stability tendencies of the airplane were shown to be a function of the geometric and aerodynamic properties of the airplane. The designer can control the degree of longitudinal and lateral directional stability by proper sizing of the horizontal and vertical tail surfaces, whereas roll stability was shown to be a consequence of dihedral effect, which is controlled by wing placement and or wing dihedral angle.

In addition to static stability, the pilot also wants sufficient control authority to keep the airplane in equilibrium (i.e. trim) or to maneuver. Aircraft response to control input and control force requirements are important flying quality characteristics which are determined by the control surface size. The stick force and stick force gradient are important parameters that influence how the pilot feels about the flying characteristics of the airplane. Stick forces must provide the pilot with a feel for the maneuver initiated. In addition, we show that the stick force gradient provides the airplane with speed stability. If the longitudinal stick force gradient is negative at the trim flight speed, then the airplane will resist disturbances in speed and will fly at a constant speed.

Finally, the relationship between static stability and control was examined. An airplane that is very stable statically will not be very maneuverable; if the airplane has very little static stability, it will be very maneuverable. The degree of maneuverability or static stability is determined by the designer on the basis of the mission requirements of the airplane being designed.

2.11 PROBLEMS

2.1. If the slope of the C_m versus C_L curve is -0.15 and the pitching moment at zero lift is equal to 0.08, determined the trim lift coefficient. If the center of gravity of the airplane is located at $X_{cg}/\bar{c} = 0.3$, determine the stick fixed neutral point.

2.2. For the data shown in Fig. P2.2, determine the following.

(a) The stick fixed neutral point.

(b) If we wish to fly the airplane at a velocity of 125 ft/s at sea level, what would be the trim lift coefficient and what would be the elevator angle for trim?

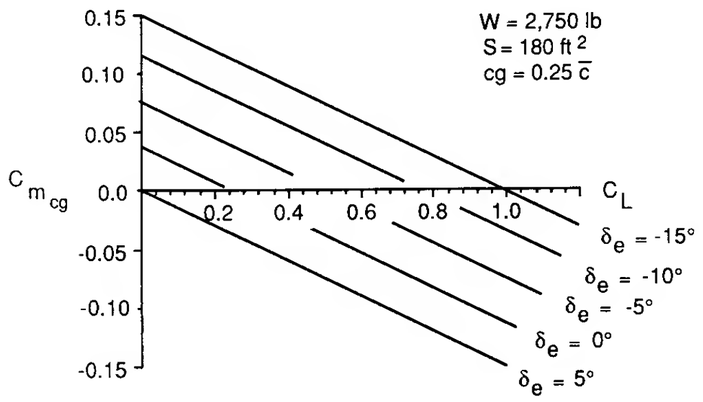

FIGURE P2.2

2.3. Analyze the canard–wing combination shown in Fig. P2.3. The canard and wing are geometrically similar and are made from the same airfoil section.

$$AR_c = AR_w \qquad S_c = 0.2S_w \qquad \bar{c}_c = 0.45\bar{c}_w$$

(a) Develop an expression for the moment coefficient about the center of gravity. You may simplify the problem by neglecting the upwash (downwash) affects between the lifting surfaces and the drag contribution to the moment. Also assume small angle approximations.

(b) Find the neutral point for this airplane.

2.4. Using the data for the business jet aircraft included in the Appendix, determine the following longitudinal stability information at subsonic speeds:

(a) wing contribution to pitching moment

(b) tail contribution to pitching moment

(c) fuselage contribution to pitching moment

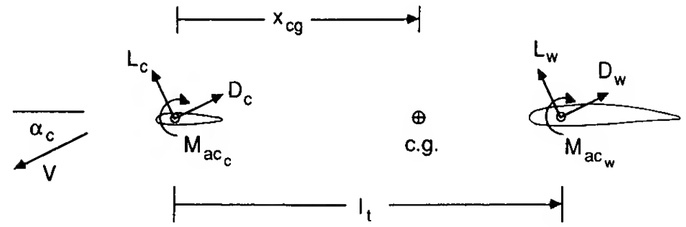

FIGURE P2.3

(d) total pitching moment

(e) plot the various contributions

(f) estimate the stick fixed neutral point

2.5. The downwash angle at zero angle of attack and the rate of change of downwash with angle of attack can be determined experimentally by several techniques. The downwash angle can be measured directly by using a five- or seven-hole pressure probe to determine the flow direction at the position of the tail surface, or it can be obtained indirectly from pitching moment data measured from wind tunnel models. This latter technique will be demonstrated by way of this problem. Suppose that a wind tunnel test was conducted to measure the pitching moment as a function of the angle of attack for various tail incidence settings as well as for the case when the tail surface is removed. Figure P2.5 is a plot of such information. Notice that the tail-off data intersect the complete configuration data at several points. At the points of intersection, the contribution of the tail surface to the pitching moment curve must be zero. For this to be the case, the lift on the tail surface is zero, which implies that the tail angle of attack is zero at these points. From the definition of the tail angle of attack,

$$\alpha_t = \alpha_w - i_w - \varepsilon + i_t$$

we obtain

$$\varepsilon = \alpha_w - i_w + i_t$$

at the interception points. Using the data of Fig. P2.5, determine the downwash angle versus the angle of attack of the wing. From this information estimate ε_0 and $d\varepsilon/d\alpha$.

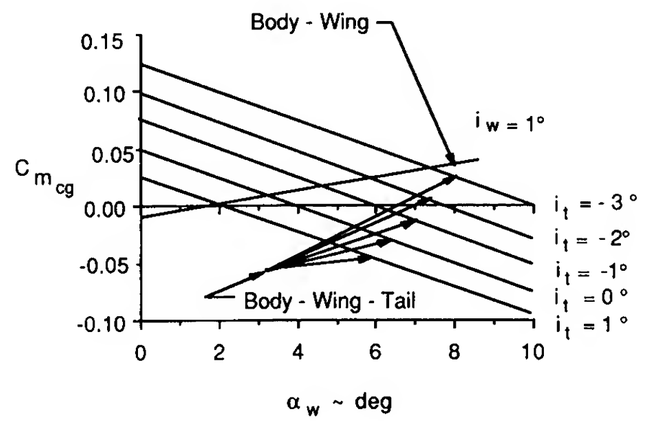

FIGURE P2.5

2.6. If the airplane in Example Problem 2.1 has the following hinge moment characteristics,

$$C_{L_{\alpha_w}} = 0.09/\text{deg} \qquad C_{h_\alpha} = -0.003/\text{deg} \qquad C_{h_\delta} = -0.005/\text{deg} \qquad V_H = 0.4$$
$$C_{L_{\alpha_t}} = 0.08/\text{deg} \qquad C_{h_0} = 0.0 \qquad S_e/S_t = 0.35 \qquad \frac{de}{d\alpha} = 0.4$$

What would be the stick free neutral point location?

2.7. As an airplane nears the ground its aerodynamic characteristics are changed by the presence of the ground plane. This change is called ground effect. A simple model for determining the influence of the ground on the lift drag and pitching moment can be obtained by representing the airplane by a horseshoe vortex system and its image as shown in Fig. P2.7. Using this sketch shown qualitatively the changes that one might expect, i.e. whether the forces and moment increase or decrease?

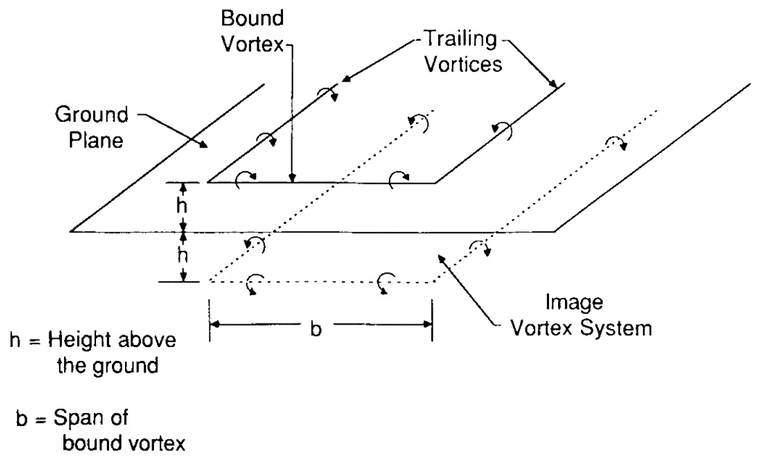

FIGURE P2.7

2.8. If the control characteristics of the elevator used in Example Problem 2.1 are as given below, determine the forward-most limit on the center of gravity travel so that the airplane can be controlled during landing, i.e. at $C_{L\max}$. Neglect ground effects on the airplane's aerodynamic characteristics.

$$C_{m\delta e} = -1.03/\text{rad} \qquad \delta_{e\max} = \begin{cases} +10^\circ \\ -20^\circ \end{cases} \qquad C_{L\max} = 1.4$$

2.9. Size the vertical tail for the airplane configuration shown in Figs. P2.9 and P2.10 so that its weathercock stability has a value of $C_{n_\beta} = +0.1\,\text{rad}^{-1}$. Clearly state your assumptions. Assume V = 150 m/s at sea level.

2.10. Figure P2.10 is a sketch of a wing planform for a business aviation airplane.
(a) Use strip theory to determine the roll control power.
(b) Comment on the accuracy of the strip theory integration technique.

2.11. Suppose the wing planform in Problem 2.10 is incorporated into a low-wing aircraft design. Find the wing dihedral angle necessary to produce a dihedral effect of $C_{l_\beta} = -0.1\,\text{rad}^{-1}$. Neglect the fuselage interference on the wing dihedral contribution.

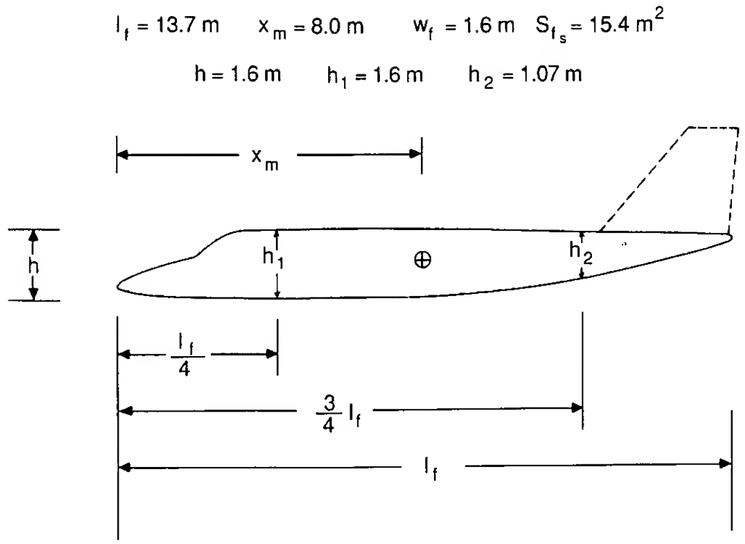

FIGURE P2.9

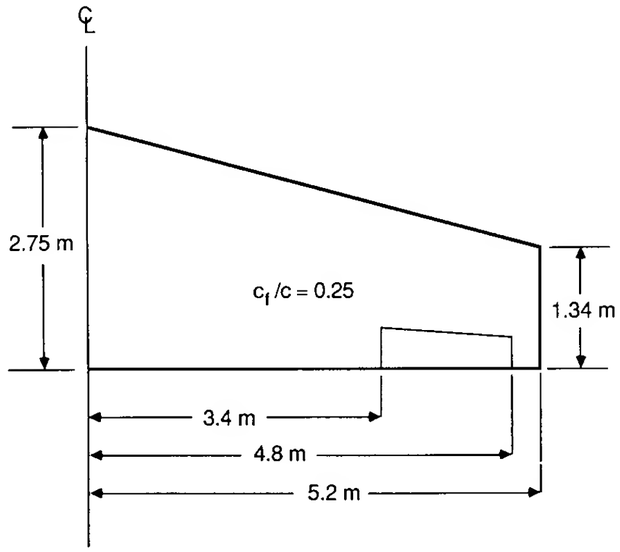

FIGURE P2.10

REFERENCES

2.1. Dickman, E. W.: *This Aviation Business*, Brentano's, New York, 1926.
2.2. Gibbs-Smith, C. H., and T. D. Crouch: "Wilbur and Orville Wright—A 75th Anniversary Commemoration," *Astronautics and Aeronautics, pp.* 8–15, *December*, 1978.
2.3. Perkins, C. D.: "Development of Airplane Stability and Control Technology," *AIAA Journal of Aircraft*, vol. 7, no. 4, 1970.
2.4. Etkin, B: *Dynamics of Flight*, Wiley, New York, 1959.
2.5. Perkins, C. D., and R. E. Hage,: *Airplane Performance Stability and Control*, Wiley, New York, 1949.

2.6. McRuer, D., I. Ashkenas, and D. Graham,: *Aircraft Dynamics and Automatic Control,* Princeton University Press, Princeton, NJ, 1973.
2.7. *USAF Stability and Control Datcom,* Flight Control Division, Air Force Flight Dynamics Laboratory, Wright Patterson Air Force Base, OH.
2.8. Munk, M. M.: *The Aerodynamic Forces on Airship Hulls,* NACA TR 184, 1924.
2.9. Multhopp, H.: *Aerodynamics of Fuselage,* NACA TM-1036, 1942.

CHAPTER 3

AIRCRAFT EQUATIONS OF MOTION

Success four flights Thursday morning all against twenty-one mile wind—started from level with engine power alone average speed through air thirty-miles—longest 57 seconds inform press home Christmas

Telegram message sent by Orville Wright/December 17, 1903

3.1 INTRODUCTION

In Chapter 2, the requirements for static stability were examined. It was shown that static stability is a tendency of the aircraft to return to its equilibrium position. In addition to static stability, the aircraft must also be dynamically stable. An airplane can be considered to be dynamically stable if, after being disturbed from its equilibrium flight condition, the ensuing motion diminishes with time. Of particular interest to the pilot and designer is the degree of dynamic stability. The required degree of dynamic stability is usually specified by the time it takes the motion to damp to half of its initial amplitude or, in the case of an unstable motion, the time it takes for the initial amplitude or disturbance to double. Also of interest is the frequency or period of the oscillation.

An understanding of the dynamic characteristics of an airplane is important in assessing the handling or flying qualities of an airplane as well as for designing autopilots. Flying qualities of an airplane are dependent upon pilot opinion, that is, the pilot's likes or dislikes with regard to the various vehicle motions. It is possible to design an airplane that has excellent performance but is considered to be an unsatisfactory airplane by the pilot. From the early 1960s to the present, there has been a considerable amount of

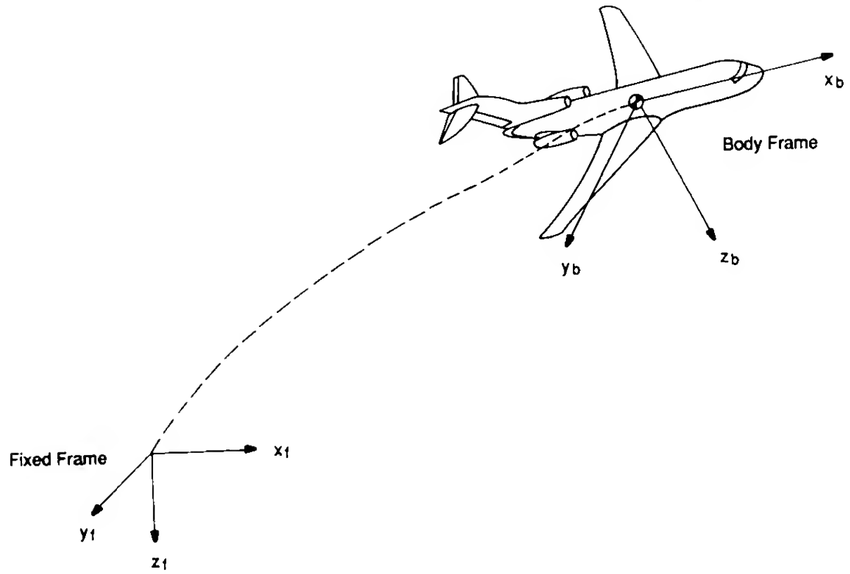

FIGURE 3.1
Body and inertial axes systems.

research directed toward quantifying pilot opinion in terms of aircraft motion characteristics, such as frequency and damping ratio of the aircraft's various modes of motion. Thus, it is important to understand the dynamic characteristics of an airplane and the relationship of the motion to the vehicle's aerodynamic characteristics and to pilot opinion.

Before developing the equations of motion, it is important to review the axis system that was specified earlier. Figure 3.1 shows the body axes system that is fixed to the aircraft and the inertial axes system that is fixed to the Earth.

3.2 DERIVATION OF RIGID BODY EQUATIONS OF MOTION

The rigid body equations of motion are obtained from Newton's second law, which states that the summation of all external forces acting on a body is equal to the time rate of change of the momentum of the body, and the summation of the external moments acting on the body is equal to the time rate of change of the moment of momentum (angular momentum). The time rates of change of linear and angular momentum are referred to an absolute or inertial reference frame. For many problems in airplane dynamics, an axis system fixed to the Earth can be used as an inertial reference frame. Newton's second law can be expressed in the following vector equations:

$$\sum \mathbf{F} = \frac{\mathrm{d}}{\mathrm{d}t}(m\mathbf{v}) \tag{3.1}$$

$$\sum \mathbf{M} = \frac{\mathrm{d}}{\mathrm{d}t}\mathbf{H} \tag{3.2}$$

The vector equations can be rewritten in scalar form and then consist of three force equations and three moment equations. The force equations can be expressed as follows:

$$F_x = \frac{\mathrm{d}}{\mathrm{d}t}(mu) \qquad F_y = \frac{\mathrm{d}}{\mathrm{d}t}(mv) \qquad F_z = \frac{\mathrm{d}}{\mathrm{d}t}(mw) \tag{3.3}$$

where F_x, F_y, F_z and u, v, w are the components of the force and velocity along the x, y and z axes, respectively. The force components are composed of contributions due to the aerodynamic, propulsive, and gravitational forces acting on the airplane. The moment equations can be expressed in a similar manner:

$$L = \frac{\mathrm{d}}{\mathrm{d}t}H_x \qquad M = \frac{\mathrm{d}}{\mathrm{d}t}H_y \qquad N = \frac{\mathrm{d}}{\mathrm{d}t}H_z \tag{3.4}$$

where L, M, N and H_x, H_y, H_z are the components of the moment and moment of momentum along the x, y and z axes, respectively.

Consider the airplane shown in Fig. 3.2. If we let δm be an element of mass of the airplane, $\mathbf{v}$ be the velocity of the elemental mass relative to an absolute or inertial frame, $\delta\mathbf{F}$ be the resulting force acting on the elemental mass; then Newton's second law yields

$$\delta\mathbf{F} = \delta m \frac{\mathrm{d}\mathbf{v}}{\mathrm{d}t} \tag{3.5}$$

and the total external force acting on the airplane is found by summing all the elements of the airplane:

$$\sum \delta\mathbf{F} = \mathbf{F} \tag{3.6}$$

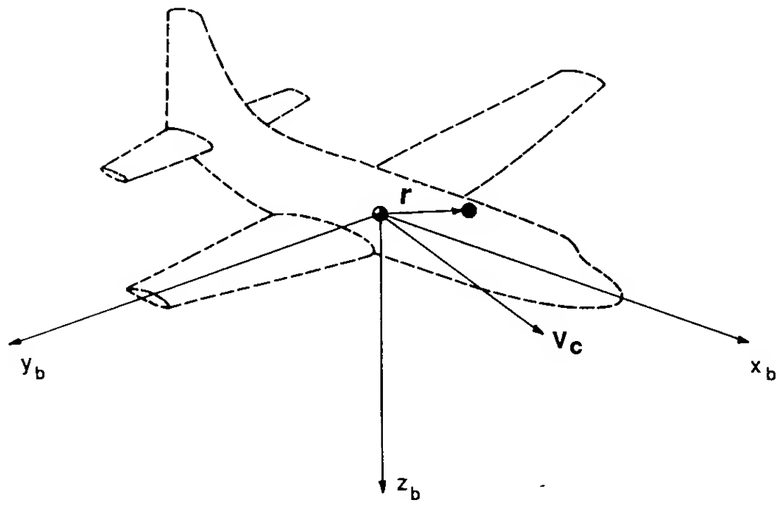

FIGURE 3.2
An element of mass on an airplane.

The velocity of the differential mass δm is

$$\mathbf{v} = \mathbf{v}_c + \frac{d\mathbf{r}}{dt} \tag{3.7}$$

where $\mathbf{v}_c$ is the velocity of the center of mass of the airplane and $d\mathbf{r}/dt$ is the velocity of the element relative to the center of mass. Substituting this expression for the velocity into Newton's second law yields

$$\sum \delta\mathbf{F} = \mathbf{F} = \frac{d}{dt}\sum\left(\mathbf{v}_c + \frac{d\mathbf{r}}{dt}\right)\delta m \tag{3.8}$$

If we assume that the mass of the vehicle is constant, Eq. (3.8), can be rewritten as

$$\mathbf{F} = m\frac{d\mathbf{v}_c}{dt} + \frac{d}{dt}\sum\frac{d\mathbf{r}}{dt}\delta m \tag{3.9}$$

or

$$\mathbf{F} = m\frac{d\mathbf{v}_c}{dt} + \frac{d^2}{dt^2}\sum\mathbf{r}\,\delta m \tag{3.10}$$

Because $\mathbf{r}$ is measured from the center of mass, the summation $\sum \mathbf{r}\,\delta m$ is equal to zero. The force equation then becomes

$$\mathbf{F} = m\frac{d\mathbf{v}_c}{dt} \tag{3.11}$$

which relates the external force on the airplane to the motion of the vehicle's center of mass.

In a similar manner, we can develop the moment equation referred to a moving center of mass. For the differential element of mass, δm, the moment equation can be written as

$$\delta\mathbf{M} = \frac{d}{dt}\delta\mathbf{H} = \frac{d}{dt}(\mathbf{r}\times\mathbf{v})\,\delta m \tag{3.12}$$

The velocity of the mass element can be expressed in terms of the velocity of the center of mass and the relative velocity of the mass element to the center of mass:

$$\mathbf{v} = \mathbf{v}_c + \frac{d\mathbf{r}}{dt} = \mathbf{v}_c + \boldsymbol{\omega}\times\mathbf{r} \tag{3.13}$$

where $\boldsymbol{\omega}$ is the angular velocity of the vehicle and $\mathbf{r}$ is the position of the mass element measured from the center of mass. The total moment of momentum can be written as

$$\mathbf{H} = \sum\delta\mathbf{H} = \sum(\mathbf{r}\times\mathbf{v}_c)\,\delta m + \sum[\mathbf{r}\times(\boldsymbol{\omega}\times\mathbf{r})]\,\delta m \tag{3.14}$$

The velocity $\mathbf{v}_c$ is a constant with respect to the summation and can be taken outside the summation sign

$$\mathbf{H} = \sum\mathbf{r}\,\delta m\times\mathbf{v}_c + \sum[\mathbf{r}\times(\boldsymbol{\omega}\times\mathbf{r})]\,\delta m \tag{3.15}$$

The first term in Eq. (3.15) is zero because the term $\sum\mathbf{r}\,\delta m = 0$, as explained previously. If we express the angular velocity and position vector as

$$\boldsymbol{\omega} = p\mathbf{i} + q\mathbf{j} + r\mathbf{k} \tag{3.16}$$

and

$$\mathbf{r} = x\mathbf{i} + y\mathbf{j} + z\mathbf{k} \tag{3.17}$$

then after expanding Eq. (3.15), $\mathbf{H}$ can be written as

$$\mathbf{H} = (p\mathbf{i}+q\mathbf{i}+r\mathbf{k})\sum(x^2+y^2+z^2)\,\delta m - \sum(x\mathbf{i}+y\mathbf{i}+z\mathbf{k})(px+qy+rz)\,\delta m \tag{3.18}$$

The scalar components of $\mathbf{H}$ are

$$\begin{aligned} H_x &= p\sum(y^2+z^2)\,\delta m - q\sum xy\,\delta m - r\sum xz\,\delta m \\ H_y &= -p\sum xy\,\delta m + q\sum(x^2+y^2)\,\delta m - r\sum yz\,\delta m \\ H_z &= -p\sum xz\,\delta m - q\sum yz\,\delta m + r\sum(x^2+y^2)\,\delta m \end{aligned} \tag{3.19}$$

The summations in the above equations are the mass moment and products of inertia of the airplane and are defined as follows:

$$\begin{aligned} I_x &= \iiint_v (y^2+z^2)\,\delta m \qquad I_{xy} = \iiint_v xy\,\delta m \\ I_y &= \iiint_v (x^2+z^2)\,\delta m \qquad I_{xz} = \iiint_v xz\,\delta m \\ I_z &= \iiint_v (x^2+y^2)\,\delta m \qquad I_{yz} = \iiint_v yz\,\delta m \end{aligned} \tag{3.20}$$

The terms I_x, I_y and I_z are the mass moments of inertia of the body about the x, y and z axes, respectively. The terms with the mixed indices are called the products of inertia. Both the moments and products of inertia depend on the shape of the body and the manner in which its mass is distributed. The larger the moments of inertia the greater the resistance the body will have to rotation. The scaler equations for the moment of momentum are given below.

$$\begin{aligned} H_x &= pI_x - qI_{xy} - rI_{xz} \\ H_y &= -pI_{xy} + qI_y - rI_{yz} \\ H_z &= -pI_{xz} - qI_{yz} + rI_z \end{aligned} \tag{3.21}$$

If the reference frame is not rotating then, as the airplane rotates, the

moments and products of inertia will vary with time. To avoid this difficulty we will fix the axis system to the aircraft (body axis system). Now we must determine the derivatives of the vectors **v** and **H** referred to the rotating body frame of reference.

It can be shown that the derivative of an arbitrary vector **A** referred to a rotating body frame having an angular velocity $\boldsymbol{\omega}$ can be represented by the following vector identity:

$$\left.\frac{d\mathbf{A}}{dt}\right|_I = \left.\frac{d\mathbf{A}}{dt}\right|_B + \boldsymbol{\omega} \times \mathbf{A} \tag{3.22}$$

where the subscript I and B refer to the inertial and body fixed frames of reference. Applying this identity to the equations derived earlier yields

$$\mathbf{F} = m\left.\frac{d\mathbf{v}_c}{dt}\right|_B + m(\boldsymbol{\omega} \times \mathbf{v}_c) \tag{3.23}$$

$$\mathbf{M} = \left.\frac{d\mathbf{H}}{dt}\right|_B + \boldsymbol{\omega} \times \mathbf{H} \tag{3.24}$$

The scalar equations are

$$\begin{aligned} F_x &= m(\dot{u} + qw - rv) \qquad F_y = m(\dot{v} + ru - pw) \qquad F_z = m(\dot{w} + pv - qu) \\ L &= \dot{H}_x + qH_z - rH_y \qquad M = \dot{H}_y + rH_x - pH_z \qquad N = \dot{H}_z + pH_y - qH_x \end{aligned} \tag{3.25}$$

The components of the force and moment acting on the airplane are composed of aerodynamic, gravitational, and propulsive contributions.

By proper positioning of the body axis system, one can make the products of inertia $I_{yz} = I_{xy} = 0$. To do this we are assuming that the xz plane is a plane of symmetry of the airplane. With this assumption, the moment equations can be written as

$$\begin{aligned} L &= I_x\dot{p} - I_{xz}\dot{r} + qr(I_z - I_y) - I_{xz}pq \\ M &= I_y\dot{q} + rp(I_x - I_z) + I_{xz}(p^2 - r^2) \\ N &= -I_{xz}\dot{p} + I_z\dot{r} + pq(I_y - I_x) + I_{xz}qr \end{aligned} \tag{3.26}$$

3.3 ORIENTATION AND POSITION OF THE AIRPLANE

The equations of motion have been derived for an axis system fixed to the airplane. Unfortunately, the position and orientation of the airplane cannot be described relative to the moving body axis frame. The orientation and position of the airplane can be defined in terms of a fixed frame of reference as shown in Fig. 3.3. At time $t = 0$, the two reference frames coincide.

The orientation of the airplane can be described by three consecutive rotations, whose order is important. The angular rotations are called the Euler angles. The orientation of the body frame with respect to the fixed frame can

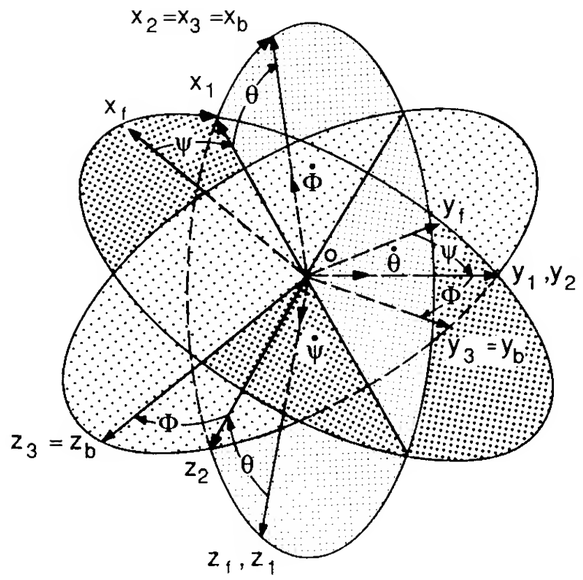

FIGURE 3.3
Relationship between body and inertial axes systems.

be determined in the following manner. Imagine the airplane to be positioned so that the body axis system is parallel to the fixed frame and then apply the following rotations:

1. Rotate the x_f, y_f, z_f frame about $0z_f$ through the yaw angle ψ to the frame to x_1, y_1, z_1.
2. Rotate the x_1, y_1, z_1 frame about $0y_1$ through the pitch angle θ bringing the frame to x_2, y_2, z_2.
3. Rotate the x_2, y_2, z_2 frame about $0x_2$ through the roll angle Φ to bring the frame to x_3, y_3, z_3, the actual orientation of the body frame relative to the fixed frame.

Remember that the order of rotation is extremely important.

Having defined the Euler angles, one can determine the flight velocities components relative to the fixed reference frame. To accomplish this, let the velocity components along the x_f, y_f, z_f frame be dx/dt, dy/dt, dz/dt and, similarly, let the subscripts 1 and 2 denote the components along x_1, y_1, z_1 and x_2, y_2, z_2, respectively. Examining Fig. 3.3, we can show that

$$\frac{dx}{dt} = u_1 \cos\psi - v_1 \sin\psi \qquad \frac{dy}{dt} = u_1 \sin\psi + v_1 \cos\psi \qquad \frac{dz}{dt} = w_1 \tag{3.27}$$

Before proceeding further, let us use the shorthand notation $S_\psi \equiv \sin\psi$, $C_\psi \equiv \cos\psi$, $S_\theta \equiv \sin\theta$, etc. In a similar manner to Eq. (3.27), u_1, v_1, and w_1 can be expressed in terms of u_2, v_2 and w_2:

$$u_1 = u_2C_\theta + w_2S_\theta \qquad v_1 = v_2 \qquad w_1 = -u_2S_\theta + w_2C_\theta \tag{3.28}$$

and

$$u_2 = u \qquad u_2 = vC_\Phi - wS_\Phi \qquad w_2 = vS_\Phi + wC_\Phi \tag{3.29}$$

where u, v and w are the velocity components along the body axes x_b, y_b, z_b.

If we back-substitute the above equations, we can determine the absolute velocity in terms of the Euler angles and velocity components in the body frame:

$$\begin{bmatrix} \frac{dx}{dt} \\ \frac{dy}{dt} \\ \frac{dz}{dt} \end{bmatrix} = \begin{bmatrix} C_\theta C_\psi & S_\Phi S_\theta C_\psi - C_\Phi S_\psi & C_\Phi S_\theta C_\psi + S_\Phi S_\psi \\ C_\theta S_\psi & S_\Phi S_\theta S_\psi + C_\Phi C_\psi & C_\Phi S_\theta S_\psi - S_\Phi C_\psi \\ -S_\theta & S_\Phi C_\theta & C_\Phi C_\theta \end{bmatrix} \begin{bmatrix} u \\ v \\ w \end{bmatrix} \tag{3.30}$$

Integration of these equations yields the airplane's position relative to the fixed frame of reference.

The relationship between the angular velocities in the body frame (p, q and r) and the Euler rates ($\dot{\psi}$, $\dot{\theta}$, and $\dot{\Phi}$) can also be determined from Fig. 3.3:

$$\begin{bmatrix} p \\ q \\ r \end{bmatrix} = \begin{bmatrix} 1 & 0 & -S_\theta \\ 0 & C_\Phi & C_\theta S_\Phi \\ 0 & -S_\Phi & C_\theta C_\Phi \end{bmatrix} \begin{bmatrix} \dot{\Phi} \\ \dot{\theta} \\ \dot{\psi} \end{bmatrix} \tag{3.31}$$

Equation (3.31) can be solved for the Euler rates in terms of the body angular velocities and is given by Eq. (3.32)

$$\begin{bmatrix} \dot{\Phi} \\ \dot{\theta} \\ \dot{\psi} \end{bmatrix} = \begin{bmatrix} 1 & S_\Phi \tan\theta & C_\Phi \tan\theta \\ 0 & C_\Phi & -S_\Phi \\ 0 & S_\Phi \sec\theta & C_\Phi \sec\theta \end{bmatrix} \begin{bmatrix} p \\ q \\ r \end{bmatrix} \tag{3.32}$$

By integrating the above equations, one can determine the Euler angles ψ, θ and Φ.

3.4 GRAVITATIONAL AND THRUST FORCES

The gravitational force acting on the airplane acts through the center of gravity of the airplane. Because the body axis system is fixed to the center of gravity, the gravitational force will not produce any moments. It will, however, contribute to the external force acting on the airplane and will have components along the respective body axes. Figure 3.4 shows that the gravitational force components acting along the body axis are a function of the airplane's orientation in space. The gravitational force components along the

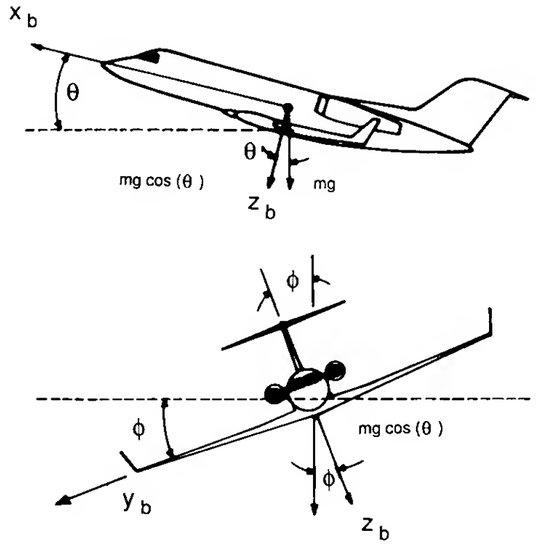

FIGURE 3.4
Components of gravitational force acting along the body axis.

x, y and z axes can be easily shown to be

$$(F_x)_{\text{gravity}} = -mg \sin\theta$$
$$(F_y)_{\text{gravity}} = mg \cos\theta \sin\Phi \tag{3.33}$$
$$(F_z)_{\text{gravity}} = mg \cos\theta \cos\Phi$$

The thrust force due to the propulsion system can have components that act along each of the body axis directions. In addition, the propulsive forces can also create moments if the thrust does not act through the center of gravity. Figure 3.5 shows some examples of moments created by the propulsive system.

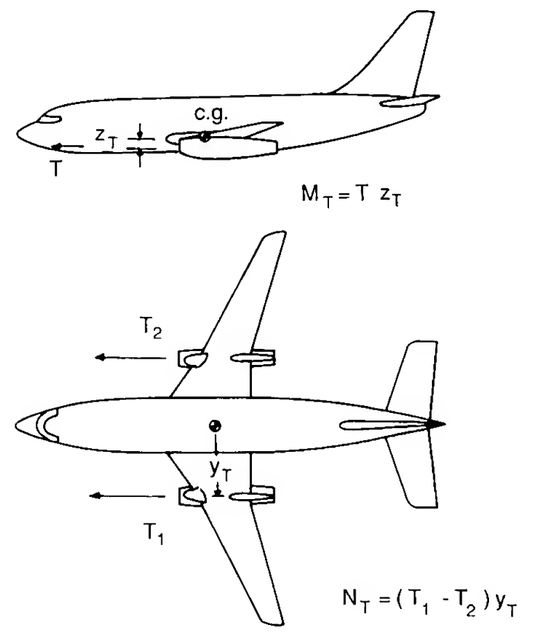

FIGURE 3.5
Force and moments due to propulsion system.

TABLE 3.1
Summary of kinematic and dynamic equations

$X - mg\,S_\theta = m(\dot{u} + qw - rv)$ $Y + mg\,C_\theta S_\Phi = m(\dot{v} + ru - pw)$ $Z + mg\,C_\theta\,C_\Phi = m(\dot{w} + pv - qu)$	Force equations
$L = I_x\dot{p} - I_{xz}\dot{r} + qr(I_z - I_y) - I_{xz}pq$ $M = I_y\dot{q} + rq(I_x - I_z) + I_{xz}(p^2 - r^2)$ $N = -I_{xz}\dot{p} + I_z\dot{r} + pq(I_y - I_x) + I_{xz}qr$	Moment equations
$p = \dot{\Phi} - \dot{\psi}\,S_\theta$ $q = \dot{\theta}C_\Phi + \dot{\psi}\,C_\theta\,S_\Phi$ $r = \dot{\psi}\,C_\theta\,C_\Phi - \dot{\theta}\,S_\Phi$	Body angular velocities in terms of Euler angles and Euler rates
$\dot{\theta} = q\,C_\Phi - r\,S_\Phi$ $\dot{\Phi} = p + q\,S_\Phi\,T_\theta + r\,C_\Phi\,T_\theta$ $\dot{\psi} = (qS_\Phi + rC_\Phi)\sec\theta$	Euler rates in terms of Euler angles and body angular velocities

Velocity of aircraft in the fixed frame in terms of Euler angles and body velocity components

$$\begin{bmatrix} \frac{dx}{dt} \\ \frac{dx}{dt} \\ \frac{dz}{dt} \end{bmatrix} = \begin{bmatrix} C_\theta C_\psi & S_\Phi S_\theta C_\psi - C_\Phi S_\psi & C_\Phi S_\theta C_\psi + S_\Phi S_\psi \\ C_\theta S_\psi & S_\Phi S_\theta S_\psi + C_\Phi C_\psi & C_\Phi S_\theta S_\psi - S_\Phi S_\psi \\ -S_\theta & S_\Phi C_\theta & C_\Phi C_\theta \end{bmatrix} \begin{bmatrix} u \\ v \\ w \end{bmatrix}$$

The propulsive forces and moments acting along the body axis system are denoted as follows:

$$(F_x)_{\text{propulsive}} = X_T \qquad (F_y)_{\text{propulsive}} = Y_T \qquad (F_z)_{\text{propulsive}} = Z_T \tag{3.34}$$

and

$$(L)_{\text{propulsive}} = L_T \qquad (M)_{\text{propulsive}} = M_T \qquad (N)_{\text{propulsive}} = N_T \tag{3.35}$$

Table 3.1 gives a summary of the rigid body equations of motion.

3.5 SMALL-DISTURBANCE THEORY

The equations developed in the previous section can be linearized by using small-disturbance theory. In applying small-disturbance theory we are assuming that the motion of the airplane consists of small deviations about a steady flight condition. Obviously, this theory cannot be applied to problems in which large-amplitude motions are to be expected (e.g. spinning or stalled flight). However, in many cases small-disturbance theory yields sufficient accuracy for practical engineering purposes.

All the variables in the equations of motion are replaced by a reference

value plus a perturbation or disturbance:

$$\begin{aligned} u &= u_0 + \Delta u & v &= v_0 + \Delta v & w &= w_0 + \Delta w \\ p &= p_0 + \Delta p & q &= q_0 + \Delta q & r &= r_0 + \Delta r \\ X &= X_0 + \Delta X & Y &= Y_0 + \Delta Y & Z &= Z_0 + \Delta Z \\ M &= M_0 + \Delta M & N &= N_0 + \Delta N & L &= L_0 + \Delta L \\ \delta &= \delta_0 + \Delta\delta \end{aligned} \tag{3.36}$$

For convenience, the reference flight condition is assumed to be symmetric and the propulsive forces are assumed to remain constant. This implies that

$$v_0 = p_0 = q_0 = r_0 = \phi_0 = \psi_0 = 0 \tag{3.37}$$

Furthermore, if we initially align the x axis so that it is along the direction of the airplane's velocity vector, then $w_0 = 0$.

Now, if we introduce the small-disturbance notation into the equations of motion, we can simplify the equations of motion. As an example, consider the X force equation:

$$X - mg\sin\theta = m(\dot{u} + qw - rv) \tag{3.38}$$

Substituting the small-disturbance variables into the above equations yields

$$\begin{aligned} &X_0 + \Delta X - mg\sin(\theta_0 + \Delta\theta) \\ &\quad = m\left[\frac{d}{dt}(u_0 + \Delta u) + (q_0 + \Delta q)(w_0 + \Delta w) - (r_0 + \Delta r)(v_0 + \Delta v)\right] \end{aligned} \tag{3.39}$$

If we neglect products of the disturbance and assume that

$$w_0 = v_0 = p_0 = q_0 = r_0 = \phi_0 = \psi_0 = 0 \tag{3.40}$$

then the X equation becomes

$$X_0 + \Delta X - mg\sin(\theta_0 + \Delta\theta) = m\,\Delta\dot{u} \tag{3.41}$$

This equation can be reduced further by applying the following trigonometric identity:

$$\sin(\theta_0 + \Delta\theta) = \sin\theta_0\cos\Delta\theta + \cos\theta_0\sin\Delta\theta = \sin\theta_0 + \Delta\theta\cos\theta_0$$

Therefore,

$$X_0 + \Delta X - mg(\sin\theta_0 + \Delta\theta\cos\theta_0) = m\,\Delta\dot{u} \tag{3.42}$$

If all the disturbance quantities are set equal to zero in the above equation, we have the reference flight condition

$$X_0 - mg\sin\theta_0 = 0 \tag{3.43}$$

This reduces the X-force equation to

$$\Delta X - mg\,\Delta\theta\cos\theta_0 = m\,\Delta\dot{u} \tag{3.44}$$

No discussion of separation of sets of equations!!

The force ΔX is the change in aerodynamic and propulsive force in the x direction and can be expressed by means of a Taylor series in terms of the perturbation variables. If we assume that ΔX is a function only of u, w, δ_e and δ_T, then ΔX can be expressed as

$$\Delta X = \frac{\partial X}{\partial u}\Delta u + \frac{\partial X}{\partial w}\Delta w + \frac{\partial X}{\partial \delta_e}\Delta\delta_e + \frac{\partial X}{\partial \delta_T}\Delta\delta_T \tag{3.45}$$

where $\partial X/\partial u$, $\partial X/\partial w$, $\partial X/\partial \delta_e$ and $\partial X/\partial \delta_T$ are called stability derivatives and are evaluated at the reference flight condition. The variables δ_e and δ_T are the change in elevator angle and throttle setting, respectively. If a canard or all-moveable stabilator is used for longitudinal control, then the control term would be replaced by

$$\frac{\partial X}{\partial \delta_H}\Delta\delta_H \qquad \text{or} \qquad \frac{\partial X}{\partial \delta_c}\Delta\delta_c$$

Substituting this expression into the force equation yields:

$$\frac{\partial X}{\partial u}\Delta u + \frac{\partial X}{\partial w}\Delta w + \frac{\partial X}{\partial \delta_e}\Delta\delta_e + \frac{\partial X}{\partial \delta_T}\Delta\delta_T - mg\,\Delta\theta\cos\theta_0 = m\,\Delta\dot{u} \tag{3.46}$$

or, upon rearranging,

$$\left(m\frac{\mathrm{d}}{\mathrm{d}t} - \frac{\partial X}{\partial u}\right)\Delta u - \left(\frac{\partial X}{\partial w}\right)\Delta w + (mg\cos\theta_0)\,\Delta\theta = \frac{\partial X}{\partial \delta_e}\Delta\delta_e + \frac{\partial X}{\partial \delta_T}\Delta\delta_T$$

The equation can be rewritten in a more convenient form by dividing through by the mass m:

Part notation confuse students

$$\left(\frac{\mathrm{d}}{\mathrm{d}t} - X_u\right)\Delta u - X_w\,\Delta w + (g\cos\theta_0)\,\Delta\theta = X_{\delta e}\,\Delta\delta_e + X_{\delta_T}\,\Delta\delta_T \tag{3.47}$$

where $X_u = \partial X/\partial u/m$, $X_w = \partial X/\partial w/m$, etc., are aerodynamic derivatives divided by the airplane mass.

The change in aerodynamic forces and moments are functions of the motion variables Δu, Δw, etc. The aerodynamic derivatives that are usually the most important for conventional airplane motion analysis are given below.

$$\left.\begin{aligned}
\Delta X &= \frac{\partial X}{\partial u}\Delta u + \frac{\partial X}{\partial w}\Delta w + \frac{\partial X}{\partial \delta_e}\Delta\delta_e + \frac{\partial X}{\partial \delta_T}\Delta\delta_T \\
\Delta Y &= \frac{\partial Y}{\partial v}\Delta v + \frac{\partial Y}{\partial p}\Delta p + \frac{\partial Y}{\partial r}\Delta r + \frac{\partial Y}{\partial \delta_r}\Delta\delta_r \\
\Delta Z &= \frac{\partial Z}{\partial u}\Delta u + \frac{\partial Z}{\partial w}\Delta w + \frac{\partial Z}{\partial \dot{w}}\Delta\dot{w} + \frac{\partial Z}{\partial q}\Delta q + \frac{\partial Z}{\partial \delta_e}\Delta\delta_e + \frac{\partial Z}{\partial \delta_T}\Delta\delta_T
\end{aligned}\right\} \tag{3.48}$$

TABLE 3.2
The linearized small-disturbance longitudinal and lateral rigid body equations of motion

Longitudinal equations

$$\left(\frac{\mathrm{d}}{\mathrm{d}t} - X_u\right)\Delta u - X_w\,\Delta w + (g\cos\theta_0)\,\Delta\theta = X_{\delta e}\,\Delta\delta_e + X_{\delta_T}\,\Delta\delta_T$$

$$-Z_u\,\Delta u + \left((1 - Z_{\dot{w}})\frac{\mathrm{d}}{\mathrm{d}t} - Z_w\right)\Delta w - \left((u_0 + Z_q)\frac{\mathrm{d}}{\mathrm{d}t} - g\sin\theta_0\right)\Delta\theta = Z_{\delta e}\,\Delta\delta_e + Z_{\delta_T}\,\Delta\delta_T$$

$$-M_u\,\Delta u - \left(M_{\dot{w}}\frac{\mathrm{d}}{\mathrm{d}t} + M_w\right)\Delta w + \left(\frac{\mathrm{d}^2}{\mathrm{d}t^2} - M_q\frac{\mathrm{d}}{\mathrm{d}t}\right)\Delta\theta = M_{\delta e}\,\Delta\delta_e + M_{\delta_T}\,\Delta\delta_T$$

Lateral equations

$$\left(\frac{\mathrm{d}}{\mathrm{d}t} - Y_v\right)\Delta v - Y_p\Delta p + (u_0 - Y_r)\,\Delta r - (g\cos\theta_0)\,\Delta\phi = Y_{\delta r}\,\Delta\delta_r$$

$$-L_v\,\Delta v + \left(\frac{\mathrm{d}}{\mathrm{d}t} - L_p\right)\Delta p - \left(\frac{I_{xz}}{I_x}\frac{\mathrm{d}}{\mathrm{d}t} + L_r\right)\Delta r = L_{\delta a}\,\Delta\delta_a + L_{\delta r}\,\Delta\delta_r$$

$$-N_v\,\Delta v - \left(\frac{I_{xz}}{I_z}\frac{\mathrm{d}}{\mathrm{d}t} + N_p\right)\Delta p + \left(\frac{\mathrm{d}}{\mathrm{d}t} - N_r\right)\Delta r = N_{\delta a}\,\Delta\delta_a + N_{\delta r}\,\Delta\delta_r$$

$$\left.\begin{aligned}
\Delta L &= \frac{\partial L}{\partial v}\Delta v + \frac{\partial L}{\partial p}\Delta p + \frac{\partial L}{\partial r}\Delta r + \frac{\partial L}{\partial \delta_r}\Delta\delta_r + \frac{\partial L}{\partial \delta_a}\Delta\delta_a \\
\Delta M &= \frac{\partial M}{\partial u}\Delta u + \frac{\partial M}{\partial w}\Delta w + \frac{\partial M}{\partial \dot{w}}\Delta\dot{w} + \frac{\partial M}{\partial q}\Delta q + \frac{\partial M}{\partial \delta_e}\Delta\delta_e + \frac{\partial M}{\partial \delta_T}\Delta\delta_T \\
\Delta N &= \frac{\partial N}{\partial v}\Delta v + \frac{\partial N}{\partial p}\Delta p + \frac{\partial N}{\partial r}\Delta r + \frac{\partial N}{\partial \delta_r}\Delta\delta_r + \frac{\partial N}{\partial \delta_a}\Delta\delta_a
\end{aligned}\right\} \tag{3.49}$$

The aerodynamic forces and moments can be expressed as a function of all the motion variables however, in the above equations only the terms that are usually significant have been retained. Note also that the longitudinal aerodynamic control surface was assumed to be an elevator. For aircraft that use either a canard or combination of longitudinal controls the elevator terms in the preceding equations can be replaced by the appropriate control derivatives and angular deflections.

The complete set of linearized equations of motion is presented in Table 3.2.

3.6 AIRCRAFT TRANSFER FUNCTIONS

The longitudinal and lateral equations of motion were described by a set of linear differential equations. A very useful concept in analysis and design of control systems is the transfer function. The transfer function gives the relationship between the output of and input to a system. In the case of dynamics it specifies the relationship between the motion variables and the

control input. The transfer function is defined as the ratio of Laplace transform of the output to the Laplace transform of the input, with all the initial conditions set to zero (i.e. the system is assumed to be initially at rest). For the reader who is not familiar with theory of Laplace transformations, a brief review of the basic concepts of Laplace transformation theory is included in one of the appendices at the end of this book.

LONGITUDINAL TRANSFER FUNCTION. The longitudinal transfer functions can be obtained from the equations of motion in the following manner. First, we simplify the equations of motion by assuming that

$$\theta_0 = 0 \rightarrow \cos\theta_0 = 1 \qquad \text{and} \qquad \sin\theta_0 = 0 \tag{3.50}$$

and

$$Z_q = Z_{\dot{w}} = 0 \tag{3.51}$$

Incorporating these assumptions yields the following set of longitudinal differential equations:

$$\begin{aligned}
&\left(\frac{\mathrm{d}}{\mathrm{d}t} - X_u\right)\Delta u - X_w\,\Delta w + g\,\Delta\theta = X_\delta\,\Delta\delta \\
&-Z_u\,\Delta u + \left(\frac{\mathrm{d}}{\mathrm{d}t} - Z_w\right)\Delta w - u_0\frac{\mathrm{d}}{\mathrm{d}t}\Delta\theta = Z_\delta\,\Delta\delta \\
&-M_u\,\Delta u - \left(M_{\dot{w}}\frac{\mathrm{d}}{\mathrm{d}t} + M_w\right)\Delta w + \frac{\mathrm{d}}{\mathrm{d}t}\left(\frac{\mathrm{d}}{\mathrm{d}t} - M_q\right)\Delta\theta = M_\delta\,\Delta\delta
\end{aligned} \tag{3.52}$$

If we take the Laplace transformation of the equations and then divide by the control deflection we can find the transfer functions $\overline{\Delta u}/\overline{\Delta\delta}$, $\overline{\Delta\theta}/\overline{\Delta\delta}$, and $\overline{\Delta w}/\overline{\Delta\delta}$.

$$\begin{aligned}
&(s - X_u)\frac{\overline{\Delta u}}{\overline{\Delta\delta}} - X_w\frac{\overline{\Delta w}}{\overline{\Delta\delta}} + g\frac{\overline{\Delta\theta}}{\overline{\Delta\delta}} = X_\delta \\
&-Z_u\frac{\overline{\Delta u}}{\overline{\Delta\delta}} + (s - Z_w)\frac{\overline{\Delta w}}{\overline{\Delta\delta}} - u_0 s\frac{\overline{\Delta\theta}}{\overline{\Delta\delta}} = Z_\delta \\
&-M_u\frac{\overline{\Delta u}}{\overline{\Delta\delta}} - (M_{\dot{w}}s + M_w)\frac{\overline{\Delta w}}{\overline{\Delta\delta}} + s(s - M_q)\frac{\overline{\Delta\theta}}{\overline{\Delta\delta}} = M_\delta
\end{aligned} \tag{3.53}$$

These equations can be solved by means of Cramer's rule to find $\overline{\Delta u}/\overline{\Delta\delta}$, $\overline{\Delta\theta}/\overline{\Delta\delta}$ and $\overline{\Delta w}/\overline{\Delta\delta}$, as follows:

$$\frac{\overline{\Delta\theta}}{\overline{\Delta\delta}} = \frac{\begin{vmatrix} s - X_u & -X_w & X_\delta \\ -Z_\mu & s - Z_w & Z_\delta \\ -M_u & -(M_{\dot{w}}s + M_w) & M_\delta \end{vmatrix}}{\begin{vmatrix} s - X_u & -X_w & g \\ -Z_u & s - Z_w & -u_0 s \\ -M_u & -(M_{\dot{w}}s + M_w) & s(s - M_q) \end{vmatrix}} \tag{3.54}$$

Expressions for $\overline{\Delta u}/\overline{\Delta\delta}$ and $\overline{\Delta w}/\overline{\Delta\delta}$ can be found in a similar fashion. By expanding the determinants, the transfer functions can be expressed as a ratio of two polynomials. For example,

$$\frac{\overline{\Delta u}}{\overline{\Delta\delta}} = \frac{N_\delta^u(s)}{\Delta_{\text{long}}} = \frac{A_u s^3 + B_u s^2 + C_u s + D_u}{\Delta_{\text{long}}} \tag{3.55}$$

$$\frac{\overline{\Delta w}}{\overline{\Delta\delta}} = \frac{N_\delta^w(s)}{\Delta_{\text{long}}} = \frac{A_w s^3 + B_w s^2 + C_w s + D_w}{\Delta_{\text{long}}} \tag{3.56}$$

and

$$\frac{\overline{\Delta\theta}}{\overline{\Delta\delta}} = \frac{N_\delta^\theta(s)}{\Delta_{\text{long}}} = \frac{A_\theta s^2 + B_\theta s + C_\theta}{\Delta_{\text{long}}} \tag{3.57}$$

where

$$\Delta_{\text{long}} = As^4 + Bs^3 + Cs^2 + Ds + E$$

The longitudinal functions are presented in Table 3.3.

LATERAL TRANSFER FUNCTIONS. The lateral transfer functions can be derived in a manner identical to that presented for the longitudinal transfer functions. If we take the Laplace transform of the lateral equations given in Table 3.2 and divide through by the control input, we obtain the following equations:

$$\begin{aligned}
&(s - Y_v)\frac{\overline{\Delta v}}{\overline{\Delta\delta}} - g\cos\theta_0\frac{\overline{\Delta\phi}}{\overline{\Delta\delta}} + (u_0 - Y_r)s\frac{\overline{\Delta\psi}}{\overline{\Delta\delta}} = Y_\delta \\
&-L_v\frac{\overline{\Delta v}}{\overline{\Delta\delta}} + (s^2 - L_p s)\frac{\overline{\Delta\phi}}{\overline{\Delta\delta}} - \left(\frac{I_{xz}}{I_x}s^2 + L_r s\right)\frac{\overline{\Delta\psi}}{\overline{\Delta\delta}} = L_\delta \\
&-N_v\frac{\overline{\Delta v}}{\overline{\Delta\delta}} - \left(\frac{I_{xz}}{I_z}s^2 + N_p s\right)\frac{\overline{\Delta\phi}}{\overline{\Delta\delta}} + (s^2 - N_r s)\frac{\overline{\Delta\psi}}{\overline{\Delta\delta}} = N_\delta
\end{aligned} \tag{3.58}$$

where Y_δ, L_δ, etc., and $\overline{\Delta\delta}$ represent either the aileron or rudder derivatives and the corresponding aileron or rudder control deflections. The lateral transfer functions $\overline{\Delta v}/\overline{\Delta\delta}$, $\overline{\Delta\phi}/\overline{\Delta\delta}$ and $\overline{\Delta\psi}/\overline{\Delta\delta}$ can be determined by solving the above equations. The transfer functions will have the following form:

$$\frac{\overline{\Delta v}}{\overline{\Delta\delta}} = \frac{A_v s^3 + B_v s^2 + C_v s + D_v}{(As^4 + Bs^3 + Cs^2 + Ds + E)} \tag{3.59}$$

where the coefficients A_v, B_v, . . . , A, B, . . . and E are functions of the lateral stability derivatives. The transfer function $\overline{\Delta v}/\overline{\Delta\delta_a}$ is obtained from Table 3.4 by replacing δ with δ_a and the control derivatives by Y_{δ_a}, L_{δ_a} etc. In a similar manner $\overline{\Delta v}/\overline{\Delta\delta_r}$ can be obtained.

no $\dot{w}$ in this table!!

TABLE 3.3
Longitudinal control transfer functions coefficients

	A	*B*	*C*	*D*	*E*
Δ_{long}	1	$-M_q - u_0 M_w - Z_w - X_u$	$-Z_w M_q - u_0 M_w - X_w Z_u + X_u(M_q + u_0 M_w + Z_w)$	$-X_u(Z_w M_q - u_0 M_w) + Z_u(X_w M_q + g M_w) - M_u(u_0 X_w - g)$	$g(Z_u M_w - M_u Z_w)$
N_δ^θ	$M_\delta + Z_\delta M_w$	$X_\delta(Z_u M_w + M_u) + Z_\delta(M_w - X_u M_w) - M_\delta(X_u + Z_w)$	$X_\delta(Z_u M_w - Z_w M_u) + Z_\delta(M_u X_w - M_w X_u) + M_\delta(Z_w X_u - X_w Z_u)$		
N_δ^w	Z_δ	$X_\delta Z_u - Z_\delta(X_u + M_q) + M_\delta u_0$	$X_\delta(u_0 M_u - Z_u M_q) + Z_\delta X_u M_q - u_0 M_\delta X_u$	$g(Z_\delta M_u - M_\delta Z_u)$	
N_δ^u	X_δ	$-X_\delta(Z_w + M_q + u_0 M_w) + Z_\delta X_w$	$X_\delta(Z_w M_q - u_0 M_w) - Z_\delta(X_w M_q + g M_w) + M_\delta(u_0 X_w - g)$	$g(M_\delta Z_w - Z_\delta M_w)$	

TABLE 3.4
Lateral control transfer functions coefficients

	A	*B*	*C*	*D*	*E*
Δ	$1 - \frac{I_{xz}^2}{I_x I_z}$	$-Y_v\left(1 - \frac{I_{xz}^2}{I_x I_z}\right) - L_p - N_r - \frac{I_{xz}}{I_x} N_p - \frac{I_{xz}}{I_z} L_r$	$u_0 N_v + L_p(Y_v + N_r) + N_p\left(\frac{I_{xz}}{I_x} Y_v - L_r\right) + Y_v\left(\frac{I_{xz}}{I_z} L_r + N_r\right) + u_0 \frac{I_{xz}}{I_z} L_v$	$-u_0 N_v L_p + Y_v(N_p L_r - L_p N_r) + u_0 N_p L_v - g\left(L_v + \frac{I_{xz}}{I_x} N_v\right)$	$g(L_v N_r - N_v L_r)$
N_δ^v	$Y_\delta\left(1 - \frac{I_{xz}^2}{I_x I_z}\right)$	$-Y_\delta\left[L_p + N_r + \frac{I_{xz}}{I_x} N_p + \frac{I_{xz}}{I_z} L_r\right] \times u_0\left(\frac{I_{xz}}{I_z} L_\delta + N_\delta\right)$	$Y_\delta(L_p N_r - N_p L_r) + u_0(N_\delta L_p - L_\delta N_p) + g\left(L_\delta + \frac{I_{xz}}{I_x} N_\beta\right)$	$g(N_\delta L_r - L_\delta N_r)$	
N_δ^φ	$L_\delta + \frac{I_{xz}}{I_x} N_\delta$	$Y_\delta\left(L_v + \frac{I_{xz}}{I_x} N_v\right) - L_\delta(N_r + Y_v) + N_\delta\left(L_r - \frac{I_{xz}}{I_x} Y_v\right)$	$Y_\delta(L_r N_v - L_v N_r) + L_\delta(Y_v N_r + u_0 N_v) - N_\delta(u_0 L_v + Y_v L_r)$		
N_δ^r	$N_\delta + \frac{I_{xz}}{I_z} L_\delta$	$Y_\delta\left(N_v + \frac{I_{xz}}{I_z} L_v\right) + L_\delta\left(N_p - \frac{I_{xz}}{I_z} Y_v\right) - N_\delta(Y_v + L_p)$	$Y_\delta(L_v N_p - N_v L_p) - L_\delta Y_v N_p + N_\delta Y_v L_p$	$g(L_\delta N_v - N_\delta L_v)$	

3.7 AERODYNAMIC FORCE AND MOMENT REPRESENTATION

In the previous sections we represented the aerodynamic force and moment contributions by means of the aerodynamic stability coefficients. We did this without explaining the rationale behind the approach.

The method of representing the aerodynamic forces and moments by stability coefficients was first introduced by Bryan over a half century ago [3.1, 3.3]. The technique proposed by Bryan assumes that the aerodynamic forces and moments can be expressed as a function of the instantaneous values of the perturbation variables. The perturbation variables are the instantaneous changes from the reference conditions of the translational velocities, angular velocities, control deflection, and their derivatives. With this assumption, we can express the aerodynamic forces and moments by means of a Taylor series expansion of the perturbation variables about the reference equilibrium condition. For example, the change in the force in the x direction can be expressed as follows:

$$\Delta X(u, \dot{u}, w, \dot{w}, \ldots, \delta_e, \dot{\delta}_e) = \frac{\partial X}{\partial u}\Delta u + \frac{\partial X}{\partial \dot{u}}\Delta \dot{u} + \cdots \frac{\partial X}{\partial \delta_e}\Delta \delta_e + \text{H.O.T.} \quad (3.60)$$

The term $\partial X/\partial u$ is called the stability derivative and is evaluated at the reference flight condition.

The contribution of the change in the velocity u to the change ΔX in the X force is just $(\partial X/\partial u)\,\Delta u$. We can also express $\partial X/\partial u$ in terms of the stability coefficient C_x as follows:

$$\frac{\partial X}{\partial u} = C_{x_u}\frac{1}{2}\rho S \quad (3.61)$$

where

$$C_{x_u} = \frac{\partial C_x}{\partial (u/u_0)} \quad (3.62)$$

Note that the stability derivative has dimensions, whereas the stability coefficient is defined so that it is nondimensional.

The preceding discussion may seem as though we are making the aerodynamic force and moment representation extremely complicated. However, by making use of the assumption that the perturbations are small, we only need to retain the linear terms in Eq. (3.60). Even though we have retained only the linear terms, the expressions may still include numerous first order terms. Fortunately, many of these terms can also be neglected because their contribution to a particular force or moment is negligible. For example, we have examined the pitching moment in detail in Chapter 2. If we express the pitching moment in terms of the perturbation variables, as indicated below,

$$M(u, v, w, \dot{u}, \dot{v}, \dot{w}, p, q, r, \delta_a, \delta_e, \delta_r) = \frac{\partial M}{\partial u}\Delta u + \frac{\partial M}{\partial v}\Delta v + \frac{\partial M}{\partial w}\Delta w + \cdots + \frac{\partial M}{\partial p}\Delta p + \cdots \quad (3.63)$$

it should be quite obvious that terms such as $(\partial M/\partial v)\,\Delta v$ and $(\partial M/\partial p)\,\Delta p$ are not going to be significant for an airplane. Therefore, we can neglect these terms in our analysis.

In the following sections, we shall use the stability derivative approach to represent the aerodynamic forces and moments acting on the airplane. The expressions developed for each of the forces and moments will only include the terms that are usually important in studying the airplane's motion. The remaining portion of this chapter is devoted to presentation of methods for predicting the longitudinal and lateral stability coefficients. We will confine our discussion to methods which are applicable to subsonic flight speeds. Note that many of the stability coefficients vary significantly with Mach number. This can be seen by examining the data on the A-4D airplane in the Appendix or by examining Fig. 3.6.

We have developed a number of relationships for estimating the various stability coefficients; for example, expressions for some of the static stability coefficients such as C_{m_α}, C_{n_β} and C_{l_β} were formulated in Chapter 2. Developing prediction methods for all of the stability derivatives necessary for performing vehicle motion analysis would be beyond the scope of this book. Therefore, we shall confine our attention to the development of several important dynamic derivatives and simply refer the reader to Ref. 3.4, the *US Air Force Stability and Control DATCOM*. This report is a comprehensive collection of aerodynamic stability and control prediction techniques which is widely used through the aviation industry.

Variation of Selected Longitudinal and Lateral Stability Derivatives

Symbol	Derivative	Variation with Mach Number
C_{m_α}	$\frac{\partial C_m}{\partial \alpha}$	$-C_{m_\alpha}$ vs M_0
$C_{m_{\dot{\alpha}}}$	$\frac{\partial C_m}{\partial \left(\frac{\dot{\alpha}\bar{c}}{2u_0}\right)}$	$-C_{m_{\dot{\alpha}}}$ vs M_0
C_{m_q}	$\frac{\partial C_m}{\left(\frac{q\bar{c}}{2u_0}\right)}$	$-C_{m_q}$ vs M_0

Symbol	Derivative	Variation with Mach Number
C_{n_β}	$\frac{\partial C_n}{\partial \beta}$	C_{n_β} vs M_0
C_{n_r}	$\frac{\partial C_n}{\partial \left(\frac{rb}{2u_0}\right)}$	$-C_{n_r}$ vs M_0
C_{l_β}	$\frac{\partial C_l}{\partial \beta}$	$-C_{l_\beta}$ vs M_0
C_{l_p}	$\frac{\partial C_l}{\partial \left(\frac{pb}{2u_0}\right)}$	$-C_{l_p}$ vs M_0

FIGURE 3.6
Variation of selected longitudinal and lateral derivatives with Mach number.

DERIVATIVES DUE TO THE CHANGE IN FORWARD SPEED. The drag, lift and pitching moment vary with changes in the airplane's forward speed. In addition the thrust of the airplane is also a function of the forward speed. The aerodynamic and propulsive forces acting on the airplane along the X body axes are the drag force and the thrust. The change in the X force i.e. ΔX due to a change in forward speed can be expressed as

$$\Delta X = \frac{\partial X}{\partial u}\Delta u = -\frac{\partial D}{\partial u}\Delta u + \frac{\partial T}{\partial u}\Delta u \tag{3.64}$$

or

$$\frac{\partial X}{\partial u} = -\frac{\partial D}{\partial u} + \frac{\partial T}{\partial u} \tag{3.65}$$

The derivative $\partial X/\partial u$ is called the speed damping derivative. Equation (3.65) can be rewritten as

$$\frac{\partial X}{\partial u} = -\frac{\rho S}{2}\left(u_0^2\frac{\partial C_D}{\partial u} + 2u_0 C_{D_0}\right) + \frac{\partial T}{\partial u} \tag{3.66}$$

where the subscript 0 indicates the reference condition. Expressing $\partial X/\partial u$ in coefficient form yields.

$$C_{X_u} = -[C_{D_u} + 2C_{D_0}] + [C_{T_u} + 2C_{T_0}] \tag{3.67}$$

where

$$C_{D_u} = \frac{\partial C_D}{\partial (u/u_0)} \quad \text{and} \quad C_{T_u} = \frac{\partial C_T}{\partial (u/u_0)} \tag{3.68}$$

are the changes in drag and thrust coefficient with forward speed. These coefficients have been made nondimensional by differentiating with respect to (u/u_0). The coefficient C_{D_u} can be estimated from a plot of the drag coefficient versus Mach number.

$$C_{D_u} = \mathbf{M}\frac{\partial C_D}{\partial \mathbf{M}} \tag{3.69}$$

where $\mathbf{M}$ is the Mach number of interest. The thrust term C_{T_u} is zero for gliding flight and is also a good approximation for jet powered aircraft. For a variable pitch propeller and piston engine power plant, C_{T_u} can be approximated by assuming it to be equal to the negative of the reference drag coefficient (i.e. $C_{T_u} = -C_D$).

The change in the Z force with respect to forward speed can be shown to be

$$\frac{\partial Z}{\partial u} = -\tfrac{1}{2}\rho S u_0[C_{L_u} + 2C_{L_0}] \tag{3.70}$$

or in coefficient form

$$C_{Z_u} = -[C_{L_u} + 2C_{L_0}] \tag{3.71}$$

The coefficient C_{L_u} arises from the change in lift coefficient with Mach number. C_{L_u} can be estimated from the Prandtl-Glauert formula which corrects the incompressible lift coefficient for Mach number effects.

$$C_L = \frac{C_L|_{M=0}}{\sqrt{1-\mathbf{M}^2}} \tag{3.72}$$

Differentiating the lift coefficient with respect to Mach number yields

$$\frac{\partial C_L}{\partial \mathbf{M}} = \frac{\mathbf{M}}{1-\mathbf{M}^2}C_L \tag{3.73}$$

but

$$C_{L_u} = \frac{\partial C_L}{\partial (u/u_0)} = \frac{u_0}{a}\frac{\partial C_L}{\partial\left(\frac{u}{a}\right)}. \tag{3.74}$$

$$= \mathbf{M}\frac{\partial C_L}{\partial \mathbf{M}} \tag{3.75}$$

where a is the speed of sound.

C_{L_u} can therefore be expressed as

$$C_{L_u} = \frac{\mathbf{M}^2}{1-\mathbf{M}^2}C_{L_0} \tag{3.76}$$

This coefficient can be neglected at low flight speeds but can become quite large near the critical Mach number for the airplane.

The change in the pitching moment due to variations in the forward speed can be expressed as

$$\Delta M = \frac{\partial M}{\partial u}\Delta u \tag{3.77}$$

or

$$\frac{\partial M}{\partial u} = C_{m_u}\rho S\bar{c}u_0 \tag{3.78}$$

The coefficient C_{m_u} can be estimated as follows.

$$C_{m_u} = \frac{\partial C_m}{\partial \mathbf{M}}\mathbf{M} \tag{3.79}$$

The coefficient C_{m_u} depends upon Mach number but is also affected by the elastic properties of the airframe. At high speeds aeroelastic bending of the airplane can cause large changes in the magnitude of C_{m_u}.

DERIVATIVES DUE TO PITCHING VELOCITY q. The stability coefficients C_{z_q} and C_{m_q} represent the change in the Z force and pitching moment coefficients with respect to the pitching velocity q. The aerodynamic characteristics of both the wing and horizontal tail are affected by the pitching motion

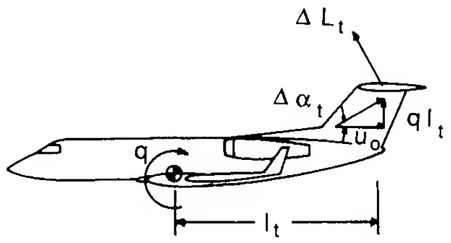

FIGURE 3.7
Mechanism for aerodynamic force due to pitch rate.

of the airplane. The wing contribution is usually quite small in comparison to that produced by the tail. A common practice is to compute the tail contribution and then increase it by 10 percent to account for the wing. Figure 3.7 is a sketch of an airplane undergoing a pitching motion.

As illustrated in Fig. 3.7, the pitching rate q causes a change in the angle of attack at the tail, which results in a change in the lift force acting on the tail:

$$\Delta L_t = C_{L_{\alpha_t}} \Delta\alpha_t \, Q_t S_t \tag{3.80}$$

or

$$\Delta Z = -\Delta L_t = -C_{L_{\alpha_t}} \frac{q l_t}{u_0} Q_t S_t \tag{3.81}$$

$$C_Z = \frac{Z}{Q_w S} \tag{3.82}$$

$$\Delta C_Z = -C_{L_{\alpha_t}} \frac{q l_t}{u_0} \eta \frac{S_t}{S} \tag{3.83}$$

$$C_{Zq} \equiv \frac{\partial C_z}{\partial (q\bar{c}/2u_0)} = \frac{2u_0}{\bar{c}} \frac{\partial C_z}{\partial q} \tag{3.84}$$

$$C_{Zq} = -2C_{L_{\alpha_t}} \eta V_H \tag{3.85}$$

The pitching moment due to the change in lift on the tail can be calculated as follows:

$$\Delta M_{cg} = -l_t \, \Delta L_t \tag{3.86}$$

$$\Delta C_{mcg} = -V_H \eta C_{L_{\alpha_t}} \frac{q l_t}{u_0} \tag{3.87}$$

$$C_{m_q} \equiv \frac{\partial C_m}{\partial (q\bar{c}/2u_0)} = \frac{2u_0}{\bar{c}} \frac{\partial C_m}{\partial q} \tag{3.88}$$

$$C_{m_q} = -2C_{L_{\alpha_t}} \eta V_H \frac{l_t}{\bar{c}} \tag{3.89}$$

Equations (3.85) and (3.89) represent the tail contribution to C_{z_q} and C_{m_q} respectively. The coefficients for the complete airplane are obtained by

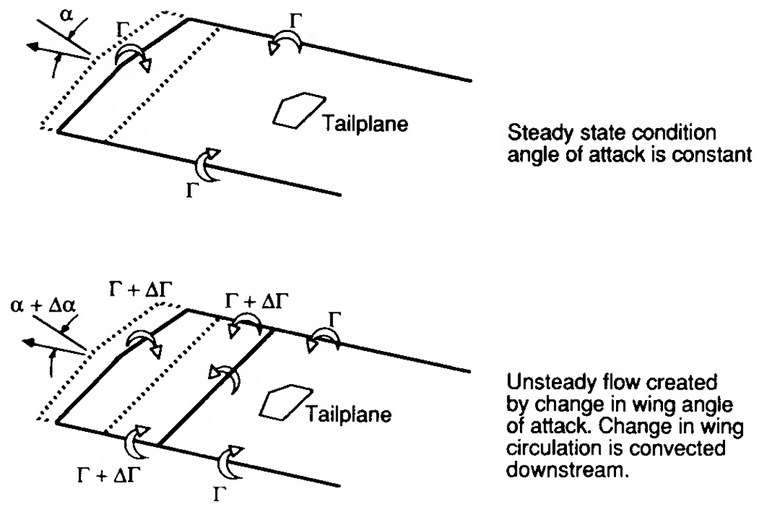

FIGURE 3.8
Mechanism for aerodynamic force due to the lag in flow field development.

increasing the tail values by 10 percent to account for the wing and fuselage contributions.

DERIVATIVES DUE TO THE TIME RATE OF CHANGE OF THE ANGLE OF ATTACK. The stability coefficients $C_{z_{\dot\alpha}}$ and $C_{m_{\dot\alpha}}$ arise because of the lag in the wing downwash getting to the tail. As the wing angle of attack changes, the circulation around the wing will be altered. The change in circulation alters the downwash at the tail; however, it takes a finite time for the alteration to occur. Figure 3.8 illustrates the lag in flow field development. If the airplane is traveling with a forward velocity u_0, then a change in circulation imparted to the trailing vortex wake will take the increment in time $\Delta t = l_t/u_0$ to reach the tail surface.

The lag in angle of attack at the tail can be expressed as:

$$\Delta\alpha_t = \frac{d\varepsilon}{dt} \Delta t \tag{3.90}$$

where

$$\Delta t = l_t/u_0 \tag{3.91}$$

or

$$\Delta\alpha_t = \frac{d\varepsilon}{dt} \frac{l_t}{u_0} = \frac{d\varepsilon}{d\alpha} \frac{d\alpha}{dt} \frac{l_t}{u_0} \tag{3.92}$$

$$\Delta\alpha_t = \frac{d\varepsilon}{d\alpha} \dot\alpha \frac{l_t}{u_0} \tag{3.93}$$

$$\Delta L_t = C_{L_{\alpha_t}} \Delta\alpha_t \, Q_t S_t \tag{3.94}$$

$$\Delta C_z = -\frac{\Delta L_t}{Q_w S} = -C_{L_{\alpha_t}} \Delta\alpha_t \eta \frac{S_t}{S} \tag{3.95}$$

$$= -C_{L_\alpha} \frac{\mathrm{d}\varepsilon}{\mathrm{d}\alpha} \frac{\dot{\alpha} l_t}{u_0} \eta \frac{S_t}{S} \tag{3.96}$$

$$C_{z_{\dot{\alpha}}} = \frac{\partial C_z}{\partial(\dot{\alpha}\bar{c}/2u_0)} = \frac{2u_0}{\bar{c}} \frac{\partial C_z}{\partial \dot{\alpha}} \tag{3.97}$$

$$C_{z_{\dot{\alpha}}} = -2V_H \eta C_{L_{\alpha_t}} \frac{\mathrm{d}\varepsilon}{\mathrm{d}\alpha} \tag{3.98}$$

The pitching moment due to the lag in the downwash field can be calculated as follows:

$$\Delta M_{cg} = -l_t \Delta L_t = -l_t C_{L_{\alpha_t}} \Delta\alpha_t Q_t S_t \tag{3.99}$$

$$\Delta C_{m_{cg}} = -V_H \eta C_{L_{\alpha_t}} \frac{\mathrm{d}\varepsilon}{\mathrm{d}\alpha} \dot{\alpha} \frac{l_t}{u_0} \tag{3.100}$$

$$C_{m_{\dot{\alpha}}} = \frac{\partial C_m}{\partial(\dot{\alpha}\bar{c}/2u_0)} = \frac{2u_0}{\bar{c}} \frac{\partial C_m}{\partial \dot{\alpha}} \tag{3.101}$$

$$C_{m_{\dot{\alpha}}} = -2C_{L_{\alpha_t}} \eta V_H \frac{l_t}{\bar{c}} \frac{\mathrm{d}\varepsilon}{\mathrm{d}\alpha} \tag{3.102}$$

Equations (3.99) and (3.102) yield only the tail contribution to these stability coefficients. To obtain an estimate for the complete airplane these coefficients are increased by 10 percent.

The stability coefficients C_{l_p}, C_{n_r}, C_{z_q}, C_{m_q}, $C_{z_{\dot{\alpha}}}$, and $C_{m_{\dot{\alpha}}}$ all oppose the motion of the vehicle and thus can be considered as damping terms. This will become more apparent as we analyze the motion of an airplane in Chapters 4 and 5.

As noted earlier, there are many more derivatives for which we could develop prediction methods. The few simple examples presented here should give the reader an appreciation of how one would go about determining estimates of the aerodynamic stability coefficients. A summary of some of the theoretical prediction methods for some of the more important longitudinal and lateral stability coefficients is presented in Tables 3.5 and 3.6.

3.8 SUMMARY

The nonlinear differential equations of motion of a rigid airplane were developed from Newton's second law of motion. Linearization of these equations was accomplished using small-disturbance theory. In following chapters we shall solve the linearized equations of motion. These solutions will yield valuable information on the dynamic characteristics of airplane motions.

TABLE 3.5
Equations for estimating the longitudinal stability coefficients

	X-force derivatives	*Z*-force derivatives	Pitching moment derivatives
u	$C_{X_u} = -[C_{D_u} + 2C_{D_0}] + C_{T_u}$	$C_{Z_u} = -\frac{M^2}{1-M^2} C_{L_0} - 2C_{L_0}$	$C_{m_u} = \frac{\partial C_m}{\partial M} M_0$
α	$C_{X_\alpha} = C_{L_0} - \frac{2C_{L_0}}{\pi e} \frac{C_{L_\alpha}}{AR}$	$C_{Z_\alpha} = -(C_{L_\alpha} + C_{D_0})$	$C_{m_\alpha} = C_{L_{\alpha_w}} \left(\frac{X_{cg}}{\bar{c}} - \frac{X_{ac}}{\bar{c}} \right) + C_{m_{\alpha_{fus}}} - \eta V_H C_{L_{\alpha_t}} \left(1 - \frac{\mathrm{d}\varepsilon}{\mathrm{d}\alpha} \right)$
$\dot{\alpha}$	0	$C_{Z_{\dot{\alpha}}} = -2\eta C_{L_{\alpha_t}} V_H \frac{\mathrm{d}\varepsilon}{\mathrm{d}\alpha}$	$C_{m_{\dot{\alpha}}} = -2\eta C_{L_{\alpha_t}} V_H \frac{l_t}{\bar{c}} \frac{\mathrm{d}\varepsilon}{\mathrm{d}\alpha}$
q	0	$C_{Z_q} = -2\eta C_{L_{\alpha_t}} V_H$	$C_{m_q} = -2\eta C_{L_{\alpha_t}} V_H \frac{l_t}{\bar{c}}$
δ_e	0	$C_{Z_{\delta_e}} = -C_{L_{\delta_e}} = -\frac{S_t}{S} \eta \frac{\mathrm{d}C_{L_t}}{\mathrm{d}\delta_e}$	$C_{m_{\delta_e}} = -\eta V_H \frac{\mathrm{d}C_{L_t}}{\mathrm{d}\delta_e}$

* Subscript 0 indicates reference values and M is the Mach number.

AR	Aspect ratio	S	Wing area
b	Wing span	S_t	Horizontal tail area
C_{D_0}	Reference drag coefficient	S_v	Vertical tail area
C_{L_0}	Reference lift coefficient	z_v	Distance from center of pressure of vertical tail to fuselage centerline
C_{L_α}	Airplane lift curve slope	Γ	Wing dihedral angle
$C_{L_{\alpha_w}}$	Wing lift curve slope	Λ	Wing sweep angle
$C_{L_{\alpha_t}}$	Tail lift curve slope	$\frac{\mathrm{d}\varepsilon}{\mathrm{d}\alpha}$	Change in downwash due to a change in angle of attack
$\bar{c}$	Mean aerodynamic chord	η	Efficiency factor of the horizontal tail
e	Oswald's span efficiency factor	η_v	Efficiency factor of the vertical tail
l_t	Distance from c.g. to tail quarter chord	λ	Taper ratio (tip chord/root chord)
l_v	Distance from c.g. to vertical tail aerodynamic center	$\frac{\mathrm{d}\sigma}{\mathrm{d}\beta}$	Change in sidewash angle with a change in side slip angle
V_H	Horizontal tail volume ratio		
V_v	Vertical tail volume ratio		
M	Flight mach number		

TABLE 3.6
Equations for estimating the lateral stability coefficients

	Y-force derivatives	Yawing moment derivatives	Rolling moment derivatives
β	$C_{y_\beta} = -\eta_v \frac{S_v}{S} C_{L_{\alpha_v}} \left(1 + \frac{d\sigma}{d\beta}\right)$	$C_{n_\beta} = C_{n_{\beta_{fus}}} + \eta_v V_v C_{L_{\alpha_v}} \left(1 + \frac{d\sigma}{d\beta}\right)$	$C_{l_\beta} = \left(\frac{C_{l_\beta}}{\Gamma}\right)\Gamma + \Delta C_{l_\beta}$ (see Fig. 3.9)
p	$C_{y_p} = C_L \frac{AR + \cos\Lambda}{AR + 4\cos\Lambda} \tan\Lambda$	$C_{n_p} = -\frac{C_L}{8}$	$C_{l_p} = -\frac{C_{L_\alpha}}{12} \frac{1+3\lambda}{1+\lambda}$
r	$C_{y_r} = -2\left(\frac{l_v}{b}\right)(C_{Y_\beta})_{tail}$	$C_{n_r} = -2\eta_v V_v \left(\frac{l_v}{b}\right) C_{L_{\alpha_v}}$	$C_{l_r} = \frac{C_L}{4} - 2\frac{l_v}{b}\frac{z_v}{b} C_{y_{\beta_{tail}}}$
δ_a	0	$C_{n_{\delta_a}} = 2KC_{L_0}C_{l_{\delta_a}}$ (see Fig. 3.10)	$C_{l_{\delta_a}} = \frac{2C_{L_\alpha}\tau}{Sb}\int_{y_1}^{y_2} cy\, dy$
δ_r	$C_{y_{\delta_r}} = \frac{S_v}{S}\tau C_{L_{\alpha_v}}$	$C_{n_{\delta_r}} = -V_v\eta_v\tau C_{L_{\alpha_v}}$	$C_{l_{\delta_r}} = \frac{S_v}{S}\left(\frac{z_v}{b}\right)\tau C_{L_{\alpha_v}}$

AR	Aspect ratio	S	Wing area
b	Wing span	S_t	Horizontal tail area
C_{D_0}	Reference drag coefficient	S_v	Vertical tail area
C_{L_0}	Reference lift coefficient	z_v	Distance from center of pressure of vertical tail to fuselage centerline
C_{L_α}	Airplane lift curve slope	Γ	Wing dihedral angle
$C_{L_{\alpha_w}}$	Wing lift curve slope	Λ	Wing sweep angle
$C_{L_{\alpha_t}}$	Tail lift curve slope	$\frac{d\varepsilon}{d\alpha}$	Change in downwash due to a change in angle of attack
$\bar{c}$	Mean aerodynamic chord	η	Efficiency factor of the horizontal tail
e	Oswald's span efficiency factor	η_v	Efficiency factor of the vertical tail
l_t	Distance from c.g. to tail quarter chord	λ	Taper ratio (tip chord/root chord)
l_v	Distance from c.g. to vertical tail aerodynamic center	$\frac{d\sigma}{d\beta}$	Change in sidewash angle with a change in side slip angle
V_H	Horizontal tail volume ratio		
V_v	Vertical tail volume ratio		
M	Flight mach number		

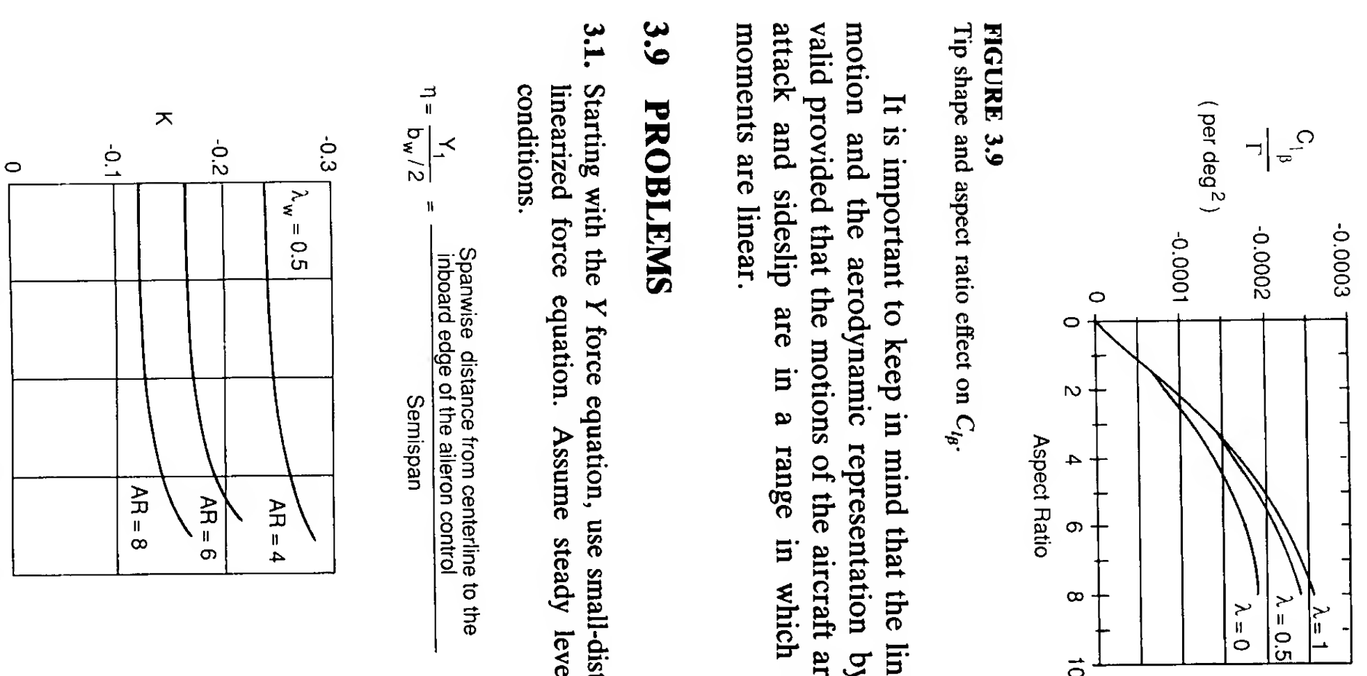

FIGURE 3.9
Tip shape and aspect ratio effect on C_{l_β}.

It is important to keep in mind that the linearization of the equations of motion and the aerodynamic representation by stability derivatives is only valid provided that the motions of the aircraft are small and that the angles of attack and sideslip are in a range in which the aerodynamic forces and moments are linear.

3.9 PROBLEMS

3.1. Starting with the Y force equation, use small-disturbance theory to determine the linearized force equation. Assume steady level flight for the reference flight conditions.

FIGURE 3.10
Empirical factor for $C_{n_{\delta_a}}$ estimate.

3.2. Starting with the Z force equation, use small-disturbance theory to determine the linearized force equations. Assume steady level flight for the reference flight conditions.

3.3. Repeat Problem 3.2 assuming the airplane is experiencing a steady pull up maneuver, i.e. $q_0 = \text{constant}$.

3.4. Using the geometric data given below and in Figure P3.4, estimate C_{m_α}, $C_{m_{\dot\alpha}}$, C_{m_q} and $C_{m_{\delta_e}}$.

Geometric Data

$S = 232\ \text{ft}^2$ $\quad b = 36$
$S_H = 54\ \text{ft}^2$ $\quad l_t = 21\ \text{ft}$
$S_v = 37.4\ \text{ft}^2$ $\quad l_v = 18.5\ \text{ft}$
$\Gamma = 2.5°$

Assume

Wing: $C_{L_{\alpha_w}} = 0.1/\text{deg}$ $\quad C_{m_{a_{c_w}}} = -0.02$
$\alpha_{0_L} = -1.0°$
tail: $C_{L_{\alpha_t}} = 0.1/\text{deg}$ $\quad C_{m_{a_{c_t}}} = 0.00$
$\alpha_{0_L} = 0°$

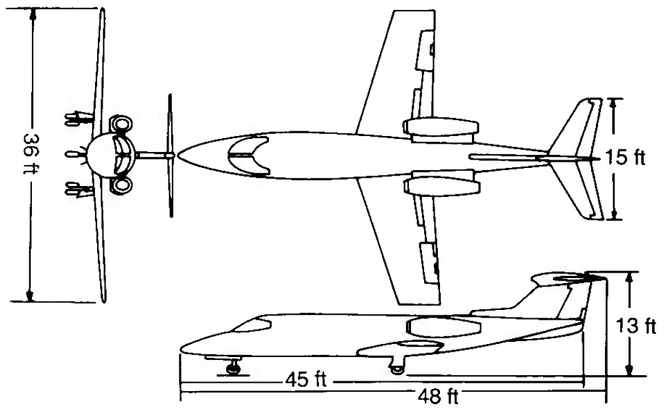

FIGURE P3.4a
Three view sketch of a Business jet.

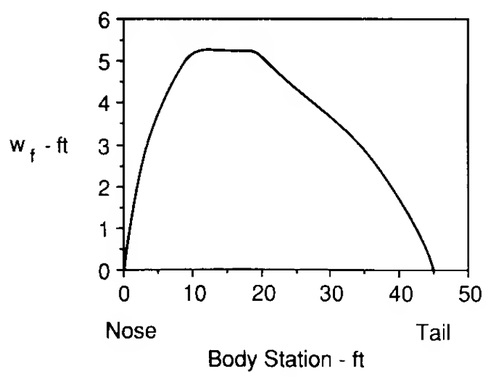

FIGURE P3.4b
Aircraft fuselage width as a function of body station.

3.5. Estimate C_{l_p} and C_{n_r} for the airplane described in Problem 3.4.

3.6. Develop an expression for the yaw moment due to yaw rate, C_{n_r}. Consider only the vertical tail in your analysis.

3.7. Develop an expression for C_{m_q} due to a canard surface.

3.8. Estimate C_{y_β}, C_{n_β} and C_{n_r} for the Boeing 747 at subsonic speeds. Compare your predictions with the data in the Appendix.

3.9. Explain why deflecting the ailerons produces a yawing moment.

REFERENCES

3.1. McRuer, D., I. Ashkemas, and D. Graham, *Aircraft Dynamics and Automatic Control,* Princeton University Press, Princeton, NJ, 1973.
3.2. Bryan, G. H., and W. E. Williams: "The Longitudinal Stability of Aerial Gliders," *Proceedings of the Royal Society of London, Series A,* Vol. 73, pp. 110–116, 1904.
3.3. Bryan, G. H.: *Stability in Aviation,* Macmillan, London, England, 1911.
3.4. *USAF Stability and Control DATCOM,* Flight Control Division, Air Force Flight Dynamics Laboratory, Wright-Patterson Air Force Base, Oh.
3.5. Smetana, F. O., D. C. Summey, and W. D. Johnson: *Riding and Handling Qualities of Light Aircraft—A Review and Analysis,* NASA CR-1975, March 1972.

CHAPTER 4

LONGITUDINAL MOTION (STICK FIXED)

"The equilibrium and stability of a bird in flight, or an aerodome or flying machine, has in the past been the subject of considerable speculation, and no adequate explanation of the principles involved has hitherto been given".
From Frederick W. Lanchester's book *Aerodonetics* published in 1908 in which he develops an elementary theory of longitudinal dynamic stability. [4.1]

4.1 HISTORICAL PERSPECTIVE

The theoretical basis for the analysis of flight vehicle motions developed almost concurrently with the successful demonstration of a powered flight of a man-carrying airplane. As early as 1897, Frederick Lanchester was studying the motion of gliders. He conducted experiments with hand-launched gliders and found that his gliders would fly along a straight path if they were launched at what he called the glider's "natural speed". Launching the glider at a higher or lower speed would result in an oscillatory motion. He also noticed that, if the glider were launched at its "natural speed" and then disturbed from its flight path, the glider would start oscillating along its flight trajectory. What Lanchester had discovered was that all flight vehicles possess certain natural frequencies or motions when disturbed from their equilibrium flight.

Lanchester called the oscillatory motion the phugoid motion. He wanted to use the Greek word meaning "to fly" to describe his newly discovered motion; actually, phugoid, literally means "to flee". Today, we still use the term "phugoid" to describe the long-period slowly damped oscillation associated with the longitudinal motion of an airplane.

The mathematical treatment of flight vehicle motions was first developed by G. H. Bryan. He was aware of Lanchester's experimental observations and

set out to develop the mathematical equations for dynamic stability analysis. His stability work was published in 1911. Bryan made significant contributions to the analysis of vehicle flight motions. He laid the mathematical foundation for airplane dynamic stability analysis, developed the concept of the aerodynamic stability derivative, and recognized that the equations of motion could be separated into a symmetric longitudinal motion and an unsymmetric lateral motion. Although the mathematical treatment of airplane dynamic stability was formulated shortly after the first successful human-controlled flight, the theory was not used by the inventors because of its mathematical complexity and the lack of information on the stability derivatives.

Experimental studies were initiated by L. Bairstow and B. M. Jones of the National Physical Laboratory (NPL) in England, and by Jerome Hunsaker of the Massachusetts Institute of Technology (MIT) to determine estimates of the aerodynamic stability derivatives used in Bryan's theory. In addition to determining stability derivatives from wind-tunnel tests of scale models, Bairstow and Jones nondimensionalized the equations of motion and showed that, with certain assumptions, there were two independent solutions, i.e. one longitudinal and one lateral. During the same period, Hunsaker and his group at MIT were conducting wind-tunnel studies of scale models of several flying airplanes. The results from these early studies were extremely valuable in establishing relationships between aerodynamics, geometric and mass characteristics of the airplane and its dynamic stability.[1]

Although these early investigators could predict the stability of the longitudinal and lateral motions, they were unsure how to interpret their findings. They were perplexed by the fact that when their analysis predicted an airplane would be unstable, the airplane was flown successfully. They wondered how the stability analysis could be used to assess whether an airplane was of good or bad design. The missing factor in analyzing airplane stability in these early studies was the failure to consider the pilot as an essential part of the airplane system.

In the late 1930s the National Advisory Committee of Aeronautics (NACA) conducted an extensive flight test program. Many airplanes were tested with the goal of quantitatively relating the measured dynamic characteristics of the airplane with the pilot's opinion of its handling characteristics. These experiments laid the foundation for modern flying qualities research. In 1943, R. Gilruth published the results of the NACA research program in the form of flying qualities' specifications. For the first time, the designer had a list of specifications which could be used in designing the airplane. If the design complied with the specifications, one could be reasonably sure that the airplane would have good flying qualities [4.1–4.4].

In this chapter we shall examine the longitudinal motion of an airplane

[1] The first technical report by the National Advisory Committee of Aeronautics, NACA (forerunner of the National Aeronautics and Space Administration, (NASA)), summarizes the MIT research in dynamic stability.

disturbed from its equilibrium state. Several different analytical techniques will be presented for solving the longitudinal differential equations. Our objectives are for the student to understand the various analytical techniques employed in airplane motion analysis and to develop an appreciation of the importance of aerodynamic or configuration changes on the airplane's dynamic stability characteristics. Later, we shall discuss what constitutes good flying qualities in terms of the dynamic characteristics presented here. Before attempting to solve the longitudinal equations of motion, we will examine the solution of a simplified aircraft motion. By studying the simpler motions with a single degree of freedom, we shall gain some insight into the more complicated longitudinal motions we shall study later in this chapter.

4.2 SECOND-ORDER DIFFERENTIAL EQUATIONS

Many physical systems can be modeled by second-order differential equations. For example, control servomotors, special cases of aircraft dynamics, as well as many electrical and mechanical systems, are governed by second-order differential equations. Because the second-order differential equation plays such an important role in aircraft dynamics we shall examine its characteristics before proceeding with our discussion of aircraft motions.

To illustrate the properties of a second-order differential equation, we shall examine the motion of a mechanical system composed of a mass, a spring, and a damping device. The forces acting on the system are shown in Fig. 4.1. The spring provides a linear restoring force that is proportional to the extension of the spring, and the damping device provides a damping force that is proportional to the velocity of the mass. The differential equation for the system can be written as

$$m\frac{d^2x}{dt^2}+c\frac{dx}{dt}+kx=F(t) \tag{4.1}$$

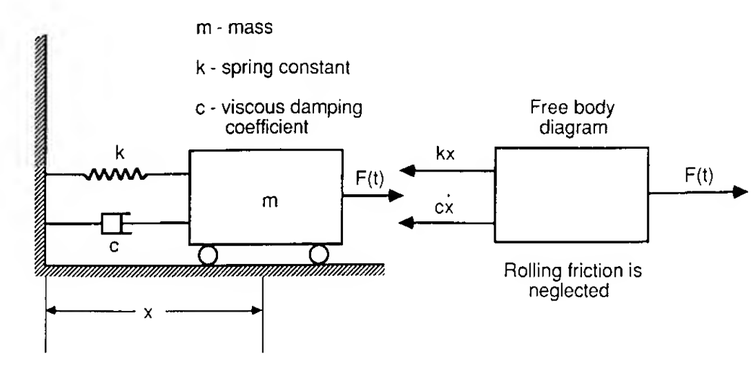

FIGURE 4.1
Sketch of a spring mass damper system.

or

$$\frac{d^2x}{dt^2}+\frac{c}{m}\frac{dx}{dt}+\frac{k}{m}x=\frac{1}{m}F(t) \tag{4.2}$$

This is a nonhomogeneous, second-order differential equation with constant coefficients. The coefficients in the equation are determined from the physical characteristics of the mechanical system being modeled, i.e. its mass, damping coefficient, and spring constant. The function $F(t)$ is called the forcing function. If the forcing function is zero, the response of the system is referred to as the free response. When the system is driven by a forcing function $F(t)$ the response is referred to as the forced response. The general solution of the nonhomogeneous differential equation is the sum of the homogeneous and particular solutions. The homogeneous solution is the solution of the differential equation when the right-hand side of the equation is zero. This corresponds to the free response of the system. The particular solution is a solution which when substituted into the left-hand side of the differential equation yields the nonhomogeneous or right-hand side of the differential equation. In the following section we will restrict our discussion to the solution of the free response or homogeneous equation.

The solution of the differential equation with constant coefficients is found by letting

$$x=Ae^{\lambda t} \tag{4.3}$$

and substituting into the differential equation yields.

$$\lambda^2Ae^{\lambda t}+\frac{c}{m}\lambda Ae^{\lambda t}+\frac{k}{m}Ae^{\lambda t}=0 \tag{4.4}$$

Clearing the equation of $Ae^{\lambda t}$ yields

$$\lambda^2+\frac{c}{m}\lambda+\frac{k}{m}=0 \tag{4.5}$$

which is called the characteristic equation. The roots of the characteristic equation are called the characteristic roots or eigenvalues of the system.

The roots of Eq. (4.5) are

$$\lambda_{1,2}=-\frac{c}{2m}\pm\sqrt{\left(\frac{c}{2m}\right)^2-\frac{k}{m}} \tag{4.6}$$

The solution of the differential equation can now be written as

$$x(t)=C_1e^{\lambda_1 t}+C_2e^{\lambda_2 t} \tag{4.7}$$

where C_1 and C_2 are arbitrary constants that are determined from the initial conditions of the problem. The type of motion that occurs if the system is displaced from its equilibrium position and released depends upon the value of λ. But λ depends upon the physical constants of the problem, namely m, c, and k. We shall consider three possible cases for λ.

When $(c/2m) > \sqrt{k/m}$, the roots are negative and real, which means that the motion will die out exponentially with time. This type of motion is referred to as an overdamped motion. The equation of motion is given by

$$x(t) = C_1 \exp\left[-\frac{c}{2m} + \sqrt{\left(\frac{c}{2m}\right)^2 - \frac{k}{m}}\right]t + C_2 \exp\left[-\frac{c}{2m} - \sqrt{\left(\frac{c}{2m}\right)^2 - \frac{k}{m}}\right]t \tag{4.8}$$

For the case where $(c/2m) < \sqrt{k/m}$, the roots are complex:

$$\lambda = -\frac{c}{2m} \pm i\sqrt{\frac{k}{m} - \left(\frac{c}{2m}\right)^2} \tag{4.9}$$

The equation of motion is as follows:

$$x(t) = \exp\left(-\frac{c}{2m}t\right)\left[C_1 \exp\left(i\sqrt{\frac{k}{m} - \left(\frac{c}{2m}\right)^2}\, t\right) + C_2 \exp\left(-i\sqrt{\frac{k}{m} - \left(\frac{c}{2m}\right)^2}\, t\right)\right] \tag{4.10}$$

which can be rewritten as

$$x(t) = \exp\left(-\frac{c}{2m}t\right)\left[A \cos\left(\sqrt{\frac{k}{m} - \left(\frac{c}{2m}\right)^2}\, t\right) + B \sin\left(\sqrt{\frac{k}{m} - \left(\frac{c}{2m}\right)^2}\, t\right)\right] \tag{4.11}$$

The solution given by Eq. (4.11) is a damped sinusoid having a natural frequency given by

$$\omega = \sqrt{\frac{k}{m} - \left(\frac{c}{2m}\right)^2} \tag{4.12}$$

The last case we consider is when $(c/2m) = \sqrt{k/m}$. This represents the boundary between the overdamped exponential motion and the damped sinusoidal motion. This particular motion is referred to as the critically damped motion. The roots of the characteristic equation are identical, i.e.

$$\lambda_{1,2} = -\frac{c}{2m} \tag{4.13}$$

The general solution for repeated roots has the form

$$x(t) = (C_1 + C_2 t)e^{\lambda t} \tag{4.14}$$

If λ is a negative constant, then $e^{\lambda t}$ will go to zero faster than $C_2 t$ goes to infinity as time increases. Figure 4.2 shows the motion for the three cases analyzed here.

The constant for the critically damped case is called the critical damping constant and is defined as

$$c_{cr} = 2\sqrt{km} \tag{4.15}$$

For oscillatory motion, the damping can be specified in terms of the critical

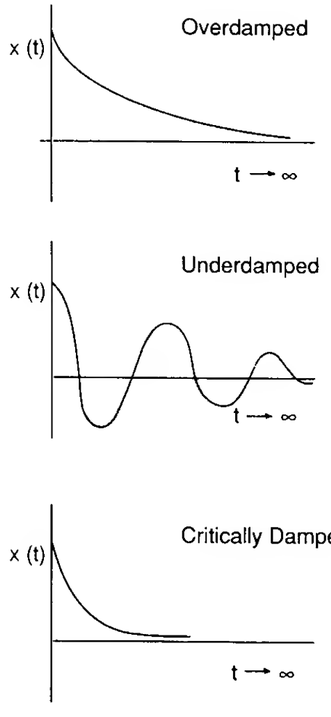

FIGURE 4.2
Typical motions of a dynamic system.

damping:

$$c = \zeta c_{cr} \tag{4.16}$$

where ζ is called the damping ratio,

$$\zeta = \frac{c}{c_{cr}} \tag{4.17}$$

For a system that has no damping, i.e. $c = 0$, which implies that the $\zeta = 0$ the motion is an undamped oscillation. The natural frequency is called the undamped natural frequency and can be obtained from Eq. (4.12) by setting $c = 0$:

$$\omega_n = \sqrt{\frac{k}{m}} \tag{4.18}$$

Since both the damping ratio and undamped natural frequency are specified as functions of the system physical constants, we can rewrite the differential equation in terms of the damping ratio and undamped natural frequency as follows:

$$\frac{d^2x}{dt^2} + 2\zeta\omega_n \frac{dx}{dt} + \omega_n^2 x = f(t) \tag{4.19}$$

Equation (4.19) is referred to as the standard form of a second-order differential equation with constant coefficients. Although we developed the

standard form of a second-order differential equation from a mechanical mass–spring–damper system, the equation could have been developed using any one of an almost limitless number of physical systems. For example, a torsional spring–mass–damper equation of motion is given by

$$\frac{d^2\theta}{dt^2}+\frac{c}{I}\frac{d\theta}{dt}+\frac{k}{I}\theta=f(t) \tag{4.20}$$

where c, k and I are the torsional damping coefficient, torsional spring constant and moment of inertia, respectively.

The characteristic equation for the standard form of the second-order differential equation with constant coefficients can be shown to be

$$\lambda^2+2\zeta\omega_n\lambda+\omega_n^2=0 \tag{4.21}$$

The roots of the characteristic equation are

$$\lambda_{1,2}=-\zeta\omega_n\pm i\omega_n\sqrt{1-\zeta^2} \tag{4.22}$$

or

$$\lambda_{1,2}=\eta\pm i\omega \tag{4.23}$$

where

$$\eta=-\zeta\omega_n \tag{4.24}$$

$$\omega=\omega_n\sqrt{1-\zeta^2} \tag{4.25}$$

The real η of the root governs the damping of the response and ω is the damped natural frequency.

Figure 4.3 shows the relationship between the roots of the characteristic

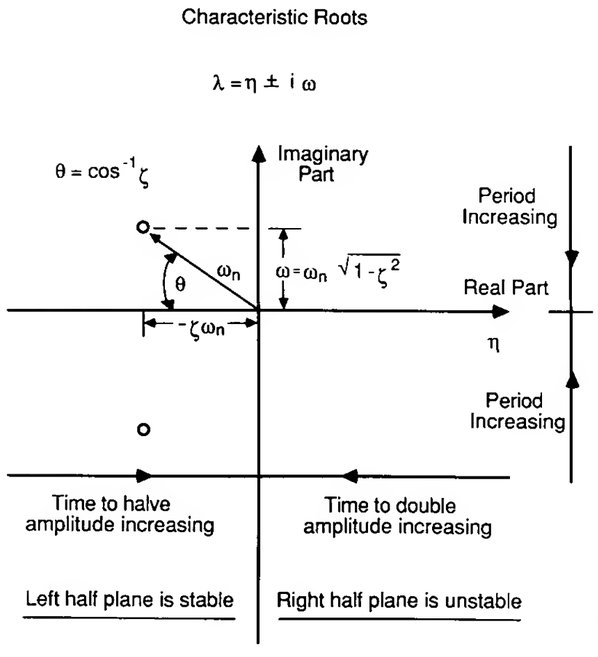

FIGURE 4.3
Relationship between η, ω, ζ and ω_n.

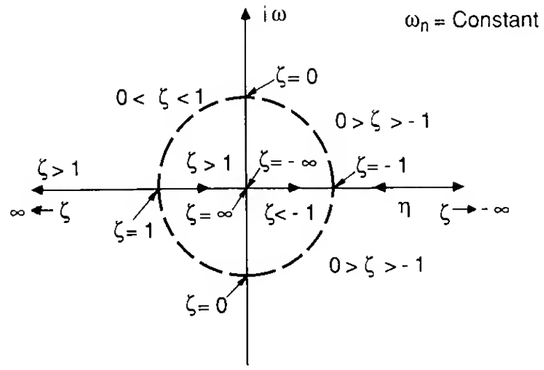

FIGURE 4.4
Variation of roots with damping ratio.

equation and η, ω, ζ and ω_n. When the roots are complex, the radial distance from the origin to the root is the undamped natural frequency. The system damping η is the real part of the complex root and the damped natural frequency is the imaginary part of the root. The damping ratio ζ is equal to the cosine of the angle between the negative real axis and the radial line from the origin to the root:

$$\cos(\pi-\theta)=-\cos\theta=\frac{-\zeta\omega_n}{\omega_n} \tag{4.26}$$

or

$$\zeta=\cos\theta \tag{4.27}$$

The influence of the damping ratio on the roots of the characteristic equation can be examined by holding the undamped natural frequency constant and varying ζ from $-\infty$ to ∞ as shown in Fig. 4.4. The response of the homogeneous equation to a displacement from its equilibrium condition can take on many forms depending upon the magnitude of the damping ratio. The classification of the response is given in Table 4.1.

TABLE 4.1
Variation of response with damping ratio

Magnitude of damping ratio	Type of root	Time response
$\zeta<-1$	Two positive real distinct roots	Exponentially growing motion
$0>\zeta>-1$	Complex roots with positive real part	Exponentially growing sinusoidal motion
$\zeta=0$	Complex roots with real part zero	Undamped sinusoidal motion Pure harmonic motion
$0<\zeta<1$	Complex roots with real part negative	Underdamped exponentially decaying sinusoidal motion
$\zeta=1$	Two negative equal real roots	Critically damped exponentially decaying motion
$\zeta>1$	Two negative distinct real roots	Overdamped exponentially decaying motion

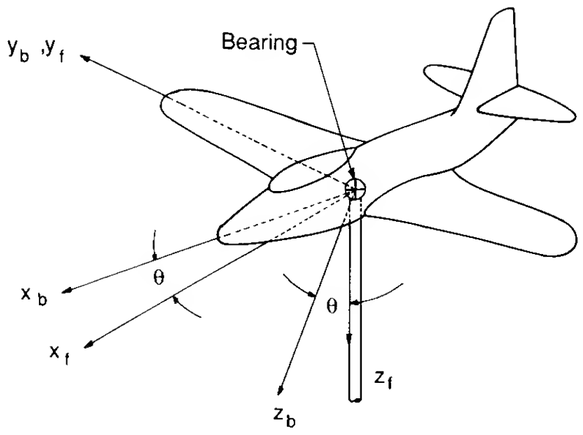

FIGURE 4.5
A model constrained to a pure pitching motion.

4.3 PURE PITCHING MOTION

Consider the case in which the airplane's center of gravity is constrained to move in a straight line at constant speed but the aircraft is free to pitch about its center of gravity. Figure 4.5 is the sketch of a wind-tunnel model constrained so that it can perform only in a pitching motion.

The equation of motion can be developed from the rigid body equations developed in Chapter 3 by making the appropriate assumptions. However, to aid our understanding of this simple motion, we shall rederive the governing equation from first principles. The equation governing this motion is obtained from Newton's second law:

$$\sum \text{Pitching moments} = \sum M_{cg} = I_y \ddot{\theta} \tag{4.28}$$

The pitching moment M and pitch angle θ can be expressed in terms of an initial reference value indicated by a subscript (0) and the perturbation by the Δ symbol.

$$M = M_0 + \Delta M \tag{4.29}$$

$$\theta = \theta_0 + \Delta\theta \tag{4.30}$$

Equation (4.28) then reduces to

$$\Delta M = I_y \, \Delta\ddot{\theta} \tag{4.31}$$

For the restricted motion that we are examining, the variables are the angle of attack, pitch angle, the time rate of change of these variables, and the elevator angle. The pitching moment is not a function of the pitch angle but is a function of the other variables and can be expressed in functional form as follows:

$$\Delta M = \text{fn}(\Delta\alpha, \Delta\dot{\alpha}, \Delta q, \Delta\delta_e) \tag{4.32}$$

Equation (4.32) can be expanded in terms of the perturbation variables by

means of a Taylor series:

$$\Delta M = \frac{\partial M}{\partial \alpha}\Delta\alpha + \frac{\partial M}{\partial \dot{\alpha}}\Delta\dot{\alpha} + \frac{\partial M}{\partial q}\Delta q + \frac{\partial M}{\partial \delta_e}\Delta\delta_e \tag{4.33}$$

If we align the body and fixed frames so they coincide at $t = 0$, the change in angle of attack and pitch angles are identical, i.e.

$$\Delta\alpha = \Delta\theta \qquad \text{and} \qquad \Delta\dot{\theta} = \Delta q = \Delta\dot{\alpha} \tag{4.34}$$

This is true only for the special cases where the center of gravity is constrained. Substituting this information into Eq. (4.31) yields

$$\Delta\ddot{\alpha} - (M_q + M_{\dot{\alpha}})\,\Delta\dot{\alpha} - M_\alpha\,\Delta\alpha = M_{\delta e}\,\Delta\delta_e \tag{4.35}$$

where

$$M_q = \frac{\partial M}{\partial q}\Big/ I_y, \qquad M_{\dot{\alpha}} = \frac{\partial M}{\partial \dot{\alpha}}\Big/ I_y \quad \text{etc.}$$

Equation (4.35) is a nonhomogeneous second-order differential equation, having constant coefficients. This equation is similar to a torsional spring–mass–damper system with a forcing function, which was mentioned briefly in the previous section. The static stability of the airplane can be thought of as the equivalent of an aerodynamic spring, while the aerodynamic damping terms are similar to a torsional damping device. The characteristic equation for Eq. (4.35) is

$$\lambda^2 - (M_q + M_{\dot{\alpha}})\lambda - M_\alpha = 0 \tag{4.36}$$

This equation can be compared with the standard equation of a second-order system:

$$\lambda^2 + 2\zeta\omega_n\lambda + \omega_n^2 = 0 \tag{4.37}$$

where ζ is the damping ratio and ω_n is the undamped natural frequency. By inspection, we see that

$$\omega_n = \sqrt{-M_\alpha} \tag{4.38}$$

and

$$\zeta = \frac{-(M_q + M_{\dot{\alpha}})}{2\sqrt{-M_\alpha}} \tag{4.39}$$

Note that the frequency is related to the airplane's static stability and that the damping ratio is a function of the aerodynamic damping and static stability.

If we solve the characteristic Eq. (4.37), we obtain the following roots:

$$\lambda_{1,2} = \frac{-2\zeta\omega_n \pm \sqrt{4\zeta^2\omega_n^2 - 4\omega_n^2}}{2} \tag{4.40}$$

or

$$\lambda_{1,2} = -\zeta\omega_n \pm i\omega_n\sqrt{1-\zeta^2} \tag{4.41}$$

Expressing the characteristic roots as

$$\lambda_{1,2} = \eta \pm i\omega \tag{4.42}$$

and comparing Eq. (4.42) with Eq. (4.41), yields

$$\eta = -\zeta\omega_n \tag{4.43}$$

and

$$\omega = \omega_n\sqrt{1-\zeta^2} \tag{4.44}$$

which are the real and imaginary parts of the characteristic roots. The angular frequency ω is called the damped natural frequency of the system.

The general solution to Eq. (4.35) for a step change $\Delta\delta_e$ in the elevator angle can be expressed as

$$\Delta\alpha(t) = \Delta\alpha_{\text{trim}}\left[\left(1 + \frac{e^{-\zeta\omega_n t}}{\sqrt{1-\zeta^2}}\sin(\sqrt{1-\zeta^2}\,\omega_n t + \phi)\right)\right] \tag{4.45}$$

where $\Delta\alpha_{\text{trim}}$ = change in trim angle of attack = $-(M_{\delta e}\,\Delta\delta_e)/M_\alpha$

$$\zeta = \text{damping ratio} = -\frac{(M_q + M_{\dot\alpha})}{2\sqrt{-M_\alpha}}$$

$$\omega_n = \text{undamped natural frequency} = \sqrt{-M_\alpha}$$

$$\phi = \text{phase angle} = \tan^{-1}(-\sqrt{1-\zeta^2}/-\zeta)$$

The solution is a damped sinusoidal motion with the frequency a function of C_{m_α} and the damping rate a function of $C_{m_q} + C_{m_{\dot\alpha}}$ and C_{m_α}. Figure 4.6 illustrates the angle of attack time history for various values of the damping ratio ζ. Note that as the system damping is increased the maximum overshoot of the response diminishes.

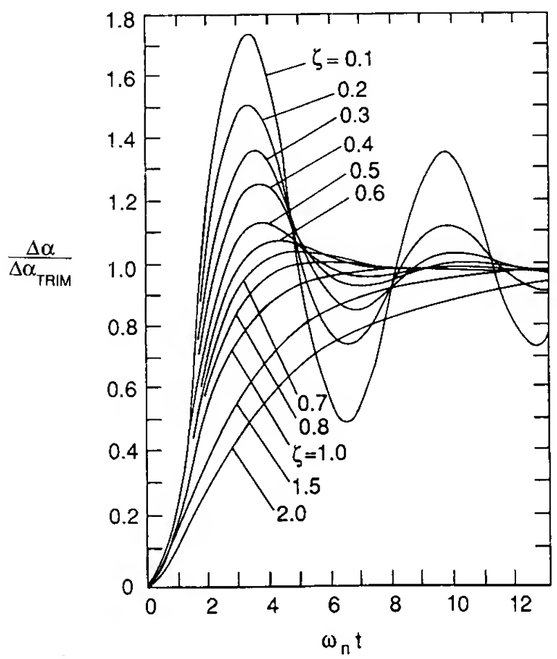

FIGURE 4.6
Angle of attack time history of a pitching model for various damping ratios.

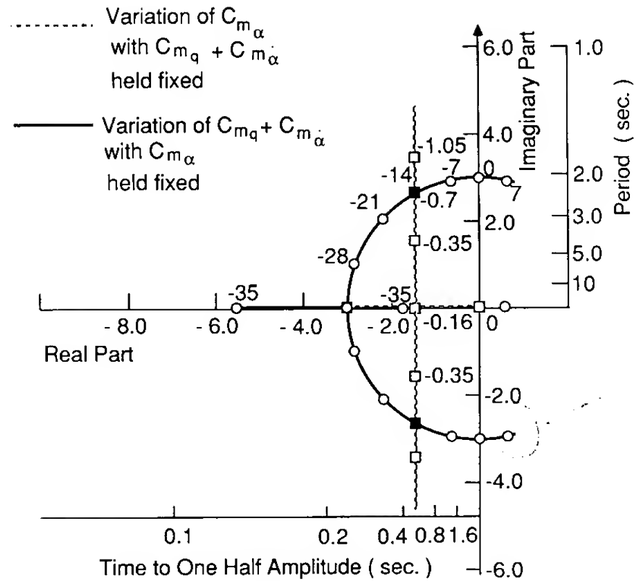

FIGURE 4.7
Variation of the characteristic roots of the pitching motion as a function of the stability coefficients.

The influence of the stability coefficients on the roots of the characteristic equation can be seen in Fig. 4.7. The curves show the effect of variations in C_{m_α} and $C_{m_q} + C_{m_{\dot\alpha}}$ on the roots. This type of curve is referred to as a root locus plot. Notice that, as the roots move into the right half-plane, the vehicle will become unstable.

The roots of the characteristic equation tell us what type of response our airplane will have. If the roots are real, the response will be either a pure divergence or a pure subsidence, depending upon whether the root is positive or negative. If the roots are complex, the motion will be either a damped or an undamped sinusoidal oscillation. The period of the oscillation is related to the imaginary part of the root, as follows:

$$\text{Period} = \frac{2\pi}{\omega} \tag{4.46}$$

The rate of growth or decay of the oscillation is determined by the sign of the real part of the complex root. A negative real part produces a decaying oscillation, whereas a positive real part causes the motion to grow. A measure of the rate of growth or decay of the oscillation can be obtained from the time for halving or doubling the initial amplitude of the disturbance. Figure 4.8 shows a damped and undamped oscillation and how the time for halving or doubling of the amplitude can be calculated. The expression for the time for doubling or halving of the amplitude is

$$t_{\text{double}} \text{ or } t_{\text{halve}} = \frac{0.693}{|\eta|} \tag{4.47}$$

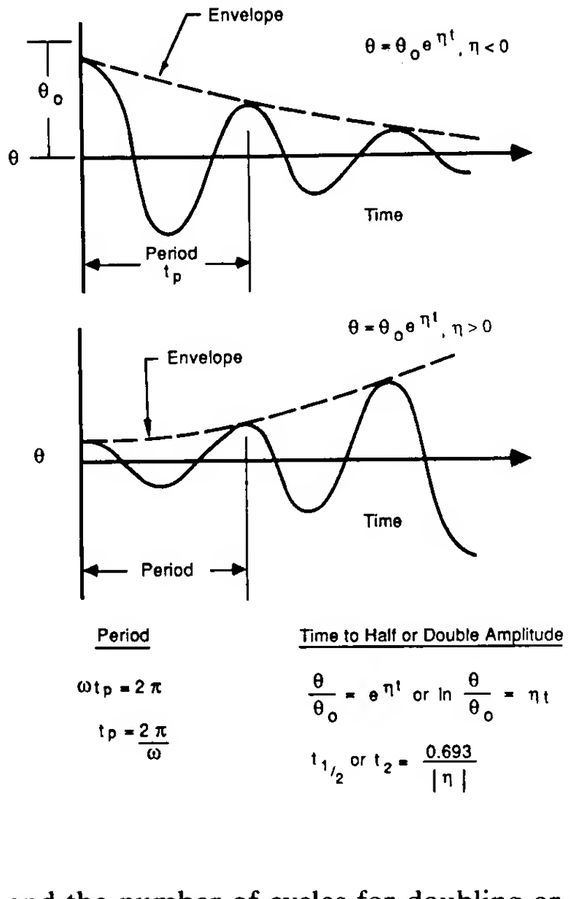

FIGURE 4.8
Relationships for time to halve or double amplitude and the period.

and the number of cycles for doubling or halving of the amplitude is

$$N(\text{cycles})_{\text{double or halve}} = 0.110 \frac{|\omega|}{|\eta|} \tag{4.48}$$

4.4 STICK FIXED LONGITUDINAL MOTION

The motion of an airplane in free flight can be extremely complicated. The airplane has three translational motions (vertical, horizontal, and transverse), three rotational motions (pitch, yaw, and roll) and numerous elastic degrees of freedom. To analyze the response of an elastic airplane is beyond the scope of this book.

The problem we shall address in this section is the solution of the rigid body equations of motion. This may seem to be a formidable task; however, we can make some simplifying assumptions which will reduce the complexity of the problem. First, we shall assume that the aircraft's motion consists of small deviations from its equilibrium flight condition. Second, we shall assume that the motion of the airplane can be analyzed by separating the equations into two groups. The X-force, Z-force and pitching moment equations comprise the longitudinal equations, and the Y-force, rolling and yawing moment

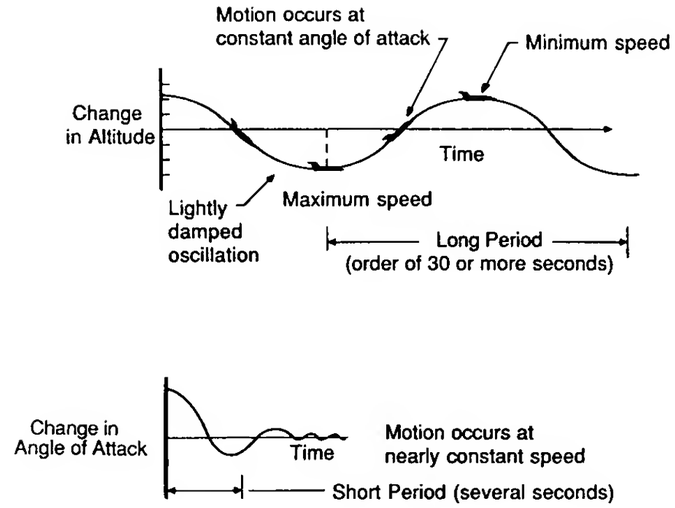

FIGURE 4.9
Sketch of the phugoid and short period motions.

equations are called the lateral equations. To separate the equations in this manner, the longitudinal and lateral equations must not be coupled. These are all reasonable assumptions provided the airplane is not undergoing a large-amplitude or very rapid maneuver.

In aircraft motion studies, one must always be sure that the assumptions made in an analysis are appropriate for the problem at hand. Students are all too eager to use the first equation they can find to solve their homework problems. This type of approach can lead to many incorrect or ridiculous solutions. To avoid such embarrassment, one must always verify that the assumptions used in developing the equations one wishes to use are consistent with the problem one is attempting to solve. This is particularly important when solving problems related to aircraft dynamics.

In the following sections we shall examine the longitudinal motion of an airplane without control input. The longitudinal motion of an airplane (controls fixed) disturbed from its equilibrium flight condition is characterized by two oscillatory modes of motion. Figure 4.9 illustrates these basic modes. We see that one mode is lightly damped and has a long period. This mode is called the long-period or phugoid mode. The second basic mode is heavily damped and has a very short period; it is appropriately called the short-period mode.

STATE VARIABLE REPRESENTATION OF THE EQUATIONS OF MOTION. The linearized longitudinal equations developed in Chapter 3 are simple, ordinary linear differential equations with constant coefficients. The coefficients in the differential equations are made up of the aerodynamic stability derivatives, mass, and inertia characteristics of the airplane. These

equations can be written as a set of first-order differential equations. When the equations are written as a system of first-order differential equations they are called the state-space or state variable equations and are represented mathematically as

$$\dot{\mathbf{x}} = \mathbf{A}\mathbf{x} + \mathbf{B}\eta \tag{4.49}$$

where $\mathbf{x}$ is the state vector, η is the control vector and the matrices $\mathbf{A}$ and $\mathbf{B}$ contain the aircraft's dimensional stability derivatives.

The linearized longitudinal equations developed earlier are repeated below.

$$\begin{aligned}
&\left(\frac{\mathrm{d}}{\mathrm{d}t} - X_u\right)\Delta u - X_w\,\Delta w + (g\cos\theta_0)\,\Delta\theta = X_\delta\,\Delta\delta + X_{\delta_T}\Delta\delta_T \\
&-Z_u\,\Delta u + \left((1 - Z_{\dot{w}})\frac{\mathrm{d}}{\mathrm{d}t} - Z_w\right)\Delta w - \left((u_0 + Z_q)\frac{\mathrm{d}}{\mathrm{d}t} - g\sin\theta_0\right)\Delta\theta \\
&\qquad\qquad = Z_\delta\,\Delta\delta + Z_{\delta_T}\Delta\delta_T \\
&-M_u\,\Delta u - \left(M_{\dot{w}}\frac{\mathrm{d}}{\mathrm{d}t} + M_w\right)\Delta w + \left(\frac{\mathrm{d}^2}{\mathrm{d}t^2} - M_q\frac{\mathrm{d}}{\mathrm{d}t}\right)\Delta\theta = M_\delta\,\Delta\delta + M_{\delta_T}\Delta\delta_T
\end{aligned} \tag{4.50}$$

In practice, the force derivatives Z_q and $Z_{\dot{w}}$ are usually neglected because they contribute very little to the aircraft response. Therefore, to simplify our presentation of the equations of motion in the state space form we will neglect both Z_q and $Z_{\dot{w}}$. Rewriting the equations in the state-space form yields

$$\begin{bmatrix} \Delta\dot{u} \\ \Delta\dot{w} \\ \Delta\dot{q} \\ \Delta\dot{\theta} \end{bmatrix} = \begin{bmatrix} X_u & X_w & 0 & -g \\ Z_u & Z_w & u_0 & 0 \\ M_u + M_{\dot{w}}Z_u & M_w + M_{\dot{w}}Z_w & M_q + M_{\dot{w}}u_0 & 0 \\ 0 & 0 & 1 & 0 \end{bmatrix} \begin{bmatrix} \Delta u \\ \Delta w \\ \Delta q \\ \Delta\theta \end{bmatrix} + \begin{bmatrix} X_\delta & X_{\delta_T} \\ Z_\delta & Z_{\delta_T} \\ M_\delta + M_{\dot{w}}Z_\delta & M_{\delta_T} + M_{\dot{w}}Z_{\delta_T} \\ 0 & 0 \end{bmatrix} \begin{bmatrix} \Delta\delta \\ \Delta\delta_T \end{bmatrix} \tag{4.51}$$

where the state vector $\mathbf{x}$ and control vector η are given by

$$x = \begin{bmatrix} \Delta u \\ \Delta w \\ \Delta q \\ \Delta\theta \end{bmatrix} \qquad \eta = \begin{bmatrix} \Delta\delta \\ \Delta\delta_T \end{bmatrix} \tag{4.52}$$

and the matrices $\mathbf{A}$ and $\mathbf{B}$ are given by

$$\mathbf{A} = \begin{bmatrix} X_u & X_w & 0 & -g \\ Z_u & Z_w & u_0 & 0 \\ M_u + M_{\dot{w}}Z_u & M_w + M_{\dot{w}}Z_w & M_q + M_{\dot{w}}u_0 & 0 \\ 0 & 0 & 1 & 0 \end{bmatrix} \tag{4.53}$$

$$\mathbf{B} = \begin{bmatrix} X_\delta & X_{\delta_T} \\ Z_\delta & Z_{\delta_T} \\ M_\delta + M_{\dot{w}}Z_\delta & M_{\delta_T} + M_{\dot{w}}Z_{\delta_T} \\ 0 & 0 \end{bmatrix} \tag{4.54}$$

The force and moment derivatives in the matrices have been divided by the mass of the airplane or the moment of inertia, respectively as indicated below:

$$X_u = \frac{\partial X/\partial u}{m} \qquad M_u = \frac{\partial M/\partial u}{I_y} \qquad \text{etc.} \tag{4.55}$$

Table 4.2 includes a list of the definitions of the longitudinal stability derivatives. Methods for estimating the stability coefficients were discussed in Chapter 3.

The homogeneous solution to Eq. (4.49) can be obtained by assuming a solution of the form

$$\mathbf{x} = \mathbf{x}_r e^{\lambda_r t} \tag{4.56}$$

TABLE 4.2
Summary of longitudinal derivatives*

$X_u = \dfrac{-(C_{D_u} + 2C_{D_0})QS}{mu_0}$	$X_w = \dfrac{-(C_{D_\alpha} - C_{L_0})QS}{mu_0}$
$Z_u = \dfrac{-(C_{L_u} + 2C_{L_0})QS}{mu_0}$	
$Z_w = \dfrac{-(C_{L_\alpha} + C_{D_0})QS}{mu_0}$	$Z_{\dot{w}} = C_{Z_{\dot{\alpha}}}\dfrac{\bar{c}}{2u_0}QS/(u_0 m)$
$Z_\alpha = u_0 Z_w$	$Z_{\dot{\alpha}} = u_0 Z_{\dot{w}}$
$Z_q = C_{Z_q}\dfrac{\bar{c}}{2u_0}QS/m$	$Z_{\delta e} = C_{Z_{\delta e}}QS/m$
$M_u = C_{m_u}\dfrac{(QS\bar{c})}{u_0 I_y}$	
$M_w = C_{m_\alpha}\dfrac{(QS\bar{c})}{u_0 I_y}$	$M_{\dot{w}} = C_{m_{\dot{\alpha}}}\dfrac{\bar{c}}{2u_0}\dfrac{QS\bar{c}}{u_0 I_y}$
$M_\alpha = u_0 M_w$	$M_{\dot{\alpha}} = u_0 M_{\dot{w}}$
$M_q = C_{m_q}\dfrac{\bar{c}}{2u_0}(QS\bar{c})/I_y$	$M_{\delta e} = C_{m_{\delta e}}(QS\bar{c})/I_y$

Substituting Eq. (4.56) into Eq. (4.49) yields

$$[\lambda_r \mathbf{I} - \mathbf{A}]\mathbf{x}_r = 0 \tag{4.57}$$

where $\mathbf{I}$ is the identity matrix

$$\mathbf{I} = \begin{bmatrix} 1 & 0 & 0 & 0 \\ 0 & 1 & 0 & 0 \\ 0 & 0 & 1 & 0 \\ 0 & 0 & 0 & 1 \end{bmatrix} \tag{4.58}$$

For a nontrivial solution to exist, the determinant

$$|\lambda_r \mathbf{I} - \mathbf{A}| = 0 \tag{4.59}$$

must be zero. The roots λ_r of Eq. (4.59) are called the characteristic roots or eigenvalues. The solution of Eq. (4.59) can be accomplished easily using a digital computer. Most computer facilities will have a subroutine package for determining the eigenvalues of a matrix.

The eigenvectors for the system can be determined once the eigenvalues are known from Eq. (4.60).

$$[\lambda_j \mathbf{I} - \mathbf{A}]\mathbf{P}_{ij} = 0 \tag{4.60}$$

where $\mathbf{P}_{ij}$ is the eigenvector corresponding to the jth eigenvalue. The set of equations making up Eq. (4.60) are linearly dependent and homogeneous; therefore, the eigenvectors cannot be unique. A technique for finding these eigenvectors will be presented later in this chapter.

4.5 LONGITUDINAL APPROXIMATIONS

We can think of the long-period or phugoid mode as a gradual interchange of potential and kinetic energy about the equilibrium altitude and airspeed. This is illustrated in Fig. 4.9. Here we see that the long-period mode is characterized by changes in pitch attitude, altitude, and velocity at a nearly constant angle of attack. An approximation to the long-period mode can be obtained by neglecting the pitching moment equation and assuming that the change in angle of attack is zero, i.e.

$$\Delta\alpha = \frac{\Delta w}{u_0} \qquad \Delta\alpha = 0 \rightarrow \Delta w = 0 \tag{4.61}$$

Making these assumptions, the homogeneous longitudinal state equations reduce to the following:

$$\begin{bmatrix} \Delta\dot{u} \\ \Delta\dot{\theta} \end{bmatrix} = \begin{bmatrix} X_u & -g \\ \dfrac{-Z_u}{u_0} & 0 \end{bmatrix} \begin{bmatrix} \Delta u \\ \Delta\theta \end{bmatrix} \tag{4.62}$$

The eigenvalues of the long period approximation are obtained by solving the

equation

$$|\lambda \mathbf{I} - \mathbf{A}| = 0 \tag{4.63}$$

or

$$\begin{vmatrix} \lambda - X_u & g \\ \dfrac{Z_u}{u_0} & \lambda \end{vmatrix} = 0 \tag{4.64}$$

Expanding the above determinant yields

$$\lambda^2 - X_u\lambda - \frac{Z_u g}{u_0} = 0 \tag{4.65}$$

or

$$\lambda_p = \left[X_u \pm \sqrt{X_u^2 + 4\frac{Z_u g}{u_0}} \right] \Big/ 2.0 \tag{4.66}$$

The frequency and damping ratio can be expressed as

$$\omega_{n_p} = \sqrt{\frac{-Z_u g}{u_0}} \tag{4.67}$$

$$\zeta_p = \frac{-X_u}{2\omega_{n_p}} \tag{4.68}$$

If we neglect compressibility effects, the frequency and damping ratios for the long-period motion can be approximated by the following equations:

$$\omega_{n_p} = \sqrt{2}\frac{g}{u_0} \tag{4.69}$$

$$\zeta_p = \frac{1}{\sqrt{2}}\frac{1}{L/D} \tag{4.70}$$

Notice that the frequency of oscillation and the damping ratio are inversely proportional to the forward speed and the lift-to-drag ratio, respectively. We see from this approximation that the phugoid damping is degraded as the aerodynamic efficiency (L/D) is increased. When pilots are flying an airplane under visual flight rules, the phugoid damping and frequency can vary over a wide range and they will still find the airplane acceptable to fly. On the other hand, if they are flying the airplane under instrument flight rules, low phugoid damping will become very objectable to them. To improve the damping of the phugoid motion, the designer would have to reduce the lift-to-drag ratio of the airplane. Because this would degrade the performance of the airplane, the designer would find such a choice unacceptable and would look for another alternative, such as an automatic stabilization system to provide the proper damping characteristics.

SHORT-PERIOD APPROXIMATION. An approximation to the short-period mode of motion can be obtained by assuming $\Delta u = 0$ and dropping the X-force equation. The longitudinal state-space equations reduce to the following:

$$\begin{bmatrix} \Delta\dot{w} \\ \Delta\dot{q} \end{bmatrix} = \begin{bmatrix} Z_w & u_0 \\ M_w + M_{\dot{w}}Z_w & M_q + M_{\dot{w}}u_0 \end{bmatrix} \begin{bmatrix} \Delta w \\ \Delta q \end{bmatrix} \tag{4.71}$$

The above equation can be written in terms of the angle of attack by using the relationship

$$\Delta\alpha = \frac{\Delta w}{u_0} \tag{4.72}$$

In addition, one can replace the derivatives due to w and $\dot{w}$ with derivatives due to α and $\dot{\alpha}$ by using the following equations. The definition of the derivative M_α is

$$M_\alpha = \frac{1}{I_y}\frac{\partial M}{\partial \alpha} = \frac{1}{I_y}\frac{\partial M}{\partial(\Delta w/u_0)} = \frac{u_0}{I_y}\frac{\partial M}{\partial w} = u_0 M_w \tag{4.73}$$

In a similar way we can show that

$$Z_\alpha = u_0 Z_w \qquad \text{and} \qquad M_{\dot{\alpha}} = u_0 M_{\dot{w}} \tag{4.74}$$

Using the above expressions, the state equations for the short-period approximation can be rewritten as

$$\begin{bmatrix} \Delta\dot{\alpha} \\ \Delta\dot{q} \end{bmatrix} = \begin{bmatrix} \dfrac{Z_\alpha}{u_0} & 1 \\ M_\alpha + M_{\dot{\alpha}}\dfrac{Z_\alpha}{u_0} & M_q + M_{\dot{\alpha}} \end{bmatrix} \begin{bmatrix} \Delta\alpha \\ \Delta q \end{bmatrix} \tag{4.75}$$

The eigenvalues of the state equation can again be determined by solving the equation

$$|\lambda\mathbf{I} - \mathbf{A}| = 0 \tag{4.76}$$

which yields

$$\begin{vmatrix} \lambda - \dfrac{Z_\alpha}{u_0} & -1 \\ -M_\alpha - M_{\dot{\alpha}}\dfrac{Z_\alpha}{u_0} & \lambda - (M_q + M_{\dot{\alpha}}) \end{vmatrix} = 0 \tag{4.77}$$

The characteristic equation for the above determinant is

$$\lambda^2 - \left(M_q + M_{\dot{\alpha}} + \frac{Z_\alpha}{u_0}\right)\lambda + M_q\frac{Z_\alpha}{u_0} - M_\alpha = 0 \tag{4.78}$$

TABLE 4.3
Summary of longitudinal approximations

	Long-period (phugoid)	Short-period
Frequency	$\omega_{np} = \sqrt{\dfrac{-Z_u g}{u_0}}$	$\omega_{nsp} = \sqrt{\dfrac{Z_\alpha M_q}{u_0} - M_\alpha}$
Damping ratio	$\zeta_p = \dfrac{-X_u}{2\omega_{np}}$	$\zeta_{sp} = -\dfrac{M_q + M_{\dot{\alpha}} + \dfrac{Z_\alpha}{u_0}}{2\omega_{nsp}}$

The approximate short-period roots can be obtained easily from the characteristic equation and are given below:

$$\lambda_{sp} = \left(M_q + M_{\dot{\alpha}} + \frac{Z_\alpha}{u_0}\right)\Big/2 \pm \left[\left(M_q + M_{\dot{\alpha}} + \frac{Z_\alpha}{u_0}\right)^2 - 4\left(M_q\frac{Z_\alpha}{u_0} - M_\alpha\right)\right]^{1/2}\Big/2 \tag{4.79}$$

or in terms of the damping and frequency

$$\omega_{n_{sp}} = \left[\left(M_q\frac{Z_\alpha}{u_0} - M_\alpha\right)\right]^{1/2} \tag{4.80}$$

$$\zeta_{sp} = -\left[M_q + M_{\dot{\alpha}} + \frac{Z_\alpha}{u_0}\right]\Big/(2\omega_{n_{sp}}) \tag{4.81}$$

Equations (4.80) and (4.81) should look familiar to the reader. They are very similar to the equations derived for the case of a constrained pitching motion. If we neglect the Z_α term (i.e. neglect the vertical motion), Eqs (4.80) and (4.81) are identical to Eqs (4.38) and (4.39).

A summary of the approximate formulas is presented in Table 4.3.

To help clarify the preceding analysis, we shall determine the longitudinal characteristics of the general aviation airplane included in Appendix B.

Example Problem 4.1. Find the longitudinal eigenvalues and eigenvectors for the general aviation airplane included in Appendix B and compare these results with the answers obtained by using the phugoid and short period approximations.

Solution. First, we must determine the numerical values of the dimensional longitudinal stability derivatives. The dynamic pressure Q and the terms QS, $QS\bar{c}$ and $\bar{c}/2u_0$ are

$$Q = \tfrac{1}{2}\rho u_0^2 = (0.5)(0.002378)(176)^2 = 36.8 \text{ lb/ft}^2$$

$$QS = (36.8)(184) = 6771 \text{ lb}$$

$$QS\bar{c} = (6771)(5.7) = 38596 \text{ ft·lb}$$

$$(c/2u_0) = (5.7)/(2 \times 176) = 0.016 \text{ s}$$

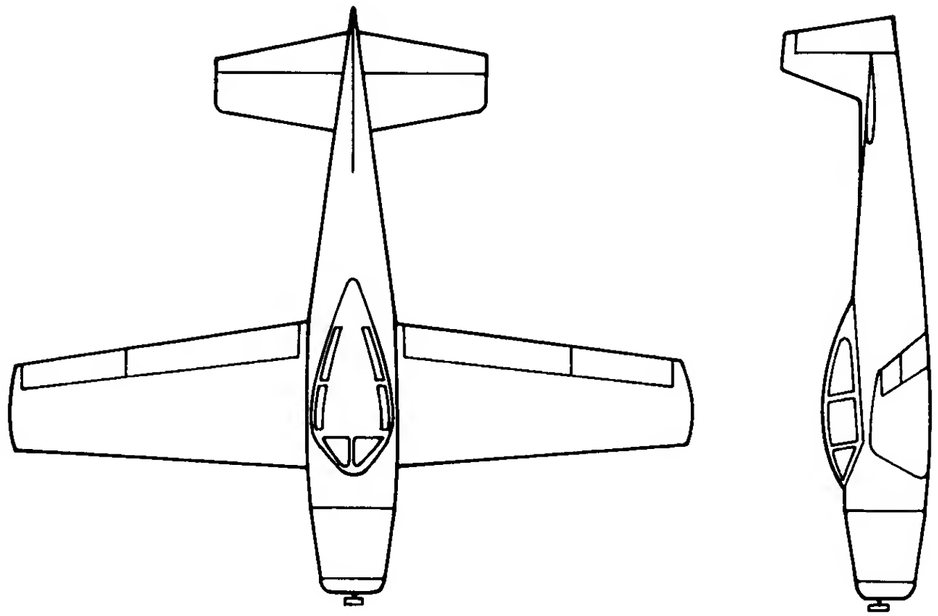

Nominal Flight Condition

h (ft) = 0; M = .158; V_{T_o} = 176 ft / sec

W = 2750 lb
CG at 29.5 % MAC
I_x = 1048 slug - ft^2
I_y = 3000 slug - ft^2
I_z = 3530 slug - ft^2
I_{xz} = 0

References Geometry

S = 184 ft^2
b = 33.4 ft
$\bar{c}$ = 5.7 ft

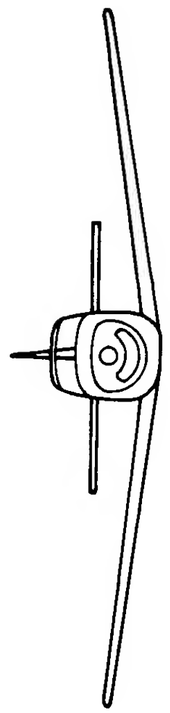

FIGURE 4.10
Geometric, mass, and aerodynamic properties of a general aviation airplane.

The longitudinal derivatives can be estimated from the formulas in Table 4.2.

***U*-derivatives**

$$X_u = -(C_{D_u} + 2C_{D_0})QS/(u_0 m)$$
$$= -(0.0 + 2(0.05))(6771)/((176)(85.5))$$
$$= -0.045\ (s^{-1})$$

$$Z_u = -(C_{L_u} + 2C_{L_0})QS/(u_0 m)$$
$$= -(0.0 + 2(0.41))(6771)/((176)(85.5))$$
$$= -0.369\ (s^{-1})$$

$$M_u = 0$$

***W*-derivatives**

$$X_w = -(C_{D_\alpha} - C_{L_0})QS/(u_0 m)$$
$$= -(0.33 - 0.41)(6771)/((176)(85.5))$$
$$= 0.036\ (s^{-1})$$

$$Z_w = -(C_{L_\alpha} + C_{D_0})QS/(u_0 m)$$
$$= -(4.44 + 0.05)(6771)/((176)(85.4))$$
$$= -2.02\ (s^{-1})$$

$$M_w = C_{m_\alpha} QS\bar{c}/(u_0 I_y)$$
$$= (-0.683)(38\,596)/((176)(3000))$$
$$= -0.05\ (1/(ft \cdot s))$$

***Ẇ*-derivatives**

$$X_{\dot{w}} = 0$$
$$Z_{\dot{w}} = 0$$
$$M_{\dot{w}} = C_{m_{\dot{\alpha}}} \frac{\bar{c}}{2u_0} QS\bar{c}/(u_0 I_y)$$
$$= (-4.36)(0.016)(38\,596)/((176)(3000))$$
$$= -0.0051\ (ft^{-1})$$

***q*-derivatives**

$$X_q = 0$$
$$Z_q = 0$$
$$M_q = C_{m_q} \frac{\bar{c}}{2u_0} QS\bar{c}/I_y$$
$$= (-9.96)(0.016)(38\,596)/(3000)$$
$$= -2.05\ (s^{-1})$$

Substituting the numerical values of the stability derivatives into Eq. (4.51), we

can obtain the stability matrix:

$$\dot{\mathbf{x}} = \mathbf{A}\mathbf{x}$$

or

$$\begin{bmatrix} \Delta\dot{u} \\ \Delta\dot{w} \\ \Delta\dot{q} \\ \Delta\dot{\theta} \end{bmatrix} = \begin{bmatrix} -0.045 & 0.036 & 0.0000 & -32.2 \\ -0.369 & -2.02 & 168.8 & 0.0000 \\ 0.0019 & -0.0396 & -2.948 & 0.000 \\ 0.0000 & 0.0000 & 1.0000 & 0.0000 \end{bmatrix} \begin{bmatrix} \Delta u \\ \Delta w \\ \Delta q \\ \Delta\theta \end{bmatrix}$$

The eigenvalues can be determined by finding eigenvalues of the matrix **A**:

$$|\lambda\mathbf{I} - \mathbf{A}| = 0$$

The resulting characteristic equation is

$$\lambda^4 + 5.0\lambda^3 + 12.9\lambda^2 + 0.66\lambda + 0.59 = 0$$

The solution of the characteristic equation yields the eigenvalues:

$$\lambda_{1,2} = -0.0169 \pm \mathrm{i}(0.215) \qquad \text{(phugoid)}$$

$$\lambda_{3,4} = -2.48 \pm \mathrm{i}(2.55) \qquad \text{(short-period)}$$

The period, time, and number of cycles to half-amplitude are readily obtained once the eigenvalues are known.

Phugoid (long-period)	**Short-period**
$t_{1/2} = 0.69/\lvert\eta\rvert = \dfrac{0.69}{-0.0169}$	$t_{1/2} = 0.69/\lvert\eta\rvert = \dfrac{0.69}{-2.48}$
$t_{1/2} = 40.8$ s Period $= 2\pi/\omega = 2\pi/0.215$ Period $= 29.2$ s	$t_{1/2} = 0.28$ s Period $= 2\pi/\omega = 2\pi/2.55$ Period $= 2.46$ s
Number of cycles to half-amplitude	**Number of cycles to half-amplitude**
$N_{1/2} = \dfrac{t_{1/2}}{P} = 0.110\dfrac{\omega}{\lvert\eta\rvert}$ $= \dfrac{[0.110][0.215]}{\lvert-0.0169\rvert}$ $N_{1/2} = 1.40$ cycles	$N_{1/2} = 0.110\dfrac{\omega}{\lvert\eta\rvert}$ $= \dfrac{[0.110][2.55]}{\lvert-2.48\rvert}$ $N_{1/2} = 0.11$ cycles

Now let us estimate the above parameters by means of the long- and short-period approximations. The damping ratio and undamped natural frequency for the long-period motion was given by Eqs (4.69), (4.70), (4.80) and (4.81).

Phugoid-approximation

$$\omega_{n_p} = \sqrt{\frac{-Z_u g}{u_0}} = \left[\frac{-[-0.369][32.21]}{[176]}\right]^{1/2} = 0.26 \text{ rad/s}$$

$$\zeta_p = \frac{-X_u}{2\omega_{n_p}} = \frac{-[-0.045]}{2[0.26]} = 0.087$$

$$\lambda_{1,2} = -\zeta_p\omega_{n_p} \pm \mathrm{i}\omega_n\sqrt{1-\zeta^2}$$
$$= -[0.087][0.26] \pm \mathrm{i}[0.26]\sqrt{1-[0.087]^2}$$
$$= -0.023 \pm \mathrm{i}0.26$$

$$\text{Period} = \frac{2\pi}{\omega} = \frac{2\pi}{0.26} = 24.2 \text{ s}$$

$$t_{1/2} = \frac{0.69}{\eta} = \frac{0.69}{|-0.023|} = 30 \text{ s}$$

$$N_{1/2} = 0.110\frac{\omega}{|\eta|} = 0.110\frac{[0.26]}{0.023} = 1.24 \text{ cycles}$$

Short-period approximation

$$\omega_{n_{sp}} = \sqrt{\frac{Z_\alpha M_q}{u_0} - M_\alpha}$$

Recall that $Z_\alpha = u_0 Z_w$, $M_\alpha = u_0 M_w$ and $M_{\dot{\alpha}} = u_0 M_{\dot{w}}$.

$$\omega_{n_{sp}} = ((-2.02)(-2.05) - (-0.05)(176))^{1/2} = 3.6 \text{ rad/s}$$

$$\zeta_{sp} = \left(M_q + M_{\dot{\alpha}} + \frac{Z_\alpha}{u_0}\right)\Big/[2\omega_{\omega_{n_{sp}}}]$$
$$= ((-2.05) + (-0.88) + (-2.02))/((2)(3.6))$$
$$= 0.688$$

$$\lambda_{1,2,sp} = -\zeta_{sp}\omega_{n_{sp}} \pm \mathrm{i}\omega_n\sqrt{1-\zeta_{sp}^2}$$
$$= -(0.688)(3.6) \pm \mathrm{i}(3.6)\sqrt{1-(0.688)^2}$$
$$= -2.48 \pm \mathrm{i}2.61$$

$$\text{Period} = \frac{2\pi}{\omega} = \frac{2\pi}{2.} = 2.4 \text{ s}$$

$$t_{1/2} = \frac{0.69}{|\eta|} = \frac{0.69}{|-2.|} = 0.278 \text{ s}$$

$$N_{1/2} = 0.110\frac{\omega}{|\eta|} = 0.110\frac{2.78}{|-2.|} = 0.116 \text{ cycles}$$

A summary of the results from the exact and approximate analysis is included in Table 4.4. In this analysis, the short-period approximation was found to be in closer agreement with the exact solution than the phugoid approximation. In general, the short-period approximation is the more accurate approximation.

The eigenvectors for this problem can be determined by a variety of techniques; however, we will discuss only one relatively straight forward method. For additional information on other techniques, readers should go to their mathematics library or computer center. Most computer facilities maintain digital computer programs suitable for extracting eigenvalues and eigenvectors of large-order systems.

TABLE 4.4
Comparison of exact and approximate methods

	Exact method	Approximate method	Difference
Phugoid	$t_{1/2} = 40.8$ s $P = 29.2$ s	$t_{1/2} = 30$ s $P = 24.2$ s	26.4% 17.1%
Short-period	$t_{1/2} = 0.280$ s $P = 2.46$ s	$t_{1/2} = 0.278$ s $P = 2.4$ s	0% 2.4%

To obtain the longitudinal eigenvectors for this example problem, we will start with Eq. (4.60) which is expanded as follows:

$$(\lambda_j - A_{11})\,\Delta u_j - A_{12}\,\Delta w_j - A_{13}\,\Delta q_j - A_{14}\,\Delta\theta_j = 0$$

$$-A_{21}\,\Delta u_j + (\lambda_j - A_{22})\,\Delta w_j - A_{23} q_j - A_{24}\,\Delta\theta_j = 0$$

$$-A_{31}\,\Delta u_j - A_{32}\,\Delta w_j + (\lambda_j - A_{33})\,\Delta q_j - A_{34}\,\Delta\theta_j = 0$$

$$-A_{41}\,\Delta u_j - A_{42}\,\Delta w_j - A_{43}\,\Delta q_j + (\lambda_j - A_{44})\,\Delta\theta_j = 0$$

In this set of equations, the only unknowns are the components of the eigenvector, the eigenvalues λ_j and the elements of the **A** matrix were determined previously. Dividing the preceding equations by any one of the unknowns (for this example we will use $\Delta\theta_j$), we obtain four equations for the three unknown ratios. Any three of the four equations can be used to find the eigenvectors. If we drop the fourth equation, we will have a set of three equations with the three unknown ratios, as follows:

$$(\lambda_j - A_{11})\left(\frac{\Delta u}{\Delta\theta}\right)_j - A_{12}\left(\frac{\Delta w}{\Delta\theta}\right)_j - A_{13}\left(\frac{\Delta q}{\Delta\theta}\right)_j = A_{14}$$

$$-A_{21}\left(\frac{\Delta u}{\Delta\theta}\right)_j + (\lambda_j - A_{22})\left(\frac{\Delta w}{\Delta\theta}\right)_j - A_{23}\left(\frac{\Delta q}{\Delta\theta}\right)_j = A_{24}$$

$$-A_{31}\left(\frac{\Delta u}{\Delta\theta}\right)_j - A_{32}\left(\frac{\Delta w}{\Delta\theta}\right)_j + (\lambda_j - A_{33})\left(\frac{\Delta q}{\Delta\theta}\right)_j = A_{34}$$

This set of equations can easily be solved by conventional techniques to yield the eigenvector $[\Delta u/\Delta\theta,\ \Delta w/\Delta\theta,\ \Delta q/\Delta\theta,\ 1]$.

The nondimensional eigenvectors for the example problem have been computed and are listed in Table 4.5. The longitudinal modes can now be examined by means of a vector or Argand diagram. The magnitude of the eigenvectors are arbitrary so only the relative length of the vectors is important.

Figure 4.11 is an Argand diagram illustrating the long-period and short-period modes. In this diagram the lengths of the vectors are decreasing exponentially with time, while the vectors are rotating with the angular rate ω. The motion of the airplane can be imagined as the projection of the eigenvectors along the real axis.

On close examination of Fig. 4.11, several observations can be made. For the long-period mode, we see the changes in angle of attack and pitch rate are

TABLE 4.5
Longitudinal eigenvectors for general aviation

Eigenvector	Long-period	Short-period
		Eigenvalue
	$\lambda = -0.0165 \pm 0.214$i	$\lambda = -2.436 \pm 2.52$i
$\dfrac{\Delta u/u_0}{\Delta\theta}$	-0.114 ± 0.837i	0.034 ± 0.025i
$\dfrac{\Delta w/u_0}{\Delta\theta} = \dfrac{\Delta\alpha}{\Delta\theta}$	0.008 ± 0.05i	1.0895 ± 0.733i
$\dfrac{\Delta(qc/2u_0)}{\Delta\theta}$	-0.000027 ± 0.00347i	-0.039 ± 0.041i

negligible. The motion is characterized by changes in speed and pitch attitude. Notice that the velocity vector leads the pitch attitude by nearly 90° in phase. In contrast, the short-period mode is characterized by changes in angle of attack and pitch attitude with negligible speed variations. As we can see from the vector diagrams, the assumptions we made earlier in developing the long- and short-period approximations are, indeed, consistent with the exact solution.

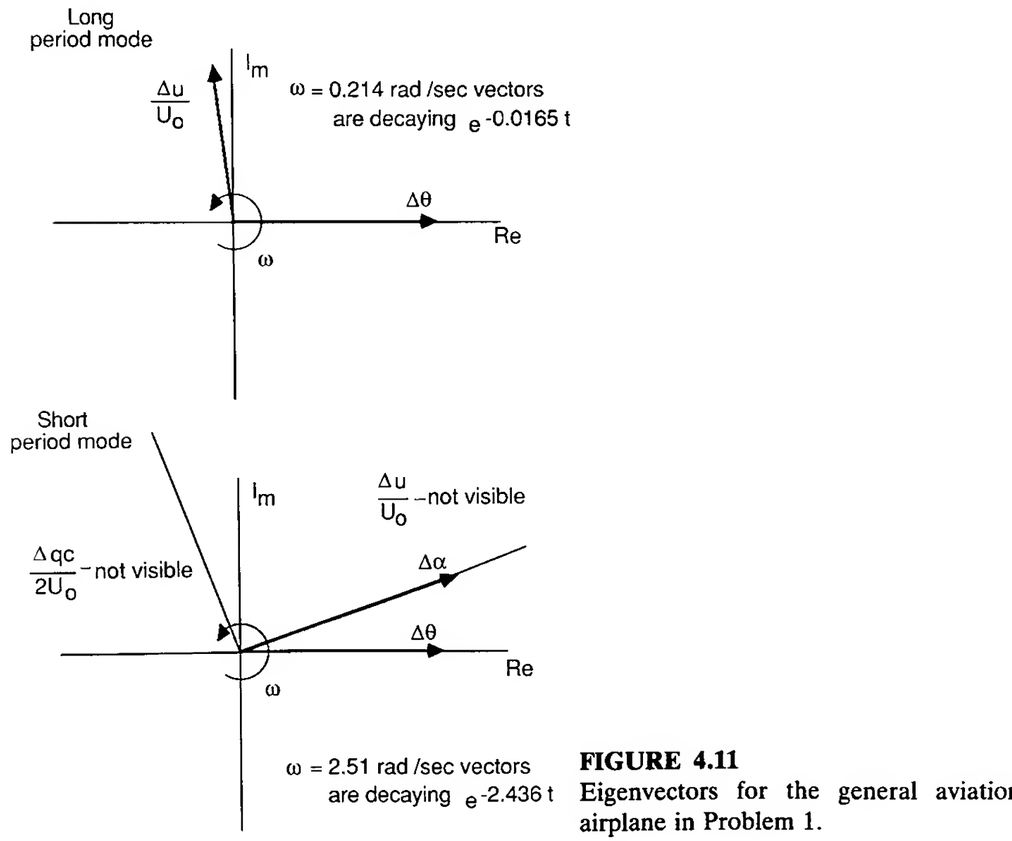

FIGURE 4.11
Eigenvectors for the general aviation airplane in Problem 1.

4.6 THE INFLUENCE OF STABILITY DERIVATIVES ON THE LONGITUDINAL MODES OF MOTION

The type of response we obtain from solving the differential equations of motion depends on the magnitude of the stability coefficients. This can easily be seen by examining the expressions for the damping ratio and frequency of the long- and short-period approximations. Table 4.6 summarizes the effect of each derivative on the longitudinal motion.

Of the two characteristic modes, the short-period mode is the most important. If this mode has a high frequency and is heavily damped, then the airplane will respond rapidly to an elevator input without any undesirable overshoot. When the short-period mode is lightly damped or has a relatively low frequency, the airplane will be difficult to control and, in some cases, may even be dangerous to fly.

The phugoid or long-period mode occurs so slowly that the pilot can easily negate the disturbance by small control movements. Even though the pilot can easily correct for the phugoid mode, it would become extremely fatiguing if the damping were too low.

Figures 4.12 and 4.13 show the effects of varying the center of gravity position and the horizontal tail area size on the long- and short-period response. As the center of gravity is moved rearward, the longitudinal modes become aperiodic and, eventually, unstable.

From a performance standpoint, it would be desirable to move the center of gravity further aft so that trim drags during the cruise portion of the flight could be reduced. Unfortunately, this leads to a less stable airplane. By using an active control stability augmentation system, the requirement of static stability can be relaxed without degrading the airplane's flying qualities.

Recent studies by the commercial aircraft industry have shown that fuel savings of three or four percent are possible if relaxed stability requirements

TABLE 4.6
Influence of stability derivatives on the long and short period motions

Stability derivative	Mode affected	How affected
$M_q + M_{\dot{\alpha}}$	Damping of short-period mode of motion	Increasing $M_q + M_{\dot{\alpha}}$ increases damping
M_α	Frequency of short-period mode of motion	Increasing M_α or static stability increases the frequency
X_u	Damping of the phugoid or long-period mode of motion	Increasing X_u increases damping
Z_u	Frequency of phugoid mode of motion	Increasing Z_u increases the frequency

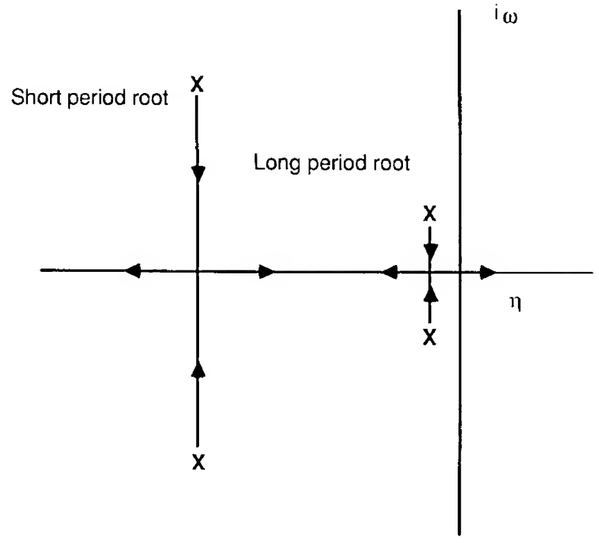

FIGURE 4.12
Influence of center of gravity position on longitudinal response.

and active control stability augmentation are incorporated into the design. With the ever rising costs of jet fuel, this small percentage could mean the savings of many millions of dollars for the commercial airlines.

4.7 FLYING QUALITIES

In the previous sections we examined the stick fixed longitudinal characteristics of an airplane. The damping and frequency of both the short- and long-period motions were determined in terms of the aerodynamic stability derivatives.

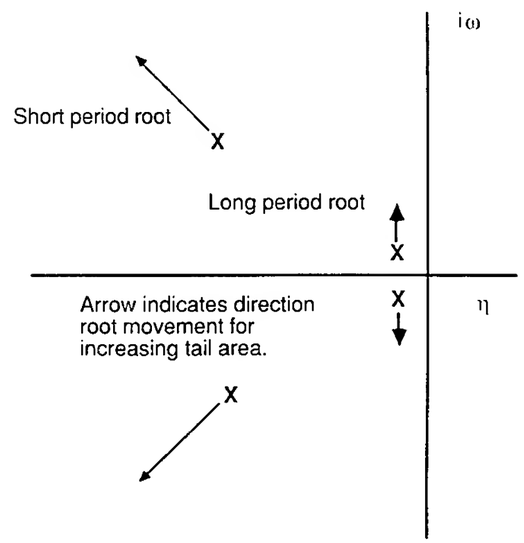

FIGURE 4.13
Influence of horizontal tail area on longitudinal response.

Because the stability derivatives are a function of the geometric and aerodynamic characteristics of the airplane, designers have some control over the longitudinal dynamics by their selection of the vehicle's geometric and aerodynamic characteristics. For example, increasing the tail size would increase both the static stability of the airplane and the damping of the short-period motion.[2] However, the increased tail area would also increase the weight and drag of the airplane and thereby reduce the airplane's performance. The designer is faced with the challenge of providing an airplane with optimum performance that is both safe and easy to fly. To achieve such a goal, the designer needs to know what degree of stability and control is required for the pilot to consider the airplane safe and flyable.

The flying qualities of an airplane are related to the stability and control characteristics and can be defined as those stability and control characteristics that are important in forming the pilot's impression of the airplane. The pilot forms subjective opinions about the ease or difficulty of controlling the airplane in steady and maneuvering flight. In addition to the longitudinal dynamics, the pilot's impression of the airplane is also influenced by the feel of the airplane that is provided to the pilot by the stick force and stick force gradients. The Department of Defense and Federal Aviation Administration has made a list of specifications dealing with airplane flying qualities. These requirements are used by the procuring and regulatory agencies to determine whether an airplane is acceptable for certification. The purpose of these requirements is to ensure that the airplane has flying qualities which do not place any limitation on the vehicle's flight safety or restrict the ability of the airplane to perform its intended mission. The specification of the requirements for airplane flying qualities can be found in Ref. 4.5.

As one might guess, the flying qualities expected by the pilot depend upon the type of aircraft and the flight phase. Aircraft are classified according to size and maneuverability as shown in Table 4.7. The flight phase is divided into three categories as shown in Table 4.8. Category A deals exclusively with military aircraft. Most of the flight phases listed in categories B and C are applicable to either commercial or military aircraft. The flying qualities are specified in terms of three levels:

Level 1 Flying qualities clearly adequate for the mission flight phase.

Level 2 Flying qualities adequate to accomplish the mission flight phase, but some increase in pilot workload or degradation in mission effectiveness, or both, exists.

Level 3 Flying qualities such that the airplane can be controlled safely, but pilot workload is excessive or mission effectiveness is inadequate, or both. Category A flight phases can be terminated safely, and Category B and C flight phases can be completed.

[2] Because the aerodynamic derivatives are also a function of Mach number, the designer can only optimize the dynamic characteristics for one flight regime. To provide suitable dynamic characteristics over the entire flight envelope, the designer must provide artificial damping by using stability augmentation.

TABLE 4.7
Classification of airplanes

Class I	Small, light airplanes, such as light utility, primary trainer, and light observation craft
Class II	Medium-weight, low-to-medium maneuverability airplanes, such as heavy utility/search and rescue, light or medium transport/cargo/tanker, reconnaissance, tactical bomber, heavy attack and trainer for Class II
Class III	Large, heavy, low-to-medium maneuverability airplanes, such as heavy transport/cargo/tanker, heavy bomber and trainer for Class III
Class IV	High-maneuverability airplanes, such as fighter/interceptor, attack, tactical reconnaissance, observation and trainer for Class IV

The levels are determined on the basis of the pilot's opinion of the flying characteristics of the airplane.

Extensive research programs have been conducted by the government and the aviation industry to quantify the stability and control characteristics of the airplane with the pilot's opinion of the airplane's flying qualities. Figure 4.14 is an example of the type of data generated from flying qualities research. This figure shows the relationship between the level of flying qualities and the damping ratio and undamped natural frequency of the short-period mode. This kind of figure is sometimes referred to as a thumbprint plot. Table 4.9 is a summary of the longitudinal specifications for the phugoid and short-period motions which is valid for all classes of aircraft.

TABLE 4.8
Flight phase categories

Nonterminal flight phase	
Category A	Nonterminal flight phases that require rapid maneuvering, precision tracking, or precise flight-path control. Included in the category are air-to-air combat ground attack, weapon delivery/launch, aerial recovery, reconnaissance, in-flight refueling (receiver), terrain-following, antisubmarine search, and close-formation flying
Category B	Nonterminal flight phases that are normally accomplished using gradual maneuvers and without precision tracking, although accurate flight-path control may be required. Included in the category are climb, cruise, loiter, in-flight refueling (tanker), descent, emergency descent, emergency deceleration, and aerial delivery.
Terminal Flight Phases:	
Category C	Terminal flight phases are normally accomplished using gradual maneuvers and usually require accurate flight-path control. Included in this category are takeoff, catapult takeoff, approach, wave-off/go-around and landing.

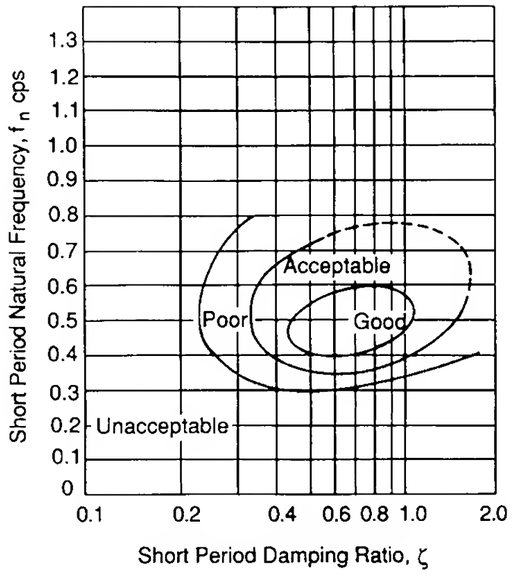

FIGURE 4.14
Short-period flying qualities.

The information provided by Table 4.9 provides the designer with valuable design data. As we showed earlier, the longitudinal response characteristics of an airplane are related to its stability derivatives. Because the stability derivatives are related to the airplane's geometric and aerodynamic characteristics it is possible for the designer to consider flying qualities in the preliminary design phase.

TABLE 4.9
Longitudinal flying qualities

Phugoid mode				
	Level 1	$\zeta > 0.04$		
	Level 2	$\zeta > 0$		
	Level 3	$T_2 > 55$ s		
Short-period mode				
	Categories A & C		**Category B**	
Level	ζ_{sp} min	ζ_{sp} max	ζ_{sp} min	ζ_{sp} max
1	0.35	1.30	0.3	2.0
2	0.25	2.00	0.2	2.0
3	0.15	—	0.15	—

Example Problem 4.2. A fighter aircraft has the aerodynamic, mass and geometric characteristics given below. Determine the short-period flying qualities at sea level, at 25 000 ft and at 50 000 ft for a true airspeed of 800 ft/s. How can the designer improve the flying qualities of this airplane?

$$W = 17\,580 \text{ lb} \qquad I_y = 25\,900 \text{ slug·ft}^2$$

$$S = 260 \text{ ft}^2 \qquad \bar{c} = 10.9 \text{ ft}$$

$$C_{L_\alpha} = 4.0 \text{ rad}^{-1} \qquad C_{m_\alpha} = -0.4 \text{ rad}^{-1} \qquad C_{m_q} = -4.3 \text{ rad}^{-1} \qquad C_{m_{\dot{\alpha}}} = -1.7 \text{ rad}^{-1}$$

Solution. The approximate formulas for the short-period damping ratio and frequency are given by Eqs (4.80) and (4.81):

$$\omega_{n_{sp}} = \sqrt{\frac{Z_\alpha M_q}{u_0} - M_\alpha}$$

$$\zeta_{sp} = -\frac{(M_q + M_{\dot{\alpha}} + Z_\alpha/u_0)}{2\omega_{n_{sp}}}$$

where

$$Z_\alpha = -C_{L_\alpha} QS/m$$

$$M_q = C_{m_q}\left(\frac{\bar{c}}{2u_0}\right)\frac{QS\bar{c}}{I_y}$$

$$M_\alpha = C_{m_\alpha}\frac{QS\bar{c}}{I_y}$$

$$M_{\dot{\alpha}} = C_{m_{\dot{\alpha}}}\left(\frac{\bar{c}}{2u_0}\right)\frac{QS\bar{c}}{I_y}$$

If we neglect the effect of Mach number changes on the stability coefficient, the damping ratio and frequency can easily be calculated from the preceeding equations. Figure 4.15 is a plot of ζ_{sp} and $\omega_{n_{sp}}$ as functions of the altitude. Comparing the estimated short-period damping ratio and frequency with the pilot opinion contours in Fig. 4.14, we see that this airplane has poor handling qualities at sea level which deteriorate to unacceptable characteristics at altitude.

To improve the flying qualities of this airplane, the designer needs to provide more short-period damping. This could be accomplished by increasing the tail area and/or increasing the tail moment arm. Such geometric changes would increase the stability coefficients C_{m_α}, C_{m_q} and $C_{m_{\dot{\alpha}}}$. Unfortunately, this can not be accomplished without a penalty in flight performance. The larger tail area results in increased structural weight and empenage drag. For low-speed aircraft, geometric design changes can usually be used to provide suitable flying

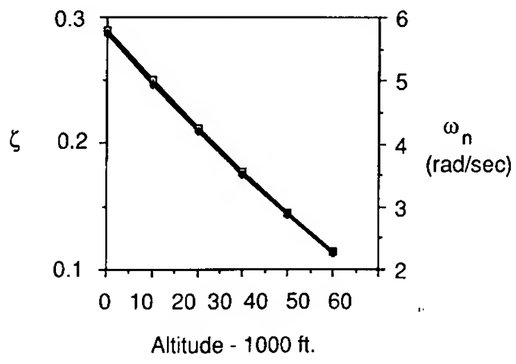

FIGURE 4.15
Variation of ζ_{sp} and $\omega_{n,sp}$ as a function of altitude.

qualities; for aircraft that have an extensive flight envelope, such as fighters, it is not possible to provide good flying qualities over the entire flight regime from geometric considerations alone. This can be accomplished, however, by using a stability augmentation system.

4.8 FLIGHT SIMULATION

To determine the flying quality specifications described in the previous section requires some very elaborate test facilities. Both ground-based and in-flight simulators are used to evaluate pilot opinion on aircraft response characteristics, stick force requirements and human factors data such as instrument design, size, and location.

The ground-based flight simulator provides the pilot with the "feel" of flight by using a combination of simulator motions and visual images. The more sophisticated flight simulators provide six degrees of freedom to the simulator cockpit. Hydraulic servo actuators are attached to the bottom of the simulator cabin and are driven by computers to produce the desired motion. The visual images produced on the windscreen of the simulator are created by projecting images from a camera mounted over a detailed terrain board or by computer-generated images. Figure 4.16 is a sketch of a ground-based simulator.

An example of an in-flight simulator is shown in Fig. 4.17. This figure is a sketch of the U.S. Air Force's Total in Flight Simulator (TIFS) which is a modified C131 transport. By using special force producing control surfaces such as direct lift flaps and side force generators, this airplane can be used to simulate a wide range of larger aircraft. The TIFS has been used to simulate the B-1, C-5 and Space Shuttle among other craft.

The stability characteristics of the simulator can be changed through the computer. This capability permits researchers to establish the relationship between pilot opinion and aircraft stability characteristics. For example, the short-period characteristics of the simulator could be varied and the simulator pilot would be asked to evaluate the case or difficulty of flying the simulator. In this manner, the researcher can establish the pilot's preference for particular airplane response characteristics.

4.9 SUMMARY

In this chapter we have examined the stick fixed longitudinal motion of an airplane using the linearized equations of motion developed in Chapter 3. It was shown that the longitudinal dynamic motion consists of two distinct and separate modes; a long-period oscillation which is lightly damped, and a very short-period but heavily damped oscillation.

Approximate relationships for the long- and short-period modes were developed by assuming that the long-period mode occurred at constant angle of attack and the short-period mode occurred at a constant speed. These

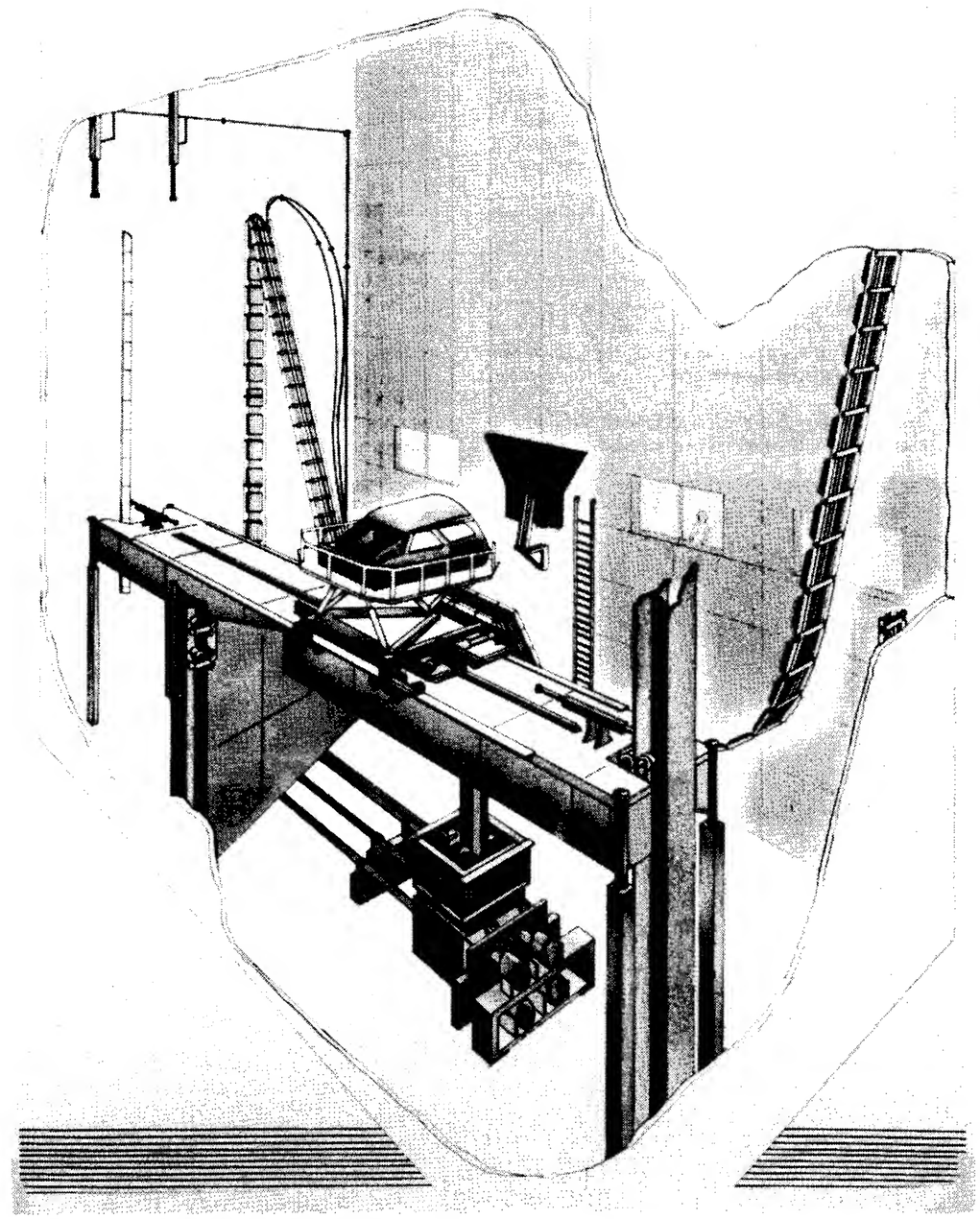

FIGURE 4.16
Sketch of a NASA ground based motion simulator. (Courtesy of SAE Aerospace Engineering magazine).

assumptions were verified by an examination of the exact solution. The approximate formulas permitted us to examine the relationship of the stability derivatives on the longitudinal motion.

Before concluding, it seems appropriate to discuss several areas of research that will affect how we analyze aircraft motions. As mentioned, active control technology in commercial aircraft can be used to improve aerodynamic

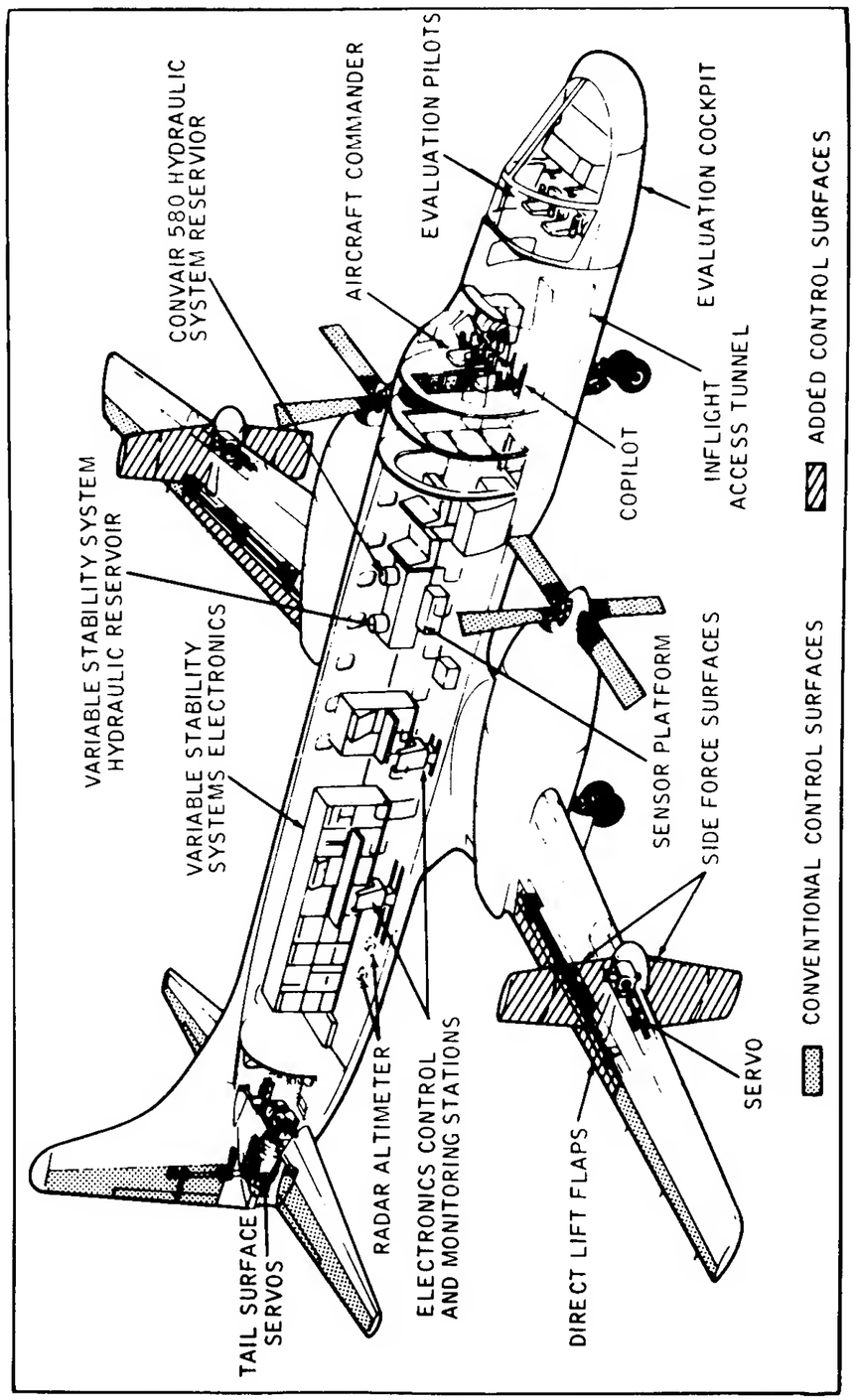

FIGURE 4.17
Airborne flight simulator.

efficiency. With active controls, the aircraft can be flown safely with more aft center of gravity position than would be possible with a standard control system. By shifting the center of gravity further aft, the trim drag can be reduced substantially. This allows for improved fuel economy during the cruise portion of the flight.

Active control technology can also be used to improve ride comfort and reduce wing bending during flight in turbulent air. With active controls located on the wing, a constant load factor can be maintained. This alleviates most of the unwanted response associated with encounters with a vertical gust field. In addition to improving the ride for passengers, the gust alleviation system reduces the wing bending moments, which means the wing can be lighter. Again, this will result in potential fuel savings.

One final topic that has a bearing on the material presented in this chapter is the influence of high angle of attack flight on dynamic stability [4.6, 4.7]. The flight envelopes of high-performance aircraft and missiles have expanded considerably in recent years owing to the increased demands for improved maneuverability. As a result, many of these vehicles encounter higher angles of attack and angular rates than in the past.

As the angle of attack of the airplane increases, the flow around the fuselage separates. The separated flow field can cause non-linear static and dynamic aerodynamic characteristics. An example of the complexity of the leeward wake flows around a slender aircraft and a missile is sketched in Fig. 4.18. Notice that, as the angle of attack becomes large, the separated body vortex flow can become asymmetric. The occurrence of this asymmetry in the flow can give rise to large side forces, yawing, and rolling moments on the airplane or missile even though the vehicle is performing a symmetric maneuver (i.e. sideslip angle equals zero). The asymmetric shedding of the nose vortices is believed to be one of the major contributions to the stall spin departure characteristics of many high-performance airplanes.

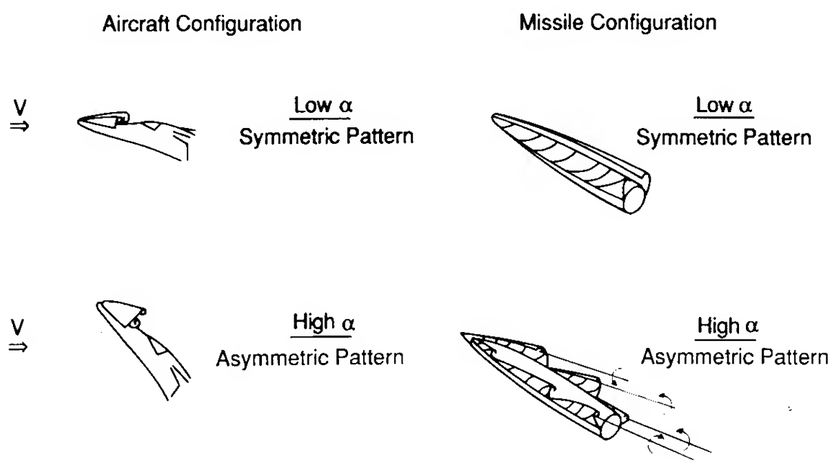

FIGURE 4.18
Vortex flows around an aircraft at large angles of attack.

The asymmetric vortex wake can lead to aerodynamic cross-coupling between the longitudinal and lateral equations of motion. Analyzing these motions requires a much more sophisticated analysis than that presented in this chapter.

4.10 PROBLEMS

4.1. Starting with Newton's second law of motion, develop the equation of motion for the simple torsional pendulum shown in Fig. P4.1. The concept of the torsional pendulum can be used to determine the mass moment of inertia of aerospace vehicles and/or components. Discuss how one could use the torsional pendulum concept to determine experimentally the mass moment of inertia of a test vehicle.

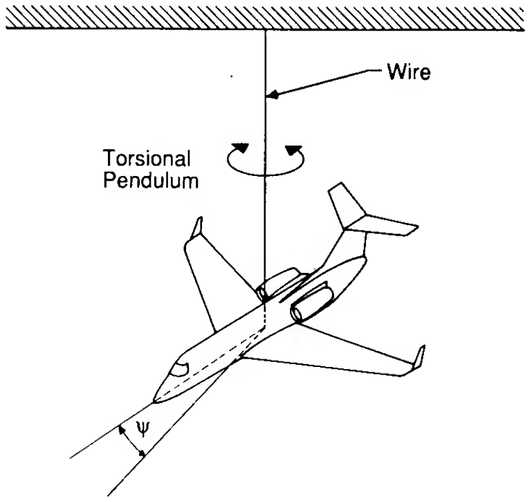

FIGURE P4.1
Sketch of aircraft model swinging as a torsional pendulum.

4.2. A mass weighing 5 lb is attached to a spring as shown in Fig. P4.2A. The spring is observed to extend 1 inch when the mass is attached to the spring. Suppose the mass is given an instantaneous velocity of 10 ft/s in the downward direction from the equilibrium position. Determine the displacement of the mass as a function of time. Repeat your analysis for the spring mass damper system Fig. P4.2B, assume $F = -c\dot{y}$ where $c = 0.6$ (lb-sec/ft.).

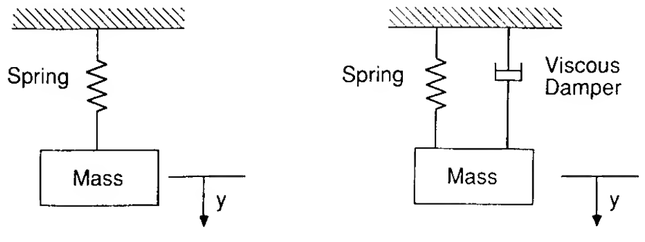

A. Mass - spring system B. Mass - spring - damper system

FIGURE P4.2
Spring mass and spring mass damper systems.

4.3. The differential equation for the constrained center of gravity pitching motion of an airplane is computed to be:

$$\ddot{\alpha} + 4\dot{\alpha} + 36\alpha = 0$$

Find the following:

(a) ω_n, natural frequency, rad/s

(b) ζ, damping ratio

(c) ω_d damped natural frequency, rad/s

4.4. Determine the eigenvalues and eigenvectors for the following matrix:

$$\mathbf{A} = \begin{bmatrix} 2 & -3 & 1 \\ 3 & 1 & 3 \\ -5 & 2 & -4 \end{bmatrix}$$

4.5. The characteristic roots of a second-order system are shown in Fig. P4.5. If this system is disturbed from equilibrium, find the time to half-amplitude, the number of cycles to half-amplitude, and the period of motion.

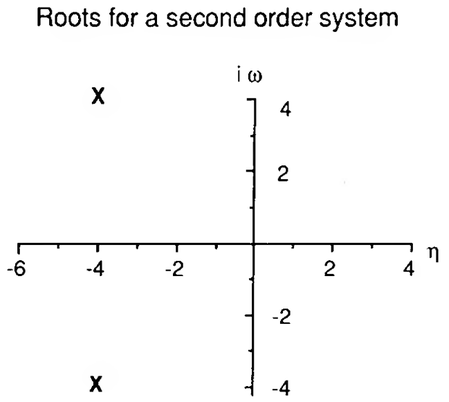

FIGURE P4.5
Second order system roots.

4.6. The missile shown in Fig. P4.6 is constrained so that only a pitching motion is possible. Assume that the aerodynamic damping and static stability come completely from the tail surface (i.e., neglect the body contribution). If the model is displaced 10° from its trim angle of attack ($\alpha_t = 0$) and then released, determine the angle of attack time history. Plot your results. What effect would moving the center of gravity have on the motion of the model?

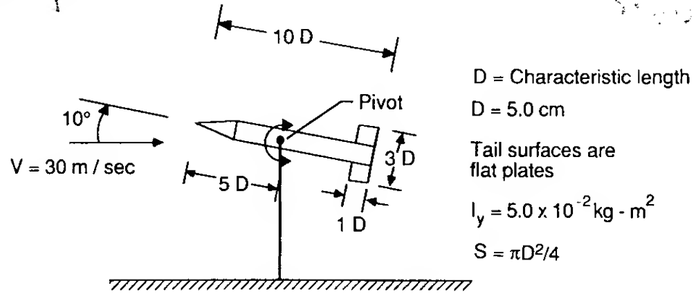

FIGURE P4.6
Pitching wind tunnel model.

4.7. Use the short- and long-period approximations to find the damping ratio for the executive jet airplane described in Appendix B.

4.8. Show that if one neglects compressibility effects, the frequency and damping ratio

for the phugoid mode can be expressed as:

$$\omega_{np} = \sqrt{2}\frac{g}{u_0} \qquad \text{and} \qquad \zeta_p = \frac{1}{\sqrt{2}}\frac{1}{L/D}$$

4.9. What effect will increasing altitude have on the short- and long-period modes? Use the approximate formulas in your analysis.

4.10. Develop the equation of motion for an airplane that has freedom only along the flight path, i.e. variations in forward speed. If the airplane is perturbed from its equilibrium state what type of motion would you expect? Clearly state all of your assumptions.

4.11. Develop a computer program to compute the eigenvalues for the longitudinal equations of motion. Use your program to determine the characteristic roots for the executive jet airplane described in Appendix B. Compare your results with those obtained in Problem 4.7.

4.12. An airplane has the following stability and inertial characteristics:

$W = 564\,000$ lb	$C_L = 1.11$
$I_x = 13.7 \times 10^6$ slug·ft^2	$C_D = 0.102$
$I_y = 30.5 \times 10^6$ slug·ft^2	$C_{L_\alpha} = 5.7$ rad^{-1}
$I_z = 43.1 \times 10^6$ slug·ft^2	$C_{D\alpha} = 0.66$ rad^{-1}
$h =$ sea level	$C_{m_\alpha} = -1.26$ rad^{-1}
$S = 5500$ ft^2	$C_{m_{\dot\alpha}} = -3.2$ rad^{-1}
$b = 195.68$ ft	$C_{m_q} = -20.8$ rad^{-1}
$\bar c = 27.3$ ft	
$V = 280$ ft/sec	

(a) Find the frequency and damping ratios of the short- and long-period modes.

(b) Find the time to half-amplitude for each mode.

(c) Discuss the influence of the coefficients C_{m_q} and C_{m_α} on the longitudinal motion.

4.13. From data in Fig. P4.13, estimate the time to half-amplitude and the number of cycles for both the short- and long-period modes.

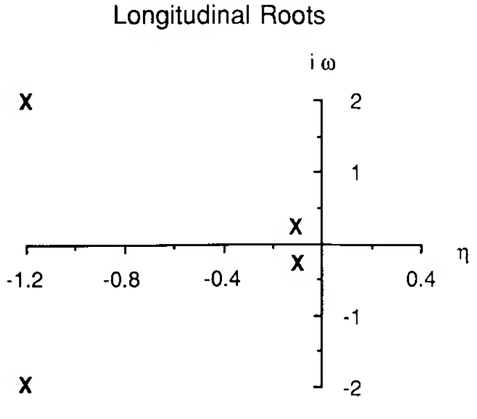

FIGURE P4.13

4.14. A wind-tunnel model is constrained so that only a pitching motion can occur. The model is in equilibrium when the angle of attack is zero. When the model is displaced from its equilibrium state and released, the motion shown in Fig. P4.14 is recorded. Using the data given below determine C_{m_α} and $C_{m_q} + C_{m_{\dot\alpha}}$.

$$u_0 = 100 \text{ ft/sec} \qquad \bar c = 0.2 \text{ ft}$$
$$Q = 11.9 \text{ lb/ft}^2 \qquad I_y = 0.01 \text{ slug-ft}^2$$
$$S = 0.5 \text{ ft}^2$$

Assume that equation of motion is

$$\theta(t) = \theta_0 e^{\eta t} \cos \omega t$$

where

$$\eta = (M_q + M_{\dot\alpha})/2.0$$

and

$$\omega = \sqrt{-M_\alpha}$$

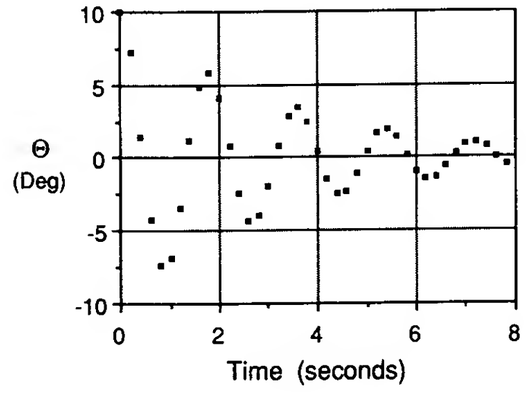

FIGURE P4.14

REFERENCES

4.1. Lanchester, F. W.: *Aerodonetics,* Archibald Constable, London, 1908.

4.2. Perkins, C. D.: "Development of Airplane Stability and Control Technology," *AIAA Journal of Aircraft,* vol. 7, no. 4, 1970 pp. 290–301.

4.3. Bairstow, L.: *Applied Aerodynamics,* 2nd ed., Longmans, Green, New York, 1939.

4.4. Garber, P. E.: 'The Wright Brothers' Contribution to Airplane Design," from *Proceedings of the AIAA Diamond Jubilee of Powered Flight—The Evolution of Aircraft Design,* AIAA, New York, 1978.

4.5. *MIL-F-8785B Military Specifications—Flying Qualities of Piloted Airplanes,* August 1969.

4.6. Curry, W. H., and K. J. Orlick-Ruckermann: "Sensitivity of Aircraft Motion to Aerodynamic Cross-Coupling at high Angles of Attack," paper presented at the AGARD Fluid Dynamics Panel Symposium on Dynamic Stability Parameters held in Athens, Greece, May 22–24, 1978.

4.7. Butler, R. W., and T. F. Langham: "Aircraft Motion Sensitivity to Variations in Dynamic Stability parameters," paper presented at the AGARD Fluid Dynamics Panel Symposium on Dynamic Stability Parameters held in Athens, Greece, May 22–24, 1978.

CHAPTER 5

LATERAL MOTION (STICK FIXED)

"Dutch Roll is a complex oscillating motion of an aircraft involving rolling, yawing and sideslipping. So named for the resemblance to the characteristic rhythm of an ice skater".

[5.1]

5.1 INTRODUCTION

The stick fixed lateral motion of an airplane disturbed from its equilibrium state is a complicated combination of rolling, yawing, and sideslipping motions. As was shown in Chapter 2, an airplane produces both yawing and rolling moments due to sideslip angle. This interaction between roll and yaw produces the coupled motion. There are three potential lateral dynamic instabilities of interest to the airplane designer: they are directional divergence, spiral divergence, and the so-called Dutch roll oscillation.

Directional divergence can occur when the airplane does not possess directional or weathercock stability. If such an airplane is disturbed from its equilibrium state, it will tend to rotate to ever-increasing angles of sideslip. Owing to the side force acting on the airplane, it will fly a curved path at large sideslip angles. For an airplane that has lateral static stability (i.e. dihedral effect) the motion can occur without any significant change in bank angle. Obviously, such a motion cannot be tolerated and can readily be avoided by proper design of the vertical tail surface to ensure directional stability.

Spiral divergence is a nonoscillatory divergent motion which can occur when directional stability is large and lateral stability is small. When disturbed from equilibrium, the airplane enters a gradual spiraling motion. The spiral

becomes tighter and steeper as time proceeds and can result in a high-speed spiral dive if corrective action is not taken. This motion normally occurs so gradually that the pilot unconsciously corrects for it.

The Dutch roll oscillation is a coupled lateral-directional oscillation which can be quite objectionable to pilots and passengers. The motion is characterized by a combination of rolling and yawing oscillations which have the same frequency but are out of phase with each other. The period can be of the order of 3 to 15 seconds, so that if the amplitude is appreciable the motion can be very annoying.

Before analyzing the complete set of lateral equations we shall examine several motions with a single degree of freedom. The purpose of examining the single degree of freedom equations is to gain an appreciation of the more complicated motion comprising the stick fixed lateral motion of an airplane.

5.2 PURE ROLLING MOTION

A wind-tunnel model free to roll about its x axis is shown in Fig. 5.1. The equation of motion for this example of a pure rolling motion is

$$\sum \text{Rolling moments} = I_x \ddot{\phi} \tag{5.1}$$

or

$$\frac{\partial L}{\partial \delta_a}\delta_a + \frac{\partial L}{\partial p}p = I_x \ddot{\phi} \tag{5.2}$$

where $(\partial L/\partial \delta_a)\delta_a$ is the roll moment due to the deflection of the ailerons and $(\partial L/\partial p)p$ is the roll-damping moment. Methods for estimating these derivatives were presented in Chapters 2 and 3. The roll angle ϕ is the angle between

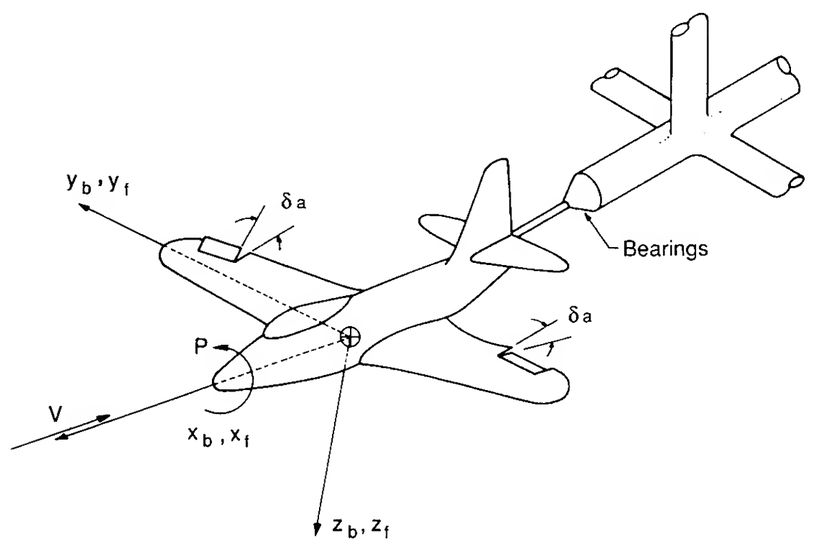

FIGURE 5.1
Wind tunnel model constrained to a pure rolling motion.

z_b of the body axes and z_f of the fixed axis system. The roll rate p is equal to $\dot{\phi}$, which will allow us to re-write Eq. (5.2) as follows:

$$\tau \frac{dp}{dt} + p = -\frac{L_{\delta a}\,\Delta\delta_a}{L_p} \tag{5.3}$$

where τ, L_p and $L_{\delta a}$ are defined as follows:

$$\tau = -\frac{1}{L_p} \quad \text{and} \quad L_p = \frac{\partial L/\partial p}{I_x} \quad L_{\delta a} = \frac{\partial L/\partial \delta_a}{I_x} \tag{5.4}$$

The parameter τ is referred to as the time constant of the system. The time constant tells us how fast our system approaches a new steady-state condition after being disturbed. If the time constant is small, the system will respond very rapidly; if the time constant is large, the system will respond very slowly.

The solution of Eq. (5.3) for a step change in the aileron angle is

$$p(t) = -\frac{L_{\delta a}}{L_p}(1 - e^{-t/\tau})\,\Delta\delta_a \tag{5.5}$$

Recall that C_{lp} is negative; therefore, the time constant will be positive. The roll rate time history for this example will be similar to that shown in Fig. 5.2. The steady-state roll rate can be obtained from Eq. (5.5), by assuming that time t is large enough that $e^{-t/\tau}$ is essentially zero:

$$p_{ss} = \frac{-L_{\delta a}}{L_p}\Delta\delta_a \tag{5.6}$$

$$p_{ss} = \frac{-C_{l_{\delta a}} QSb/I_x}{C_{l_p}(b/2u_0)QSb/I_x}\Delta\delta_a \tag{5.7}$$

$$\frac{p_{ss} b}{2u_0} = -\frac{C_{l_{\delta a}}}{C_{lp}}\Delta\delta_a$$

The term $(p_{ss}b/2u_0)$ for full aileron deflection can be used for sizing the aileron. The minimum requirement for this ratio is a function of the class of airplane under consideration:

Cargo or transport airplanes: $pb/2u_0 = 0.07$
Fighter airplanes: $pb/2u_0 = 0.09$

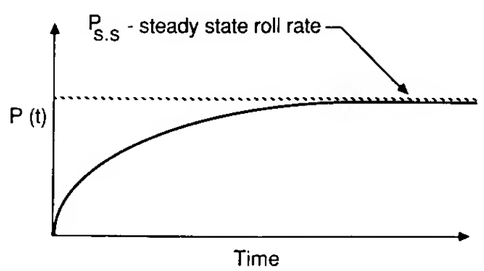

FIGURE 5.2
Typical roll response due to aileron deflection.

Example Problem 5.1. Calculate the roll response of the F104A to a 5° step change in aileron deflection. Assume the airplane is flying at sea level with a velocity of 87 m/s. The F104A has the following aerodynamic and geometric characteristics:

$$C_{l_p} = 0.285\ \text{rad}^{-1} \qquad S = 18\ \text{m}^2$$
$$C_{l_{\delta a}} = 0.039\ \text{rad}^{-1} \qquad b = 6.7\ \text{m}$$
$$I_x = 4676\ \text{kg·m}^2$$
$$\frac{b}{2u_0} = \frac{6.7}{2(87\ \text{m/s})} = 0.039\ \text{s}$$

$$Q = \tfrac{1}{2}\rho u_0^2 = (0.5)(1.225\ \text{kg/m}^3)(87\ \text{m/s})^2 = 4636\ \text{N/m}^2$$

$$L_p = C_{lp}\frac{b}{2u_0}QSb/I_x$$

$$= (-0.285\ \text{rad}^{-1})(0.039\ \text{s}^{-1})(4636\ \text{N/m}^2)(18\ \text{m}^2)(6.7\ \text{m})(4676\ \text{kg·m}^2)$$

$$L_p = -1.3\ (\text{s}^{-1})$$

$$\tau = -\frac{1}{L_p} = -\frac{1}{(-1.3\ \text{s}^{-1})} = 0.77\ \text{s}$$

Steady state roll rate

$$p_{ss} = -\frac{L_{\delta a}}{L_p}\Delta\delta_a$$

$$L_{\delta a} = C_{l\delta a}QSb/I_x$$

$$L_{\delta a} = (0.039\ \text{rad}^{-1})(4636\ \text{N/m}^2)(18\ \text{m}^2)(6.7\ \text{m})/(4676\ \text{kg·m}^2) = 4.66\ (\text{s}^{-2})$$

$$p_{ss} = -(4.66\,1\ \text{s}^{-2})(5\ \text{deg})/(-1.3\ \text{s}^{-1})(57.3\ \text{deg/rad})) = 0.31\ \text{rad/s}$$

Figure 5.4 is a plot of the role rate time history for a step change in aileron deflection.

Let us reconsider this problem. Suppose that Fig. 5.3 is a measured roll

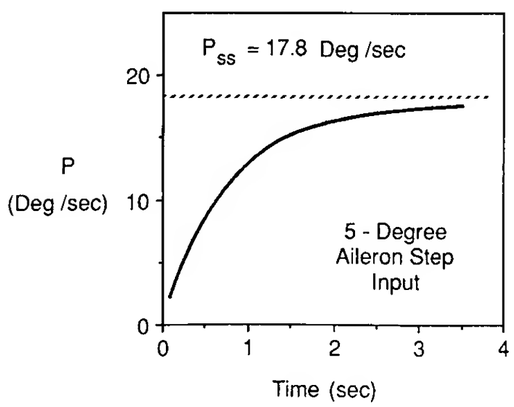

FIGURE 5.3
Roll time history of an F104A to a 5-degree step change in aileron deflection.

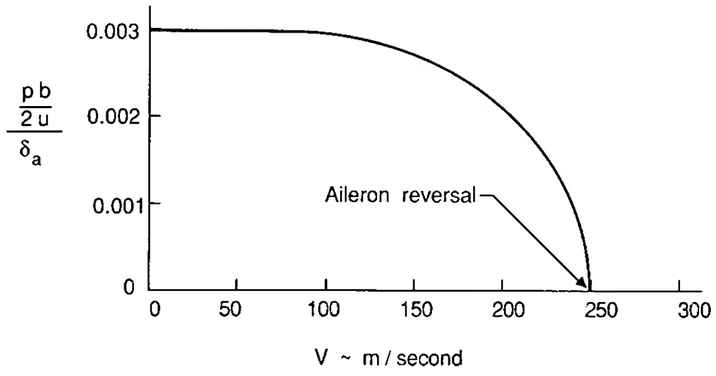

FIGURE 5.4
Aileron control power per degree versus flight velocity.

rate instead of a calculated response. The roll rate of the airplane could be measured by means of a rate gyro appropriately located on the airplane. If we know the mass and geometric properties of the airplane, we can extract the aerodynamic stability coefficients from the measured motion data.

If we fit the solution to the differential equation of motion to the response, we can obtain values for $C_{l_{\delta a}}$ and C_{l_p}. It can be shown that after one time constant, the response of a first-order system to a step input is 63% of its final value. With this in mind, we can obtain the time constant from Fig. 5.3. The steady-state roll rate can also be measured directly from this figure. Knowing τ and p_{ss}, we can compute $L_{\delta a}$ and L_p and, in turn, $C_{l_{\delta a}}$ and C_{l_p}. The technique of extracting aerodynamic data from the measured response is often called the "inverse problem" or "parameter identification".

ROLL CONTROL REVERSAL. The aileron control power per degree, $(pb/2u_0)/\delta_a$ is shown in Fig. 5.4. Note that $(pb/2u_0)/\delta_a$ is essentially a constant, independent of speeds below 140 m/s. However, at high speeds $(pb/2u_0)/\delta_a$ decreases until a point is reached where roll control is lost. The point at which $(pb/2u_0)/\delta_a = 0$ is called the aileron reversal speed. The loss and ultimate reversal of aileron control is due to the elasticity of the wing.

Some understanding of this aeroelastic phenomenon can be obtained from the following simplified analysis. Figure 5.5 is a sketch of a two-dimensional wing with an aileron. As the aileron is deflected downwards, it

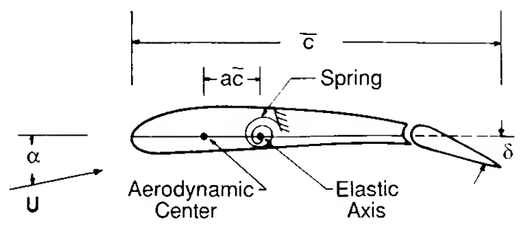

FIGURE 5.5
Two-dimensional wing and aileron.

increases the lift acting on the wing. The increased lift produces a rolling moment. Deflecting the aileron also produces a nose-down aerodynamic pitching moment which tends to twist the wing downward. Such a rotation will reduce the lift and rolling moment. The aerodynamic forces vary with the square of the airplane's velocity, whereas the elastic stiffness of the wing is independent of the flight speed. Thus, it is possible that the wing may twist enough that the ailerons become ineffective. The speed at which the ailerons become ineffective is called the critical aileron reversal speed.

To determine the aileron reversal speed, we shall use the information in Fig. 5.5. The torsional stiffness of the wing will be modeled by the simple torsional spring located at the elastic axis of the wing. The lift and moment coefficients for the two-dimensional airfoil can be expressed as functions of the stability coefficients:

$$C_l = C_{l_\alpha}\alpha + C_{l_\delta}\delta \tag{5.8}$$

$$C_m = C_{m_{ac}} + C_{m_\delta}\delta \tag{5.9}$$

where δ is the flap angle, i.e. aileron. Aileron reversal occurs when the rate of change of lift with aileron deflection is zero:

$$L = (C_{l_\alpha}\alpha + C_{l_\delta}\delta)Q\bar{c} \tag{5.10}$$

$$\frac{dL}{d\delta} = \left(C_{l_\alpha}\frac{d\alpha}{d\delta} + C_{l_\delta}\right)Q\bar{c} = 0 \tag{5.11}$$

or

$$\frac{d\alpha}{d\delta} = -\frac{C_{l_\delta}}{C_{l_\alpha}} \tag{5.12}$$

Note that the angle of attack is a function of the flap angle because the wing can twist. The aerodynamic moment acting about the elastic axis is

$$M = [C_{m_{ac}} + C_{m_\delta}\delta + (C_{l_\alpha}\alpha + C_{l_\delta}\delta)a]Q\bar{c}^2 \tag{5.13}$$

This moment is balanced by the torsional moment of the wing:

$$k\alpha = [C_{m_{ac}} + C_{m_\delta}\delta + (C_{l_\alpha}\alpha + C_{l_\delta}\delta)a]Q\bar{c}^2 \tag{5.14}$$

Differentiating Eq. (5.14) with respect to δ yields

$$k\frac{d\alpha}{d\delta} = \left[C_{m_\delta} + \left(C_{l_\alpha}\frac{d\alpha}{d\delta} + C_{l_\delta}\right)a\right]Q\bar{c}^2 \tag{5.15}$$

Substituting Eq. (5.12) into (5.15) and solving for Q yields the critical dynamic pressure:

$$Q_{rev} = -\frac{kC_{l_\delta}}{c^2 C_{l_\alpha} C_{m_\delta}} \tag{5.16}$$

The reversal speed is given by

$$U_{\text{rev}} = \sqrt{-\frac{2kC_{l_\delta}}{\rho c^2 C_{l_\alpha} C_{m_\delta}}} \tag{5.17}$$

Note that the reversal speed increases with increasing torsional stiffness and increasing altitude.

5.3 PURE YAWING MOTION

As our last example of a motion with a single degree of freedom, we shall examine the motion of an airplane constrained so that it can perform only a simple yawing motion. Figure 5.6 is a sketch of a wind-tunnel model which can only perform yawing motions. The equation of motion can be written as follows:

$$\sum \text{Yawing moments} = I_z \ddot{\psi} \tag{5.18}$$

The yawing moment N and the yaw angle ψ can be expressed as

$$N = N_0 + \Delta N \qquad \psi = \psi_0 + \Delta\psi \tag{5.19}$$

The yawing moment equation reduces to

$$\Delta N = I_z \, \Delta\ddot{\psi} \tag{5.20}$$

where

$$\Delta N = \frac{\partial N}{\partial \beta}\Delta\beta + \frac{\partial N}{\partial \dot{\beta}}\Delta\dot{\beta} + \frac{\partial N}{\partial r}\Delta r + \frac{\partial N}{\partial \delta_r}\Delta\delta_r \tag{5.21}$$

Because the centre of gravity is constrained, the yaw angle ψ and the sideslip

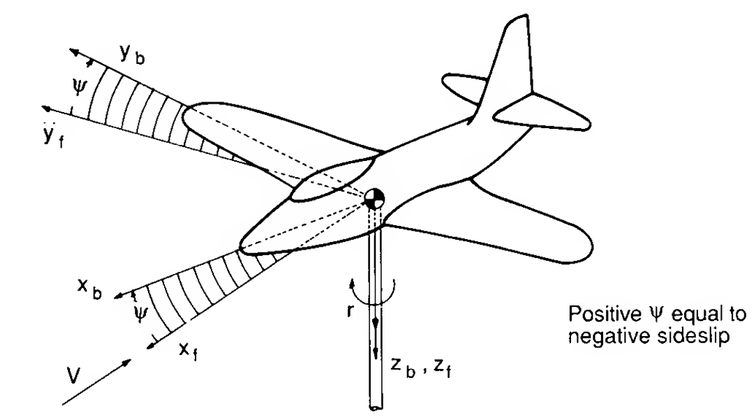

FIGURE 5.6
Wind tunnel model constrained to a pure yawing motion.

angle β are related by the expression

$$\Delta\psi = -\Delta\beta \qquad \Delta\dot{\psi} = -\Delta\dot{\beta} \qquad \Delta\ddot{\psi} = \Delta r \tag{5.22}$$

Substituting these relationships into Eq. (5.20) and rearranging, yields

$$\Delta\ddot{\psi} - (N_r - N_{\dot{\beta}})\,\Delta\dot{\psi} + N_\beta\,\Delta\psi = N_{\delta r}\,\Delta\delta_r \tag{5.23}$$

where

$$N_r = \frac{\partial N/\partial r}{I_z} \qquad \text{etc.}$$

For airplanes, the term $N_{\dot{\beta}}$ is usually negligible and will be eliminated in future expressions.

The characteristic equation for Eq. (5.23) is

$$\lambda^2 - N_r\lambda + N_\beta = 0 \tag{5.24}$$

The damping ratio ζ and the undamped natural frequency ω_n can be determined directly from Eq. (5.24):

$$\omega_n = \sqrt{N_\beta} \tag{5.25}$$

$$\zeta = -\frac{N_r}{2\sqrt{N_\beta}} \tag{5.26}$$

The solution of Eq. (5.23) for a step change in the rudder control will result in a damped sinusoidal motion, provided the airplane has sufficient aerodynamic damping. As in the case of the pure pitching, we see that the frequency of oscillation is a function of the airplane's static stability (weathercock or directional stability) and the damping ratio is a function of the aerodynamic damping derivative. Figure 5.7 is a sketch of the yawing motion

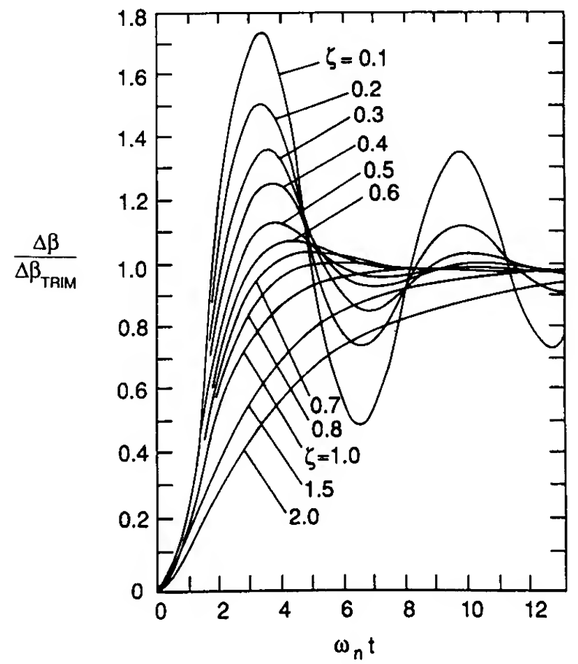

FIGURE 5.7
Yawing motion due to rudder deflection.

due to a step change in rudder deflections for different levels of aerodynamic damping.

5.4 LATERAL-DIRECTIONAL EQUATIONS OF MOTION

The lateral-directional equations of motion consist of the side force, rolling moment and yawing moment equations of motion. The lateral equations of motion can be rearranged into the state space form in the following manner. We start with Eq. (5.27) shown below.

$$\left(\frac{\mathrm{d}}{\mathrm{d}t} - Y_v\right)\Delta v - Y_p\,\Delta p + (u_0 - Y_r)\,\Delta r - g\cos\theta_0\,\Delta\phi = Y_{\delta r}\,\Delta\delta_r$$

$$-L_v\,\Delta v + \left(\frac{\mathrm{d}}{\mathrm{d}t} - L_p\right)\Delta p - \left(\frac{I_{xz}}{I_x}\frac{\mathrm{d}}{\mathrm{d}t} + L_r\right)\Delta r = L_{\delta a}\,\Delta\delta_a + L_{\delta r}\,\Delta\delta_r \qquad (5.27)$$

$$-N_v\,\Delta v - \left(\frac{I_{xz}}{I_z}\frac{\mathrm{d}}{\mathrm{d}t} + N_p\right)\Delta p + \left(\frac{\mathrm{d}}{\mathrm{d}t} - N_r\right)\Delta r = N_{\delta a}\,\Delta\delta_a + N_{\delta r}\,\Delta\delta_r$$

Rearranging and collecting terms the above equations can be written in the state variable form:

$$\dot{\mathbf{x}} = \mathbf{A}\mathbf{x} + \mathbf{B}\boldsymbol{\eta} \qquad (5.28)$$

The matrices **A** and **B** are defined as follows:

$$\mathbf{A} = \begin{bmatrix} Y_v & Y_p & -(u_0 - Y_r) & g\cos\theta_0 \\ L_v^* + \frac{I_{xz}}{I_x}N_v^* & L_p^* + \frac{I_{xz}}{I_x}N_p^* & L_r^* + \frac{I_{xz}}{I_x}N_r^* & 0 \\ N_v^* + \frac{I_{xz}}{I_z}L_v^* & N_p^* + \frac{I_{xz}}{I_z}L_p^* & N_r^* + \frac{I_{xz}}{I_z}L_r^* & 0 \\ 0 & 1 & 0 & 0 \end{bmatrix} \qquad (5.29)$$

$$\mathbf{B} = \begin{bmatrix} 0 & Y_{\delta r} \\ L_{\delta_a}^* + \frac{I_{xz}}{I_x}N_{\delta_a}^* & L_{\delta_r}^* + \frac{I_{xz}}{I_x}N_{\delta_r}^* \\ N_{\delta_a}^* + \frac{I_{xz}}{I_z}L_{\delta_a}^* & N_{\delta_r}^* + \frac{I_{xz}}{I_z}L_{\delta_r}^* \\ 0 & 0 \end{bmatrix} \qquad (5.30)$$

$$\mathbf{x} = \begin{bmatrix} \Delta v \\ \Delta p \\ \Delta r \\ \Delta\phi \end{bmatrix} \quad \text{and} \quad \boldsymbol{\eta} = \begin{bmatrix} \Delta\delta_a \\ \Delta\delta_r \end{bmatrix} \qquad (5.31)$$

The starred derivatives are defined as follows:

$$L_v^* = \frac{L_v}{[1 - (I_{xz}^2/I_xI_z)]} \qquad N_v^* = \frac{N_v}{[1 - (I_{xz}^2/I_zI_x)]} \qquad \text{etc.} \qquad (5.32)$$

If the product of inertia $I_{xz} = 0$, the equations of motion reduce to the following form:

$$\begin{bmatrix} \Delta\dot{v} \\ \Delta\dot{p} \\ \Delta\dot{r} \\ \Delta\dot{\phi} \end{bmatrix} = \begin{bmatrix} Y_v & Y_p & -(u_0 - Y_r) & g\cos\theta_0 \\ L_v & L_p & L_r & 0 \\ N_v & N_p & N_r & 0 \\ 0 & 1 & 0 & 0 \end{bmatrix}\begin{bmatrix} \Delta v \\ \Delta p \\ \Delta r \\ \Delta\phi \end{bmatrix} + \begin{bmatrix} 0 & Y_{\delta r} \\ L_{\delta a} & L_{\delta r} \\ N_{\delta a} & N_{\delta r} \\ 0 & 0 \end{bmatrix}\begin{bmatrix} \Delta\delta_a \\ \Delta\delta_r \end{bmatrix} \qquad (5.33)$$

It is sometimes convenient to use the sideslip angle $\Delta\beta$ instead of the side velocity Δv. These two quantities are related to each other in the following way:

$$\Delta\beta \approx \tan^{-1}\frac{\Delta v}{u_0} = \frac{\Delta v}{u_0} \qquad (5.34)$$

Using this relationship, Eqs (5.33) can be expressed in terms of $\Delta\beta$:

$$\begin{bmatrix} \Delta\dot{\beta} \\ \Delta\dot{p} \\ \Delta\dot{r} \\ \Delta\dot{\phi} \end{bmatrix} = \begin{bmatrix} \frac{Y_\beta}{u_0} & \frac{Y_p}{u_0} & -\left(1 - \frac{Y_r}{u_0}\right) & \frac{g\cos\theta_0}{u_0} \\ L_\beta & L_p & L_r & 0 \\ N_\beta & N_p & N_r & 0 \\ 0 & 1 & 0 & 0 \end{bmatrix}\begin{bmatrix} \Delta\beta \\ \Delta p \\ \Delta r \\ \Delta\phi \end{bmatrix} + \begin{bmatrix} 0 & \frac{Y_{\delta r}}{u_0} \\ L_{\delta_a} & L_{\delta_r} \\ N_{\delta_a} & N_{\delta_r} \\ 0 & 0 \end{bmatrix}\begin{bmatrix} \Delta\delta_a \\ \Delta\delta_r \end{bmatrix} \qquad (5.35)$$

The solution of Eq. (5.35) is obtained in the same manner as we solved the state equations in Chapter 4. The characteristic equation is obtained by expanding the following determinant.

$$|\lambda_r\mathbf{I} - \mathbf{A}| = 0 \qquad (5.36)$$

where **I** and **A** are the identity and lateral stability matrices, respectively. The characteristic equation determined from the stability matrix **A** yields a quartic equation:

$$A\lambda^4 + B\lambda^3 + C\lambda^2 + D\lambda + E = 0 \qquad (5.37)$$

where A, B, C, D, and E are functions of the stability derivatives, mass, and inertia characteristics of the airplane.

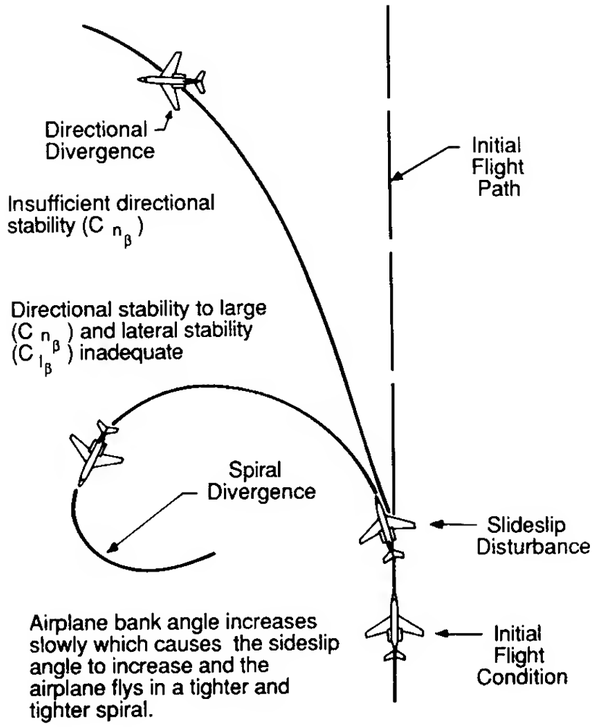

FIGURE 5.8
Sketch of the spiral motion.

In general, we will find the roots to the lateral-directional characteristic equation to be composed of two real roots and a pair of complex roots. The roots will be such that the airplane response can be characterized by the following motions:

(a) a slowly convergent or divergent motion, called the spiral mode
(b) a highly convergent motion, called the rolling mode
(c) a lightly damped oscillatory motion having a low frequency, called the Dutch roll mode.

Figures 5.8, 5.9 and 5.10 are sketches of the spiral, roll and Dutch roll motions. An unstable spiral mode results in a turning flight trajectory. The airplane's bank angle increases slowly and the airplane flies an ever tightening spiral dive. The rolling motion is usually highly damped and will reach a steady

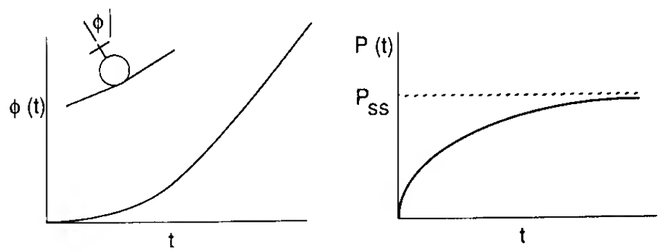

FIGURE 5.9
Sketch of the roll motion.

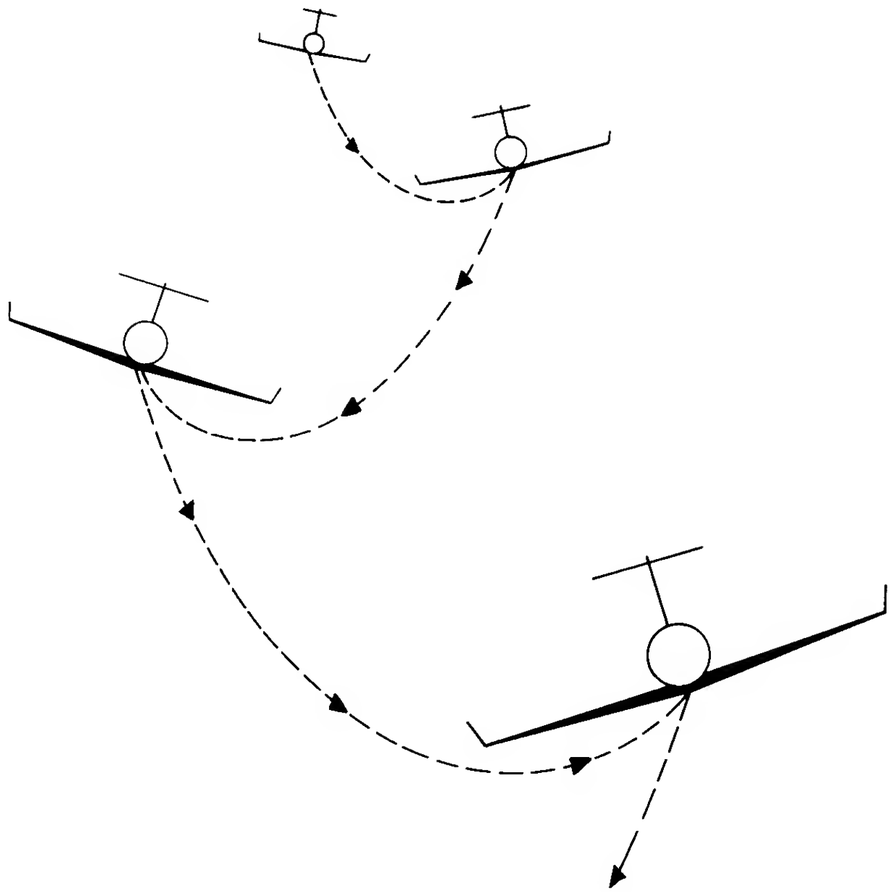

FIGURE 5.10
Sketch of the Dutch roll motion.

state in a very short time. The combination of the yawing and rolling oscillations is called the Dutch roll motion because it resembles the weaving motion of an ice skater.

SPIRAL APPROXIMATION. As indicated in Fig. 5.8, the spiral mode is characterized by changes in bank angle ϕ and heading angle ψ. The sideslip angle is usually quite small but cannot be neglected because the aerodynamic moments do not depend on the roll angle ϕ or the heading angle ψ, but on the sideslip angle β, roll rate p, and yawing rate r.

The aerodynamic contributions due to β and r are usually of the same order of magnitude. Therefore, to obtain an approximation of the spiral mode, we shall neglect the side force equation and $\Delta\phi$. With these assumptions, the equations of motion for the approximation can be obtained from Eqs (5.35):

$$L_\beta \Delta\beta + L_r \Delta r = 0 \tag{5.38}$$

$$\Delta\dot{r} = N_\beta \Delta\beta + N_r \Delta r \tag{5.39}$$

or

$$\dot{\Delta r} + \frac{L_r N_\beta - L_\beta N_r}{L_\beta} \Delta r = 0 \tag{5.40}$$

The characteristic root for the above equation is

$$\lambda_{\text{spiral}} = \frac{L_\beta N_r - L_r N_\beta}{L_\beta} \tag{5.41}$$

The stability derivatives L_β (dihedral effect) and N_r (yaw rate damping), are usually negative quantities. On the other hand, N_β (directional stability) and L_r (roll moment due to yaw rate) are generally positive quantities. If the derivatives have the usual sign, then the condition for a stable spiral model is

$$L_\beta N_r - N_\beta L_r > 0 \tag{5.42}$$

or

$$L_\beta N_r > N_\beta L_r \tag{5.43}$$

Increasing the dihedral effect L_β and/or the yaw damping can be used to make the spiral mode stable.

ROLL APPROXIMATION. This motion can be approximated by the single degree of freedom rolling motion which was analyzed earlier in the chapter:

$$\tau \frac{dp}{dt} + p = 0$$

where τ is the roll time constant. Therefore

$$\lambda_{\text{roll}} = -\frac{1}{\tau} = L_p \tag{5.44}$$

The magnitude of the roll damping L_p is determined by the wing and tail surfaces.

DUTCH ROLL APPROXIMATION. If we consider the Dutch roll mode to consist primarily of sideslipping and yawing motions, then we can neglect the rolling moment equation. With these assumptions, Eq. (5.35) reduces to

$$\begin{bmatrix} \Delta\dot{\beta} \\ \Delta\dot{r} \end{bmatrix} = \begin{bmatrix} \frac{Y_\beta}{u_0} & -\left(1 - \frac{Y_r}{u_0}\right) \\ N_\beta & N_r \end{bmatrix} \begin{bmatrix} \Delta\beta \\ \Delta r \end{bmatrix} \tag{5.45}$$

Solving for the characteristic equation yields

$$\lambda^2 - \left(\frac{Y_\beta + u_0 N_r}{u_0}\right)\lambda + \frac{Y_\beta N_r - N_\beta Y_r + u_0 N_\beta}{u_0} = 0 \tag{5.46}$$

From this expression we can determine the undamped natural frequency and

the damping ratio as follows:

$$\omega_{n_{\text{DR}}} = \sqrt{\frac{Y_\beta N_r - N_\beta Y_r + u_0 N_\beta}{u_0}} \tag{5.47}$$

$$\zeta_{\text{DR}} = -\frac{1}{2\omega_{n_{\text{DR}}}} \left(\frac{Y_\beta + u_0 N_r}{u_0}\right) \tag{5.48}$$

The approximations developed in this section give, at best, only a rough estimate of the spiral and Dutch roll modes. The approximate formulas should, therefore, be used with caution. The reason for the poor agreement between the approximate and exact solutions is that the Dutch roll motion is truly a three degree of freedom motion with strong coupling between the equations.

Example Problem 5.2. Find the lateral eigenvalues for the general aviation airplane described in Chapter 4 and compare these results with the answers obtained using the lateral approximations. A summary of the aerodynamic and geometric data needed for this analysis is included in the appendices. The stick fixed lateral equations are shown below.

$$\begin{bmatrix} \Delta\dot{\beta} \\ \Delta\dot{p} \\ \Delta\dot{r} \\ \Delta\dot{\phi} \end{bmatrix} = \begin{bmatrix} \frac{Y_\beta}{u_0} & \frac{Y_p}{u_0} & -\left(1 - \frac{Y_r}{u_0}\right) & \frac{g}{u_0}\cos\theta_0 \\ L_\beta & L_p & L_r & 0 \\ N_\beta & N_p & N_r & 0 \\ 0 & 1 & 0 & 0 \end{bmatrix} \begin{bmatrix} \Delta\beta \\ \Delta p \\ \Delta r \\ \Delta\phi \end{bmatrix}$$

Before we can determine the eigenvalues of the stability matrix **A**, we must first calculate the lateral stability derivatives. Table 5.1 is a summary of the lateral stability derivative definitions and Table 5.2 gives a summary of the values of these derivatives for the general aviation airplane.

Substituting the lateral stability derivatives into the stick fixed lateral equations yields

$$\dot{\mathbf{x}} = \mathbf{A}\mathbf{x}$$

or

$$\begin{bmatrix} \Delta\dot{\beta} \\ \Delta\dot{p} \\ \Delta\dot{r} \\ \Delta\dot{\phi} \end{bmatrix} = \begin{bmatrix} -0.254 & 0 & -1.0 & 0.182 \\ -16.02 & -8.40 & 2.19 & 0 \\ 4.488 & -0.350 & -0.760 & 0 \\ 0 & 1 & 0 & 0 \end{bmatrix} \begin{bmatrix} \Delta\beta \\ \Delta p \\ \Delta r \\ \Delta\phi \end{bmatrix}$$

The eigenvalues can be determined by finding the eignevalues of the matrix **A**:

$$|\lambda_r \mathbf{I} - \mathbf{A}| = 0$$

The resulting characteristic equation is

$$\lambda^4 + 9.417\lambda^3 + 13.982\lambda^2 + 48.102\lambda + 0.4205 = 0$$

TABLE 5.1
Summary of lateral directional derivatives

$Y_\beta = \frac{QSC_{y\beta}}{m}$ (ft s^{-2})	$N_\beta = \frac{QSbC_{n\beta}}{I_z}$ (s^{-2})	$L_\beta = \frac{QSbC_{l\beta}}{I_x}$ (s^{-2})	
$Y_p = \frac{QSbC_{yp}}{2mu_0}$ (ft/s) or (m/s)	$N_p = \frac{QSb^2C_{np}}{2I_zu_0}$ (s^{-1})		
$L_p = \frac{QSb^2C_{lp}}{2I_xu_0}$ (s^{-1})			
$Y_r = \frac{QSbC_{yr}}{2mu_0}$ (ft/s) or (m/s)	$N_r = \frac{QSb^2C_{nr}}{2I_zu_0}$ (s^{-1})		
$L_r = \frac{QSb^2C_{lr}}{2I_xu_0}$ (s^{-1})			
$Y_{\delta a} = \frac{QSC_{y\delta a}}{m}$ (ft/s^2) or (m/s^2)	$Y_{\delta r} = \frac{QSC_{y\delta r}}{m}$ (ft/s^2) or (m/s^2)		
$N_{\delta a} = \frac{QSbC_{n\delta a}}{I_z}$ (s^{-2})	$N_{\delta r} = \frac{QSbC_{n\delta r}}{I_z}$ (s^{-2})		
$L_{\delta a} = \frac{QSbC_{l\delta a}}{I_x}$ (s^{-2})	$L_{\delta r} = \frac{QSbC_{l\delta r}}{I_x}$ (s^{-2})		

Solution of the characteristic equation yields the lateral eigenvalues:

$\lambda = -0.00877$ (Spiral mode)

$\lambda = -8.435$ (Roll mode)

$\lambda = -0.487 \pm i(2.335)$ (Dutch roll mode)

$$\lambda_{\text{sprial}} = \frac{L_\beta N_r - L_r N_\beta}{L_\beta}$$

TABLE 5.2
Lateral derivatives for the general aviation airplane

$Y_v = -0.254$ (s^{-1})	$L_v = -0.091$ (ft·s)$^{-1}$
$Y_\beta = -45.72$ (ft/s^2)	$L_\beta = -16.02$ (s^{-2})
$Y_p = 0$	$L_p = -8.4$ (s^{-1})
$Y_r = 0$	$L_r = 2.19$ (s^{-1})
$N_v = 0.025$ (ft·s)$^{-1}$	
$N_\beta = 4.49$ (s^{-2})	
$N_p = -0.35$ (s^{-1})	
$N_r = -0.76$ (s^{-1})	

Substituting in the numerical values for the derivatives yields

$$\lambda_{\text{spiral}} = [(-16.02)(-0.76) - (2.19)(4.49)]/(-16.02)$$
$$= -0.144$$
$$\lambda_{\text{roll}} = L_p = -8.4$$

The Dutch roll roots are determined from the characteristic equation given by Equation (5.44):

$$\lambda^2 - \frac{(Y_\beta + u_0 N_r)}{u_0}\lambda + \frac{Y_\beta N_r - N_\beta Y_r + u_0 N_\beta}{u_0} = 0$$

or

$$\lambda^2 + 1.102\lambda + 4.71 = 0$$

which yields the following roots

$$\lambda_{\text{DR}} = -0.51 \pm 2.109i$$

and

$$\omega_{n\text{DR}} = 2.17 \text{ rad/s}$$
$$\zeta_{\text{DR}} = 0.254$$

Table 5.3 compares the results of the exact and approximate analysis. For this example, the roll and Dutch roll roots are in good agreement. On the other hand, the spiral root approximation is very poor.

The relationship between good spiral and Dutch roll characteristics presents a challenge to the airplane designer. In Chapter 2 is was stated that an airplane should possess static stability in both the directional and roll modes. This implies the $C_{n_\beta} > 0$ and $C_{l_\beta} < 0$. However, if we examine the influence of these stability coefficients on the lateral roots by means of a root locus plot, we observe the following. As the dihedral effect is increased, i.e., C_{l_β} becomes more negative, the Dutch roll root moves towards the right half-plane which means the Dutch roll root is becoming less stable, whereas the spiral root is moving in the direction of increased stability. These observations are clearly shown in Figs. 5.11 and 5.12.

Increasing directional stability of the airplane, i.e. C_{n_β} becomes more

TABLE 5.3
Comparison of exact and approximate roots

	Exact			Approximate		
	$T_{1/2}$, s	T_2, s	P, s	$T_{1/2}$, s	T_2, s	P, s
Spiral	78.7	—	—	4.79	—	—
Roll	0.082	—	—	0.082	—	—
Dutch roll	1.42	—	2.69	1.35	—	2.98

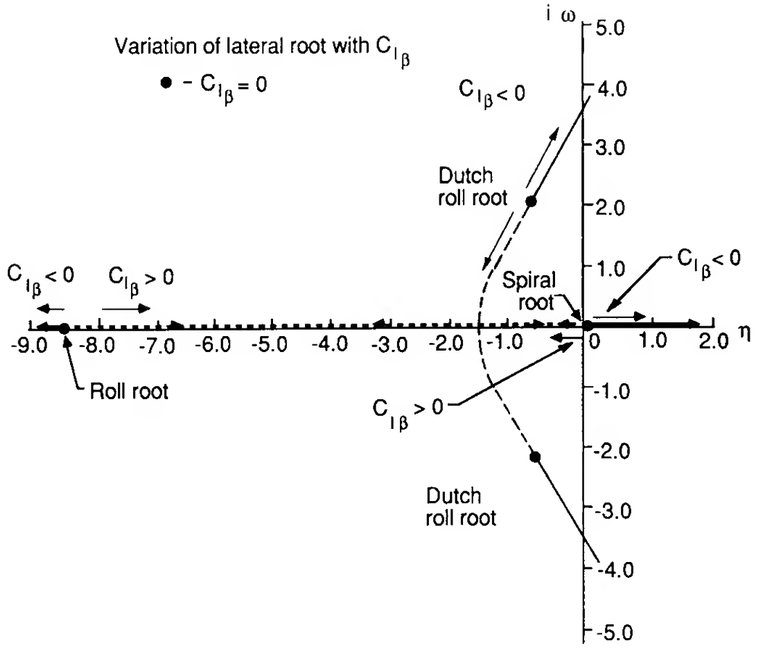

FIGURE 5.11
Variation of lateral roots with C_{l_β}.

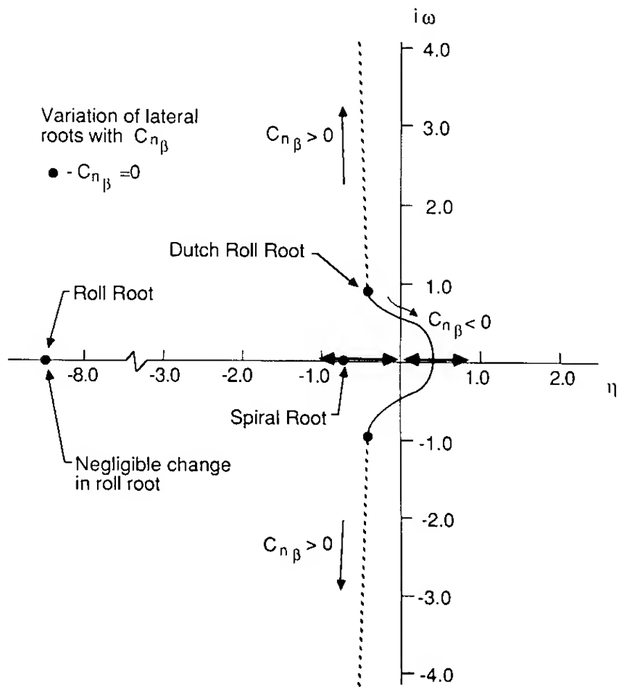

FIGURE 5.12
Variation of lateral roots with C_{n_β}.

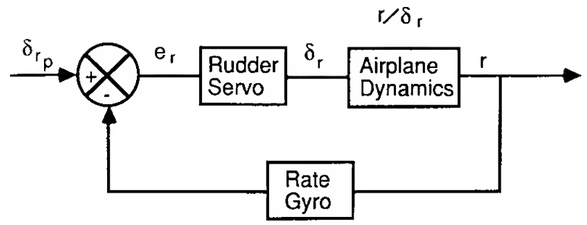

FIGURE 5.13
Sketch of a simple yaw damper.

positive, causing the spiral root to become less stable while the frequency of the Dutch roll root is increased. This is illustrated in the root locus plot of Fig. 5.13. Increasing the yaw damping, i.e. C_{n_r} becomes more negative, will result in better Dutch roll damping. Unfortunately, this is not that easy to achieve simply by geometric design changes. Many airplanes are provided with a rate damper to artificially provide adequate damping in Dutch roll.

5.5 LATERAL FLYING QUALITIES

In this chapter we have examined the lateral direction characteristics of an airplane. The relationship between the aerodynamic stability and control derivatives and the lateral response was discussed. We have developed the necessary equations and analysis procedures to calculate the lateral dynamics. Although these techniques will allow us to determine whether our airplane design is stable or unstable, the analysis does not by itself tell us whether the airplane will be judged by the pilot as having acceptable flying characteristics. To determine whether the airplane will have acceptable flying qualities, the designer needs to know what dynamic characteristics are considered favorable by the pilots who will fly the airplane. This information is available through the lateral-directional flying quality specifications.

The lateral-directional flying quality requirements are listed in Tables 5.4, 5.5 and 5.6. The definition of class and category were presented in Chapter 4. For Example Problem 5.2 the aircraft would be considered as a class 1 vehicle and the flight phase as category B. Using the information from Table 5.4, we find that the aircraft studied here has level 1 flying qualities.

TABLE 5.4
Spiral mode flying qualities

Spiral mode—minumum time to double amplitude				
Class	**Category**	**Level 1**	**Level 2**	**Level 3**
I & IV	A	12 s	12 s	4 s
	B & C	20 s	12 s	4 s
II & III	A11	20 s	12 s	4 s

TABLE 5.5
Roll mode flying qualities

Roll mode—maximum roll time constant, seconds				
Class	**Category**	**Level 1**	**Level 2**	**Level 3**
I, IV II, III	A	1.0 1.4	1.4 3.0	10
A11	B	1.4	3.0	10
I, IV II, III	C	1.0 1.4	1.4 3.0	10

TABLE 5.6
Dutch roll flying qualities

Dutch roll					
Level	**Category**	**Class**	**Min ζ***	**Min $\zeta\omega_n$,* rad/s**	**Min ω_n, rad/s**
1	A	I, IV	0.19	0.35	1.0
		II, III	0.19	0.35	0.4
	B	A11	0.08	0.15	0.4
	C	I, II-*C* IV	0.08	0.15	1.0
		II-*L*, III	0.08	0.15	0.4
2	A11	A11	0.02	0.05	0.4
3	A11	A11	0.02	—	0.4

Where *C* and *L* denote carrier or land based aircraft.
* The governing damping requirement is that yielding the larger value of ζ.

Example Problem 5.3. As was shown earlier, the Dutch roll motion can be improved by increasing the magnitude of the yaw damping term N_r. One means of increasing N_r is by increasing the vertical tail area. Unfortunately, increasing the vertical tail area will add additional drag to the airplane as well as increasing the directional stability. The increase in directional stability will cause the spiral characteristics of the airplane to be degraded. For most transport and fighter aircraft, increased damping is provided artificially by means of a yaw damper.

In this example we shall examine the basic idea behind a yaw damper. More detailed information on stability augmentation systems and autopilots will be provided in Chapters 7 and 8. To examine how a yaw damper can be used to provide damping for an airplane, let us consider the yawing moment equation developed earlier:

$$\Delta\ddot{\psi} - N_r\,\Delta\dot{\psi} + N_\beta\,\Delta\psi = N_{\delta r}\,\Delta\delta_r$$

Suppose that for a particular airplane the static directional stability, yaw

damping and control derivatives were as follows:

$$N_\beta = 1.77\ \text{s}^{-2} \qquad N_r = -0.10\ \text{s}^{-1} \qquad N_{\delta r} = -0.84\ \text{s}^{-1}$$

For this airplane, the damping ratio and undamped natural frequency would be

$$\zeta = -\frac{N_r}{2\sqrt{N_\beta}} = 0.037 \qquad \omega_n = \sqrt{N_\beta} = 1.33\ \text{rad/s}$$

The low damping ratio would result in a free response that would have a large overshoot and poor damping. Such an airplane would be very difficult for the pilot to fly. However, we could design a feedback control system such that the rudder deflection is proportional to the yaw rate, i.e.

$$\delta_r = -k\,\Delta\dot{\psi}$$

Substituting the control deflection expression into the equation of motion and rearranging yields

$$\Delta\ddot{\psi} - (N_r - kN_{\delta r})\,\Delta\dot{\psi} + N_\beta\,\Delta\psi = 0$$

By proper selection of k we can provide the airplane with whatever damping characteristics we desire. For the purpose of this example, let us consider the simple yawing motion to be an approximation of the Dutch roll motion. The flying quality specifications included in Table 5.6 state that a level 1 flying quality rating would be achieved for the landing flight phase if

$$\zeta > 0.08 \qquad \zeta\omega_n > 0.15\ \text{rad/s} \qquad \omega_n > 0.4\ \text{rad/s}$$

A damping ratio of 0.2 and a frequency of 1.33 would be considered acceptable by pilots. The problem now is one of selecting the unknown gain k so that the airplane has the desired damping characteristics. If we compare the yaw moment equation of motion to the standard form for a second-order system, we can establish a relationship for k as follows:

$$2\zeta\omega_n = -(N_r - kN_{\delta r}) \qquad 0.532 = -[-0.1 - k(-0.84)] \qquad k = -0.514$$

Figure 5.14 is a sketch of a simple yaw damper stability augmentation system.

Although we designed a feedback system to provide improved damping, it is possible to control both the damping and the frequency. This can be accomplished by making the rudder deflection proportional to both the yaw rate and yaw angle, i.e.

$$\delta_r = -k_1\,\Delta\dot{\psi} - k_2\,\Delta\psi$$

Substituting this expression back into the differential equation yields

$$\Delta\ddot{\psi} - (N_r - k_1N_{\delta r})\,\Delta\dot{\psi} + (N_\beta + k_2)\,\Delta\psi = 0$$

The gains k_1 and k_2 are then selected so that the characteristic equation has the desired damping ratio and frequency. The use of feedback control to augment the stability characteristics of an airplane plays an important role in the design of modern aircraft. By using stability augmentation systems, the designer can ensure good flying qualities over the entire flight regime. Furthermore, with the addition of a stability augmentation system, the designer can reduce the inherent aerodynamic static stability of the airplane by reducing the vertical tail size. Thus, the designer can achieve an improvement in performance without compromising the level of flying qualities.

5.6 INERTIAL COUPLING

In the analysis presented in this and the previous chapter, we have treated the longitudinal and lateral equations separately. In so doing we have assumed that there is no coupling between the equations. However, slender high-performance fighter aircraft can experience significant roll coupling which can result in divergence from the desired flight path, causing loss of control or structural failure.

The mechanisms that cause this undesirable behavior can be due to inertial and/or aerodynamic coupling of the equations of motion. To explain how inertial coupling occurs, we examine the non-linearized moment equations developed in Chapter 3. The moment equations are reproduced in Eq. (5.49).

$$\begin{aligned} \sum \text{Roll moments} &= I_x\dot{p} + qr(I_z - I_y) - (\dot{r} + qp)I_{xz} \\ \sum \text{Pitching moments} &= I_y\dot{q} + pr(I_x - I_z) + (p^2 - r^2)I_{xz} \\ \sum \text{Yawing moments} &= I_z\dot{r} + pq(I_y - I_x) + (qr - \dot{p})I_{xz} \end{aligned} \tag{5.49}$$

The first cases of inertial coupling started to appear when fighter aircraft designs were developed for supersonic flight. These aircraft were designed with low aspect ratio wings and long, slender fuselages. In these designs, more of the aircraft's weight was concentrated in the fuselage than in the earlier subsonic fighters. With the weight concentrated in the fuselage, the moments of inertia around the pitch angle yaw axis increased, while the inertia around the roll axis decreased in comparison with subsonic fighter aircraft.

Upon examining Eq. (5.49), we see that the second term in the pitch equation could be significant if the difference in the moments of inertia becomes large. For the case of a slender high performance fighter executing a rapid rolling maneuver the term $pr(I_x - I_z)$ can become large enough to produce an uncontrollable pitching motion.

A similar argument can be made for the product of inertia terms in the equations of motion. The product of inertia I_{xz} is a measure of the uniformity of the distribution of mass about the x axis. For modern fighter aircraft I_{xz} is typically not zero. Again we see that if the airplane is executing a rapid roll maneuver, the term $(p^2 - r^2)I_{xz}$ may be as significant as the other terms in the equation.

Finally, aerodynamic coupling must also be considered when aircraft are maneuvering at high angular rates or at high angles of attack. As was discussed in Chapter 4, high angle of attack flow asymmetries can cause out-of-plane forces and moments even for symmetric flight conditions. Such forces and moments couple the longitudinal and lateral equations of motion.

5.7 SUMMARY

In this chapter we examined the lateral modes of motion. The Dutch roll and spiral motions were shown to be influenced by static directional stability and dihedral effect in an opposing manner. The designer is faced with the dilemma of trying to satisfy the flying quality specifications for both the spiral and Dutch roll modes. This becomes particularly difficult for airplanes that have extended flight envelopes. One way designers have solved this problem is by incorporating a yaw damper in the design. The yaw damper is an automatic system that artificially improves the system damping. The increased damping provided by the yaw damper improves both the spiral and Dutch roll characteristics.

5.8 PROBLEMS

5.1. Determine the response of the A-4D to a 5° step change in aileron deflection. Plot the roll rate versus time. Assume sea-level standard conditions and that the airplane is flying at $M = 0.4$. What is the steady-state roll rate and time constant for this motion?

5.2. For the roll response shown in the Fig. P5.2, estimate the aileron control power L_{δ_a} and the roll damping derivative L_p. Information on the characteristics of the airplane is as follows:

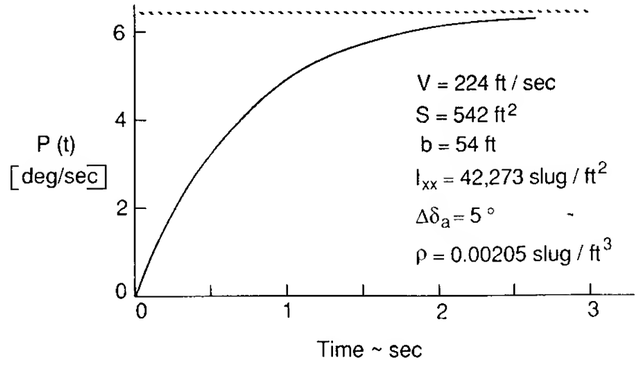

FIGURE P5.2
Roll rate time history.

5.3. A wind-tunnel model free to rotate about its X axis is spun up to 10.5 rad/s by means of a motor drive system. When the motor drive is disengaged, the model spin decays as shown in Fig. P5.3. From the spin time history determine the roll damping derivative L_p.

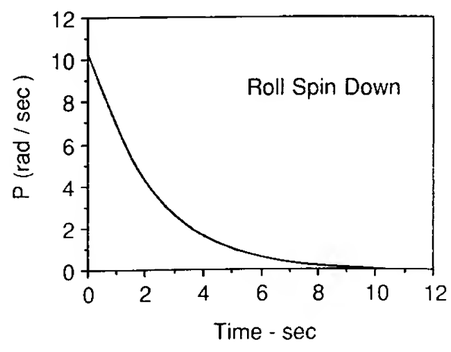

FIGURE P5.3
Roll rate time history.

5.4. Assume the cruciform finned model in Fig. P5.4 is mounted in the wind tunnel so that it is constrained to a pure yawing motion. The model is displaced from its trim position by 10° and then released. Neglect $\dot{\beta}$ contribution, and assume $S = \pi D^2/4$.

(a) Find the time for the motion to damp to half its initial amplitude.

(b) What is the period of the motion?

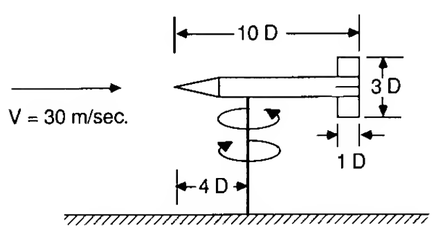

D = Characteristic length
D = 5.0 cm
Tail surfaces are flat plates
$I_z = 5.0 \times 10^{-2}$ kg - m^2
$S = \pi D^2/4$

FIGURE P5.4
Yawing Wind Tunnel model.

5.5. Figure P5.5. shows the stick fixed lateral roots of a jet transport airplane. Identify the roots and determine the time for the amplitude and period to halve or double where applicable.

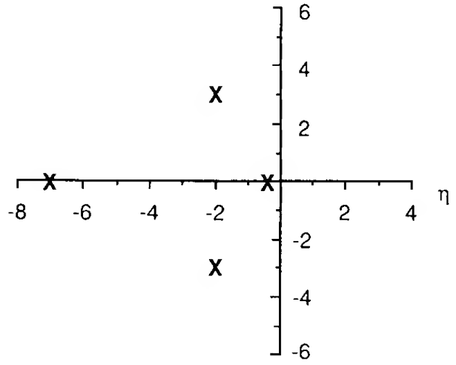

FIGURE P5.5
Lateral roots for a jet transport.

5.6. Develop a computer code to obtain the stick fixed lateral eigenvalues from the lateral stability matrix. Use your computer program to analyze the lateral motion of the 747 jet transport. Estimated aerodynamic, mass and geometric characteristics of the 747 are included in the appendices.

5.7. Using the program developed for Problem 5.6, examine the effect that increasing altitude has on the stick fixed lateral characteristics.

5.8. Using the Dutch roll approximation, determine the state feedback gains so that the damping ratio and frequency of the Dutch roll are 0.3 and 1.0 rad/s, respectively. Assume the airplane has the following characteristics:

$$Y_\beta = -19.5\ \text{ft/s}^2 \qquad Y_r = 1.3\ \text{ft/s}$$
$$N_\beta = 1.5\ \text{s}^{-2} \qquad N_r = -0.21\ \text{s}^{-1}$$
$$Y_{\delta r} = 4.7\ \text{ft/s}^2 \qquad N_{\delta r} = -0.082\ \text{s}^{-2}$$
$$u_0 = 400\ \text{ft/s}$$

REFERENCES

5.1. Adams, F. D.: *Aeronautical Dictionary,* National Aeronautics and Space Administration, United States Government Printing Office, Washington, DC., 1959.

5.2. Seckel, E.: *Statility and Control of Airplanes and Helicopters,* Academic Press, New York, 1964.

5.3. Etkin, B.: *Dynamics of Flight,* Wiley, New York, 1972.

5.4. Hage, R. E., and C. D. Perkins: *Airplane Performance, Stability and Control,* Wiley, New York, 1949.

5.5. Roskam, J.: *Flight Dynamics of Rigid and Elastic Airplanes,* University of Kansas Press, 1972.

5.6. Fung, Y. C.: *The Theory of Aeroelasticity,* Wiley, New York, 1955.

5.7. Bisplinghoff, R. L., H. Ashley, and R. L. Halfman: *Aeroelasticity,* Addison Wesley, Reading, MA, 1955.

5.8. Scanlan, R. H., and R. Rosenbaum: *Introduction to the Study of Aircraft Vibration and Flutter,* MacMillan, New York, 1951.

5.9. Abramson, H.: *The Dynamics of Airplanes,* Ronald Press, New York, 1958.

CHAPTER 6

AIRCRAFT RESPONSE TO CONTROL OR ATMOSPHERIC INPUTS

6.1 INTRODUCTION

In the previous chapters we have examined the free response of an airplane as well as several simple examples of single degree of freedom motions with step changes in control input. Another useful input function is the sinusoidal input. The step and sinusoidal input function are important for two reasons. First, the input to many physical systems takes the form of either a step change or sinusoidal signal. Second, an arbitrary function can be represented by a series of step changes or a periodic function can be decomposed by means of Fourier analysis into a series of sinusoidal waves. If we know the response of a linear system to either a step or sinusoidal input, then we can construct the response of the system to an arbitrary input by the principle of superposition.

Of particular importance to the study of aircraft response to control or atmospheric inputs is the steady-state response to a sinusoidal input. If the input to a linear stable system is sinusoidal, then, after the transients have died out, the response of the system will also be a sinusoid of the same frequency. The response of the system is completely described by the ratio of the output to input amplitude and the phase difference, over the frequency range from zero to infinity. The magnitude and phase relationship between the input and output signals is called the frequency response. The frequency response can

readily be obtained from the system transfer function by replacing the Laplace variable s by $i\omega$. The frequency response information is usually presented in graphical form using either rectangular, polar, log–log or semi-log plots of the magnitude and phase angle versus the frequency. At first it might appear that the construction of the magnitude and phase plots would be extremely difficult for all but the simplest transfer functions. Fortunately, this is not the case. Consider the factored form of a transfer function, given by

$$G(s) = \frac{k(1 + T_a s)(1 + T_b s) \cdots}{s^m (1 + T_1 s)(1 + T_2 s) \cdots \left(1 + \frac{2\zeta}{\omega_n} s + \frac{s^2}{\omega_n^2}\right)} \tag{6.1}$$

The transfer function has been factored into first- and second-order terms. Replacing the Laplace variable s by $i\omega$ and rewriting the transfer function in polar form yields

$$M(\omega) = |G(i\omega)| = \frac{|k| \times |1 + T_a i\omega| \times |1 + T_b i\omega| \cdots}{|(i\omega)^m| \times |1 + T_1 i\omega| \cdots \times \left|1 - \left(\frac{\omega}{\omega_n}\right)^2 + 2\zeta \frac{\omega}{\omega_n} i\right| \cdots} \times \exp[i(\phi_a + \phi_b \cdots - \phi_1 - \phi_2 \cdots)] \tag{6.2}$$

Now, if we take the logarithm of the above equation, we obtain

$$\begin{aligned} \log M(\omega) = {} & \log k + \log |1 + T_a i\omega| + \log |1 + T_b i\omega| \cdots - m \log |i\omega| \\ & - \log |1 + T_1 i\omega| - \log |1 + T_2 i\omega| \\ & - \log \left|1 - \left(\frac{\omega}{\omega_n}\right)^2 + 2\zeta \frac{\omega}{\omega_n} i\right| - \cdots \end{aligned} \tag{6.3}$$

or

$$\begin{aligned} \angle G(i\omega) = {} & \tan^{-1} \omega T_a + \tan^{-1} \omega T_b + \cdots m(90°) \\ & - \tan^{-1} \omega T_1 + \cdots - \tan^{-1}\left(\frac{2\zeta\omega_n\omega}{\omega_n^2 - \omega^2}\right) \end{aligned} \tag{6.4}$$

By expressing the magnitude in terms of logarithms, the magnitude of the transfer function is readily obtained by the addition of the individual factors. The contribution of each of the basic factors, i.e. gain, pole at the origin, simple poles and zeros, and complex poles and zeros are presented in an appendix at the end of this book. In practice, the log-magnitude is often expressed in units called decibels (dB). The magnitude in decibels is found by multiplying each term in Eq. (6.3) by 20:

$$\text{Magnitude in dB} = 20 \log |G(i\omega)| \tag{6.5}$$

The frequency response information of a transfer function is represented by two graphs, one of the magnitude and the other of the phase angle, both versus the frequency on a logarithmic scale. When the frequency response data are presented in this manner, the plots are referred to as Bode diagrams after

H. W. Bode who made significant contributions to frequency response analysis.

We shall now look at the application of the frequency response techniques to the longitudinal control transfer functions. As the first example, let us consider the longitudinal pitch angle to elevator transfer function developed in Chapter 3. For example, the longitudinal pitch angle to elevator transfer function was found to be

$$\frac{\theta(s)}{\delta_e(s)} = \frac{A_\theta s^2 + B_\theta s + C_\theta}{As^4 + Bs^3 + Cs^2 + Ds + E} \tag{6.6}$$

which can be written in the factored form:

$$\frac{\theta(s)}{\delta_e(s)} = \frac{k_{\theta\delta}(T_{\theta 1}s + 1)(T_{\theta 2}s + 1)}{\left(\frac{s^2}{\omega_{nsp}^2} + \frac{2\zeta_{sp}}{\omega_{nsp}}s + 1\right)\left(\frac{s^2}{\omega_{np}^2} + \frac{2\zeta_p}{\omega_{np}}s + 1\right)} \tag{6.7}$$

The magnitude and phase angle of the pitch angle of the pitch altitude elevator control transfer function is obtained by replacing s by $j\omega$ as follows:

$$\left|\frac{\theta(i\omega)}{\delta_e(i\omega)}\right| = \frac{|k_{\theta\delta}|\,|T_{\theta 1}i\omega + 1|}{\left|\frac{(i\omega)^2}{\omega_{nsp}^2} + \frac{2\zeta_{sp}}{\omega_{nsp}}i\omega + 1\right|} \frac{|T_{\theta 2}i\omega + 1|}{\left|\frac{(i\omega)^2}{\omega_{np}^2} + \frac{2\zeta_p}{\omega_{np}}i\omega + 1\right|} \tag{6.8}$$

$$\angle\theta(i\omega)/\delta_e(i\omega) = \tan^{-1}\omega T_{\theta 1} + \tan^{-1}\omega T_{\theta 2} - \tan^{-1}[2\zeta_{sp}\omega_{nsp}\omega/(\omega_{nsp}^2 - \omega^2)] - \tan^{-1}[2\zeta_p\omega_{np}\omega/(\omega_{np}^2 - \omega^2)]$$

The frequency response for the pitch attitude to control deflection for the corporate business jet described in the Appendix is shown in Fig. 6.1. The amplitude ratio at both the phugoid and short period frequency are of comparable magnitude. At very large frequencies the amplitude ratio is very small, which indicates that the elevator has a negligible effect on the pitch attitude in this frequency range.

The frequency response for the change in forward speed and angle of

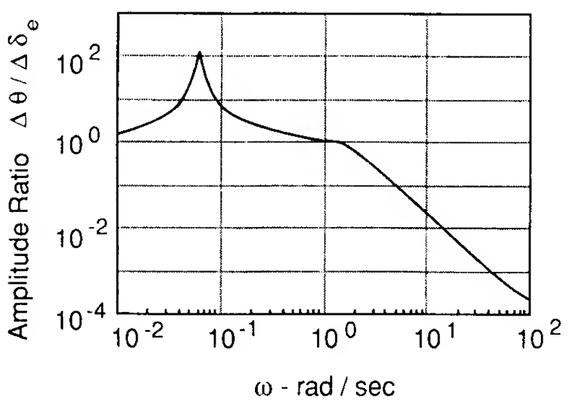

FIGURE 6.1

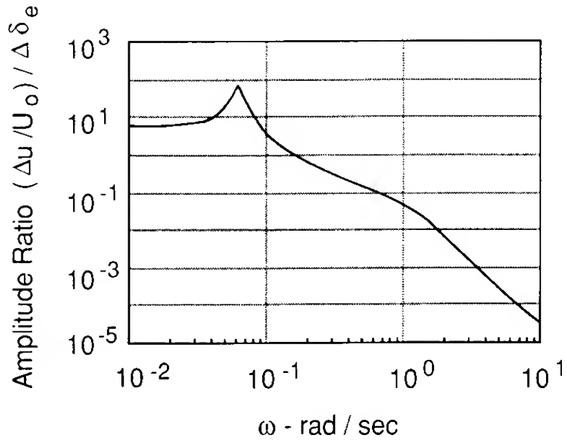

FIGURE 6.2

attack to control input is shown in Figs 6.2 and 6.3 for the same aircraft. For the speed elevator transfer function the amplitude ratio is large at the phugoid frequency and very small at the short-period frequency. Recall that in Chapter 4 we assumed that the short-period motion occurred at essentially constant speed. The frequency response plot confirms the validity of this assumption. Figure 6.3 shows the amplitude ratio of the angle of attack to elevator deflection; here we see that angle of attack is constant at the low frequencies. This again is in keeping with the assumption we made regarding the phugoid approximation. Recall that in the phugoid approximation the angle of attack was assumed to be constant. The phase plot shows that there is a large phase lag in the response of the speed change to elevator inputs. The phase lag for α/δ is much smaller, which means that the angle of attack will respond faster than the change in forward speed to an elevator input.

A similar type of analysis can be conducted for the lateral response to aileron or rudder control input. Several problems dealing with the lateral frequency response are presented at the end of this chapter.

Frequency response techniques are also useful in studying the motion of an aircraft encountering atmosphere turbulence. In Chapter 3, the equations of

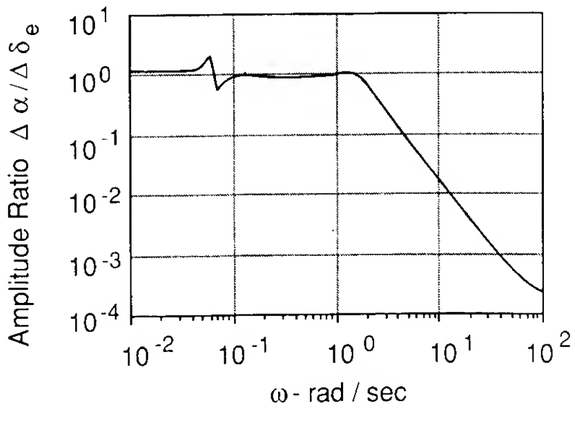

FIGURE 6.3

motion were developed for flight in a stationary atmosphere. In the following sections we shall discuss the influence of wind gusts, i.e. turbulence, on aircraft response.

6.2 EQUATIONS OF MOTION IN A NONUNIFORM ATMOSPHERE

The atmosphere is rarely calm but is usually characterized by winds, gusts, and turbulence. In order to study the influence of atmospheric disturbances on aircraft motions, the equations must be modified. The aerodynamic forces and moments acting on the airplane depend on the relative motion of the airplane to the atmosphere and not on the inertial velocities. Therefore, to account for atmospheric disturbances such as winds, gusts, or turbulence, the forces and moments must be related to the relative motion with respect to the atmosphere. This is accomplished by expressing the velocities used in calculating the aerodynamics in terms of the inertial and gust velocities as shown below.

$$\begin{aligned} \Delta u_a &= \Delta u - u_g \qquad \Delta v_a = \Delta v - v_g \qquad \Delta w_a = \Delta w - w_g \\ \Delta p_a &= \Delta p - p_g \qquad \Delta q_a = \Delta q - q_g \qquad \Delta r_a = \Delta r - r_g \end{aligned} \tag{6.9}$$

where the Δ quantities are the perturbations in the inertial variables and the subscripted variables are the gust velocities. The aerodynamic forces and moments can now be expressed as follows:

$$\begin{aligned} \Delta X &= \frac{\partial X}{\partial u}(\Delta u - u_g) + \frac{\partial X}{\partial w}(\Delta w - w_g) + \frac{\partial X}{\partial \dot{w}}(\Delta \dot{w} - \dot{w}_g) \\ &\quad + \frac{\partial X}{\partial q}(\Delta q - q_g) + \frac{\partial X}{\partial \delta_e}\Delta\delta_e \\ \Delta Z &= \frac{\partial Z}{\partial u}(\Delta u - u_g) + \frac{\partial Z}{\partial w}(\Delta w - w_g) + \frac{\partial Z}{\partial \dot{w}}(\Delta \dot{w} - \dot{w}_g) + \cdots \\ &\vdots \\ \Delta N &= \frac{\partial N}{\partial v}(\Delta v - v_g) + \frac{\partial N}{\partial r}(\Delta r - r_g) + \frac{\partial N}{\partial p}(\Delta p - p_g) \end{aligned} \tag{6.10}$$

The disturbances in the atmosphere can be described by the spatial and temporal variations in the gust components. The rotational gusts q_g, p_g, etc., included in Eqs (6.10) arise from the variation of u_g, v_g and w_g with position and time.

The rotary gusts p_g, q_g and r_g occur due to the spatial variations of the gust components. For example if the gust field wavelength is large in comparison with the airplane, as shown in Fig. 6.4, the vertical gust produces a spanwise variation of velocity along the span of the wing. The linear variation of velocity across the span is the same as that produced on a rolling wing. The

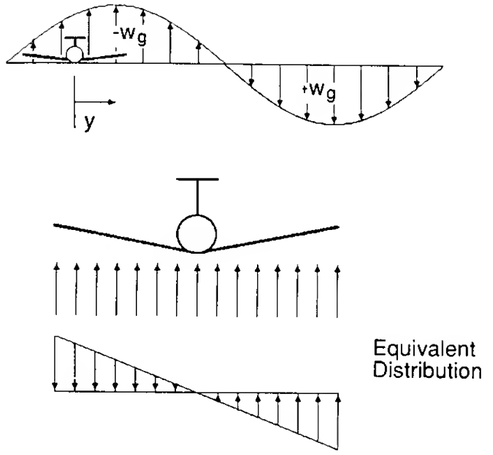

FIGURE 6.4

velocity normal to the wing at some point along the span is given by

$$w = py \tag{6.11}$$

or

$$\frac{\partial w}{\partial y} = p \tag{6.12}$$

Using this analogy, we can express the rotary gust velocity in terms of the gradient in the vertical gust field;

$$p_g = \frac{\partial w_g}{\partial y} \tag{6.13}$$

In a similar manner, the q_g can be developed. The variation of the vertical gust velocity along the X axis of the airplane is similar to the velocity distribution created on a pitching airplane. Figure 6.5 helps to show the origin of rotary

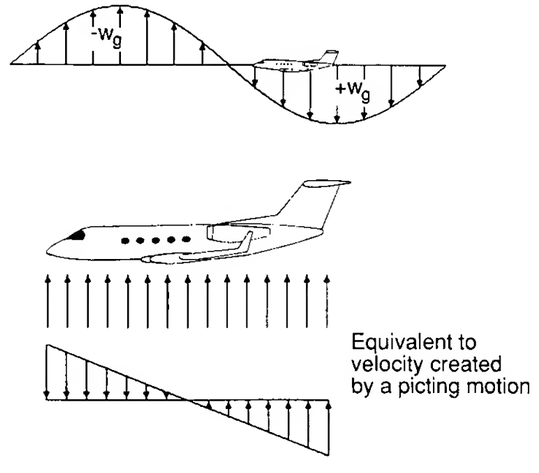

FIGURE 6.5

gust q_g:

$$q_g = \frac{\partial w_g}{\partial x} \tag{6.14}$$

or

$$q_g = -\frac{\partial w_g/\partial t}{\partial x/\partial t} = -\dot{w}_g/u_0 \tag{6.15}$$

The equations of motion, modified to account for atmospheric disturbances, can be written in the state-space form as follows:

$$\dot{\mathbf{x}} = \mathbf{A}\mathbf{x} + \mathbf{B}\eta + \mathbf{C}\xi \tag{6.16}$$

where $\mathbf{x}$, $\boldsymbol{\eta}$ and $\boldsymbol{\xi}$ are the state, control and gust disturbance vectors. The longitudinal equations are

$$\begin{bmatrix} \Delta\dot{u} \\ \Delta\dot{w} \\ \Delta\dot{q} \\ \Delta\dot{\theta} \end{bmatrix} = \begin{bmatrix} X_u & X_w & 0 & -g \\ Z_u & Z_w & u_0 & 0 \\ M_u & M_w & M_q & 0 \\ 0 & 0 & 1 & 0 \end{bmatrix} \begin{bmatrix} \Delta u \\ \Delta w \\ \Delta q \\ \Delta\theta \end{bmatrix} + \begin{bmatrix} X_\delta & X_{\delta t} \\ Z_\delta & Z_{\delta t} \\ M_\delta & M_{\delta t} \\ 0 & 0 \end{bmatrix} \begin{bmatrix} \Delta\delta_e \\ \Delta\delta_t \end{bmatrix}$$
$$+ \begin{bmatrix} -X_u & -X_w & 0 \\ -Z_u & -Z_w & 0 \\ -M_u & -M_w & -M_q \\ 0 & 0 & 0 \end{bmatrix} \begin{bmatrix} u_g \\ w_g \\ q_g \end{bmatrix} \tag{6.17}$$

and the lateral equations are

$$\begin{bmatrix} \Delta\dot{v} \\ \Delta\dot{p} \\ \Delta\dot{r} \\ \Delta\dot{\phi} \end{bmatrix} = \begin{bmatrix} Y_v & 0 & (Y_r - u_0) & g \\ L_v & L_p & L_r & 0 \\ N_v & N_p & N_r & 0 \\ 0 & 1 & 0 & 0 \end{bmatrix} \begin{bmatrix} \Delta v \\ \Delta p \\ \Delta r \\ \Delta\phi \end{bmatrix} + \begin{bmatrix} 0 & Y_{\delta r} \\ L_{\delta a} & L_{\delta r} \\ N_{\delta a} & N_{\delta r} \\ 0 & 0 \end{bmatrix} \begin{bmatrix} \Delta\delta_a \\ \Delta\delta_r \end{bmatrix}$$
$$+ \begin{bmatrix} -Y_v & 0 & 0 \\ -L_v & -L_p & -L_r \\ -N_v & -N_p & -N_r \\ 0 & 0 & 0 \end{bmatrix} \begin{bmatrix} v_g \\ p_g \\ r_g \end{bmatrix} \tag{6.18}$$

The longitudinal and lateral gust transfer functions can be determined by taking the Laplace transform of Eq. (6.17) and (6.18) and then dividing by the gust function. A linear set of algebraic equations in terms of $\Delta\bar{u}/\bar{u}_g$ are obtained. These equations can then be solved for the transfer functions.

To provide some insight into the influence of atmospheric disturbances on aircraft response, we shall examine the vertical motion of an airplane that encounters a vertical gust field.

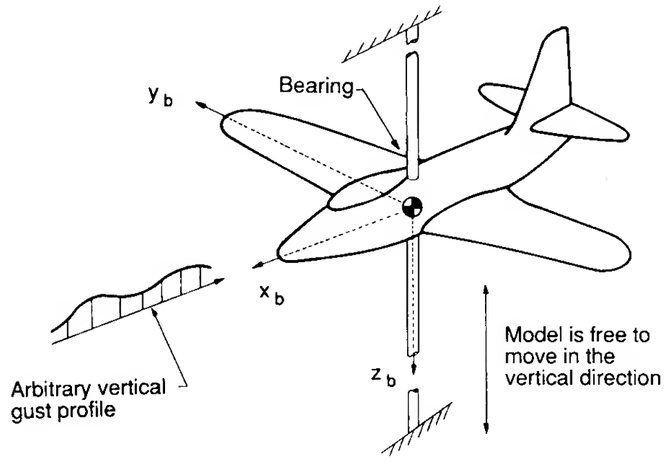

FIGURE 6.6

6.3 PURE VERTICAL OR PLUNGING MOTION

Consider an airplane constrained so that only movement in the vertical direction is possible. This type of motion could be simulated in the wind tunnel using a model constrained by a vertical rod, as illustrated in Fig. 6.6. The model is free to move up or down along the rod, but no other motion is possible.

Now let us examine the response of this constrained airplane subjected to an external disturbance such as a wind gust. The equation of motion for this example is obtained by applying Newton's second law, i.e.

$$\sum \text{Forces in the vertical direction} = m\frac{\mathrm{d}w}{\mathrm{d}t} \tag{6.19}$$

$$Z + WT = m\frac{\mathrm{d}w}{\mathrm{d}t} \tag{6.20}$$

where Z is the aerodynamic force in the z direction and WT is the weight of the airplane model. If we assume the motion of the airplane will be confined to small perturbations from an initial unaccelerated flight condition, then the aerodynamic force and vertical velocity can be expressed as the sum of the reference flight condition plus the perturbation:

$$Z = Z_0 + \Delta Z \qquad w = w_0 + \Delta w \tag{6.21}$$

Substituting Eq. (6.21) into Eq. (6.20) yields

$$Z_0 + \Delta Z + WT = m\frac{\mathrm{d}}{\mathrm{d}t}(w_0 + \Delta w) \tag{6.22}$$

This equation can be simplified by recognizing that in unaccelerated flight the

condition for equilibrium is

$$Z_0 + WT = 0 \tag{6.23}$$

Therefore, Eq. (6.22) reduces to

$$\Delta Z/m = \frac{\mathrm{d}}{\mathrm{d}t}\Delta w \tag{6.24}$$

The aerodynamic force acting on the airplane is a function of the angle of attack and time rate of change of the attack, and can be expressed in terms of the stability derivatives as follows

$$\Delta Z/m = Z_\alpha\,\Delta\alpha + Z_{\dot\alpha}\,\Delta\dot\alpha \tag{6.25}$$

or

$$\Delta Z/m = C_{z_\alpha}\,\Delta\alpha\,QS/m + C_{z_{\dot\alpha}}\frac{\Delta\dot\alpha c}{2u_0}QS/m \tag{6.26}$$

where

$$C_{z\alpha} = -C_{L_\alpha} \qquad C_{z\dot\alpha} = -C_{L_{\dot\alpha}}$$

To simplify our analysis we will assume that the lag in lift term, $Z_{\dot\alpha}\,\Delta\dot\alpha$, is negligible in comparison to the $Z_\alpha\,\Delta\alpha$ term.

The change in angle of attack experienced by the airplane is due to its motion in the vertical direction and also to the vertical wind gust. The angle of attack can be written as

$$\Delta\alpha = \frac{\Delta w}{u_0} - \frac{w_g(t)}{u_0} \tag{6.27}$$

Substituting Eqs (6.25) and (6.27) into Eq. (6.24), and rearranging, yields

$$u_0\frac{\mathrm{d}\,\Delta w}{\mathrm{d}t} - Z_\alpha\,\Delta w = -Z_\alpha w_g(t) \tag{6.28}$$

or

$$-\frac{u_0}{Z_\alpha}\frac{\mathrm{d}\,\Delta w}{\mathrm{d}t} + \Delta w = w_g(t) \tag{6.29}$$

Equation (6.29) is a first-order differential equation with constant coefficients. Systems characterized by first-order differential equations are referred to as first-order systems. We rewrite Eq. (6.29) to have the form:

$$\tau\frac{\mathrm{d}\,\Delta w}{\mathrm{d}t} + \Delta w = \left(\tau\frac{\mathrm{d}}{\mathrm{d}t} + 1\right)\Delta w = w_g(t) \tag{6.30}$$

where

$$\tau = -\frac{u_0}{Z_\alpha} \tag{6.31}$$

and $w_g(t)$ is the gust velocity as a function of time.

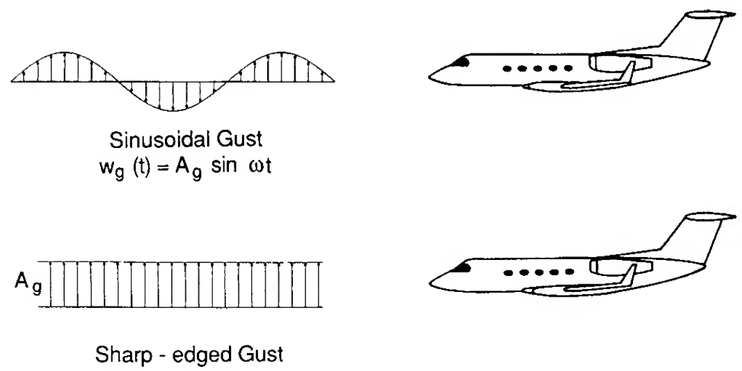

FIGURE 6.7

The solution of Eq. (6.30) for a sharp-edged or sinusoidal gust will now be examined. Figure 6.7 shows an airplane encountering a sharp edged or step gust and a sinusoidal gust profile. The reason for selecting these two types of gust inputs is that they occur quite often in nature. Furthermore, as was mentioned earlier, both the step function and sinusoidal inputs can be used to construct an arbitrary gust profile. For example, Fig. 6.8 shows the construction of an arbitrary gust profile as a series of step changes. Also in the case of an arbitrary-period gust function, the profile can be decomposed into a series of sine waves by Fourier analysis.

The transient response of an airplane to an encounter with a sharp-edged

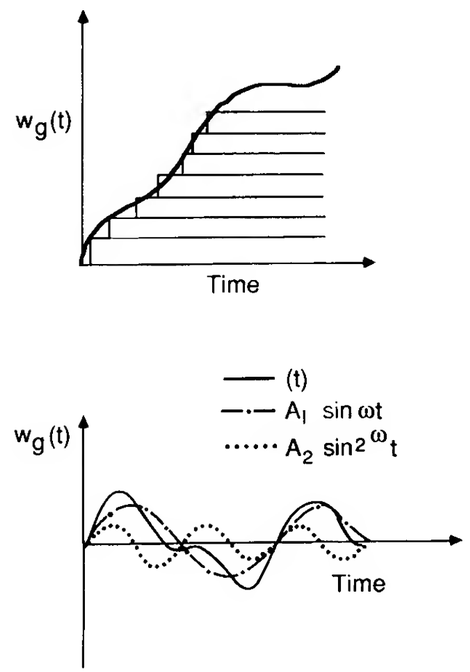

FIGURE 6.8

gust can be modeled by expressing the gust profile as a step function:

$$w_g(t) = \begin{cases} 0 & t = 0^- \\ A_g u(t) & t = 0^+ \end{cases} \tag{6.32}$$

where $u(t)$ is a unit step change and A_g is the magnitude of the gust. The solution of Eq. (6.30) for a step input can be obtained by taking the Laplace transformation of the differential equation

$$\tau s\, \Delta w(s) + \Delta w(s) = w_g(s) \tag{6.33}$$

or solving for the ratio of the output to input yields

$$\frac{\Delta w(s)}{w_g(s)} = \frac{1}{\tau s + 1} \tag{6.34}$$

Equation (6.34) is the transfer function of the change in vertical velocity to the vertical gust input. When the forcing function or input is a step change in the gust velocity, then

$$w_g(s) = \frac{A_g}{s} \tag{6.35}$$

or

$$\Delta w(s) = \frac{A_g}{s(\tau s + 1)} \tag{6.36}$$

Expanding Eq. (6.36) by the method of partial factions, and then taking the inverse Laplace transformation, yields

$$\Delta w(t) = A_g(1 - e^{-t/\tau}) \tag{6.37}$$

The vertical velocity of the airplane grows exponentially from zero to a final value of A_g. The initial slope of the curve at $t = 0$ is given by the derivative

$$\frac{dw}{dt} = \frac{A_g}{\tau} e^{-t/\tau} \qquad \left.\frac{dw}{dt}\right|_{t\to 0} = \frac{A_g}{\tau} \tag{6.38}$$

The parameter τ is referred to as the time constant of the system. The time constant tells us how fast our system approaches a new steady-state condition after being disturbed. If the time constant is small, the system will respond very rapidly; if the time constant is large, the system will respond very slowly. Figure 6.9 shows the response of the airplane to a sharp-edged gust. Notice that the output of the system approaches the final value asymptotically; however, the response is within 2 percent of the final value after only four time constants.

Additional insight into the vehicle's response can be obtained by looking at the maximum acceleration of the airplane. The maximum acceleration

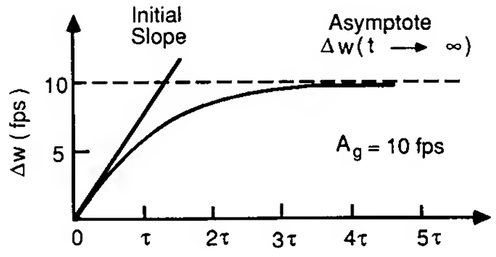

t	$\Delta w/w_g = 1 - e^{-t/\tau}$
0	0
τ	0.632
2τ	0.865
3τ	0.950
4τ	0.982
5τ	0.993
6τ	0.998

FIGURE 6.9

occurs at $t = 0$:

$$\Delta \dot{w} = \frac{C_{L_\alpha} QS}{mu_0} A_g = \frac{A_g}{\tau} \tag{6.39}$$

Dividing Eq. (6.39) by the gravitational constant g we obtain an equation for the change in load factor due to a sharp-edged gust:

$$\frac{\Delta \dot{w}}{g} = \frac{C_{L_\alpha} QS}{mu_0 g} A_g = \frac{\Delta L}{WT} = \Delta n \tag{6.40}$$

or

$$\Delta n = C_{L_\alpha} \frac{\rho u_0}{2} \frac{A_g}{WT/S} \tag{6.41}$$

Equation (6.41) indicates that airplanes having low wing loading WT/S will be much more responsive to the influence of vertical wing gust than airplanes with high wing loadings.

The takeoff and landing performance of an airplane can be shown to be a function of wing loading WT/S. Airplanes having a low wing loading will, in general, have short takeoff and landing field requirements. Airplanes designed for minimum runway requirements such as short-takeoff-and-landing (STOL) aircraft will have low wing loadings compared with conventional transport and fighter airplanes and, therefore, should be more responsive to atmospheric disturbances.

If the gust profile encountered by the airplane is sinusoidal, the response will consist of a transient phase followed by a steady-state sinusoidal

oscillation. The steady-state response to a sinusoidal gust can be written as

$$\Delta w(t) = A_g \frac{1}{\sqrt{1+\tau^2\omega^2}} \sin(\omega t - \phi) \tag{6.42}$$

where

$$\phi = -\tan^{-1}(\tau\omega)$$

The steady-state response of the airplane will have the following characteristics:

1. The same frequency as the gust wave
2. The amplitude of the response will be

$$\text{Amplitude} = \frac{A_g}{\sqrt{1+\tau^2\omega^2}}$$

   where the amplitude of the gust is A_g.
3. The phase angle of the response is $\phi = -\tan^{-1}(\tau\omega)$; the phase angle of the input gust is zero. The response of the airplane lags the gust wave by the angle ϕ.

Figure 6.10 shows the vertical response of an airplane to a sinusoidal gust encountered for values of $\omega\tau$. Remember that ω is the frequency of the gust and τ is the time constant of the airplane. Notice for small values of $\omega\tau$, i.e. low-frequency gusts or small airplane time constants, the phase angle ϕ is very small and the ratio of the response to gust input amplitudes is near unity. In this situation, the response is in phase with the gust wave and the amplitude of response of the airplane is nearly equal to the amplitude of the gust profile.

For very large values of $\omega\tau$, the response amplitude tends to zero, that is, the airplane is unaffected by the gust profile. These trends are easily observed in the frequency response curve shown in Fig. 6.11. This analysis shows us that the rigid body motion of the airplane is excited by the low frequency or long wave length gusts, and that the high frequency or short wave length gusts have little effect on the airplane's motion. Although the high frequency gusts do not

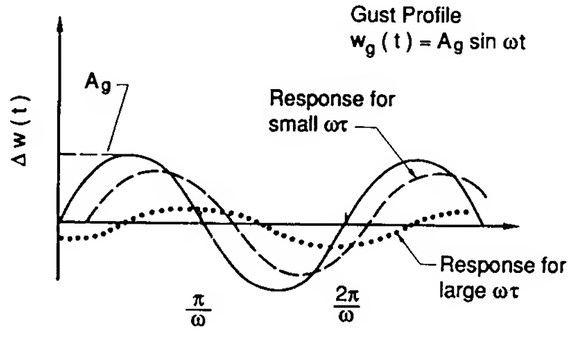

FIGURE 6.10

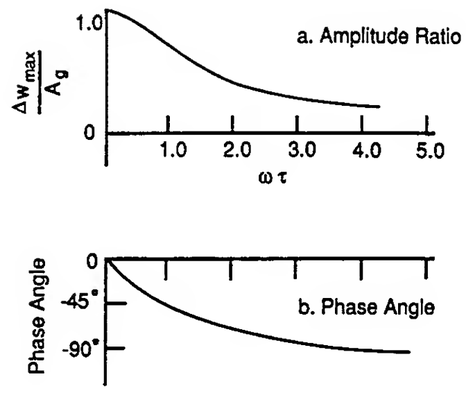

Curves a and b are called Frequency Response Curves

FIGURE 6.11

influence the rigid body motion they will excite the structural modes of the airplane.

Although this example gives us some insight into how atmospheric gusts will affect an airplane, the turbulence in the atmosphere is not deterministic. That is to say, there are no analytical expressions that completely describe atmospheric turbulence. Rather, turbulence is a stochastic process, or random process, and can only be described in a statistical manner.

6.4 ATMOSPHERIC TURBULENCE

The atmosphere is in a continuous state of motion. The winds and wind gusts created by the movement of atmospheric air masses can degrade the performance and flying qualities of an airplane. In addition, the atmospheric gusts impose structural loads that must be accounted for in the structural design of an airplane. The movement of atmospheric air masses is driven by solar heating, the Earth's rotation and various chemical, thermodynamic, and electromagnetic processes.

The velocity field within the atmosphere varies in both space and time in a random manner. This random velocity field is called atmospheric turbulence. The velocity variations in a turbulent flow can be decomposed into a mean and a fluctuating part. Figure 6.12 shows a typical atmospheric turbulence profile. The size or scale of the fluctuations vary from small wavelengths, of the order of centimeters, to wavelengths of the order of kilometers. Because atmospheric turbulence is a random phenomenon, it can only be described in a statistical way.

To predict the effect of atmospheric disturbances on aircraft response, flying qualities, autopilot performance, and structural loads requires a mathematical model of atmospheric turbulence. In the following sections the discussion will include a description of statistical functions used in describing

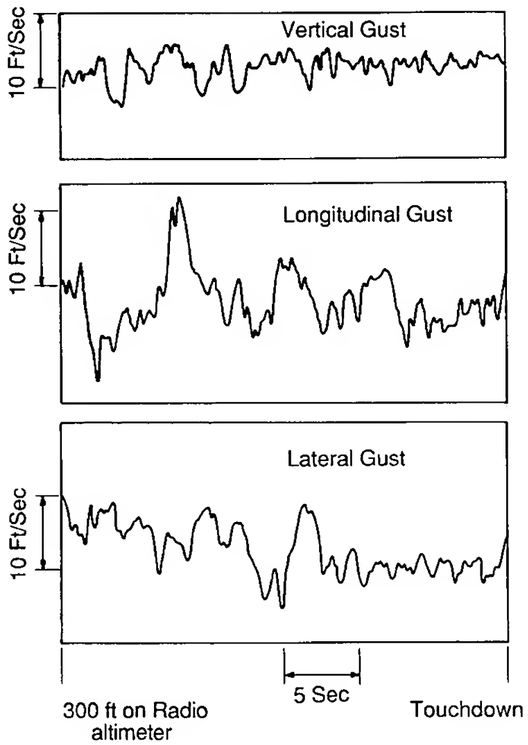

FIGURE 6.12

atmospheric turbulence, a mathematical model of turbulence, and finally an indication of how the turbulence model can be used to determine the response of an airplane to atmospheric disturbances.

Before presenting the mathematical model of turbulence, it is necessary to review some of the basic concepts used to describe turbulence. The discussion will be, at best, only a cursory review of an extremely complicated subject. The reader is referred to Refs 6.2 and 6.3 for a more informative treatment of the subject.

6.5 HARMONIC ANALYSIS

An arbitrary periodic signal having a period T can be represented as an infinite series of cosine and sine functions as follows:

$$f(t) = a_0 + \sum_{n=1}^{\infty} a_n \cos(n\omega t) + \sum_{m=1}^{\infty} b_n \sin(m\omega t) \tag{6.43}$$

where the angular frequency $\omega = 2\pi/T$ and the Fourier coefficients are found from the relationship

$$a_0 = \frac{\omega}{2\pi} \int_{t_0}^{t_0+2\pi/\omega} f(t)\, dt \tag{6.44}$$

$$a_n = \frac{\omega}{\pi} \int_{t_0}^{t_0+2\pi/\omega} f(t) \cos(\omega t)\, dt \tag{6.45}$$

$$b_n = \frac{\omega}{\pi} \int_{t_0}^{t_0+2\pi/\omega} f(t) \sin(n\omega t)\, dt \tag{6.46}$$

When the function is not periodic, the technique can still be used by allowing the period T to go to infinity; then the Fourier series becomes a Fourier integral:

$$f(t) = \frac{1}{\pi} \int_{-\infty}^{\infty} e^{i\omega t}\, d\omega \int_{-\infty}^{\infty} f(\tau) e^{-i\omega\tau}\, d\tau \tag{6.47}$$

If we define the second integral to be

$$G(\omega) = \int_{-\infty}^{\infty} f(\tau) e^{-i\omega\tau}\, d\omega \tag{6.48}$$

then

$$f(t) = \frac{1}{2\pi} \int_{-\infty}^{\infty} G(\omega) e^{i\omega t}\, d\omega \tag{6.49}$$

where $G(\omega)$ and $f(t)$ are a Fourier transform pair. The integrand $G(\omega)\, d\omega$ gives the contribution of the harmonic components of $f(t)$ between the frequencies ω and $\omega + d\omega$. Unfortunately, the harmonic analysis discussed above does not hold for turbulence. In order for the Fourier integral to be applicable, the integrals must be convergent. The nonperiodic turbulence disturbances persist for long periods of time without dying out in time. The persistence of turbulence yields integrals that do not converge.

To obtain a frequency representation for a continuing disturbance requires the use of the theory of random processes. A random process is one which is random by its nature, so that a deterministic description is not practical. For example, we are all familiar with board games we play for relaxation and enjoyment. In most of these games we must roll dice to in order to move around the board. The rolling of the dice constitutes a random experiment. If we denote the sum of the points on the two dice as X, then X is a random variable that can assume integer values between 2 and 12. If we roll the dice a sufficient number of times, we can determine the probabilities of the random variable X assuming any value in the range of X. A function $f(X)$ that yields the probabilities is called the probability or frequency function of a random variable.

Atmospheric turbulence is also a random process, and the magnitude of the gust fields can only be described by statistical parameters. That is, we can conduct experiments to determine the magnitude of a gust component and its probability of occurrence. The properties of atmospheric turbulence include that it is homogeneous and stationary. The property of homogeneity means that the statistical properties of turbulence are the same throughout the region

of interest; stationarity implies that the statistical properties are independent of time.

For the case when $f(t)$ is a stationary random process, the mean square $\overline{f^2(t)}$ is defined as

$$\overline{f^2(t)} = \lim_{T\to\infty} \frac{1}{T}\int_0^T [f(t)]^2\,dt \tag{6.50}$$

where $\overline{f^2(t)}$ represents a measure of the disturbance intensity. The disturbance function $f(t)$ can be thought of as an infinite number of sinusoidal components having frequencies ranging from zero to infinity. That portion of $\overline{f^2(t)}$ that occurs from ω to $d\omega$ is called the power spectral density and is denoted by the symbol $\Phi(\omega)$. The intensity of the random process can be related to the power spectral density.

The response of a physical system such as an airplane to a random disturbance such as atmospheric turbulence can be obtained from the power spectral density of the input function and the system transfer function. If $G(i\omega)$ represents the system frequency response function and $\Phi_i(\omega)$ is the power spectral density of the disturbance input function, then the output $\Phi_0(\omega)$ is given by

$$\Phi_0(\omega) = \Phi_i(\omega)\,|G(i\omega)|^2 \tag{6.51}$$

With Eq. (6.51) we can determine the response of an airplane to atmospheric disturbances. The transfer function G is the gust transfer described earlier. All that remains now is to describe $\Phi_i(\omega)$ for the gust input.

TURBULENCE MODELS. There are two spectral forms of random continuous turbulence used to model atmospheric turbulence for aircraft response studies. They are the mathematical models named after von Karman and Dryden, the scientists who first proposed them. Because the von Karman model is more widely used in practice, it will be the only one described here. The power spectral density for the turbulence velocities is given by

$$\Phi_{ug}(\Omega) = \sigma_u^2 \frac{2L_u}{\pi} \frac{1}{[1+(1.339L_u\Omega)^2]^{5/6}} \tag{6.52}$$

$$\Phi_{vg}(\Omega) = \sigma_v^2 \frac{2L_v}{\pi} \frac{1+\frac{8}{3}(1.339L_v\Omega)^2}{[1+(1.339L_v\Omega)^2]^{11/6}} \tag{6.53}$$

$$\Phi_{wg}(\Omega) = \sigma_w^2 \frac{2L_w}{\pi} \frac{1+\frac{8}{3}(1.339L_w\Omega)^2}{[1+(1.339L_w\Omega)^2]^{11/6}} \tag{6.54}$$

where σ is the root mean square intensity of the gust component, Ω is the spatial frequency, defined by $2\pi/\lambda$, where λ is the wavelength of a sinusoidal component, and L is the scale of the turbulence. The subscripts u, v, w refer to the gust components. The scales and intensities of atmospheric turbulence depend on altitude and the type of turbulence, i.e. clear air (high or low altitude) and thunderstorm turbulences.

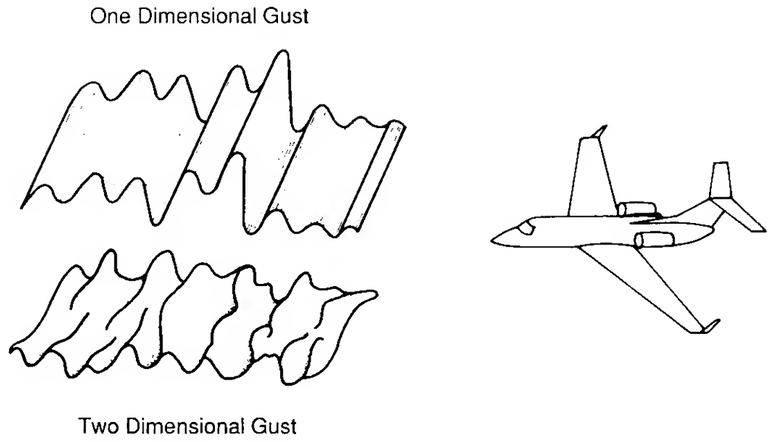

FIGURE 6.13

For an airplane passing through a gust field, it is assumed that the turbulence encountered is independent of time (i.e. the turbulence is stationary). This assumption can be visualized by considering the gust field to be frozen in both time and space, as illustrated in Fig. 6.13. Assuming the frozen-field concept, the turbulence-induced motion is due only to the motion of the airplane relative to the gust field.

The three power spectral densities presented earlier were a function of a spatial frequency; however, as the airplane passes through the frozen turbulent field it senses a temporal frequency. The relationship between the spatial and temporal frequency is given by

$$\Omega = \omega/u_0 \tag{6.55}$$

where ω is in radians/s and u_0 is the velocity of the airplane relative to the air mass it is passing through.

6.6 WIND SHEAR

Wind shear is defined as a local variation of the wind vector. The variations in wind speed and direction are measured in the vertical and horizontal directions. A vertical wind shear is one in which the wind speed and direction varies with changing altitude; horizontal wind shear refers to wind variations along some horizontal distance.

Wind shears are created by the movement of air masses relative to one another or to the earth's surface. Thunderstorms, frontal systems, and the Earth's boundary layer all produce wind shear profiles which, at times, can be hazardous to aircraft flying at low altitudes. The strong gust fronts associated with thunderstorms are created by downdrafts within the storm system. As the downdrafts approach the ground, they turn and move outward along the

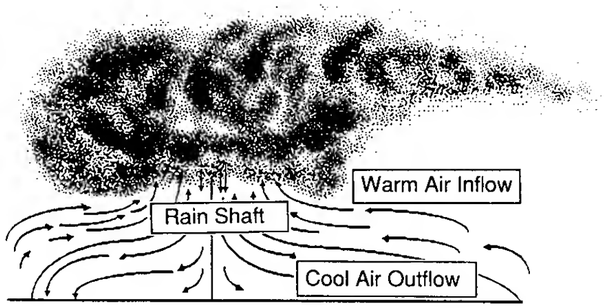

FIGURE 6.14

Earth's surface. The wind shear produced by the gust front can be quite severe.

The wind shear created by a frontal system occurs at the transition zone between two different air masses. The wind shear is created by the interaction of the winds in the two air masses. If the transition zone is gradual, the wind shear will be small. However, if the transition zone is small, the conflicting wind speeds and directions of the air masses can produce a very strong wind shear. Figure 6.14 shows some of the mechanisms that create a wind shear and Fig. 6.15 shows an experimentally measured shear profile near the ground.

There are no simple mathematical formulations to characterize the wind shears produced by the passage of frontal systems or thunderstorms. Generally, these shears are represented in simulation studies by tables of wind speed components with altitude.

The surface boundary layer also produces wind shear. The shape of the profile is determined, primarily, by local terrain and atmospheric conditions. Additional problems arise when there is an abrupt change in surface roughness (which can be expected near airports), resulting in additional internal boundary layers, and when the direction of the wind varies with altitude.

To analyze the influence of wind shear on aircraft motion, the characteristics of wind shear must be known. The magnitude of the shear can be expressed in terms of the change in wind speed with respect to altitude, du/dz, where a positive wind shear is one which increases with increasing altitude. The qualitative criteria for judging the severity of wind shear were proposed to the International Civil Aviation Organization (ICAO). It was suggested that

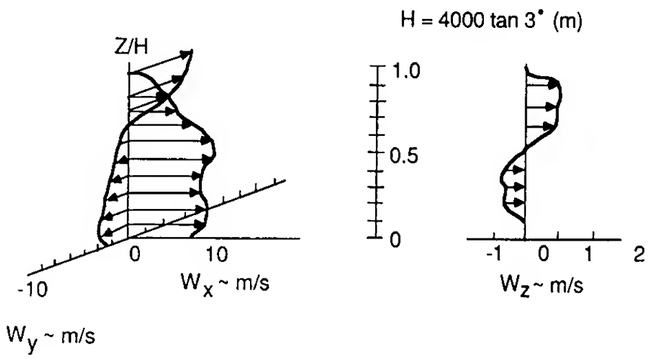

FIGURE 6.15

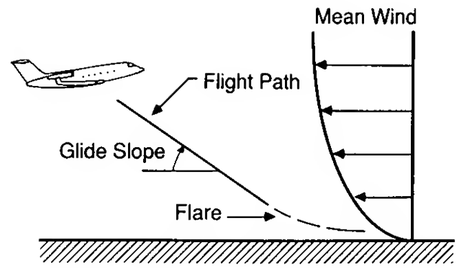

FIGURE 6.16

shear be considered light if du/dh ranged from 0 to $0.08\,s^{-1}$; moderate for $0.08–0.15\,s^{-1}$; strong for $0.15–0.20\,s^{-1}$; and severe if greater than $0.2\,s^{-1}$. These criteria are useful in giving an idea of the magnitude of wind shear, but the ICAO did not accept them. A shear which is moderate for an airplane with high stall speed may be strong for one with low stall speed, so that universal criteria are impossible owing to differences between aircraft types.

Example Problem 6.1. Consider an airplane on final approach encountering a vertical wind shear, i.e. the variation of horizontal wind velocity with altitude. Figure 6.16 shows an airplane flying into a wind shear. To analyse this problem we can use Eq. (6.17). The change in wind velocity is represented by

$$u_g = \frac{du}{dh}\,dh$$

where du/dh is the velocity gradient and dh is the change in altitude. If we assume that the controls are fixed, Eq. (6.17) reduces to

$$\begin{bmatrix} \Delta\dot{u} \\ \Delta\dot{w} \\ \Delta\dot{q} \\ \Delta\dot{\theta} \end{bmatrix} = \begin{bmatrix} X_u & X_w & 0 & -g \\ Z_u & Z_w & u_0 & 0 \\ M_u & M_w & M_q & 0 \\ 0 & 0 & 1 & 0 \end{bmatrix} \begin{bmatrix} \Delta u \\ \Delta w \\ \Delta q \\ \Delta\theta \end{bmatrix} + \begin{bmatrix} -X_u \\ -Z_u \\ -M_u \\ 0 \end{bmatrix} [u_g]$$

But u_g is a function of altitude and therefore we must add other equations to the system. The vertical velocity of the airplane can be expressed as the time rate of change of altitude as follows:

$$\Delta\dot{h} = u_0(\Delta\alpha - \Delta\theta)$$

Adding this equation to the state equations, and substituting for u_g, yields

$$\begin{bmatrix} \Delta\dot{u} \\ \Delta\dot{\alpha} \\ \Delta\dot{q} \\ \Delta\dot{\theta} \\ \Delta\dot{h} \end{bmatrix} = \begin{bmatrix} X_u & X_\alpha & 0 & -g & -X_u\dfrac{du}{dh} \\ \dfrac{Z_u}{u_0} & \dfrac{Z_\alpha}{\mu_0} & 1 & 0 & \dfrac{-Z_u}{u_0}\dfrac{du}{dh} \\ M_u & M_\alpha & M_q & 0 & -M_u\dfrac{du}{dh} \\ 0 & 0 & 1 & 0 & 0 \\ 0 & u_0 & 0 & -u_0 & 0 \end{bmatrix} \begin{bmatrix} \Delta u \\ \Delta\alpha \\ \Delta q \\ \Delta\theta \\ \Delta h \end{bmatrix}$$

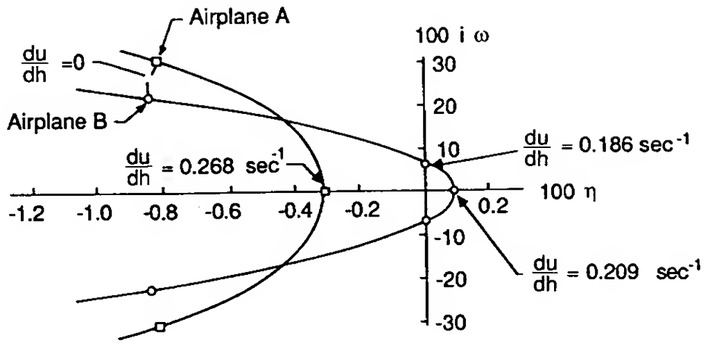

FIGURE 6.17

The solution of this system of equations yields five eigenvalues: two complex pairs representing the phugoid and short-period modes and a fifth, real, root indicating a non-oscillatory motion. The above equations were solved in Ref. 6.6 for STOL aircraft for various magnitudes of the velocity gradient. The results showed that wind shear had very little affect on the short-period motion; however, the phugoid motion was found to be quite sensitive to du/dh. Figure 6.17 shows a root locus plot of the phugoid roots for variations in du/dh. For very large gradients, the phugoid mode can become unstable. An unstable phugoid mode would make the landing approach very difficult for the pilot to control. Therefore, strong wind shears must be avoided for reasons of flight safety.

6.7 SUMMARY

In this chapter we have examined some of the analytical techniques available to the flight control engineers to study the dynamic response of an airplane to control deflection or atmospheric disturbances. Apart from the fact that they create an uncomfortable ride for the pilot and passengers, the loads imposed on the airframe structure by the gust fields must be calculated so that the structure can be properly designed.

Wind shear has been shown recently to be a greater hazard to commercial aviation than had been appreciated. Wind shears created by thunderstorm systems have been identified as the major contributor to several airline crashes. The techniques outlined in this chapter can be used by stability and control engineers to study the effects of atmospheric disturbances on aircraft flight characteristics. Such studies can be used to improve flight safety.

6.8 PROBLEMS

6.1. For the business jet aircraft whose details are included in the Appendix, determine the lateral response curves for an aileron input. Present your results in the form of frequency response curves.

6.2. The vertical motion of an airplane subjected to a sharp-edged gust is described by the equation

$$\Delta w(t) = A_g(1 - e^{-t/\tau})$$

where Δw is in the vertical velocity, A_g is the magnitude of the gust, and τ is the time constant of the airplane. Using the information in Fig. P6.2, determine the maximum vertical acceleration and the time constant of the airplane.

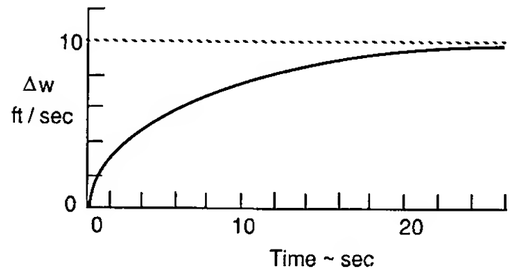

FIGURE P6.2

6.3. For the general aviation airplane whose details are included in the Appendix, determine the vertical response to a sinusoidal gust field. Assume the problem can be modeled by a single degree of freedom vertical equation of motion. Present your results in the form of frequency response curves.

6.4. Discuss how changes in the aerodynamic stability characteristics would effect the response curves obtained in Problem 6.3.

6.5. Assume that an airplane is on final approach and encounters a wind shear which can be represented as

$$u_g = \frac{du}{dh} dh$$

where du/dh is the wind gradient. Assume that the pitch attitude of the airplane is maintained by an automatic control system. Develop the equations of motion governing the vertical and horizontal velocity of the airplane. How does the wind gradient effect the two-dimensional response?

REFERENCES

6.1. McRuer, D., I. Ashkenas, and D. Graham: *Aircraft Dynamics and Automatic Control,* Princeton University Press, Princeton, NJ, 1973.

6.2. Batchelor, G. K.: *The Theory of Homogeneous Turbulence,* Cambridge University Press, London, 1956.

6.3. Lumley, J. L., and H. A. Panofsky: *The Structure of Atmospheric Turbulence,* Interscience, New York, 1964.

6.4. Houbolt, J. C., R. Steiner, and K. G. Pratt: *Dynamic Response of Airplanes to Atmospheric Turbulence Including Flight Data on Input and Response,* NASA TR-R-199, June 1964.

6.5. Press, H., M. T. Meadows, and I. Hadlock: *A Reevaluation of Data on Atmospheric Turbulence and Airplane Gust Loads for Application to Spectral Calculations,* NACA Report 1272, 1956.

6.6. Nelson, R. C., M. M. Curtin, and F. M. Payne: *A Combined Experimental and Analytical Investigation of the Influence of Low Level Wind Shear on the Handling Characteristics of Aircraft,* DOT Report-DOT/RSPA/ADMA-50/83/29, October 1979.

CHAPTER 7

AUTOMATIC CONTROL: APPLICATION OF CONVENTIONAL CONTROL THEORY

"The application of automatic control systems to aircraft promises to bring about the most important new advances in aeronautics in the future". From William Bollay–14th Wright Brothers Lecture[1]

7.1 INTRODUCTION

The development of automatic control systems has played an important role in the growth of civil and military aviation. Modern aircraft include a variety of automatic control systems that aid the flight crew in navigation, flight management and augmenting the stability characteristics of the airplane. In this chapter we shall discuss the application of control theory to the design of simple autopilots that can be used by the flight crew to lessen their work load during cruise and to help them land their aircraft during adverse weather conditions. In addition, we shall also discuss how automatic control systems can be used to provide artificial stability to improve the flying qualities of an airplane.

The development of autopilots closely followed the successful development of a powered man-carrying airplane by the Wright brothers. In 1914 the Sperry brothers demonstrated the first successful autopilot. The autopilot was capable of maintaining pitch, roll, and heading angles. To demonstrate the effectiveness of their design, Lawrence Sperry trimmed his airplane for straight and level flight and then engaged the autopilot. He then proceeded to stand in the cockpit with his hands raised above his head while his mechanic walked out along the wings in an attempt to upset the airplane's equilibrium. Figure 7.1

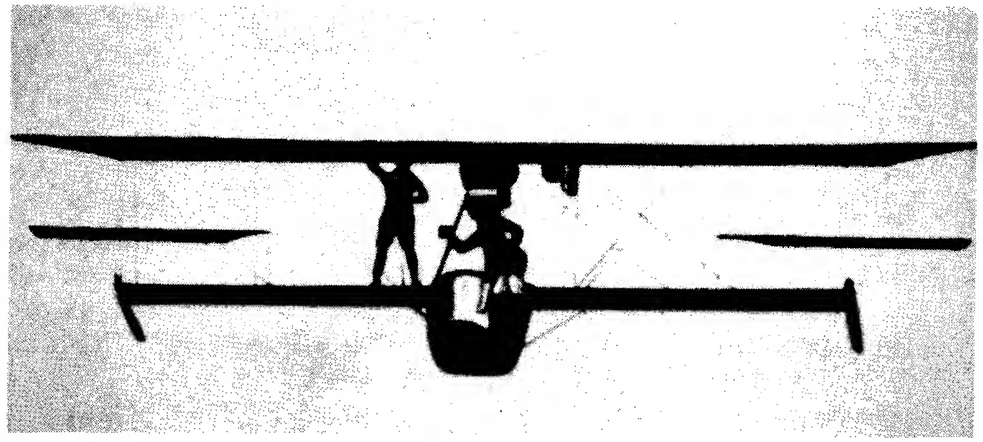

FIGURE 7.1
Photograph of Sperry's flight demonstration of a three axes automatic control system.

shows a photograph of the remarkable flight. The autopilot provided aileron, rudder, and elevator commands to that the airplane remained in a wings-level attitude.

Before examining some simple autopilot designs, we will review some of the basic concepts of control theory. Control systems can be classified as either open-loop or closed-loop systems. An open-loop control system is the simplest and least complex of all control devices. In an open-loop system the control action is independent of the output. A closed-loop system is one in which the control action depends on the output of the system. Closed-loop control systems are called feedback control systems. The advantage of the closed-loop control system is its accuracy.

To obtain a more accurate control system, some form of feedback between the output and input must be established. This can be accomplished by comparing the controlled signal (output) with the commanded or reference input. A feedback system is defined as a system in which one or more feedback loops are used to compare the controlled signal with the command signal so as to generate an error signal. The error signal is then used to drive the output signal into agreement with the desired input signal. The typical closed-loop feedback system shown in Fig. 7.2 is composed of a forward path, a feedback path and an error-detection device called a comparator. Each component of the control system is defined in terms of its transfer function. The transfer function T.F. is defined as the ratio of the Laplace transform of the output to the Laplace transform of the input where the initial conditions are assumed to be zero:

$$\text{T.F.} = \frac{\text{Laplace transform of the output}}{\text{Laplace transform of the input}} \tag{7.1}$$

The transfer function of each element of the control system can be determined

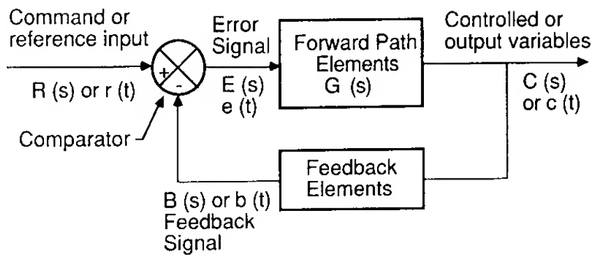

FIGURE 7.2
Block diagram representation of a feedback control system.

from the equations that govern the dynamic characteristics of the element. The aircraft transfer functions were developed in Chapter 3 from the equations of motion.

The closed-loop transfer function for the feedback control system shown in Fig. 7.2 can be developed from the block diagram. The symbols used in the block diagram are defined as follows:

$R(s)$	reference input
$C(s)$	output signal (variable to be controlled)
$B(s)$	feedback signal
$E(s)$	error or actuating signal
$G(s)$	$C(s)/E(s)$ forward path or open-loop transfer function
$M(s)$	$C(s)/R(s)$ the closed-loop transfer function
$H(s)$	feedback transfer function
$G(s)H(s)$	loop transfer function

The closed-loop transfer function $C(s)/R(s)$ can be obtained by simple algebraic manipulation of the block diagram. The actuating or error signal is the difference between the input and feedback signals:

$$E(s) = R(s) - B(s) \tag{7.2}$$

The feedback signal $B(s)$ can be expressed in terms of the feedback transfer function and the output signal:

$$B(s) = H(s)C(s) \tag{7.3}$$

and the output signal $C(s)$ is related to the error signal and forward path transfer function in the following manner:

$$C(s) = G(s)E(s) \tag{7.4}$$

Substituting Eqs (7.2) and (7.3) into Eq. (7.4) yields

$$C(s) = G(s)R(s) - G(s)H(s)C(s) \tag{7.5}$$

Equation (7.5) can be solved for the closed-loop transfer function $C(s)/R(s)$,

$$\frac{C(s)}{R(s)} = \frac{G(s)}{1 + G(s)H(s)} \tag{7.6}$$

which is the ratio of the system output to the input. Most control systems are

much more complex than the one shown in Fig. 7.2. However, theoretically, the more complex control systems consisting of many feedback elements can be reduced to the simple form described above.

The feedback systems described here can be designed to control accurately the output to some desired tolerance. However, feedback in itself does not ensure that the system will be stable. Therefore, to design a feedback control system one needs analysis tools which permit the designer to select system parameters so that the system will be stable. In addition to determining the absolute stability, the relative stability of the control system must also be determined. A system which is stable in the absolute sense may not be a satisfactory control system. For example, if the system damping is too low, the output will be characterized by large amplitude oscillations about the desired output. The large overshooting of the response may make the system unacceptable.

Autopilots can be designed using either frequency- or time-domain methods developed from servomechanism theory, or by time-domain analysis using state feedback design. In this chapter the techniques from servomechanism theory will be discussed and several simple applications of the design techniques will be demonstrated by applying the techniques to the design of autopilots.

The servomechanism design techniques include the Routh criterion, root locus, Bode, and Nyquist methods. A brief description of these techniques is presented either in the following sections or in the appendices at the end of this book. For a more rigorous treatment of this material, the reader is referred to Refs [7.2–7.5].

7.2 ROUTH'S CRITERION

As noted earlier, the roots of the characteristic equation tell us whether or not the system is dynamically stable. If all the roots of the characteristic equation have negative real parts, the system will be dynamically stable. On the other hand, if any root of the characteristic equation has a positive real part, the system will be unstable. The system is considered to be marginally stable if one or more of the roots is a pure imaginary number. The marginally stable system represents the boundary between a dynamically stable or unstable system. For a closed-loop control system the denominator of Eq. (7.6) is the characteristic equation of the system.

A simple means of determining the absolute stability of a system can be obtained by the Routh stability criterion. The method allows us to determine whether any of the roots of the characteristic equation have positive real parts, without actually solving for the roots. Consider the characteristic equation

$$a_n\lambda^n + a_{n-1}\lambda^{n-1} + a_{n-2}\lambda^{n-2} \cdots a_1\lambda + a_0 = 0 \tag{7.7}$$

In order that there be no roots of Eq. (7.7) with positive real parts, the

TABLE 7.1
Definition of Routh array

Routh table				
λ^n	a_n	a_{n-2}	a_{n-4}	$\cdots$
λ^{n-1}	a_{n-1}	a_{n-3}	a_{n-5}	$\cdots$
λ^{n-2}	b_1	b_2	b_3	$\cdots$
$\vdots$	c_1	c_2	c_3	$\cdots$

where a_n, $a_{n-1}, \ldots a_0$ are the coefficients of the characteristic equation and the coefficients b_1, b_2, b_3, c_1, c_2, etc., are given by:

$$b_1 \equiv \frac{a_{n-1}a_{n-2} - a_n a_{n-3}}{a_{n-1}} \qquad b_2 \equiv \frac{a_{n-1}a_{n-4} - a_n a_{n-5}}{a_{n-1}} \qquad \text{etc.}$$

$$c_1 \equiv \frac{b_1 a_{n-3} - a_{n-1}b_2}{b_1} \qquad c_2 \equiv \frac{b_1 a_{n-5} - a_{n-1}b_3}{b_1} \qquad \text{etc.}$$

$$d_1 \equiv \frac{c_1 b_2 - c_2 b_1}{c_1} \qquad \text{etc.}$$

necessary, but not sufficient, conditions are that:

1. All the coefficients of the characteristic equation must have the same sign.
2. All the coefficients must exist.

To apply the Routh criterion, we must first define the Routh array as in Table 7.1. The Routh array is continued horizontally and vertically until only zeros are obtained. The last step is to investigate the signs of the numbers in the first column of the Routh table. The Routh stability criterion states:

1. If all the numbers of the first column have the same sign, then the roots of the characteristic polynominal have negative real parts. The system is, therefore, stable.
2. If the numbers in the first column change sign, then the number of sign changes indicates the number of roots of the characteristic equation having positive real parts. Therefore, if there is a sign change in the first column, the system will be unstable.

When developing the Routh array, several difficulties may occur. For example, the first number in one of the rows may be zero, but the other numbers in the row may not be. Obviously, if a zero appears in the first position of a row, the elements in the following row will be infinite. In this case, the Routh test breaks down. Another possibility is that all the numbers in a row are zero. Methods for handling these special cases can be found in most textbooks on automatic control theory.

Several examples of applying the Routh stability criterion are shown in Example Problem 7.1.

Example Problem 7.1. Determine whether the characteristic equation

$$\lambda^3 + 6\lambda^2 + 12\lambda + 8 = 0$$

has any roots with positive real parts. The first two rows of the array are written down by inspection and the succeeding rows are obtained by using the relationship for each row element as presented previously:

1	12	0
6	8	0
64	0	
6		
8		

There are no sign changes in column 1; therefore, the system is stable.

As another example, consider the characteristic equation

$$2\lambda^3 + 4\lambda^2 + 4\lambda + 12 = 0$$

The Routh array can be written as follows.

2	4	0
4	12	0
−2	0	
12		

Note that there are two sign changes in column 1; therefore, the characteristic equation has two roots with positive real parts. The system is unstable.

The Routh stability criterion can be applied to the quartic characteristic equation which describes either the longitudinal or lateral motion of an airplane. The quartic characteristic equation for either the longitudinal or lateral equation of motion can be expressed as

$$A\lambda^4 + B\lambda^3 + C\lambda^2 + D\lambda + E = 0$$

where A, B, C, D and E are functions of the longitudinal or lateral stability derivatives. Forming the Routh array from the characteristic equation yields

A	C	E
B	D	0
$\dfrac{BC - AD}{B}$	E	0
$\dfrac{[D(BC - AD)/B] - BE}{(BC - AD)/B}$	0	
E		

The condition that the airplane is stable requires that

$$\begin{aligned} A,B,C,D,E &> 0 \\ BC - AD &> 0 \\ D(BC - AD) - B^2E &> 0 \end{aligned}$$

The last two inequalities were obtained by inspection of the first column of the Routh array.

7.3 ROOT LOCUS TECHNIQUE

In designing a control system, it is desirable to be able to investigate the performance of the control system when one or more parameters of the system are varied. As has been shown repeatedly, the characteristic equation plays an important role in the dynamic behavior or aircraft motions. The same is true for linear control systems. In control system design, a powerful tool for analyzing the performance of a system is the root locus technique. Basically, the technique provides graphical information in the s plane on the trajectory of the roots of the characteristic equation for variations in one or more of the system parameters. Typically, most root locus plots consist of only one parametric variation. The root locus technique was introduced by W. R. Evans in 1949. The root locus method allows the control engineer to obtain accurate time-domain response as well as frequency response information of closed-loop control systems.

A brief discussion of the root locus technique will be presented here. Recall that the closed-loop transfer function of a feedback control system can be expressed as

$$\frac{C(s)}{R(s)} = \frac{G(s)}{1 + G(s)H(s)} \tag{7.8}$$

The characteristic equation of the closed loop system is found by setting the denominator of the transfer function equal to zero.

$$1 + G(s)H(s) = 0 \tag{7.9}$$

The loop transfer function $G(s)H(s)$ can be expressed in the factored form as follows:

$$G(s)H(s) = \frac{k(s + z_1)(s + z_2) \cdots (s + z_m)}{(s + p_1)(s + p_2) \cdots (s + p_n)} \tag{7.10}$$

where the z's, p's, and k are the zeros, poles, and gain of the transfer function. The zeros are the roots of the numerator and the poles are the roots of the denominator of the transfer function. As stated earlier, the root locus is a graphical presentation of the trajectory of the roots of the characteristic equation or the poles of the closed-loop transfer function for variation of one of the system parameters. Let us examine the root locus plot for the above equation as the system gain k is varied. The characteristic equation can be rewritten as

$$G(s)H(s) = -1 \tag{7.11}$$

or

$$\frac{k(s + z_1)(s + z_2) \cdots (s + z_m)}{(s + p_1)(s + p_2) \cdots (s + p_n)} = -1 \tag{7.12}$$

For the case when $k = 0$, the points on the root locus plot are the poles of

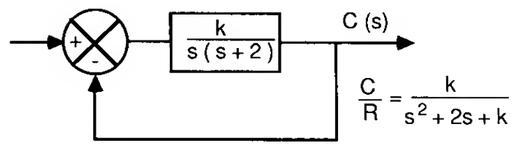

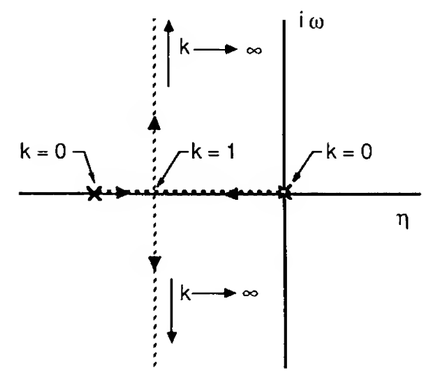

FIGURE 7.3
Root locus sketch for a second order system.

the loop transfer function $G(s)H(s)$. On the other hand, when $k \to \infty$ the points on the root locus are the zeros of the loop transfer function. Thus we see that the roots of the closed-loop transfer function migrate from the poles to the zeros of the loop transfer function as k is varied from 0 to ∞. Furthermore, the points on the root locus for intermediate values of k must satisfy the equation

$$\frac{|k|\,|s + z_1|\,|s + z_2| \cdots |s + z_m|}{|s + p_1|\,|s + p_2| \cdots |s + p_n|} = 1 \tag{7.13}$$

and

$$\sum_{i=1}^{m} \angle(s + z_i) - \sum_{i=1}^{n} \angle(s + p_i) = (2q + 1)\pi \tag{7.14}$$

where $q = 0, \pm 1, \pm 2 \ldots$ all integers.

Figure 7.3 is a sketch of a root locus plot for a second-order control system. The root locus diagram gives the roots of the closed loop characteristic equation as k is varied from 0 to ∞. When $k = 0$ the roots are located at the origin and $s = -2$. As k is increased, the roots move along the real axis towards one another until they meet at $s = -1$. Further increases in k cause the roots to become complex and they move away from the real axis along a line perpendicular to the real axis. When the roots are complex, the system is underdamped and a measure of the system damping ratio is obtained by measuring the angle of a line drawn from the origin to a point on the complex portion of the root locus. The system damping ratio is given by the equation

$$\zeta = \cos^{-1}\theta \tag{7.15}$$

The roots of the closed-loop characteristic equation can be obtained using

root-solving algorithms that can be coded on digital computers. Such computer software can be used to obtain root locus contours for variations of system parameters. In addition, there is a simple graphical technique that can be used to rapidly construct the root locus diagram of a control system. An outline of the graphical procedure is presented in one of the appendices.

7.4 FREQUENCY DOMAIN TECHNIQUES

The frequency response of a dynamic system was discussed in Chapter 6. The same techniques can be applied to the design of feedback control systems. The transfer function for a closed-loop feedback system can be written as

$$M(s) = \frac{C(s)}{R(s)} = \frac{G(s)}{1 + G(s)H(s)} \tag{7.16}$$

If we excite the system with a sinusoidal input such as

$$r(t) = A \sin(\omega t) \tag{7.17}$$

the steady-state output of the system will have the form

$$c(t) = B \sin(\omega t + \phi) \tag{7.18}$$

The magnitude and phase relationship between the input and output signal is called the frequency response of the system. The ratio of output to input for a sinusoidal steady state can be obtained by replacing the Laplace transform variable s with $i\omega$.

$$M(i\omega) = \frac{G(i\omega)}{1 + G(i\omega)H(i\omega)} \tag{7.19}$$

Expressing the previous equation in terms of its magnitude and phase angle yields

$$M(i\omega) = M(\omega)\underline{/\phi(\omega)} \tag{7.20}$$

where

$$M(\omega) = \left| \frac{G(i\omega)}{1 + G(i\omega)H(i\omega)} \right| \tag{7.21}$$

and

$$\phi(\omega) = \underline{/G(i\omega)} - \underline{/[1 + G(i\omega)H(i\omega)]} \tag{7.22}$$

The frequency response information can be plotted in rectangular, polar, or logarithmic (Bode) plots. Figure 7.4 is a sketch of the various ways of presenting the frequency response data. The relationship between the frequency- and time-domain performance of a control system is discussed in the next section.

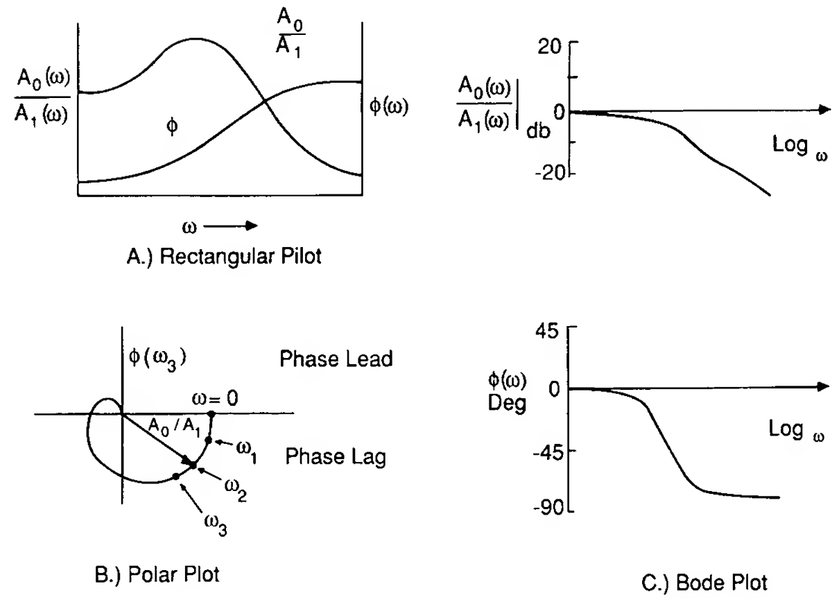

FIGURE 7.4
Various graphical ways of presenting frequency response data.

7.5 TIME-DOMAIN AND FREQUENCY-DOMAIN SPECIFICATIONS

The first step in the design of a feedback control system is to determine a set of specifications of the desired system performance. In the following section we shall present both time- and frequency-domain specifications and their relationship to one another for a second-order system. The transfer function of a second-order system can be expressed as

$$\frac{C(s)}{R(s)} = \frac{\omega_n^2}{s^2 + 2\zeta\omega_n s + \omega_n^2} \tag{7.23}$$

where ζ is the damping ratio and ω_n is the undamped natural frequency of the system. Figure 7.5 is a sketch of the response to a step input of an underdamped second-order system. The performance of the second-order system is characterized by the overshoot, delay time, rise time, and settling time of the transient response to a unit step. The time response of a second-order system to a step input for an underdamped system, i.e. $\zeta < 1$, is given by Eqs (7.24) and (7.25):

$$c(t) = 1 + \frac{e^{-\zeta\omega_n t}}{\sqrt{1-\zeta^2}} \sin(\omega_n \sqrt{1-\zeta^2}\, t - \phi) \tag{7.24}$$

$$\phi = \tan^{-1}\left(\frac{\sqrt{1-\zeta^2}}{-\zeta}\right) \tag{7.25}$$

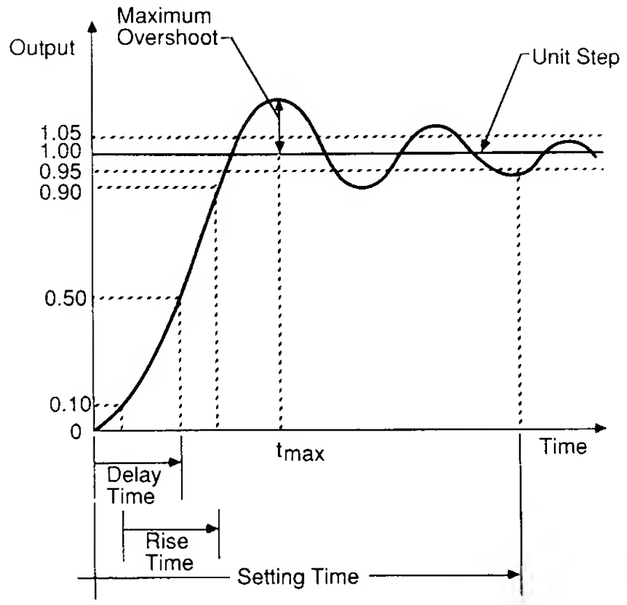

FIGURE 7.5
Time response of a second order system.

The delay and rise time give a measure of how fast the system responds to a step input. Delay time t_d is the time it takes for the response to reach for the first time 50 percent of the final value of the response. The rise time t_r is the time required for the response to rise from 10 percent to 90 percent of the final value. The other two parameters of interest are the settling time and peak overshoot. Settling time t_s is the time it takes for the response to stay within a specified tolerance band of 5 percent of the final value. The peak overshoot is a measure of the oscillations about the final output. From the standpoint of control system design, we would like to have a system that responds rapidly with minimum overshoot. Equations (7.24) and (7.25) can be used to determine the relationships between the time-domain specifications t_d, t_r, etc., and the damping ratio ζ and undamped natural frequency ω_n. Table 7.2 is a summary of these relationships.

Figure 7.6 is a sketch of the typical magnitude and phase characteristics of a feedback control system. As was the case in the time-domain analysis, it is desirable to have a set of specifications to describe the control system performance in the frequency domain. In the frequency domain the design specifications are given in terms of the resonance peak M_r, the resonant frequency ω_r, the system bandwidth ω_B, and the gain and phase margins. The maximum value of $M(\omega)$ is called the resonance peak and is an indication of the relative stability of the control system. If M_r is large, the system will have a large peak overshoot to a step input. The resonant frequency ω_r is the frequency at which the resonance peak occurs and is related to the frequency of the oscillations and speed of the transient response. The band width ω_B is the band of frequencies from zero to the frequency at which the magnitude $M(\omega)$ drops to 70 percent of the zero-frequency magnitude. The bandwidth

TABLE 7.2
Time domain specifications

Delay time t_d	**Rise time, t_r**
$t_d \approx \dfrac{1+0.6\zeta+0.15\zeta^2}{\omega_n}$	$t_r \approx \dfrac{1+1.1\zeta+1.4\zeta^2}{\omega_n}$
Time to peak amplitude, t_p	**Settling time, t_s**
$t_p = \dfrac{\pi}{\omega_n\sqrt{1-\zeta^2}}$	$t_s = \dfrac{3.0}{\omega_n\zeta}$

Peak overshoot, M_p

$$M_p = \frac{c(t_p)-c(\infty)}{c(\infty)} \times 100\%$$

For a unit step

Percent maximum overshoot $= 100\exp(-\pi\zeta/\sqrt{1-\zeta^2})$

gives an indication of the transient response of the system. If the bandwidth is large, the system will respond rapidly, whereas a small bandwidth will result in a sluggish control system.

The gain and phase margins are measures of the relative stability of the system and are related to the closeness of the poles of the closed-loop system to the $i\omega$ axis.

For a second-order system the frequency domain characteristics M_r, ω_r, and ω_B can be related to the system damping ratio and the undamped natural frequency ω_n. The relationships will be presented here without proof:

$$M_r = \frac{1}{2\zeta\sqrt{1-\zeta^2}} \tag{7.26}$$

$$\omega_r = \omega_n\sqrt{1-2\zeta^2} \tag{7.27}$$

$$\omega_B = \omega_n[(1-2\zeta^2)+\sqrt{4\zeta^4-4\zeta^2+2}]^{1/2} \tag{7.28}$$

The peak resonance and the peak overshoot of the transient response in the time domain is given by the following approximation:

$$c(t)_{\max} \leq 1.17M_r \tag{7.29}$$

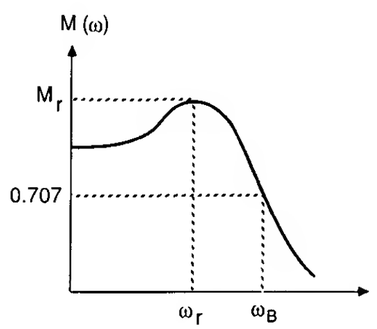

FIGURE 7.6
Frequency response of a closed loop control system.

The phase margin of a second-order system can be related to the system damping ratio as follows:

$$\phi = \tan^{-1}\left[2\zeta\left(\frac{1}{(4\zeta^2+1)^{1/2}-2\zeta^2}\right)^{1/2}\right] \tag{7.30}$$

This very formidable equation can be approximated by the simple relationship

$$\zeta \approx 0.1\phi \qquad \text{for} \qquad \zeta \leq 0.7 \tag{7.31}$$

The phase margin ϕ is in degrees.

From the above relationships developed for the second-order system the following observations can be made.

1. The maximum overshoot for a unit step in the time domain is a function only of ζ.
2. The resonance peak of the closed loop system is only a function of ζ.
3. The maximum peak overshoot and resonance peak are related through the damping ratio.
4. The rise time increases while the bandwidth decreases for increases in system damping for a fixed ω_n. The bandwidth and rise time are inversely proportional to one another.
5. The bandwidth is directly proportional to ω_n.
6. The higher the bandwidth, the larger the resonance peak.

HIGHER-ORDER SYSTEMS. Most feedback control systems are usually of a higher order than the second-order system discussed in the previous sections. However, many higher-order control systems can be analyzed by approximating the system by a second-order system. Obviously, when this can be accomplished, the design and analysis of the equivalent system is greatly simplified.

For a higher-order system to be replaced by an equivalent second-order system, the transient response of the higher-order system must be dominated by a pair of complex conjugate poles. These poles are called the dominant poles or roots and are located closest to the origin in a pole–zero plot. The other poles must be located far to the left of the dominant poles or be located near a zero of the system. The transient response caused by the poles located to the far left of the dominant poles will diminish rapidly in comparison with the dominant root response. On the other hand, if the pole is not located to the far left of the dominant poles, then the poles must be near a zero of the system transfer function. The transient response of a pole located near a zero is characterized by a very small amplitude motion, which can readily be neglected.

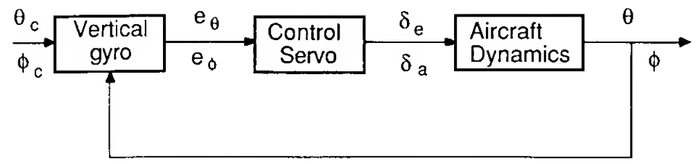

FIGURE 7.7
Block diagram of a roll or pitch displacement autopilot.

7.6 THE DISPLACEMENT AUTOPILOT

One of the earliest autopilots to be used for aircraft control is the so-called displacement autopilot. A displacement type autopilot can be used to control the angular orientation of the airplane. Conceptually, the displacement autopilot works in the following manner. In a pitch attitude displacement autopilot, the pitch angle is sensed by a vertical gyro and compared with the desired pitch angle to create an error angle. The difference or error in pitch attitude is used to produce proportional displacements of the elevator so that the error signal is reduced. Figure 7.7 is a sketch showing the block diagram representation of either a pitch or roll angle displacement autopilot.

The heading angle of the airplane can also be controlled using a similar scheme to that outlined above. The heading angle is sensed by a directional gyro and the error signal is used to displace the rudder so that the error signal is reduced. A sketch of a displacement heading autopilot is shown in Fig. 7.8.

In practise, the displacement autopilot is engaged once the airplane has been trimmed in straight and level flight. To maneuver the airplane while the autopilot is engaged, the pilot adjusts the commanded signals. For example, the airplane can be made to climb or descend by changing the pitch command. Turns can be achieved by introducing the desired bank angle while simultaneously changing the heading command. In the following section we shall examine several displacement autopilot concepts.

PITCH DISPLACEMENT AUTOPILOT. The basic components of a pitch attitude control system are shown in Fig. 7.7. For this design the reference pitch angle is compared with the actual angle measured by a gyro to produce an error signal to activate the control servo. In general, the error signal is amplified and sent to the control surface actuator to deflect the control surface. Movement of the control surface causes the aircraft to achieve a new pitch orientation, which is fed back to close the loop.

To illustrate how such an autopilot would be designed, we will examine this particular pitch displacement autopilot concept for a business jet aircraft.

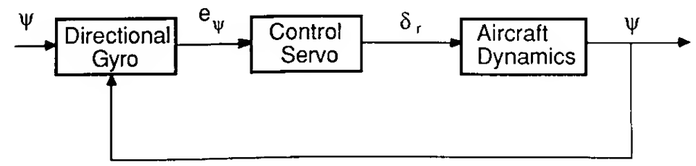

FIGURE 7.8
Block diagram of a leading displacement autopilot.

Once we have decided upon a control concept, our next step must be to evaluate the performance of the control system. To accomplish this we must define the transfer functions for each of the elements in the block diagram describing the system. For the purposes of this discussion we will assume that the transfer functions of both the gyro and amplifier can be represented by simple gains. The elevator servo transfer function can be represented as a first-order system:

$$\frac{\delta_e}{v} = \frac{1}{\tau s + 1} \tag{7.32}$$

where δ_e, v, and τ are the elevator deflection angle, input voltage, and servomotor time constant. Time constants for typical servomotors fall in a range 0.05–0.25 s. For our discussion we assume a time constant of 0.1 s. Finally, we need to specify the transfer function for the airplane. The transfer function relating the pitch attitude to elevator deflection was developed in Chapter 3. To keep the description of this design as simple as possible, we represent the aircraft dynamics by using the short-period approximation. The short-period transfer function for the business jet can be shown to be

$$\frac{\Delta\theta}{\Delta\delta_e} = \frac{-2.0(s + 0.3)}{s(s^2 + 0.65s + 2.15)} \tag{7.33}$$

Figure 7.9 is the block diagram representation of the autopilot. The problem now is one of determining the gain k so that the control system will have the desired performance. Selection of the gain k can be determined using a root locus plot of the loop transfer function. Figure 7.10 is the root locus plot for the business jet pitch autopilot. As the gain is increased from zero, the system damping decreases rapidly and the system becomes unstable. Even for low values of k, the system damping would be too low for satisfactory dynamic performance. The reason for the poor performance of this design is that the airplane has very little natural damping. To improve the design we could increase the damping of the short-period mode by adding an inner feedback loop. Figure 7.11 is a block diagram representation of a displacement autopilot with pitch rate feedback for improved damping. In the inner loop the pitch

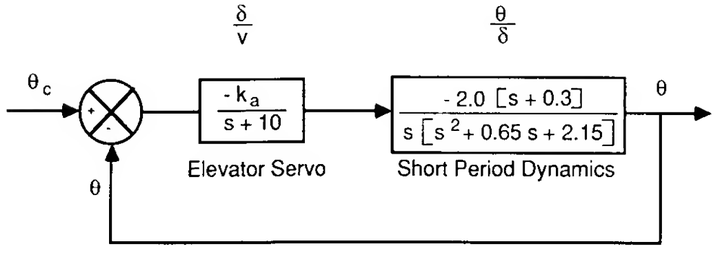

FIGURE 7.9
Block diagram of a pitch displacement autopilot for a business jet.

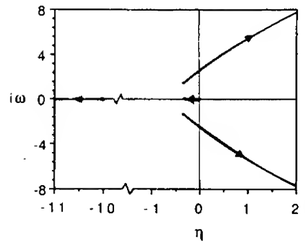

FIGURE 7.10
Root locus plot of the system gain for a pitch displacement autopilot.

rate is measured by a rate gyro and fed back to be added with the error signal generated by the difference in pitch attitude. Figure 7.12 shows the block diagram for the business jet when pitch rate is incorporated into the design. For this problem we now have two parameters to select, namely the gains k and k_{rg}. The root locus method can be used to pick both parameters. The procedure is essentially a trial-and-error method. First, the root locus diagram is determined for the inner loop; a gyro gain is selected, and then the outer root locus plot is constructed. Several iterations may be required until the desired overall system performance is achieved.

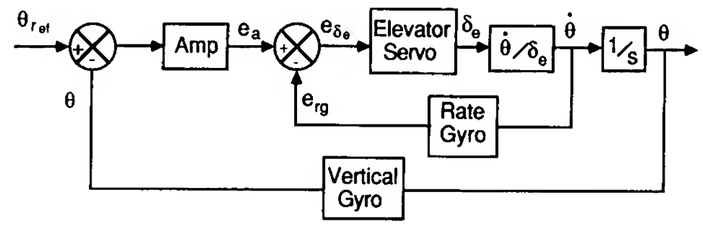

FIGURE 7.11
Block diagram of a pitch altitude control system employing pitch rate feedback.

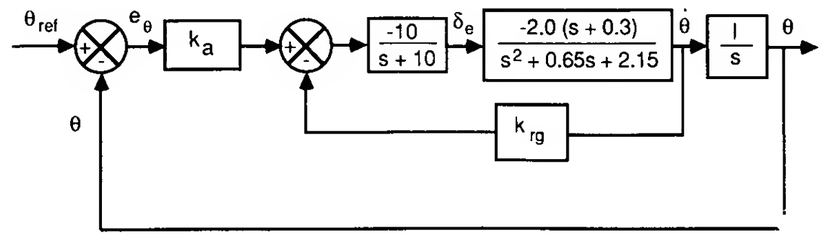

FIGURE 7.12
Block diagram of a business jet pitch attitude control system with pitch rate feedback.

Example Problem 7.2. In this example we examine the performance of a simple roll autopilot for maintaining the roll angle at some specified value. For most applications the autopilot would be used to maintain a wings-level altitude. A conceptual design of a wings-leveling autopilot would be as shown in Fig. 7.7. The aileron servomotor transfer function can again be approximated as a

first-order lag term as

$$\frac{\delta_a}{v} = \frac{1}{\tau s + 1}$$

For this example we assume that τ has a value of 0.1 s. The airplane dynamics for this example will be modeled using the single degree of freedom roll equation developed in Chapter 5. The transfer function ϕ/δ can be obtained by taking the Laplace transformation of the roll equation, which yields

$$\frac{\phi}{\delta} = \frac{L_{\delta a}}{s(s - L_p)}$$

The block diagram of the control system for a fighter aircraft having the characteristics $L_{\delta a} = 11.4$, $L_p = -1.4$ is shown in Fig. 7.13.

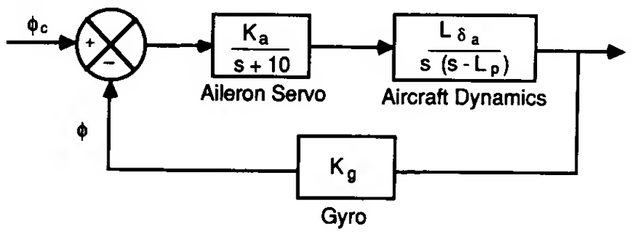

FIGURE 7.13
Block diagram of a roll control autopilot for a jet fighter.

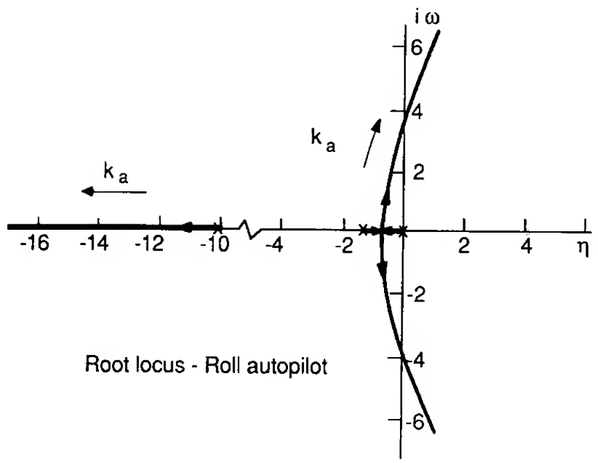

FIGURE 7.14
Root locus plot of a displacement roll control system for a fighter aircraft.

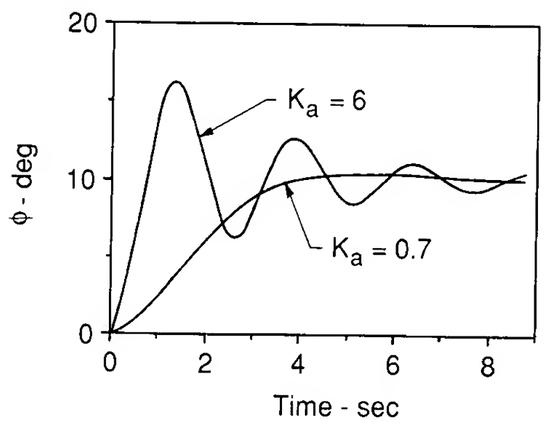

FIGURE 7.15
Roll autopilot response to initial disturbances for several different values of k_a.

The problem is now one of determining the amplifier gain k_a so that the autopilot will perform properly. The root locus analysis technique allows the designer to examine the roots of the characteristic equation of the closed-loop transfer function as one of the system parameters is varied. In this case we will vary k_a from 0 to ∞. Figure 7.14 shows the root locus plot of our autopilot design. As shown earlier, the locus starts as the poles of the open loop transfer function $G(s)H(s)$ when $k_a = 0$, and in this case move towards zeros at infinity as k_a is increased to ∞. The root starting at the servo root moves along the real axis towards $-\infty$ as k_a is increased, while the roots starting at the poles 0 and -1.4 move towards each other and eventually break away from the real axis as complex roots as k_a is increased. The complex portion of the locus intersects the imaginary axis when $k_a = 8$. Further increases in k_a result in an unstable system. Figure 7.15 shows the time-domain response for several different values of k_a.

7.7 STABILITY AUGMENTATION

Another application of automatic devices is to provide artificial stability for an airplane that has undesirable flying characteristics. Such control systems are commonly called stability augmentation systems (SAS).

As we showed earlier, the inherent stability of an airplane depends upon the aerodynamic stability derivatives. The magnitude of the derivatives affects both the damping and frequency of the longitudinal and lateral motions of an airplane. Furthermore, it was shown that the stability derivatives were a function of the airplane's aerodynamic and geometric characteristics. For a particular flight regime it would be possible to design an airplane to possess desirable flying qualities. For example, we know that the longitudinal stability coefficients are a function of the horizontal tail volume ratio. Therefore, we could select a tail size and or location so that $C_{m\alpha}$ and C_{mq} provide the proper damping and frequency for the short-period mode. However, for an airplane that will fly throughout an extended flight envelope, one can expect the stability to vary significantly, owing primarily to changes in the vehicle's configuration (lowering of flaps and landing gear), or Mach and Reynolds number effects on the stability coefficients. Because the stability derivatives vary over the flight envelope, the handling qualities will also change. Obviously, we would like to provide the flight crew with an airplane that has desirable handling qualities over its entire operational envelope. This is accomplished by employing stability augmentation systems.

Example Problem 7.3. To help us understand how a stability augmentation system works, we shall consider the case of an airplane having poor short-period dynamic characteristics. In our analysis we assume that the aircraft has only one degree of freedom—a pitching motion about the center of gravity. The equation of motion for a constrained pitching motion was developed in Chapter 4 and is reproduced below:

$$\ddot{\theta} - (M_q + M_{\dot{\alpha}})\dot{\theta} + M_\alpha \theta = M_\delta \delta$$

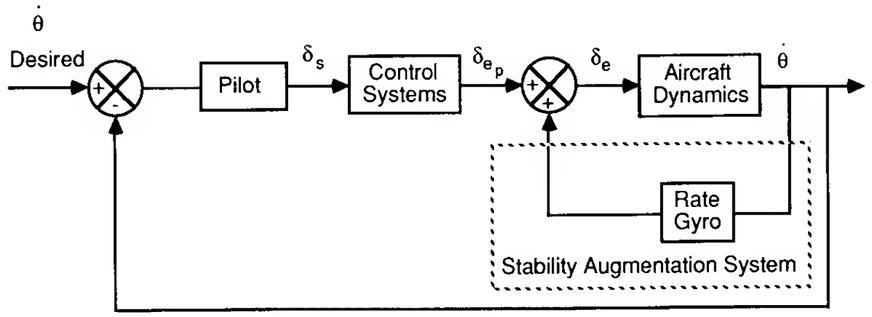

FIGURE 7.16
Stability augmentation system using pitch rate feedback.

The damping ratio and undamped natural frequency are given by

$$\zeta_{sp} = (C_{mq} + C_{m\dot{\alpha}}) \frac{\rho u_0 S c^2}{4 I_y} / (2\omega_{nsp})$$

$$\omega_{nsp}^2 = C_{m\alpha} \frac{\rho u_0^2 S c}{2 I_y}$$

If the aerodynamic and inertial characteristics of a business jet during cruise are such that the above equations have the numerical values

$$\ddot{\theta} + 0.797\dot{\theta} + 3.27\theta = -2.09\delta_e$$

then the damping ratio and frequency are given by

$$\zeta_{sp} = 0.22 \qquad \omega_{nsp} = 1.8 \text{ rad/s}$$

For these short-period characteristics the airplane has level 2 flying qualities. Upon examining the flying quality specification, we see that to provide level 1 flying qualities the short-period damping must be increased so that $\zeta_{sp} > 0.3$.

One means of improving the damping of the system is to provide rate feedback, as illustrated in Fig. 7.16. This type of system is called a pitch rate damper. The stability augmentation system provides artificial damping without interfering with the pilot's control input. This is accomplished by producing an elevator deflection in proportion to the pitch rate and adding it to the pilot's control input:

$$\delta_e = \delta_{ep} + k\dot{\theta}$$

where δ_{ep} is that part of the elevator deflection created by the pilot. A rate gyro is used to measure the pitch rate and creates an electrical signal that is used to provide elevator deflections. If we substitute the expression for the elevator angle back into the equation of motion, we obtain

$$\ddot{\theta} + (0.342 + 2.09k)\dot{\theta} + 2.07\theta = -2.09\delta_{ep}$$

Comparing this equation with the standard form of a second-order system yields

$$2\zeta\omega_n = (0.342 + 2.09k) \qquad \text{and} \qquad \omega_n^2 = 2.07$$

The short-period damping ratio is now a function of the gyro gain k and can be selected so that the damping ratio will provide level 1 handling qualities. For example, if k is chosen to be 0.25, then the damping ratio $\zeta = 0.3$.

7.8 INSTRUMENT LANDING

With the advent of the instrument landing system (ILS), aircraft were able to operate safely in weather conditions under which visibility was restricted. The instrument landing system is composed of both ground-based signal transmitters and onboard receiving equipment. The ground-based equipment includes radio transmitters for the localizer, glide path, and marker beacons. The equipment on the airplane consists of receivers for detecting the signals and indicators to display the information.

The basic function of the ILS is to provide pilots with information that will permit them to guide the airplane down through the clouds to a point where the pilot re-establishes visual sighting of the runway. In a completely automatic landing, the autopilot guides the airplane all the way down to touchdown and roll out.

Before addressing the autoland system, we briefly review the basic ideas behind the ILS equipment. To guide the airplane down toward the runway, the airplane must be guided laterally and vertically. The localizer beam is used to position the aircraft on a trajectory so that the airplane will intercept the centerline of the runway. The transmitter radiates at a frequency in a band of 108–112 MHz. The purpose of this beam is to locate the airplane relative to a centerline of the runway. This is accomplished by creating azimuth guidance signals which are detected by the onboard localizer receiver. The azimuth guidance signal is created by superimposing a 90-Hz signal that is directed towards the left and a 150-Hz signal that is directed to the right on the carrier signal. Figure 7.17 is a sketch of an instrument landing localizer signal. When the aircraft is flying directly along the projected extension of the runway centerline, both superimposed signals are detected with equal strength.

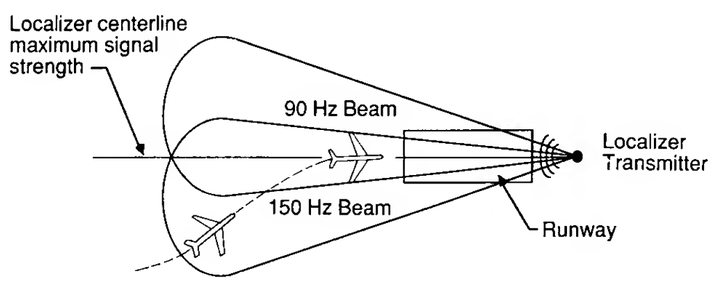

FIGURE 7.17
Sketch of a localizer beam system.

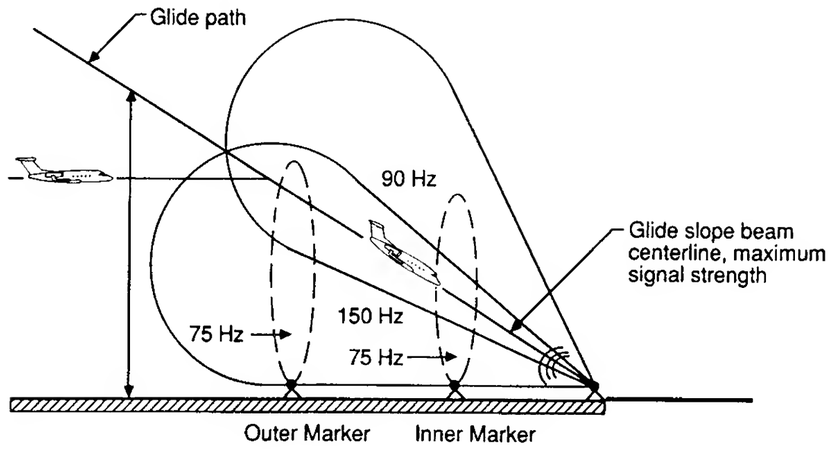

FIGURE 7.18
Sketch of a glide slope beam system.

However, when the aircraft deviates say to the right of centerline, the 150-Hz signal is stronger. The receiver in the cockpit detects the difference and directs the pilot to fly the aircraft to the left by way of a vertical bar on the ILS indicator which shows the airplane to the right of the runway. If the airplane deviates to the left, the indicator will deflect the bar to the left of the runway marker.

The glide path or glide slope beam is located near the runway threshold and radiates at a frequency in the range 329.3–335.0 MHz. Its purpose is to guide the aircraft down a predetermined descent path. The glide slope is typically an angle of 2.5–3° to the horizontal. Figure 7.18 shows a schematic of the glide path beam. As in the case of the localizer, two signals are superimposed on the carrier frequency to create an error signal if the aircraft is either high or low with respect to the glide path. This is usually indicated by a horizontal bar on the ILS indicator that moves up or down with respect to the glide path indicator. The marker beacons are used to locate the aircraft relative to the runway. Two markers are used. One is located four nautical miles from the runway and is called the outer marker. The second, or inner, marker is located 3500 ft from the runway threshold. The beams are directed vertically into the descent path at a frequency of 75 MHz. The signals are coded, and when the airplane flies overhead the signals are detected by an on-board receiver. The pilot is alerted to the passage over a marker beacon by both an audio signal and visual signal. The audio signal is heard over the aircraft's communication system and the visual signal is presented by way of a colored indicator light on the instrument panel.

In flying the airplane in poor visibility, the pilot uses the ILS equipment in the following manner. The pilot descends from cruise altitude under direction of ground control to an altitude of approximately 1200 ft above the ground. The pilot is then vectored so that the aircraft intercepts the localizer at a distance of at least six nautical miles from the runway. The pilot positions the

airplane using the localizer display so that the airplane is on a heading towards the runway centerline. When the aircraft approaches the outer marker, the glide path signal is intercepted. The aircraft is placed in its final approach configuration and the pilot flies down the glide path slope. The pilot follows the beams by maneuvering the airplane so that the vertical and horizontal bars on the ILS indicator show zero deviation from the desired flight path. The ILS system does not guide the aircraft all the way to touchdown. At some point during the approach the pilot must look away from the instruments and outside the window to establish a visual reference for the final portion of the landing. The pilot may take five or six seconds to establish an outside visual reference. Obviously the pilot must do this at sufficient altitude and distance from the runway so that if the runway is not visible the pilot can abort the landing. This gives rise to a "decision height" which is a predetermined height above the runway for which the pilot can not go beyond without visually sighting the runway.

The ILS as outlined in the previous paragraphs is an integral part of a fully automatic landing system. To be able to land an airplane without any visual reference to the runway requires an automatic landing system that can intercept the localizer and glide path signals, then guide the airplane down the glide path to some preselected altitude at which the aircraft's descent rate is reduced and the airplane executes a flare maneuver so that it touches down with an acceptable sink rate. The autoland system comprises a number of automatic control systems which include a localizer and glide path coupler, attitude and airspeed control, and an automatic flare control system.

Figure 7.19 shows an airplane descending towards the runway. The airplane shown is below the intended glide path. The deviation d of the airplane from the glide path is the normal distance of the airplane above or below the desired glide path. The angle Γ is the difference between the actual and desired glide path angle and R is the radial distance of the airplane from the glide slope transmitter. To maintain the airplane along the glide path, one must make Γ equal to zero. Figure 7.20 is a conceptual design of an autopilot

$$\dot{d} = u_o \sin\gamma = u_o \gamma$$

$$\frac{\gamma}{d} = \frac{u_o}{57.3\ s}\left[\frac{\text{degrees}}{\text{ft. or meter}}\right]$$

$$\tan\Gamma = \frac{d}{R}$$

$$\Gamma \simeq \frac{d}{R} \quad \text{or} \quad \frac{\Gamma}{d} = \frac{57.3}{R}\left[\frac{\text{degrees}}{\text{ft. or meter}}\right]$$

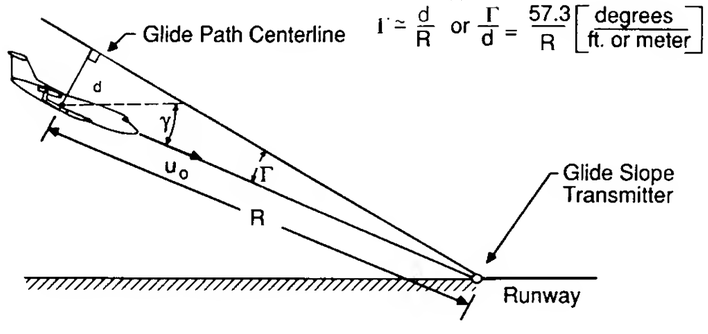

FIGURE 7.19
An airplane displaced from the glide path.

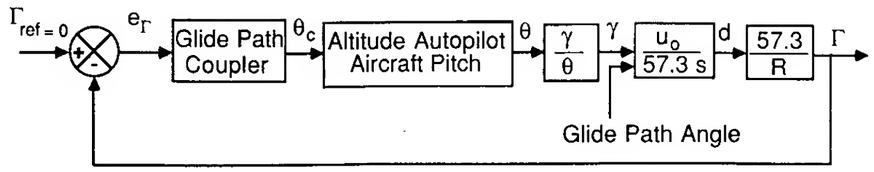

FIGURE 7.20
Conceptual design of an automatic glide path control system.

that will keep the airplane on the glide path. The transfer functions for d and Γ are obtained from the geometry and are noted in Fig. 7.19.

As the airplane descends along the glide path, its pitch attitude, and speed must be controlled. This is again accomplished by means of a pitch displacement and speed control autopilot. The pitch displacement autopilot would be conceptually the same as the one discussed earlier in this chapter. Figure 7.21 is a sketch of an automatic control system that could be used to maintain a constant speed along the flight path. The difference in flight speed is used to produce a proportional displacement of the engine throttle so that the speed difference is reduced. The component of the system labelled compensation is a device that is incorporated into the design so that the closed loop system can meet the desired performance specifications. Finally, as the airplane gets very close to the runway threshold, the glide path control system is disengaged and a flare maneuver is executed. Figure 7.22 illustrates the flare maneuver just prior to touchdown. The flare maneuver is needed to decrease the vertical descent rate to a level consistent with the ability of the landing gear to dissipate the energy of the impact at landing. An automatic flare control system is shown in Figure 7.23. A detailed discussion of the autoland system is provided by Blakelock [7.5].

7.9 SUMMARY

In this chapter we have examined briefly the use of automatic control system that can be used to reduce the pilot's workload, guide the airplane to a safe landing in poor visibility, and provide stability augmentation to improve the flying qualities of airplanes with poor stability characteristics. Additional applications of automatic control technology include load allevation and flutter suppression.

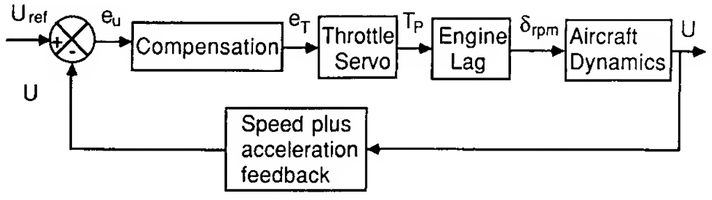

FIGURE 7.21
Conceptual design for an automatic speed control system.

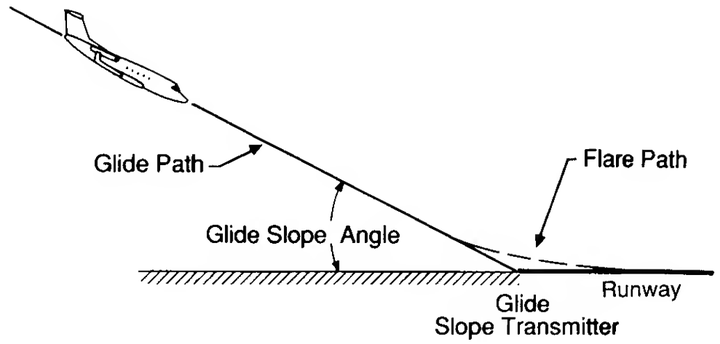

FIGURE 7.22
Sketch of a flare maneuver.

Load alleviation can be achieved by using active wing controls to reduce the wing-bending moments. By reducing the wing design loads through active controls, the designer can increase the wing span or reduce the structural weight of the wing. Increasing the wing span for a given wing area improves the aerodynamic efficiency of the wing, i.e. increases the lift-to-drag ratio. The improvement in aerodynamic efficiency and the potential for lower wing weight result in better cruise fuel efficiency.

Stability augmentation systems can also be used to improve airplane performance without degrading the vehicle's flying qualities. If the horizontal and vertical tail control surfaces are used in an active control system, the tail area can be reduced. Reducing the static stability results in smaller trim drag forces. The combination of smaller tail areas and reduced static stability yields a lower drag contribution from the tail surfaces, which will improve the performance characteristics of the airplane.

Another area in which active control can play an important role is in suppressing flutter. Flutter is an unstable structural motion that can lead to structural failure of any of the major components of an airplane, i.e. wing, tail, fuselage, or control surfaces. Flutter is caused by the interaction between structural vibration and the aerodynamic forces acting on the surface undergoing flutter. During flutter the aerodynamic surface extracts energy from the airstream to feed this undesirable motion. An automatic control system incorporating active controls can be designed to prevent flutter from occurring by controlling the structural vibration.

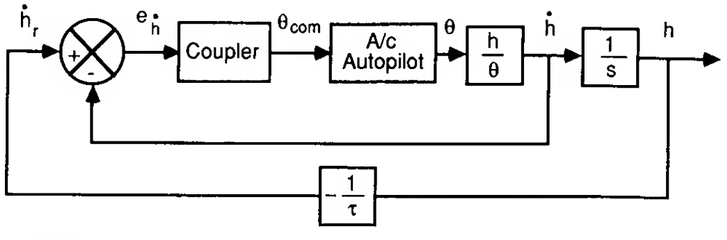

FIGURE 7.23
Conceptual design of an automatic flare control system.

7.10 PROBLEMS

7.1. Given the characteristic equation

$$\lambda^3 + 3\lambda^2 + 3\lambda + 1 + k = 0$$

find the range of values of k for which the system is stable.

7.2. Given the fourth-order characteristic equation

$$\lambda^4 + 6\lambda^3 + 11\lambda^2 + 6\lambda + k = 0$$

for what values of k will the system be stable?

7.3 The single degree of freedom pitching motion of an airplane was shown to be represented by a second order differential equation. If the equation is given as

$$\ddot{\theta} + 0.5\dot{\theta} + 2\theta = \delta_e$$

where the θ and δ_e are in radians. Estimate the rise time, peak overshoot and settling time for step input of the elevator angle of 0.10 radians.

7.4 Determine the frequency domain characteristic for problem 7.3. In particular estimate the resonance peak, M_r, resonant frequency, ω_r, bandwidth, ω_B, and the phase margin.

7.5. A simple roll control system is shown in Fig. P7.5. Sketch the root locus diagram for this system. Determine the value of the gain k when the system is neutrally stable. Assume that the aircraft characteristics are the same as example problem 7.2, except that the aileron servo gain is unity.

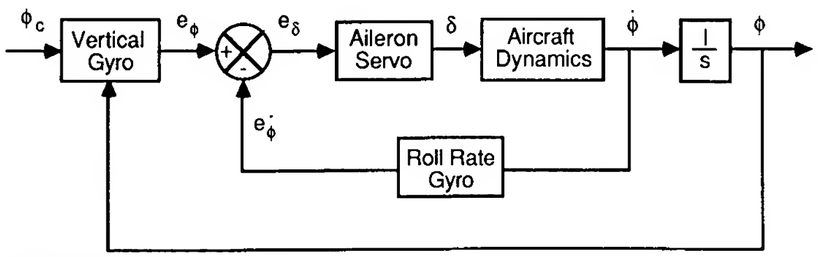

FIGURE P7.5

7.6. For the pitch rate feedback control system shown in Fig. P7.6, determine the gain necessary to improve the system characteristics so that the control system has the following performance: $\zeta = 0.3$, $\omega_n = 2.0$ rad/s. Assume that the aircraft characteristics are the same as those described earlier in Figure 7.9.

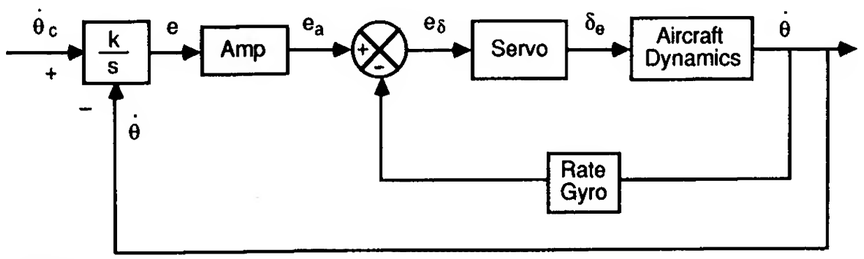

FIGURE P7.6

7.7 The Wright "Flyer" was statically and dynamically unstable. However, because the Wright brothers incorporated sufficient control authority into their design they were able to fly their airplane successfully. Although the airplane was difficult to fly the combination of the pilot and airplane could be made to be a stable system. In reference 7.7 the closed loop pilot is represented as a pure gain, k_p, and the pitch attitude to canard deflection is given as follows.

$$\frac{\theta}{\delta_c} = \frac{11.0(s + 0.5)(s + 3.0)}{(s^2 + 0.72s + 1.44)(s^2 + 5.9s - 11.9)}$$

Determine the root locus plot of the closed loop system. For what range of pilot gain is the system stable.

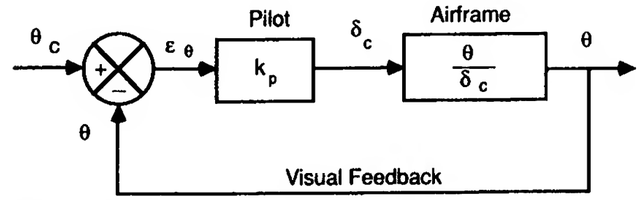

FIGURE P7.7

REFERENCES

7.1. Bollay, W.: "Aerodynamic Stability and Automatic Control," *Journal of the Aeronautical Sciences*, vol. 18, No. 9, pp. 569–617, 1951.

7.2. Raven, F. H.: *Automatic Control Engineering*, McGraw-Hill, New York, 1978.

7.3. Kuo, B. C.: *Automatic Control Systems*, Prentice Hall, Englewood Cliffs, NJ, 1975.

7.4. Shinners, S. M.: *Modern Control System Theory and Application*, Addison Wesley, Reading, MA, 1978.

7.5. Blakelock, J. H.: *Automatic Control of Aircraft and Missiles*, Wiley, New York, 1965.

7.6. Pallett, E. H. J.: *Automatic Flight Control*, Granada Publishing, London, England, 1979.

7.7. Culick, F. E. C.: "Building a 1903 Wright 'Flyer'—by Committee," *AIAA Paper* 88-0094, 1988.

CHAPTER 8

AUTOMATIC CONTROL: APPLICATION OF MODERN CONTROL THEORY

8.1 INTRODUCTION

In Chapter 7, the design of feedback control systems was accomplished using the root locus technique and Bode methods developed by Evans and Bode, respectively. These techniques are very useful in designing many practical control systems. However, the design of a control system using either the root locus or Bode techniques is essentially a trial-and-error procedure. The major advantage of these design procedures is their simplicity and ease of use. This advantage disappears quickly as the complexity of the system increases.

With the rapid development of high-speed computers during the recent decades, a new approach to control system design has evolved. This new approach is commonly called modern control theory. This theory permits a more systematic approach to control system design. In modern control theory, the control system is specified as a system of first-order differential equations. By formulating the problem in this manner, the control system designer can fully exploit the digital computer for solving complex control problems. Another advantage of modern control theory is that optimization techniques can be applied to design optimal control systems. To comprehend this theory fully one needs to have a good understanding of matrix algebra; a brief discussion of matrix algebra is included in the appendices.

It is not possible in a single chapter to present a thorough discussion of modern control theory. Our purpose is to expose the reader to some of the concepts of modern control theory and then apply the procedures to the design of aircraft autopilots. It is hoped that this brief discussion will provide the reader with an appreciation of modern control theory and its application to the design of aircraft flight control systems.

8.2 STATE-SPACE MODELING

The state-space approach to control system analysis and design is a time-domain method. As was shown in Chapters 4 and 5, the equations of motion can easily be written in the state-space form. The application of state variable techniques to control problems is called modern control theory. The state equations are simply first-order differential equations that govern the dynamics of the system being analyzed. It should be noted that any higher-order differential equation can be decomposed into a set of first-order differential equations. This will be shown later by means of an illustration.

In the mathematical sense, the state variables and state equation completely describe the system. The definition of state variables is as follows. The state variables of a system are a minimum set of variables $x_1(t) \cdots x_n(t)$ which, when known at time t_0, and along with the input, are sufficient to determine the state of the system at any other time $t > t_0$. State variables should not be confused with the output of the system. An output variable is one that can be measured, but state variables do not always satisfy this condition. The output, as we will see shortly, is defined as a function of the state variables.

Once a physical system has been reduced to a set of differential equations, the equation can be rewritten in a convenient matrix form:

$$\dot{\mathbf{x}} = \mathbf{A}\mathbf{x} + \mathbf{B}\eta \tag{8.1}$$

The output of the system is expressed in terms of the state and control inputs as follows:

$$\mathbf{y} = \mathbf{C}\mathbf{x} + \mathbf{D}\eta \tag{8.2}$$

The state, control, and output vectors are defined as follows:

$$\mathbf{x} = \begin{bmatrix} x_1(t) \\ x_1(t) \\ \vdots \\ x_n(t) \end{bmatrix} \quad \text{State vector } (n \times 1) \tag{8.3}$$

$$\eta = \begin{bmatrix} \delta_1(t) \\ \delta_2(t) \\ \vdots \\ \delta_p(t) \end{bmatrix} \quad \text{Control or input vector } (p \times 1) \tag{8.4}$$

$$\mathbf{y} = \begin{bmatrix} y_1(t) \\ y_2(t) \\ \vdots \\ y_q(t) \end{bmatrix} \quad \text{Output vector } (q \times 1) \tag{8.5}$$

The matrices **A**, **B**, **C** and **D** are defined in the following manner:

$$\mathbf{A} = \begin{bmatrix} a_{11} & a_{12} & \cdots & a_{1n} \\ a_{21} & & & \vdots \\ \vdots & & & \\ a_{n1} & a_{n2} & \cdots & a_{nn} \end{bmatrix} \quad \text{Plant matrix } (n \times n) \tag{8.6}$$

$$\mathbf{B} = \begin{bmatrix} b_{11} & b_{12} & \cdots & b_{1p} \\ b_{21} & & & \vdots \\ \vdots & & & \\ b_{n1} & b_{n2} & \cdots & b_{np} \end{bmatrix} \quad \text{Control or input matrix } (n \times p) \tag{8.7}$$

$$\mathbf{C} = \begin{bmatrix} c_{11} & c_{12} & \cdots & c_{1n} \\ c_{21} & & & \vdots \\ \vdots & & & \\ c_{q1} & & & c_{qn} \end{bmatrix} (q \times n) \tag{8.8}$$

$$\mathbf{D} = \begin{bmatrix} d_{11} & d_{12} & \cdots & d_{1p} \\ d_{21} & & & \vdots \\ \vdots & & & \\ d_{q1} & & & a_{qp} \end{bmatrix} (q \times p) \tag{8.9}$$

Figure 8.1 is a sketch of the block diagram representation of the state equation given by Eqs (8.1) and (8.2).

The state equations are a set of first-order differential equations. The matrices **A** and **B** may be either constant or functions of time. For the application we are considering, namely aircraft equations of motion, the matrices are composed of an array of constants. The constants making up either the **A** or **B** matrices are the stability and control derivatives of the airplane. It should be noted that, if the governing differential equations are of

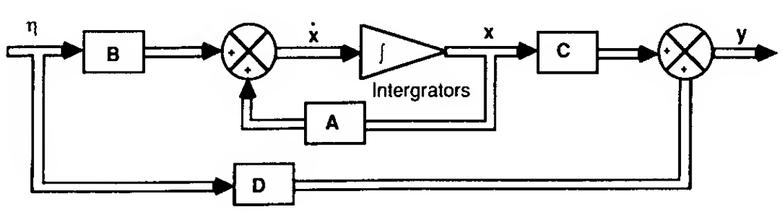

FIGURE 8.1
Block diagram of the linear state equations.

higher order, they can be reduced to a system of first-order differential equations.

For example, suppose that the physical system being modeled can be described by an nth-order differential equation:

$$\frac{d^n c(t)}{dt^n} + a_1 \frac{d^{n-1} c(t)}{dt^{n-1}} + a_2 \frac{d^{n-2} c(t)}{dt^{n-2}} + \cdots + a_{n-1} \frac{dc(t)}{dt} + a_n c(t) = r(t) \tag{8.10}$$

The variables $c(t)$ and $r(t)$ are the output and input variables, respectively. The above differential equation can be reduced to a set of first-order differential equations by defining the state variables as follows:

$$\begin{aligned} x_1(t) &= c(t) \\ x_2(t) &= \frac{dc(t)}{dt} \\ &\vdots \\ x_n(t) &= \frac{d^{n-1} c(t)}{dt^{n-1}} \end{aligned} \tag{8.11}$$

The state equations can now be written as

$$\begin{aligned} \dot{x}_1(t) &= x_2(t) \\ \dot{x}_2(t) &= x_3(t) \end{aligned} \tag{8.12}$$

$$\dot{x}_n(t) = -a_n x_1(t) - a_{n-1} x_2(t) - \cdots - a_1 x_n(t) + r(t)$$

The last equation is obtained by solving for the highest-order derivative in the original differential equation. Rewriting the equation in the state vector form yields

$$\dot{\mathbf{x}} = \mathbf{A}\mathbf{x} + \mathbf{B}\eta \tag{8.13}$$

where

$$\mathbf{A} = \begin{bmatrix} 0 & 1 & 0 & 0 & 0 & \cdot & 0 \\ 0 & 0 & 1 & 0 & 0 & \cdot & 0 \\ 0 & 0 & 0 & 1 & 0 & \cdot & 0 \\ \cdot & \cdot & \cdot & \cdot & \cdot & \cdot & \cdot \\ \cdot & \cdot & \cdot & \cdot & \cdot & \cdot & \cdot \\ 0 & 0 & 0 & 0 & 0 & \cdot & 1 \\ -a_n & -a_{n-1} & -a_{n-2} & -a_{n-3} & -a_{n-4} & \cdot & -a_1 \end{bmatrix} \tag{8.14}$$

$$\mathbf{B} = \begin{bmatrix} 0 \\ 0 \\ 0 \\ 0 \\ \cdot \\ \cdot \\ \cdot \\ 1 \end{bmatrix} \tag{8.15}$$

and the output equation is

$$y = \mathbf{C}\mathbf{x} \tag{8.16}$$

where

$$\mathbf{C} = [1\ 0\ 0\ \cdots\ 0] \tag{8.17}$$

STATE TRANSITION MATRIX. The state transition matrix is defined as a matrix that satisfies the linear homogeneous state equation, i.e.

$$\dot{\mathbf{x}} = \mathbf{A}\mathbf{x} \qquad \text{Homogeneous state equation} \tag{8.18}$$

$$\mathbf{x}(0) = \begin{bmatrix} x_1(0) \\ \vdots \\ x_n(0) \end{bmatrix} \qquad \text{Initial state at time } t = 0 \tag{8.19}$$

$$\mathbf{x}(t) = \Phi(\mathbf{t})\,\mathbf{x}(0) \tag{8.20}$$

where $\Phi(t)$ is the state transition matrix.

State transition matrix by Laplace transformation technique

$$\dot{\mathbf{x}} = \mathbf{A}\mathbf{x} \qquad \text{and} \qquad \mathbf{x}(0) = \begin{bmatrix} x_1(0) \\ \vdots \\ x_n(0) \end{bmatrix} \tag{8.21}$$

Taking the Laplace transformation of the above equation yields

$$s\mathbf{x}(s) - \mathbf{x}(0) = \mathbf{A}\mathbf{x}(s) \tag{8.22}$$

or

$$\mathbf{x}(s) = [\mathbf{sI} - \mathbf{A}]^{-1}\mathbf{x}(0) \tag{8.23}$$

The state transition matrix is obtained by taking the inverse Laplace transform of equation 8.23

$$\Phi(t) = \mathscr{L}^{-1}[(\mathbf{sI} - \mathbf{A})^{-1}] \tag{8.24}$$

State transition matrix by classical technique

The state transition matrix can also be found in the following manner

$$\mathbf{x}(t) = e^{\mathbf{A}t}\,\mathbf{x}(0) \tag{8.25}$$

where $e^{\mathbf{A}t}$ is a matrix exponential and $de^{\mathbf{A}t}/dt = \mathbf{A}e^{\mathbf{A}t}$. Substituting the above equation into the homogeneous state equation shows that it is a solution:

$$\mathbf{A}e^{\mathbf{A}t}\,\mathbf{x}(0) = \mathbf{A}e^{\mathbf{A}t}\,\mathbf{x}(0) \tag{8.26}$$

$e^{\mathbf{A}t}$ can be represented by a power series as follows:

$$e^{\mathbf{A}t} = \mathbf{I} + \mathbf{A}t + \tfrac{1}{2}\mathbf{A}^2t^2 + \tfrac{1}{3}\mathbf{A}^3t^3 + \cdots \tag{8.27}$$

The state transition matrix is

$$\Phi(t) = \mathbf{I} + \mathbf{A}t + \tfrac{1}{2}\mathbf{A}^2t^2 + \tfrac{1}{3}\mathbf{A}^3t^3 + \cdots \tag{8.28}$$

Since the state transition matrix satisfies the homogeneous state equation, it represents the free response of the system.

Properties of the state transition matrix

Some of the properties of the state transition matrix are presented below.

1. $\Phi(0) = e^{\mathbf{A}0} = \mathbf{I}$. (8.29)

2. $[\Phi(t)]^{-1} = [\Phi(-t)]$. (8.30)

3. $\Phi(t_1 + t_2) = e^{\mathbf{A}(t_1+t_2)} = e^{\mathbf{A}t_1}e^{\mathbf{A}t_2} = \Phi(t_1)\Phi(t_2) = \Phi(t_2)\Phi(t_1)$. (8.31)

4. $[\Phi(t)]^k = \Phi(kt)$, where k is an integer. (8.32)

Once the state transition matrix has been found, the solution to the nonhomogeneous equation can be determined as follows:

$$\dot{\mathbf{x}} = \mathbf{A}\mathbf{x} + \mathbf{B}\eta \tag{8.33}$$

Taking the Laplace transform of the above equation yields

$$s\mathbf{x}(s) - \mathbf{x}(0) = \mathbf{A}\mathbf{x}(s) + \mathbf{B}\eta(s) \tag{8.34}$$

solving for $\mathbf{x}(s)$

$$\mathbf{x}(s) = [\mathbf{sI} - \mathbf{A}]^{-1}\mathbf{x}(0) + [s\mathbf{I} - \mathbf{A}]^{-1}\mathbf{B}\eta(s) \tag{8.35}$$

$$\mathbf{x}(t) = \mathscr{L}^{-1}[s\mathbf{I} - \mathbf{A}]^{-1}\mathbf{x}(0) + \mathscr{L}^{-1}[[s\mathbf{I} - \mathbf{A}]^{-1}\mathbf{B}\eta(s)] \tag{8.36}$$

or

$$\mathbf{x}(t) = \Phi(t)\mathbf{x}(0) + \int_0^t \Phi(t-\tau)\mathbf{B}\eta(\tau)\,d\tau \tag{8.37}$$

Example Problem 8.1. Given a system that is described by the following equations,

$$\begin{bmatrix} \dot{x}_1 \\ \dot{x}_2 \end{bmatrix} = \begin{bmatrix} 0 & 1 \\ -3 & -4 \end{bmatrix}\begin{bmatrix} x_1 \\ x_2 \end{bmatrix} + \begin{bmatrix} 0 \\ 1 \end{bmatrix}u$$

where

$$\begin{bmatrix} x_1(0) \\ x_2(0) \end{bmatrix} = \begin{bmatrix} 0 \\ 1 \end{bmatrix}$$

and the input function u is a unit step function, determine the response of the system using the state transition matrix, which can be found as follows:

$$\Phi(s) = [s\mathbf{I} - \mathbf{A}]^{-1} = \begin{bmatrix} s & -1 \\ 3 & s+4 \end{bmatrix}^{-1}$$

$$\Phi(s) = \begin{bmatrix} \dfrac{s+4}{s^2+4s+3} & \dfrac{1}{s^2+4s+3} \\ \dfrac{-3}{s^2+4s+3} & \dfrac{s}{s^2+4s+3} \end{bmatrix}$$

Using the partial fraction expansion, the elements of the transition matrix can be written as

$$\Phi(s) = \begin{bmatrix} \frac{3}{2}\dfrac{1}{s+1} - \frac{1}{2}\dfrac{1}{s+3} & \frac{1}{2}\dfrac{1}{s+1} - \frac{1}{2}\dfrac{1}{s+3} \\ \frac{-3}{2}\dfrac{1}{s+1} + \frac{3}{2}\dfrac{1}{s+3} & \frac{-1}{2}\dfrac{1}{s+1} + \frac{3}{2}\dfrac{1}{s+3} \end{bmatrix}$$

The state transition matrix $\Phi(t)$ is determined by taking the inverse Laplace transform of $\Phi(s)$:

$$\Phi(t) = \mathscr{L}^{-1}(\Phi(s))$$

$$\Phi(t) = \begin{bmatrix} \frac{3}{2}e^{-t} - \frac{1}{2}e^{-3t} & \frac{1}{2}e^{-t} + \frac{1}{2}e^{-3t} \\ -\frac{3}{2}e^{-t} + \frac{3}{2}e^{-3t} & -\frac{1}{2}e^{-t} + \frac{3}{2}e^{-3t} \end{bmatrix}$$

The state transition matrix can also be obtained by the matrix exponential definition:

$$e^{\mathbf{A}t} = \mathbf{I} + \mathbf{A}t + \frac{1}{2!}\mathbf{A}^2t^2 + \frac{1}{3!}\mathbf{A}^3t^3 + \cdots$$

$$A^2 = \begin{bmatrix} 0 & 1 \\ -3 & -4 \end{bmatrix}\begin{bmatrix} 0 & 1 \\ -3 & -4 \end{bmatrix} = \begin{bmatrix} -3 & -4 \\ 12 & 13 \end{bmatrix}$$

etc. Then

$$e^{\mathbf{A}t} = \begin{bmatrix} 1 + 0t - \frac{3}{2}t^2 \cdots & 0 + t - 2t^2 \cdots \\ 0 - 3t + 6t^2 \cdots & 1 - 4t + \frac{13}{2}t^2 \cdots \end{bmatrix}$$

which can be shown to be identical to the equations obtained from the Laplace

transform approach. The solution of the state equation is found by

$$\mathbf{x}(t) = \Phi(t)\mathbf{x}(0) + \int_0^t \Phi(t-\tau)\mathbf{B}\eta(\tau)\,d\tau$$

$$\boldsymbol{x}(t) = \begin{bmatrix} \frac{3}{2}e^{-t} - \frac{1}{2}e^{-3t} & \frac{1}{2}e^{-t} - \frac{1}{2}e^{-3t} \\ \frac{3}{2}e^{-t} + \frac{3}{2}e^{-3t} & -\frac{1}{2}e^{-t} + \frac{3}{2}e^{-3t} \end{bmatrix}\begin{bmatrix} 0 \\ 1 \end{bmatrix}$$

$$+ \int_0^t \begin{bmatrix} \frac{3}{2}e^{-(t-\tau)} - \frac{1}{2}e^{-3(t-\tau)} & \frac{1}{2}e^{-(t-\tau)} - \frac{1}{2}e^{-3(t-\tau)} \\ -\frac{3}{2}e^{-(t-\tau)} + \frac{3}{2}e^{-3(t-\tau)} & -\frac{1}{2}e^{-(t-\tau)} + \frac{3}{2}e^{-3(t-\tau)} \end{bmatrix}\begin{bmatrix} 0 \\ 1 \end{bmatrix} d\tau$$

CONTROLLABILITY AND OBSERVABILITY. In the following sections we shall examine the application of state feedback design and optimal control theory to aircraft control problems. Two concepts that play an important role in modern control theory are the concepts of controllability and observability. Controllability is concerned with whether the states of the dynamic system are affected by the control input. A system is said to be completely controllable if there exists a control that transfers any initial state $\mathbf{x}_i(t)$ to any final state $\mathbf{x}_f(t)$ in some finite time. If one or more of the states are unaffected by the control, the system is not completely controllable.

A mathematical definition of controllability for a linear dynamical system can be expressed as follows. If the dynamic system can be described by the state equation

$$\dot{\mathbf{x}} = \mathbf{A}\mathbf{x} + \mathbf{B}\eta \tag{8.38}$$

where $\mathbf{x}$ and η are the state and control vectors of order n and m, respectively, then the necessary and sufficient condition for the system to be completely controllable is that the rank of the matrix $\mathbf{P}$ is equal to the number of states. The matrix $\mathbf{P}$ is constructed from the $\mathbf{A}$ and $\mathbf{B}$ matrices in the following way:

$$\mathbf{P} = [\mathbf{B}, \mathbf{AB}, \mathbf{A}^2\mathbf{B}, \ldots \mathbf{A}^{n-1}\mathbf{B}] \tag{8.39}$$

The rank of a matrix is defined as the largest non-zero determinant. Although this definition is abstract, the test for controllability can be easily applied.

Observability deals with whether the states of the system can be identified from the output of the system. A system is said to be completely observable if every state $\mathbf{x}$ can be determined by the measurement of the output $\mathbf{y}(t)$ over a finite time interval. If one or more states cannot be identified from the output of the system, the system is not observable. A mathematical test for observability of an nth-order dynamic system governed by the equations

$$\dot{\mathbf{x}} = \mathbf{A}\mathbf{x} + \mathbf{B}\eta \tag{8.40}$$

$$\mathbf{y} = \mathbf{C}\mathbf{x} + \mathbf{D}\eta \tag{8.41}$$

is given as follows. The necessary and sufficient condition for a system to be

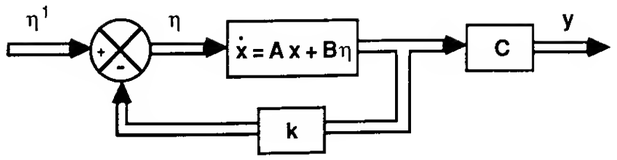

FIGURE 8.2
Block diagram of a linear system with state feedback.

completely observable is that the matrix **U**, defined as

$$\mathbf{U} = [\mathbf{C}^T, \mathbf{A}^T\mathbf{C}^T, \ldots (\mathbf{A}^T)^{n-1}\mathbf{C}^T] \tag{8.42}$$

is of the rank n.

8.3 STATE FEEDBACK DESIGN

State feedback can be used to design a control system with a specific eigenvalue structure. Consider the system represented by the state equations

$$\dot{\mathbf{x}} = \mathbf{A}\mathbf{x} + \mathbf{B}\eta \tag{8.43}$$

$$\mathbf{y} = \mathbf{C}\mathbf{x} \tag{8.44}$$

It can be shown from optimal control theory that if the system is state-controllable, then it is possible to use a linear feedback control law given by

$$\eta = -\mathbf{k}^T\mathbf{x} + \eta' \tag{8.45}$$

to achieve a specific eigenvalue structure. The matrix **k** is called the feedback gain matrix and η' is the original control system input. Figure 8.2 shows the block diagram representation of the system. If we combine Eqs (8.43) and (8.45), the closed loop system is given by

$$\dot{\mathbf{x}} = (\mathbf{A} - \mathbf{B}\mathbf{k}^T)\mathbf{x} + \mathbf{B}\eta' \tag{8.46}$$

or

$$\dot{\mathbf{x}} = \mathbf{A}^*\mathbf{x} + \mathbf{B}\eta' \tag{8.47}$$

where $\mathbf{A}^*$ is the augmented matrix. For the case in which the **A** matrix may have had undesirable eigenvalues, the augmented matrix $\mathbf{A}^*$ can be made to have specific eigenvalues by properly selecting the feedback gains.

The application of state feedback as presented here requires the states be state-controllable. As stated earlier, a system is said to be completely controllable if the control can be used to move the system from its initial state at $t = t_0$ to the desired state at $t = t_1$. Another way of stating this concept is to say that every state is affected by the control input signal.

LONGITUDINAL STABILITY AUGMENTATION. State feedback control can be used to improve the stability characteristics of airplanes that lack good flying qualities. As shown in the previous section, the problem is one of determining the feedback gains that will produce the desired flying characteristics.

Starting with the longitudinal state equations given in Chapter 4, we develop a set of linear algebraic equations in terms of the unknown feedback gains. The state equations for the longitudinal motion have been simplified by neglecting the affect of the control on the X-force equation and the stability derivative $M_{\dot{w}}$. The state equations are given below:

$$\begin{bmatrix} \Delta\dot{u} \\ \Delta\dot{w} \\ \Delta\dot{q} \\ \Delta\dot{\theta} \end{bmatrix} = \begin{bmatrix} X_u & X_w & 0 & -g \\ Z_u & Z_w & u_0 & 0 \\ M_u & M_w & M_q & 0 \\ 0 & 0 & 1 & 0 \end{bmatrix} \begin{bmatrix} \Delta u \\ \Delta w \\ \Delta q \\ \Delta\theta \end{bmatrix} + \begin{bmatrix} 0 \\ Z_\delta \\ M_\delta \\ 0 \end{bmatrix} [\Delta\delta_e] \tag{8.48}$$

or

$$\dot{\mathbf{x}} = \mathbf{A}\mathbf{x} + \mathbf{B}\eta \tag{8.49}$$

where **A** and **B** are the stability and control matrices shown above and **x** and η are the state and control vectors.

The eigenvalues of the **A** matrix are the short- and long-period roots. If these roots are unacceptable to the pilot, a stability augmentation system will be required. State feedback design can be used to provide the stability augmentation system. In state feedback design we assume a linear control law that is proportional to the states, i.e.

$$\eta = -\mathbf{k}^T\mathbf{x} + \eta_p \tag{8.50}$$

where $\mathbf{k}^T$ is the transpose of the feedback gain vector and η_p is the pilot input. Substituting the control law into the state equation yields

$$\dot{\mathbf{x}} = (\mathbf{A} - \mathbf{B}\mathbf{k}^T)\mathbf{x} + \mathbf{B}\eta_p \tag{8.51}$$

or

$$\dot{\mathbf{x}} = \mathbf{A}^*\mathbf{x} + \mathbf{B}\eta_p \tag{8.52}$$

where $\mathbf{A}^*$ is the augmented matrix and is expressed as

$$\mathbf{A}^* = \mathbf{A} - \mathbf{B}\mathbf{k}^T \tag{8.53}$$

The augmented matrix for the longitudinal system of equations is

$$\mathbf{A}^* = \begin{bmatrix} X_u & X_w & 0 & -g \\ Z_u - Z_\delta k_1 & Z_w - Z_\delta k_2 & u_0 - Z_\delta k_3 & -Z_\delta k_4 \\ M_u - M_\delta k_1 & M_w - M_\delta k_2 & M_q - M_\delta k_3 & -M_\delta k_4 \\ 0 & 0 & 1 & 0 \end{bmatrix} \tag{8.54}$$

The characteristic equation for the augmented matrix is obtained by solving the equation

$$|\lambda\mathbf{I} - \mathbf{A}^*| = 0 \tag{8.55}$$

which yields a quartic characteristic equation.

$$A\lambda^4 + B\lambda^3 + C\lambda^2 + D\lambda + E = 0 \tag{8.56}$$

where the coefficients are defined below.

$$
\begin{aligned}
A &= 1.0 \\
B &= Z_\delta k_2 + M_\delta k_3 - (X_u + Z_w + M_q) \\
C &= Z_\delta X_w k_1 + (u_0 M_\delta - X_u Z_\delta - Z_\delta M_q) k_2 \\
&\quad + (Z_\delta M_w - X_u M_\delta - Z_w M_\delta) k_3 + M_\delta k_4 \\
&\quad + X_u M_q + X_u Z_w + Z_w M_q - u_0 M_w - X_w Z_w \\
D &= (u_0 X_w M_\delta - g M_\delta - X_w Z_\delta M_q) k_1 \\
&\quad + (X_u Z_\delta M_q - u_0 X_u M_\delta) k_2 \\
&\quad + (X_u Z_w M_\delta - X_u Z_\delta M_w - X_w Z_u M_\delta + X_w Z_\delta M_u) k_3 \\
&\quad + (Z_\delta M_w - X_u M_\delta - Z_w M_\delta) k_4 \\
&\quad + g M_u - X_u Z_w M_q + u_0 X_u M_w + X_w Z_u M_q - u_0 X_w M_u \\
E &= (g Z_w M_\delta - g Z_\delta M_w) k_1 + (g Z_\delta M_u - g Z_u M_\delta) k_2 \\
&\quad + (X_u Z_w M_\delta - X_u Z_\delta M_w - X_w Z_u M_\delta + X_w Z_\delta M_u) k_4 \\
&\quad + g Z_u M_w - g Z_w M_u
\end{aligned}
\qquad (8.57)
$$

The characteristic equation of the augmented system is a function of the known stability derivatives and the unknown feedback gains. The feedback gains can be determined once the desired longitudinal characteristics are specified. For example, if the desired characteristic roots are

$$\lambda_{1,2} = -\zeta_{sp}\omega_{nsp} \pm i\omega_{nsp}\sqrt{1-\zeta_{sp}^2} \qquad (8.58)$$

and

$$\lambda_{3,4} = -\zeta_{p}\omega_{np} \pm i\omega_{np}\sqrt{1-\zeta_{p}^2} \qquad (8.59)$$

then the desired characteristic equation is

$$
\begin{aligned}
\lambda^4 - [(\lambda_1 + \lambda_2 + \lambda_3 + \lambda_4)]\lambda^3 + [\lambda_1\lambda_2\lambda_3\lambda_4 + (\lambda_1 + \lambda_2)]\lambda^2 \\
- [\lambda_1\lambda_2(\lambda_3 + \lambda_4) + \lambda_3\lambda_4(\lambda_1 + \lambda_2)]\lambda + \lambda_1\lambda_2\lambda_3\lambda_4 = 0
\end{aligned}
\qquad (8.60)
$$

By equating the coefficients of like powers of λ for the augmented and desired characteristic equations, one obtains a set of four linear algebraic equations in terms of the unknown gains. These equations can be solved for the feedback gains.

Example Problem 8.2. An airplane is found to have poor short-period flying qualities in a particular flight regime. To improve the flying qualities, a stability augmentation system using state feedback is to be employed. Determine the feedback gains so that the airplane's short-period characteristics are $\lambda_{sp} = -2.1 \pm 2.14i$. Assume that the original short-period dynamics are given by

$$\begin{bmatrix} \Delta\dot{\alpha} \\ \Delta\dot{q} \end{bmatrix} = \begin{bmatrix} -0.334 & 1.0 \\ -2.52 & -0.387 \end{bmatrix} \begin{bmatrix} \Delta\alpha \\ \Delta q \end{bmatrix} + \begin{bmatrix} -0.027 \\ -2.6 \end{bmatrix} [\Delta\delta_e]$$

The augmented matrix $\mathbf{A}^*$ can be obtained from Eq. (8.53):

$$\mathbf{A}^* = \mathbf{A} - \mathbf{B}\mathbf{k}^T$$

$$\mathbf{A}^* = \begin{bmatrix} -0.334 + 0.027k_1 & 1.0 + 0.027k_2 \\ -2.52 + 2.6k_1 & -0.387 + 2.6k_2 \end{bmatrix}$$

The eigenvalues of the augmented matrix $\mathbf{A}^*$ are determined from the characteristic equation, which is obtained from

$$|\lambda\mathbf{I} - \mathbf{A}^*| = 0$$

or

$$\begin{vmatrix} \lambda + 0.334 - 0.027k_1 & -1.0 - 0.027k_2 \\ 2.52 - 2.6k_1 & \lambda + 0.387 - 2.6k_2 \end{vmatrix} = 0$$

Expanding the determinant yields the characteristic equation of the augmented system in terms of the unknown feedback gains k_1 and k_2.

$$\lambda^2 + (0.721 - 0.027k_1 - 2.6k_2)\lambda + 2.65 - 2.61k_1 - 0.8k_2 = 0$$

The desired characteristic equation is given as

$$\lambda^2 + 4.2\lambda + 9 = 0$$

Comparing like powers of λ we obtain a set of algebraic equations for the unknown feedback gains:

$$0.721 - 0.027k_1 - 2.6k_2 = 4.2 \qquad 2.65 - 2.61k_1 - 0.8k_2 = 9$$

Solving for the gains yields

$$k_1 = -1.970 \qquad k_2 = -1.318$$

and the state feedback control is given as

$$\Delta\delta_e = 1.970\,\Delta\alpha + 1.318\,\Delta q$$

Figure 8.3 shows the response of the airplane with and without the stability augmentation system. An initial angle of attack disturbance of 5° is used to excite the airplane. Without the stability augmentation, the airplane responds in its natural short period motion. However, when the state feedback stability augmentation system is active the disturbance is quickly damped out.

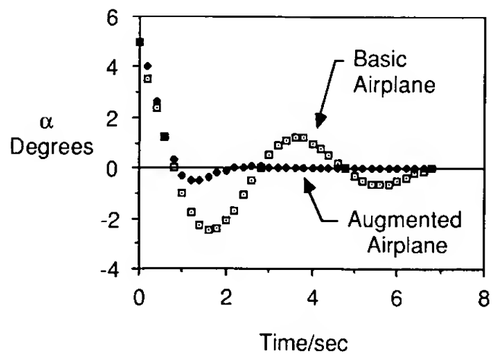

FIGURE 8.3
Longitudinal response of an airplane with and without state feedback.

LATERAL STABILITY AUGMENTATION. The lateral eigenvalues of an airplane can also be modified using state feedback. The lateral state equations were shown to be

$$\begin{bmatrix} \Delta\dot{v} \\ \Delta\dot{p} \\ \Delta\dot{r} \\ \Delta\dot{\phi} \end{bmatrix} = \begin{bmatrix} Y_v & 0 & -u_0 & g \\ L_v & L_p & L_r & 0 \\ N_v & N_p & N_r & 0 \\ 0 & 1 & 0 & 0 \end{bmatrix} \begin{bmatrix} \Delta v \\ \Delta p \\ \Delta r \\ \Delta\phi \end{bmatrix} + \begin{bmatrix} Y_{\delta,a} & Y_{\delta,r} \\ L_{\delta,a} & L_{\delta,r} \\ N_{\delta,a} & N_{\delta,r} \\ 0 & 0 \end{bmatrix} \begin{bmatrix} \Delta\delta_a \\ \Delta\delta_r \end{bmatrix} \tag{8.61}$$

which is of the form

$$\dot{\mathbf{x}} = \mathbf{A}\mathbf{x} + \mathbf{B}\eta \tag{8.62}$$

The state feedback control law can be expressed as

$$\eta = -\mathbf{c}\mathbf{k}^{\mathrm{T}}\mathbf{x} + \eta_p \tag{8.63}$$

which will locate the lateral eigenvalues of the airplane at any desired values. The procedure is identical to that for the longitudinal equations. The constant vector **c** establishes the relationship between the aileron and rudder for augmentation. Either c_1 or c_2 is equal to 1, and the ratio $c_1/c_2 = \Delta\delta a/\Delta\delta r$ is specified by control deflection limits.

Substituting the control vector into the state equation yields

$$\dot{\mathbf{x}} = (\mathbf{A} - \mathbf{B}\mathbf{c}\mathbf{k}^{\mathrm{T}})\mathbf{x} + \mathbf{B}\eta \tag{8.64}$$

or

$$\dot{\mathbf{x}} = \mathbf{A}^*\mathbf{x} + \mathbf{B}\eta \tag{8.65}$$

where $\mathbf{A}^*$ is the augmented matrix and is expressed as

$$\mathbf{A}^* = \mathbf{A} - \mathbf{B}\mathbf{c}\mathbf{k}^{\mathrm{T}} \tag{8.66}$$

The characteristic equation for the augmented system is again solved by expanding the determinant

$$|\lambda\mathbf{I} - \mathbf{A}| = 0 \tag{8.67}$$

The characteristic equation of the augmented matrix is again a quartic equation:

$$A\lambda^4 + B\lambda^3 + C\lambda^2 + D\lambda + E = 0 \tag{8.68}$$

where the coefficients A, B, C, D and E are functions of the stability derivatives and unknown feedback gains. The desired characteristic equation is known once the desired eigenvalues are specified. If the desired lateral roots are given as

$$\lambda_1 = \lambda_{\text{roll}} \qquad \lambda_2 = \lambda_{\text{spiral}} \qquad \lambda_{3,4} = -\zeta_{\text{DR}}\omega_{n\text{DR}} \pm \mathrm{i}\omega_{n\text{DR}}\sqrt{1-\zeta_{\text{DR}}^2} \tag{8.69}$$

then the desired characteristic equation is given as

$$(\lambda - \lambda_1)(\lambda - \lambda_2)(\lambda - \lambda_3)(\lambda - \lambda_4) = 0 \tag{8.70}$$

or

$$\lambda^4 - [(\lambda_1 + \lambda_2 + \lambda_3 + \lambda_4)]\lambda^3 + [(\lambda_1\lambda_2 + \lambda_3\lambda_4 + (\lambda_1 + \lambda_2)(\lambda_3 + \lambda_4)]\lambda^2 - [\lambda_1\lambda_2(\lambda_3 + \lambda_4) + \lambda_3\lambda_4(\lambda_1 + \lambda_2)]\lambda + \lambda_1\lambda_2\lambda_3\lambda_4 = 0 \tag{8.71}$$

Equating the coefficients of like powers of λ yields a set of algebraic equations in terms of the unknown gains **k**. Although simple in concept, these equations are quite long in symbolic form, and will not be presented here. However, a simple lateral state feedback augmentation system will be presented to aid the reader in understanding the basic ideas of this section.

The state feedback design described in the previous section requires that all the states be available for feedback. In practise this is not always possible because some states may not be accessible. That is, we may not be able to measure the state with the instrumentation on board the aircraft. If this is the case, it will be necessary to modify the design to include a state observer. The state observer estimates the states of the system from measurements of the input and output signals. A discussion of state observers is to be found in the next section.

Example Problem 8.3. A wind-tunnel model is mounted on a bearing system that permits angular rotation in roll and yaw. Use state feedback to position the eigenvalues of the system at λ_1 and λ_2.

For the motion described by the wind-tunnel model, the side force equation and the change in side velocity will be neglected. Furthermore, we will also assume that $I_{xz} = 0$. The equations of motion in state-space form can be written as

$$\begin{bmatrix} \Delta\dot{p} \\ \Delta\dot{r} \end{bmatrix} = \begin{bmatrix} L_p & L_r \\ N_p & N_r \end{bmatrix} \begin{bmatrix} \Delta p \\ \Delta r \end{bmatrix} + \begin{bmatrix} L_{\delta a} & L_{\delta r} \\ N_{\delta a} & N_{\delta r} \end{bmatrix} \begin{bmatrix} \delta_a \\ \delta_r \end{bmatrix}$$

or

$$\dot{\mathbf{x}} = \mathbf{A}\mathbf{x} + \mathbf{B}\eta$$

where

$$\mathbf{A} = \begin{bmatrix} L_p & L_r \\ N_p & N_r \end{bmatrix} \qquad \mathbf{B} = \begin{bmatrix} L_{\delta a} & L_{\delta r} \\ N_{\delta a} & N_{\delta r} \end{bmatrix}$$

If the state feedback is assumed to be

$$\eta = -\mathbf{c}\mathbf{k}^{\mathrm{T}}\mathbf{x}$$

then the augmented matrix $\mathbf{A}^*$ can be expressed as follows.

$$\mathbf{A}^* = \mathbf{A} - \mathbf{B}\mathbf{c}\mathbf{k}^{\mathrm{T}}$$

or

$$\mathbf{A}^* = \begin{bmatrix} L_p - k_1(c_1L_{\delta a} + c_2L_{\delta r}) & L_r - k_2(c_1L_{\delta a} + c_2L_{\delta r}) \\ N_p - k_1(c_1N_{\delta a} + c_2N_{\delta r}) & N_r - k_2(c_1N_{\delta,a} + c_2N_{\delta,r}) \end{bmatrix}$$

The eigenvalues of the augmented matrix can be obtained from

$$|\lambda\mathbf{I} - \mathbf{A}^*| = 0$$

which upon expansion yields

$$\lambda^2 + (k_1 L_c + k_2 N_c - L_p - N_r)\lambda + k_1(L_r N_c - N_r L_c) + k_2(N_p L_c - L_p N_c) + N_r L_p - N_p L_r = 0$$

where

$$L_c = C_1 L_{\delta a} + C_2 L_{\delta r} \qquad N_c = C_1 N_{\delta a} + C_2 N_{\delta r}$$

The characteristic equation for desired eigenvalues is given as

$$(\lambda - \lambda_1)(\lambda - \lambda_2) = 0 \qquad \text{or} \qquad \lambda^2 - (\lambda_1 + \lambda_2)\lambda + \lambda_1 \lambda_2 = 0$$

If we equate the coefficients of like powers of λ for the desired and augmented characteristic equation, we obtain a set of algebraic equations for the feedback gains k_1 and k_2:

$$k_1 L_c + k_2 N_c - L_p - N_r = -(\lambda_1 + \lambda_2)$$

$$k_1(L_r N_c + N_r L_c) + k_2(N_p L_c - L_p N_c) + N_r L_p - N_p L_r = \lambda_1 \lambda_2$$

The feedback gains are in terms of the known aerodynamic derivatives, the desired eigenvalues and the constants c_1 and c_2 where c_1 and c_2 establish the interconnection between the aileron and rudder. These constants establish the relationship between the aileron and rudder deflections. Once these parameters are selected the feedback gains can readily be obtained.

8.4 STATE VARIABLE RECONSTRUCTION: THE STATE OBSERVER

State feedback design as discussed in the previous section requires the measurement of each state variable. There are systems in which this is not possible, owing either to the complexity of the system or to the expense required to measure certain states. If the states cannot be measured for these reasons, the control law cannot be implemented. An alternate approach for designing the controller when all the states are not available is to use an approximation to the state vector. The approximation to the unavailable states is obtained by a subsystem called an observer. The design of a state feedback control system when some of the states are inaccessible can be divided into two phases. In the first phase, the control system is designed as though all the states were known, for example, the method discussed in the previous section. The second part of the design deals with determining the design of the system that estimates the unavailable states. Figure 8.4 is a sketch of a linear system with state feedback and a state observer.

The designer can select the eigenvalues of the state observer. In choosing the eigenvalues, it should be obvious that one would want the observer to respond faster than the observed system. This means that the eigenvalues of the observer should be more negative than the observed system. In practise, the observer eigenvalues are chosen so that they are only slightly more

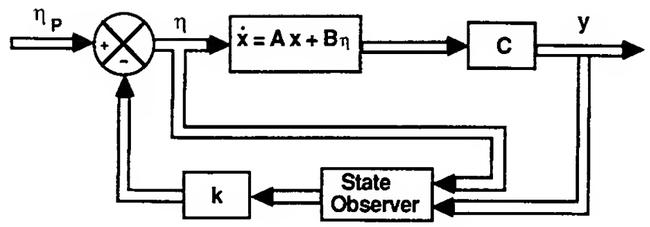

FIGURE 8.4
Block diagram representation of a linear system with state feedback and a state observer.

negative than the observed system eigenvalues. If the observer eigenvalues were chosen to be extremely large negative values, the observer would have extremely rapid response. Such an observer would be highly sensitive to noise. Hence, it has been found that good closed-loop response with an observer is best achieved by selecting eigenvalues of the observer that make the observer only slightly more responsive than the observed system.

There are a number of ways to design a state observer. The basic idea is to make the estimated state $\mathbf{x}_e$ to be very close to the actual state $\mathbf{x}$. Since $\mathbf{x}$ is unknown, there is no direct way of comparing the estimated state to the actual state of the system. However, we do know the output of the system and we can compare it with the estimated output of the observer:

$$\mathbf{y}_e = \mathbf{C}\mathbf{x}_e \tag{8.72}$$

The observer can be constructed as a state feedback problem as illustrated in Fig. 8.5. The problem now is one of determining the observer feedback gains $\mathbf{k}_e$ so that $\mathbf{y}_e$ approaches $\mathbf{y}$ as rapidly as possible. The dynamic characteristics of the observer can be expressed as

$$\dot{\mathbf{x}}_e = (\mathbf{A} - \mathbf{k}_e^{\mathrm{T}}\mathbf{C})\mathbf{x}_e + \mathbf{B}\eta + k_e^{\mathrm{T}}\mathbf{y} \tag{8.73}$$

but

$$\mathbf{y} = \mathbf{C}\mathbf{x} \tag{8.74}$$

or

$$\dot{\mathbf{x}}_e = (\mathbf{A} - \mathbf{k}_e^{\mathrm{T}}\mathbf{C})\mathbf{x}_e + \mathbf{B}\eta + k_e^{\mathrm{T}}\mathbf{C}\mathbf{x} \tag{8.75}$$

If we subtract Eq. (8.75) from the state equation for the actual system, we obtain

$$\dot{\mathbf{x}} - \dot{\mathbf{x}}_e = (\mathbf{A} - \mathbf{k}_e^{\mathrm{T}}\mathbf{C})(\mathbf{x} - \mathbf{x}_e) \tag{8.76}$$

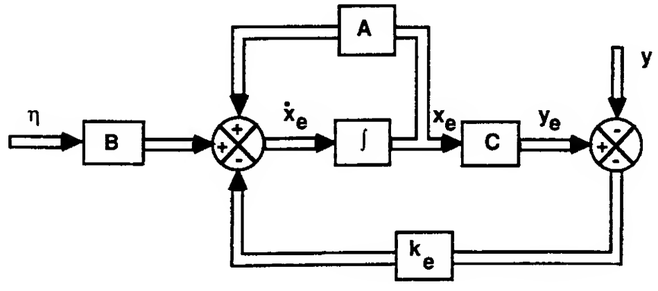

FIGURE 8.5
Design for a state observer.

The characteristic equation for the observer can be determined by solving

$$|\lambda \mathbf{I} - (\mathbf{A} - \mathbf{k}_e^{\mathrm{T}}\mathbf{C})| = 0 \tag{8.77}$$

The gain matrix of the observer is selected so that Eq. (8.76) decays rapidly to zero.

8.5 OPTIMAL STATE SPACE CONTROL SYSTEM DESIGN

The control system can be written in the state-space form

$$\dot{\mathbf{x}} = \mathbf{A}\mathbf{x} + \mathbf{B}\eta \tag{8.78}$$

For the optimal control problem, given an initial state $\mathbf{x}(t_0)$ we want to find a control vector η that drives the state $\mathbf{x}(t_0)$ to the desired final state $\mathbf{x}_d(t_f)$ in such a way that a selected performance index of the form

$$J = \int_{t_0}^{t_f} g(\mathbf{x}, \eta, t)\, \mathrm{d}t \tag{8.79}$$

is minimized. The functional form of the performance index can be expressed in a variety of forms; the most useful form is a quadratic index:

$$J = \int_0^{t_f} \mathbf{x}^{\mathrm{T}}\mathbf{Q}\mathbf{x}\, \mathrm{d}t \tag{8.80}$$

where $\mathbf{Q}$ is a weighting matrix. For many practical control problems, it is desirable to include a penalty for physical constraints such as expenditure of control energy. The performance index can be rewritten as

$$J = \int_0^{t_f} (\mathbf{x}^{\mathrm{T}}\mathbf{Q}\mathbf{x} + \eta^{\mathrm{T}}\mathbf{R}\eta)\, \mathrm{d}t \tag{8.81}$$

Using the quadratic performance index defined above, it can be shown that for a linear feedback control the optimal control law is

$$\eta = -\mathbf{k}^{\mathrm{T}}\mathbf{x} \tag{8.82}$$

where $\mathbf{k}$ is a matrix of unknown gains. This problem is often referred to as the linear regulator problem.

If we apply the principles of the calculus of variations to the minimization of the performance index, we obtain the Riccati equation. A complete development of the Ricatti equation can be found in reference 8.1. The Riccati equation is a set of nonlinear differential equations which must be solved for the Riccati gains $\mathbf{S}(t)$.

$$\frac{\mathrm{d}\mathbf{S}(t)}{\mathrm{d}t} = \mathbf{S}(t)\mathbf{B}\mathbf{R}^{-1}\mathbf{B}^{\mathrm{T}}\mathbf{S}(t) - \mathbf{S}(t)\mathbf{A} - \mathbf{A}^{\mathrm{T}}\mathbf{S}(t) - \mathbf{Q} \tag{8.83}$$

The time-varying gains are related to the Riccati gains in the following

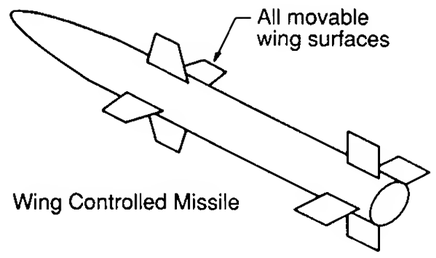

FIGURE 8.6
Sketch of a wing controlled missile.

manner:

$$\mathbf{k}(t) = \mathbf{R}^{-1}\mathbf{B}^{\mathrm{T}}\mathbf{S}(t) \tag{8.84}$$

For the case in which the final time t_f approaches infinity, the Riccati gain matrix becomes a constant matrix and reduces to

$$\mathbf{S}\mathbf{B}\mathbf{R}^{-1}\mathbf{B}^{\mathrm{T}}\mathbf{S} - \mathbf{S}\mathbf{A} - \mathbf{A}^{\mathrm{T}}\mathbf{S} - \mathbf{Q} = 0 \tag{8.85}$$

In this form the Riccati equation is a set of nonlinear algebraic equations in terms of the Riccati gains. Except for the simplest of examples, solution of Eq. (8.85) requires sophisticated computer codes.

Example Problem 8.4. Most guided missiles require that the roll attitude of the missile be kept at a fixed orientation throughout its flight so that the guidance system can function properly. A roll autopilot is needed to maintain the desired roll orientation. Figure 8.6 is a sketch of a wing-controlled missile.

In this example we shall design a feedback control system that will keep the roll orientation near zero, while not exceeding a given limit on the aileron deflection angle. The equations of motion for the rolling motion of the missile were developed in Chapter 5 and are given below:

$$I_x\dot{p} = \frac{\partial L}{\partial P}p + \frac{\partial L}{\partial \delta_a}\delta_a \qquad \dot{\phi} = p$$

Rewriting these equations as

$$\dot{p} = L_p p + L_{\delta a}\delta_a \qquad \dot{\phi} = p$$

where

$$L_p = \frac{\partial L/\partial p}{I_x} \quad \text{and} \quad L_{\delta a} = \frac{\partial L/\partial \delta_\alpha}{I_x}$$

the equations can be easily be written in the state variable form as follows:

$$\begin{bmatrix}\dot{\phi}\\ \dot{p}\end{bmatrix} = \begin{bmatrix}0 & 1\\ 0 & L_p\end{bmatrix}\begin{bmatrix}\phi\\ p\end{bmatrix} + \begin{bmatrix}0\\ L_{\delta a}\end{bmatrix}\{\delta_a\}$$

or

$$\dot{\mathbf{x}} = \mathbf{A}\mathbf{x} + \mathbf{B}\eta$$

where

$$\mathbf{A} = \begin{bmatrix} 0 & 1 \\ 0 & L_p \end{bmatrix} \quad \text{and} \quad \mathbf{B} = \begin{bmatrix} 0 \\ L_{\delta a} \end{bmatrix}$$

The quadratic performance index that is to be minimized is

$$J = \frac{1}{2}\int_0^\infty \left[\left(\frac{\phi}{\phi_{\max}}\right)^2 + \left(\frac{p}{p_{\max}}\right)^2 + \left(\frac{\delta_a}{\delta_{a\max}}\right)^2 \right] dt$$

where $\phi_{\max}$ = the maximum desired roll angle
$p_{\max}$ = the maximum desired roll rate
$\delta_{a\max}$ = maximum aileron deflection.

Comparing the performance index given here with the general form allows us to specify the matrices **Q** and **R**:

$$\mathbf{Q} = \begin{bmatrix} \frac{1}{\phi_{\max}^2} & 0 \\ 0 & \frac{1}{p_{\max}^2} \end{bmatrix} \quad \text{and} \quad \mathbf{R} = \frac{1}{\delta_{\max}^2}$$

The optimum control law is determined by solving the steady-state matrix Riccati equation,

$$\mathbf{SA} + \mathbf{A}^T\mathbf{S} + \mathbf{Q} - \mathbf{SBR}^{-1}\mathbf{BTS} = 0$$

for the values of the **S** matrix. The optimal control law is given by

$$\eta = -\mathbf{k}^T\mathbf{x}(t) \qquad \text{where} \qquad \mathbf{k} = \mathbf{R}^{-1}\mathbf{B}^T\mathbf{S}$$

Substituting the matrices **A**, **B**, **Q**, and **R** into the Ricatti equation yields a set of nonlinear algebraic equations for the unknown elements of the **S** matrix[1]:

$$\frac{1}{\phi_{\max}^2} - S_{12}^2 L_{\delta,a}^2 \delta_{\max}^2 = 0$$

$$S_{11} + S_{12}L_p - S_{12}S_{22}L_{\delta a}^2\delta_{\max}^2 = 0$$

$$2S_{12} + 2S_{22}L_p + \frac{1}{p_{\max}} - S_{22}^2 L_{\delta a}^2 \delta_{\max}^2 = 0$$

For the case in which the missile has the aerodynamic characteristics

$$L_p = -2 \text{ rad/s} \qquad L_{\delta a} = 9000 \text{ s}^{-2}$$

and

$$\phi_{\max} = 10° = 0.174 \text{ rad} \qquad p_{\max} = 300°/\text{s} = 5.23 \text{ rad/s}$$

the control law is found to be $\delta_a = -3.0\phi - 0.103p$.

[1] Remember that the **S** matrix is symmetric, so that it is only necessary to solve the equation generated for the elements along and above the diagonal of the matrix.

8.6 SUMMARY

Modern control theory provides the control systems engineer with a very valuable design tool. Unlike the classical control methods presented in Chapter 7, modern control theory is ideally suited for synthesis of a control system with multiple inputs and for determining optimal control strategies.

State feedback design can be accomplished provided that all the states are controllable. If some of the states are not available for feedback, a state observer can be incorporated into the design to estimate the unknown states provided the states are observable through the system output.

Finally, the state-space representation of the control system lends itself to mathematical techniques that permit the designer to determine optimal control laws consistent with design constraints.

8.7 PROBLEMS

8.1. Given the third-order differential equation

$$\frac{d^3c(t)}{dt^3} + 7\frac{d^2c(t)}{dt^2} + 3\frac{d^2c}{dt} + 5c(t) = r(t)$$

write the equation in state vector form.

8.2. Given the second-order differential equation

$$\frac{d^2c(t)}{dt^2} + 3\frac{dc(t)}{dt} + 2ct(t) = r(t)$$

having the initial conditions $c(0) = 1$ and $dc/dt(0) = 0$. Write the equation in state vector form.

(a) Find the state transition matrix.

(b) Determine the solution if $r(t)$ is a unit step function.

8.3. Given the linear time-invariant dynamical system that is governed by the equations

$$\begin{bmatrix} \dot{x}_1 \\ \dot{x}_2 \end{bmatrix} = \begin{bmatrix} 1 & 0 \\ 1 & 1 \end{bmatrix}\begin{bmatrix} x_1 \\ x_2 \end{bmatrix} + \begin{bmatrix} 1 \\ 1 \end{bmatrix}[\eta]$$

where

$$\begin{bmatrix} x_1(0) \\ x_2(0) \end{bmatrix} = \begin{bmatrix} 0 \\ 1 \end{bmatrix}$$

determine the state transition matrix and the response of the system if the input signal is a unit step function.

8.4. Given the state equations

$$\begin{bmatrix} \dot{x}_1 \\ \dot{x}_2 \\ \dot{x}_3 \end{bmatrix} = \begin{bmatrix} 0 & 1 & 0 \\ 0 & 0 & 1 \\ -3 & -6 & -4 \end{bmatrix}\begin{bmatrix} x_1 \\ x_2 \\ x_3 \end{bmatrix} + \begin{bmatrix} 0 \\ 0 \\ 1 \end{bmatrix}[\eta]$$

determine whether the system is completely controllable.

8.5. Given the state equations shown below, use state feedback to position the eigenvalues so closed system has eigenvalues located at $-1 \pm 2i$.

$$\begin{bmatrix} \dot{x}_1 \\ \dot{x}_2 \end{bmatrix} = \begin{bmatrix} 0 & 1 \\ -3 & -1 \end{bmatrix} \begin{bmatrix} x_1 \\ x_2 \end{bmatrix} + \begin{bmatrix} 0 \\ 1 \end{bmatrix} [\eta]$$

8.6. The longitudinal motion of an airplane is approximated by the differential equations

$$\dot{w} = -2.0w + 170\dot{\theta} - 27\delta$$

$$\ddot{\theta} = -0.25w - 15\dot{\theta} - 45\delta$$

(a) Rewrite the equations in state space form

$$\dot{\mathbf{x}} = \mathbf{A}\mathbf{x} + \mathbf{B}\eta$$

(b) Find the eigenvalues of **A**.

(c) Determine a state feedback control law

$$\eta = -\mathbf{k}^T\mathbf{x}$$

so that the augmented system has a damping ratio $\zeta = 0.5$ and the undamped natural frequency $\omega_n = 20$ rad/s.

8.7. Assume that the pitching velocity for the airplane described in Problem 8.6 cannot be measured. Discuss how you would design a state observer so that the system can achieve the desired performance.

8.8. Design an automatic control system to maintain zero vertical acceleration. The equations of motion governing the aircraft's motion are

$$\Delta\dot{\alpha} = \frac{Z_\alpha}{u_0}\Delta\alpha - \Delta q \qquad \Delta\dot{q} = M_\alpha\,\Delta\alpha + M_\delta\,\Delta\delta_e$$

Find the nonlinear algebraic equations that must be solved to determine the gains for the control law $\eta = -\mathbf{k}^T\mathbf{x}$, that satisfies the performance index

$$J = \int_0^\infty \left[\left(\frac{\delta}{\delta_0}\right)^2 + \left(\frac{\alpha}{\alpha_0}\right)^2 + \left(\frac{q}{q_0}\right)^2 \right] dt$$

where δ_0 = maximum control deflection
α_0 = maximum angle of attack
q_0 = maximum pitch rate

REFERENCES

8.1. Kuo, B. C.: *Automatic Control System,* Prentice-Hall, Englewood Cliffs, NW, 1975.
8.2. Nagrath, I. J., and M. Gopal: *Control Systems Engineering,* Helsted Press, New York, 1975.
8.3. Raven, F. H.: *Automatic Control Engineering,* McGraw-Hill, New York, 1978.
8.4. Blakelock, J. H.: *Automatic Control of Aircraft and Missiles,* Wiley, New York, 1965.
8.5. Bryson, A. E.: "Dryden Lecture: New Concepts in Control Theory 1959–1984", AIAA Paper 84-0161, January 1985.

8.6. Bryson, A. E., and Y. C. Ho: *Applied Optimal Control,* Hemisphere, Washington, DC, 1975.
8.7. Nesline, F. W., and P. Zarchan: "A Classical Look at Modern Control for Missile Autopilot Design," AIAA Paper 82-1512, August 1982.
8.8. Oehman, W. E., and J. H. Suddath: *State-Vector Control Applied to Lateral Stability of High Performance Aircraft,* NASA TN D-2984, July 1965.

APPENDIX A

ATMOSPHERIC TABLES (ICAO STANDARD ATMOSPHERE)

Geometric altitude metric units

H_G, m	H, m	T, K	P, N/m^2	$\frac{P}{P_0}$	ρ, kg/m^{-3}	$\frac{\rho}{\rho_0}$	a, m/s	ν, m^2/s
0	0	288.150	1.01325 +5	1.00000 +0	1.2250 +0	1.0000 +0	340.294	1.4607 −5
1 000	1 000	281.651	8.9876 +4	8.87009 −1	1.1117 +0	9.0748 −1	336.435	1.5813 −5
2 000	1 999	275.154	7.9501 +4	7.84618 −1	1.0066 +0	8.2168 −1	332.532	1.7147 −5
3 000	2 999	268.659	7.0121 +4	6.92042 −1	9.0925 −1	7.4225 −1	328.583	1.8628 −5
4 000	3 997	262.166	6.1660 +4	6.08541 −1	8.1935 −1	6.6885 −1	324.589	2.0275 −5
5 000	4 996	255.676	5.4048 +4	5.33415 −1	7.3643 −1	6.0117 −1	320.545	2.2110 −5
6 000	5 994	249.187	4.7217 +4	4.66001 −1	6.6011 −1	5.3887 −1	316.452	2.4162 −5
7 000	6 992	242.700	4.1105 +4	4.05677 −1	5.9002 −1	4.8165 −1	312.306	2.6461 −5
8 000	7 990	236.215	3.5651 +4	3.51854 −1	5.2579 −1	4.2921 −1	308.105	2.9044 −5
9 000	8 987	229.733	3.0800 +4	3.03979 −1	4.6706 −1	3.8128 −1	303.848	3.1957 −5
10 000	9 984	223.252	2.6500 +4	2.61533 −1	4.1351 −1	3.3756 −1	299.532	3.5251 −5
11 000	10 981	216.774	2.2700 +4	2.24031 −1	3.6480 −1	2.9780 −1	295.154	3.8988 −5
12 000	11 977	216.650	1.9399 +4	1.91457 −1	3.1194 −1	2.5464 −1	295.069	4.5574 −5
13 000	12 973	216.650	1.4170 +4	1.63628 −1	2.6660 −1	2.1763 −1	295.069	5.3325 −5
14 000	13 969	216.650	1.4170 +4	1.39851 −1	2.2786 −1	1.8600 −1	295.069	6.2391 −5
15 000	14 965	216.650	1.2112 +4	1.19534 −1	1.9475 −1	1.5898 −1	205.069	7.2995 −5
16 000	15 960	216.650	1.0353 +4	1.02174 −1	1.6647 −1	1.3589 −1	295.069	8.5397 −5
17 000	16 955	216.650	8.8496 +3	8.73399 −2	1.4230 −1	1.1616 −1	295.069	9.9902 −5
18 000	17 949	216.650	7.5652 +3	7.46629 −2	1.2165 −1	9.9304 −2	295.069	1.1686 −4
19 000	18 943	216.650	6.4674 +3	6.38291 −2	1.0400 −1	8.4894 −2	295.069	1.3670 −4
20 000	19 937	216.650	5.5293 +3	5.45700 −2	8.8910 −2	7.2579 −2	295.069	1.5989 −4
21 000	20 931	217.581	4.7274 +3	4.66709 −2	7.5715 −2	6.1808 −2	295.703	1.8843 −4
22 000	21 924	218.574	4.0420 +3	3.99456 −2	6.4510 −2	5.2661 −2	296.377	2.2201 −4
23 000	22 917	219.567	3.4562 +3	3.42153 −2	5.5006 −2	4.4903 −2	297.049	2.6135 −4
24 000	23 910	220.560	2.9554 +3	2.93288 −2	4.6938 −2	3.8317 −2	297.720	3.0743 −4
25 000	24 902	221.552	2.6077 +3	2.51588 −2	4.0084 −2	3.2722 −2	298.389	3.6135 −4
26 000	25 894	222.544	2.1632 +3	2.15976 −2	3.4257 −2	2.7965 −2	299.056	4.2439 −4
27 000	26 886	223.536	1.8555 +3	1.85539 −2	2.9298 −2	2.3917 −2	299.722	4.9805 −4
28 000	27 877	224.527	1.5949 +3	1.59506 −2	2.5076 −2	2.0470 −2	300.386	5.8405 −4
29 000	28 868	225.518	1.3737 +3	1.37224 −2	2.1478 −2	1.7533 −2	301.048	6.8438 −4
30 000	29 859	226.509	1.1855 +3	1.18138 −2	1.8410 −2	1.5029 −2	301.709	8.0134 −4

Geometric altitude english units

H_G, ft	H, ft	T, °R	P, lb/ft^2	$\frac{P}{P_0}$	ρ, slug/ft^3	$\frac{\rho}{\rho_0}$	a, ft/s	ν, ft^2/s
0	0	518.670	2.1162 +3	1.00000 +0	2.3769 −3	1.0000 +0	1116.45	1.5723 −4
2 500	2 500	509.756	1.9319 +3	9.12910	2.2079 −3	9.2887	1106.81	1.6700
5 000	4 999	500.843	1.7609 +3	8.32085 −1	2.0482 −3	8.6170 −1	1097.10	1.7755 −4
7 500	7 497	491.933	1.6023 +3	7.57172	1.8975 −3	7.9832	1087.29	1.8896
10 000	9 995	483.025	1.4556 +3	6.87832 −1	1.7556 −3	7.3859 −1	1077.40	2.0132 −4
12 500	12 493	474.120	1.3200 +3	6.23741	1.6219 −3	6.8235	1067.43	2.1472
15 000	14 989	465.216	1.1948 +3	5.64587 −1	1.4962 −3	6.2946 −1	1057.36	2.2927 −4
17 500	17 485	456.315	1.0794 +3	5.10072	1.3781 −3	5.7977	1047.19	2.4509
20 000	19 981	447.415	9.7327 +2	4.59912 −1	1.2673 −3	5.3316 −1	1036.93	2.6233 −4
22 500	22 476	438.518	8.7576 +2	4.13834	1.1634 −3	4.8947	1026.57	2.8113
25 000	24 970	429.623	7.8633 +2	3.71577 −1	1.0663 −3	4.4859 −1	1016.10	3.0167 −4
27 500	27 464	420.730	7.0447 +2	3.32892	9.7544 −4	4.1039	1005.53	3.2416
30 000	29 957	411.839	6.2962 +2	2.97544 −1	8.9068 −4	3.7473 −1	994.85	3.4882 −4
32 500	32 449	402.950	5.6144 +2	2.65305	8.1169 −4	3.415	984.05	3.7591
35 000	34 941	394.064	4.9934 +2	2.35962 −1	7.3820 −4	3.1058 −1	973.14	4.0573 −4
37 500	37 432.5	389.970	4.4312 +2	2.093965	6.6196 −4	2.78505	968.08	4.48535
40 000	39 923	389.970	3.9312 +2	1.85769	5.8727 −4	2.4708	968.08	7.70146
42 500	42 413.5	389.970	3.4878 +2	1.64816	5.2103 −4	2.1921	968.08	5.69855
45 000	44 903	389.970	3.0945 +2	1.46227 −1	4.6227 −4	1.9449 −1	968.08	6.4228 −4
47 500	47 392.5	389.970	2.7456 +2	1.29742	4.1015 −4	1.7256	968.08	7.2391
50 000	49 880	389.970	2.4361 +2	1.15116	3.6391 −4	1.5311	968.08	8.1587
52 500	52 368.5	389.970	2.1615 +2	1.02143	3.2290 −4	1.3585	968.08	9.19505
55 000	54 855	389.970	1.9180 +2	9.06336 −2	2.8652 −4	1.2055 −1	968.08	1.0363 −3
57 500	57 341.5	389.970	1.7019 +2	8.042485	2.5424 −4	1.0697	968.08	1.1678
60 000	59 828	389.970	1.5103 +2	7.13664	2.2561 −4	9.4919	968.08	1.3160
62 500	62 313.5	389.970	1.3402 +2	6.33315	2.0021 −4	8.42325	968.08	1.483
65 000	64 798	389.970	1.1893 +2	5.62015 −2	1.7767 −4	7.4749 −2	968.08	1.6711 −3
67 500	67 282.5	390.8835	1.0555 +2	4.988155	1.5767 −4	6.61885	969.21	1.891
70 000	69 766	392.246	9.3672 +1	4.42898	1.3993 −4	5.8565	970.90	2.1434
72 500	72 249	393.6085	8.3134 +1	3.93432	1.2419 −4	5.18435	972.58	2.4283
75 000	74 731	394.971	7.3784 +1	3.49635 −2	1.1022 −4	4.5914 −2	974.26	2.7498 −3
77 500	77 213	396.3325	6.5487 +1	3.10856	9.7829 −5	4.01681	975.94	3.1125
80 000	79 694	397.693	5.8125 +1	2.76491	8.6831 −5	3.6060	977.62	3.5213
82 500	82 174	399.0545	5.1592 +1	2.460355	7.7022 −5	3.19785	979.285	3.98215
85 000	84 655	400.415	4.5827 +1	2.19023 −2	6.7706 −5	2.8371 −2	980.95	4.5012 −3
87 500	87 134.5	401.7755	4.0757 +1	1.95063	5.9598 −5	2.51815	982.62	5.0857
90 000	89 613	403.135	3.6292 +1	1.73793	5.2531 −5	2.2360	984.28	5.7434
92 500	92 091.5	404.495	3.2354 +1	1.549199	4.6362 −5	1.9864	985.94	6.48345
95 000	94 569	405.854	2.8878 +1	1.38133 −2	4.0970 −5	1.7653 −2	987.59	7.3155 −3
97 500	97 046	407.2135	2.5805 +1	1.23226	3.6251 −5	1.56955	989.245	8.25085
100 000	99 523	408.572	2.3085 +1	1.09971	3.2114 −5	1.3960	990.90	9.3017

APPENDIX B

GEOMETRIC, MASS AND AERODYNAMIC CHARACTERISTICS OF SELECTED AIRPLANES

Data on the geometric, mass, and aerodynamic stability and control characteristics are presented for six airplanes. The airplanes include a general aviation airplane, two jet fighters, an executive business jet and two jet transports. The stability coefficients are presented in tabular form for each airplane. Coefficients that were unavailable have been presented with a numerical value of zero in the following tables. The stability coefficients for the A-4D are presented in graphical form as a function of Mach number and altitude. These plots show the large variations in the coefficients due to compressibility effects. The definitions of the stability coefficient and geometric data presented in the figures are given in the following nomenclature list. The information presented in this appendix was taken from the references B1 and B2 given after the nomenclature list.

NOMENCLATURE

b Wing span

$\bar{c}$ Mean chord

$C_L = \dfrac{L}{QS}$

$C_{L_\alpha} = \dfrac{\partial C_L}{\partial \alpha}\,(\text{rad}^{-1})$

$C_{L_{\dot\alpha}} = \dfrac{\partial C_L}{\partial\left(\dfrac{\dot\alpha \bar{c}}{2u_0}\right)}\,(\text{rad}^{-1})$

$C_{L_\mathbf{M}} = \dfrac{\partial C_L}{\partial \mathbf{M}}$

$C_{L_{\delta_e}} = \dfrac{\partial C_L}{\partial \delta_e}\,(\text{rad}^{-1})$

$C_D = \dfrac{D}{QS}$

$C_{D_\alpha} = \dfrac{\partial C_D}{\partial \alpha}\,(\text{rad}^{-1})$

$C_{D_\mathbf{M}} = \dfrac{\partial C_D}{\partial \mathbf{M}}$

$C_{D_{\delta_e}} = \dfrac{\partial C_D}{\partial \delta_e}\,(\text{rad}^{-1})$

$C_m = \dfrac{M}{QS\bar{c}}$

$C_{m_\alpha} = \dfrac{\partial C_M}{\partial \alpha}\,(\text{rad}^{-1})$

$C_y = \dfrac{Y}{QS}$

$C_{y_\beta} = \dfrac{\partial C_y}{\partial \beta}\,(\text{rad}^{-1})$

$C_{y_{\delta_r}} = \dfrac{\partial C_y}{\partial \delta_r}\,(\text{rad}^{-1})$

$C_l = \dfrac{L}{QSb}$

$C_{l_\beta} = \dfrac{\partial C_l}{\partial \beta}\,(\text{rad}^{-1})$

$C_{l_p} = \dfrac{\partial C_l}{\partial (pb/2u_0)}\,(\text{rad}^{-1})$

$C_{l_r} = \dfrac{\partial C_l}{\partial (rb/2u_0)}\,(\text{rad}^{-1})$

$C_{l_{\delta_a}} = \dfrac{\partial C_l}{\partial \delta_a}\,(\text{rad}^{-1})$

$C_{l_{\delta_r}} = \dfrac{\partial C_l}{\partial \delta_r}\,(\text{rad}^{-1})$

$C_n = \dfrac{N}{QSb}$

$C_{n_\beta} = \dfrac{\partial C_n}{\partial \beta}\,(\text{rad}^{-1})$

$C_{n_p} = \dfrac{\partial C_n}{\partial (pb/2u_0)}\,(\text{rad}^{-1})$

$C_{n_r} = \dfrac{\partial C_n}{\partial (rb/2u_0)}\,(\text{rad}^{-1})$

$C_{m_{\dot\alpha}} = \dfrac{\partial C_m}{\partial (\dot\alpha \bar{c}/2u_0)}\,(\text{rad}^{-1})$

$C_{m_\mathbf{M}} = \dfrac{\partial C_m}{\mathbf{M}}$

$C_{m_q} = \dfrac{\partial C_m}{\partial (q\bar{c}/2u_0)}\,(\text{rad}^{-1})$

$C_{n_{\delta_a}} = \dfrac{\partial C_n}{\partial \delta_a}\,(\text{rad}^{-1})$

$C_{n_{\delta_r}} = \dfrac{\partial C_n}{\partial \delta_r}\,(\text{rad}^{-1})$

I_x Rolling moment of inertia
I_y Pitching moment of inertia
I_z Yawing moment of inertia
I_{xz} Product of inertia about xz axis
$\mathbf{M}$ Mach number
Q Dynamic pressure
S Wing planform area
u_0 Reference flight speed

REFERENCES

B.1 Teper, G. L., *Aircraft Stability and Control Data,* System Technology, Inc., Hawthorne, California, Technical Report 176-1, April 1969.

B.2 Heffley, R. K., and Jewell, W. F., *Aircraft Handling Qualities Data,* NASA CR-2144, December 1972.

General aviation airplane: NAVION[a]

Longitudinal **M** = 0.158	C_L	C_D	C_{L_α}	C_{D_α}	C_{m_α}	$C_{L_{\dot\alpha}}$	$C_{m_{\dot\alpha}}$	C_{L_q}	C_{m_q}	C_{L_M}	C_{D_M}	C_{m_M}	$C_{L_{\delta e}}$	$C_{m_{\delta e}}$
Sea level	0.41	0.05	4.44	0.33	−0.683	0.0	−4.36	3.8	−9.96	0.0	0.0	0.0	0.355	−0.923
Lateral **M** = 0.158	C_{y_β}	C_{l_β}	C_{n_β}	C_{l_p}	C_{n_p}	C_{l_r}	C_{n_r}	$C_{l_{\delta a}}$	$C_{n_{\delta a}}$	$C_{y_{\delta r}}$	$C_{l_{\delta r}}$	$C_{n_{\delta r}}$		
Sea level	−0.564	−0.074	0.071	−0.410	−0.0575	0.107	−0.125	−0.134	−0.0035	0.157	0.107	−0.072		

[a] All derivatives are per radian.

General Aviation Airplane

Center of Gravity and Mass Characteristics

W = 2750 lbs
CG at 29.5% MAC
I_x = 1048 slug ft^2
I_y = 3000 slug ft^2
I_z = 3530 slug ft^2
I_{xz} = 0

Reference Geometry

S = 184 ft^2
$\underline{b}$ = 33.4 ft
$\overline{c}$ = 5.7 ft

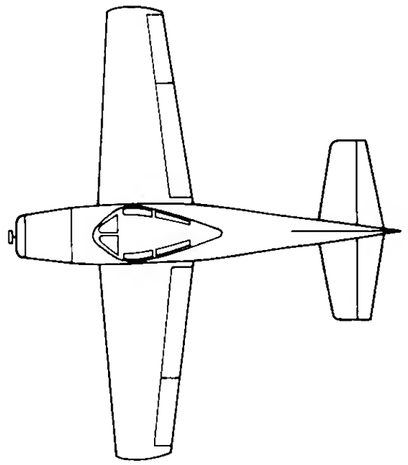

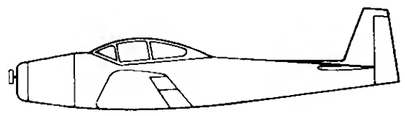

FIGURE B.1
Three-view-sketch and stability data for a general aviation airplane.

Fighter aircraft: F104-A[a]

Longitudinal **M** = 0.257	C_L	C_D	C_{L_α}	C_{D_α}	C_{m_α}	$C_{L_{\dot\alpha}}$	$C_{m_{\dot\alpha}}$	C_{L_q}	C_{m_q}	C_{L_M}	C_{D_M}	C_{m_M}	$C_{L_{\delta e}}$	$C_{m_{\delta e}}$
Sea level	0.235	0.263	3.44	0.45	−0.64	0.0	−1.6	0.0	−5.8	0.0	0.0	0.0	0.68	−1.46
M = 1.8 55,000 ft	0.2	0.055	2.0	0.38	−1.30	0.0	−2.0	0.0	−4.8	−0.2	0.0	−0.01	0.52	−0.10
Lateral **M** = 0.257	C_{y_β}	C_{l_β}	C_{n_β}	C_{l_p}	C_{n_p}	C_{l_r}	C_{n_r}	$C_{l_{\delta a}}$	$C_{n_{\delta a}}$	$C_{y_{\delta r}}$	$C_{l_{\delta r}}$	$C_{n_{\delta r}}$		
Sea level	−1.17	−0.175	0.50	−0.285	−0.14	0.265	−0.75	0.039	0.0042	0.208	0.045	−0.16		
M = 1.8 55,000 ft	−1.0	−0.09	0.24	−0.27	−0.09	0.15	−0.65	0.017	0.0025	0.05	0.008	−0.04		

[a] All derivatives are per radian.

F-104A
Fighter Airplane

Center of Gravity and Mass Characteristics

W = 16 300 lb
CG at 7 % MAC
I_x = 3 549 Slug - ft^2
I_y = 58 611 Slug - ft^2
I_z = 59 669 Slug - ft^2
I_{xz} = 0

References Geometry

S = 196.1 ft^2
b = 21.94 ft
$\overline{c}$ = 9.55 ft

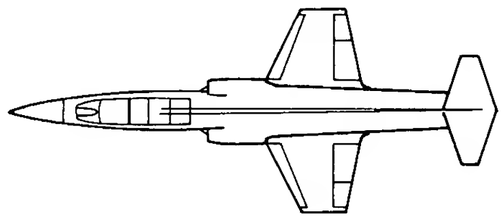

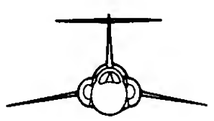

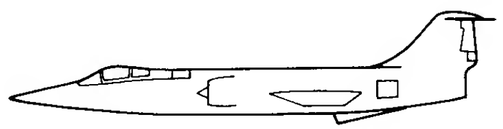

FIGURE B.2
Three-view sketch and stability data for the F-104-A fighter.

Fighter aircraft: A 4D[a]

Longitudinal	C_L	C_D	C_{L_α}	C_{D_α}	C_{m_α}	$C_{L_{\dot\alpha}}$	$C_{m_{\dot\alpha}}$	C_{L_q}	C_{m_q}	C_{L_M}	C_{D_M}	C_{m_M}	$C_{L_{\delta e}}$	$C_{m_{\delta e}}$
M = 0.4														
Sea level	0.28	0.03	3.45	0.30	−0.38	0.72	−1.1	0.0	−3.6	0.0	0.0	0.0	0.36	−0.50
M = 0.8														
35,000 ft	0.30	0.038	4.0	0.56	−0.41	1.12	−1.65	0.0	−4.3	0.15	0.03	−0.05	0.4	−0.60

Lateral	C_{y_β}	C_{l_β}	C_{n_β}	C_{l_p}	C_{n_p}	C_{l_r}	C_{n_r}	$C_{l_{\delta a}}$	$C_{n_{\delta a}}$	$C_{y_{\delta r}}$	$C_{l_{\delta r}}$	$C_{n_{\delta r}}$
M = 0.4												
Sea level	−0.98	−0.12	0.25	−0.26	0.022	0.14	−0.35	0.08	0.06	0.17	−0.105	0.032
M = 0.8												
35,000 ft	−1.04	−0.14	0.27	−0.24	0.029	0.17	−0.39	0.072	0.04	0.17	−0.105	0.032

[a] All derivatives are per radian.

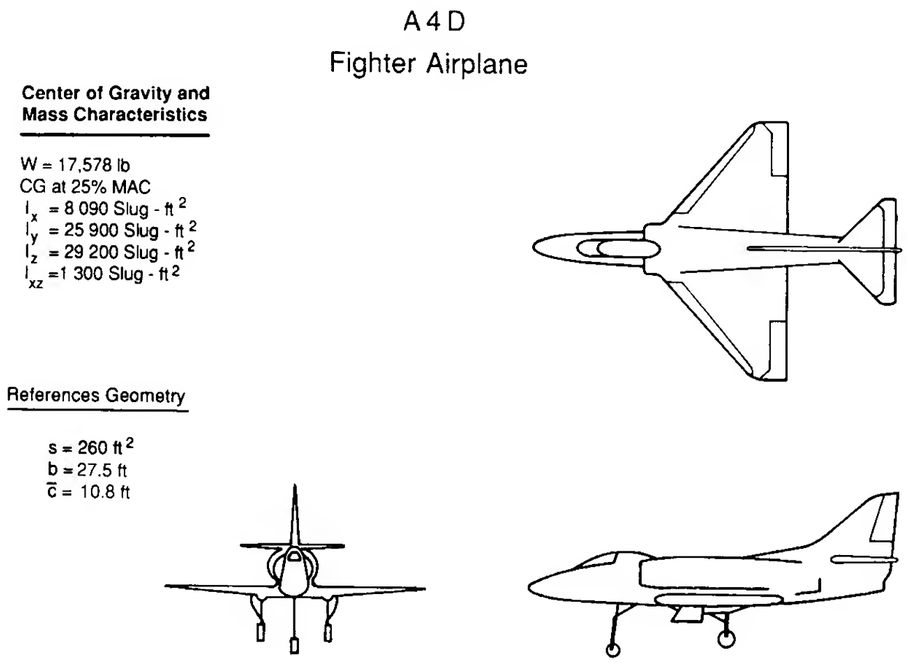

FIGURE B.3
Three-view sketch and stability data for the A-4D fighter.

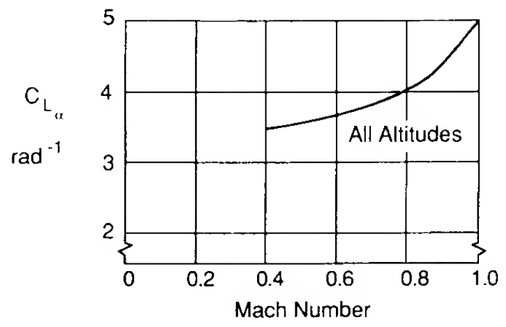

FIGURE B.4
C_{L_α} versus Mach number.

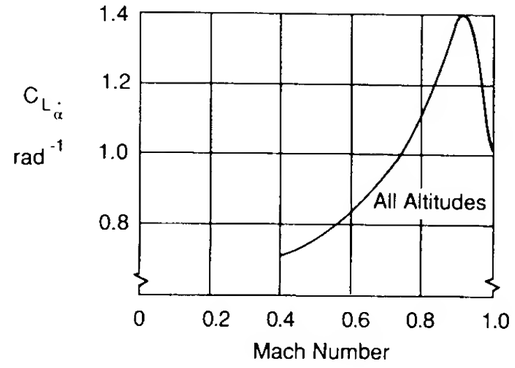

FIGURE B.5
$C_{L_{\dot\alpha}}$ versus Mach number.

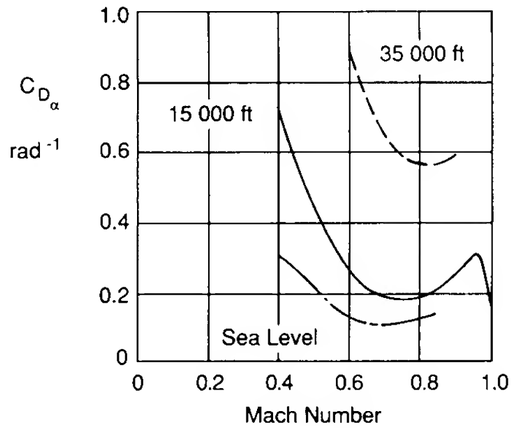

FIGURE B.6
C_{D_α} versus Mach number.

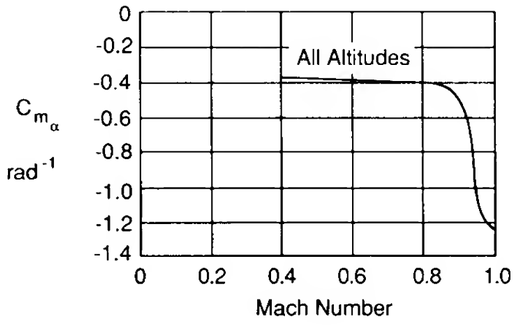

FIGURE B.7
C_{m_α} versus Mach number.

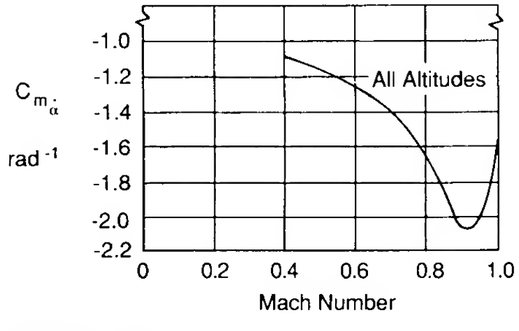

FIGURE B.8
$C_{m_{\dot\alpha}}$ versus Mach number.

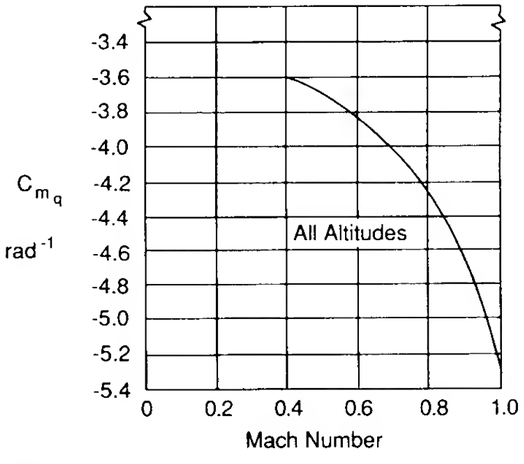

FIGURE B.9
C_{m_q} versus Mach number.

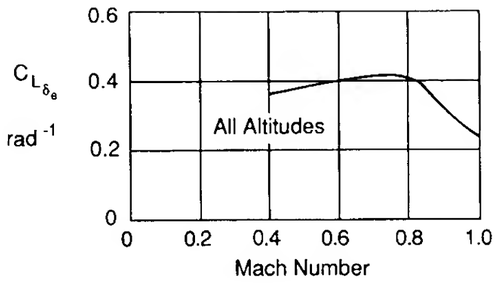

FIGURE B.10
$C_{L_{\delta_e}}$ versus Mach number.

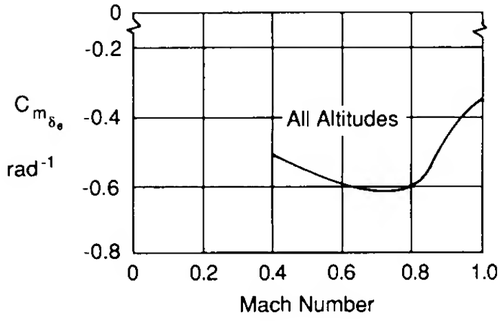

FIGURE B.11
$C_{m_{\delta_e}}$ versus Mach number.

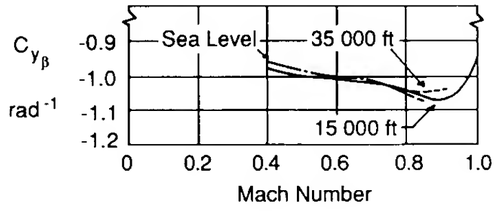

FIGURE B.12
C_{y_β} versus Mach number.

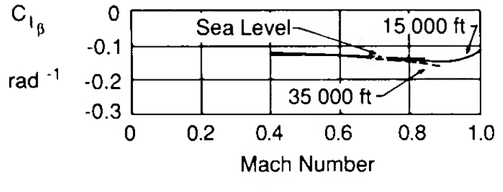

FIGURE B.13
C_{l_β} versus Mach number.

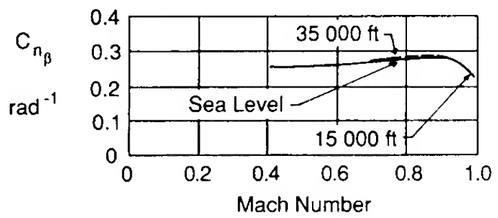

FIGURE B.14
C_{n_β} versus Mach number.

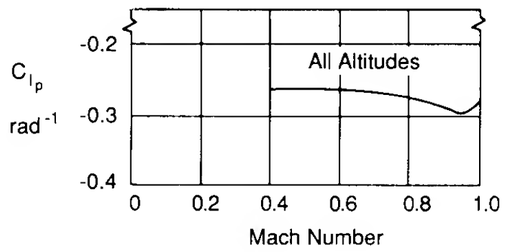

FIGURE B.15
C_{l_p} versus Mach number.

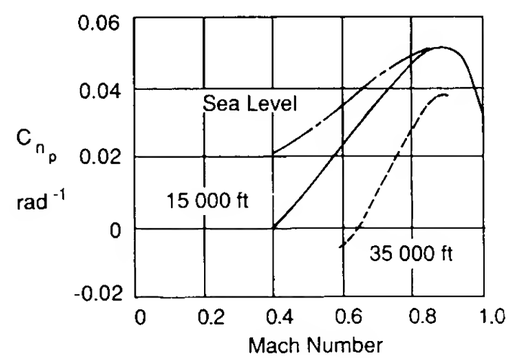

FIGURE B.16
C_{n_p} versus Mach number.

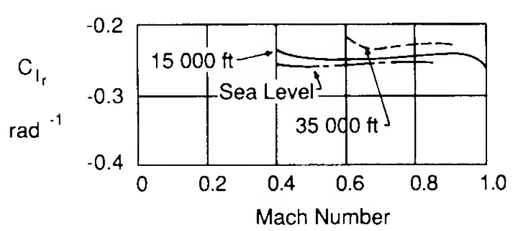

FIGURE B.17
C_{l_r} versus Mach number.

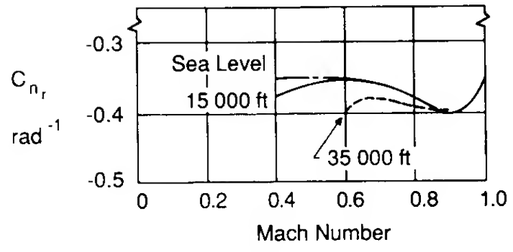

FIGURE B.18
C_{n_r} versus Mach number.

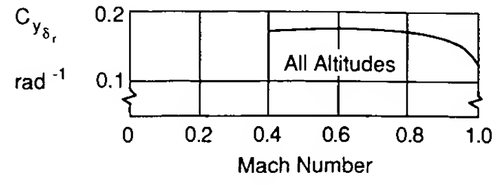

FIGURE B.19
$C_{y_{\delta_r}}$ versus Mach number.

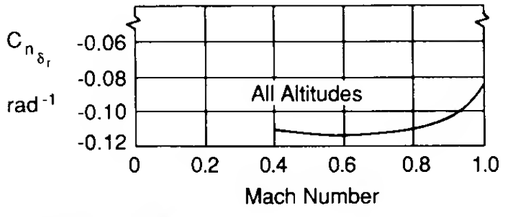

FIGURE B.20
$C_{n_{\delta_r}}$ versus Mach number.

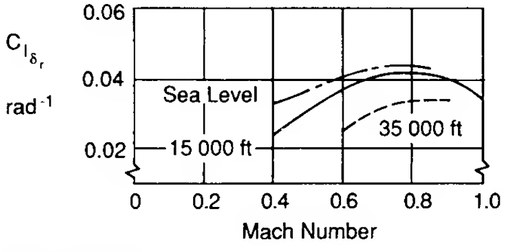

FIGURE B.21
$C_{l_{\delta_r}}$ versus Mach number.

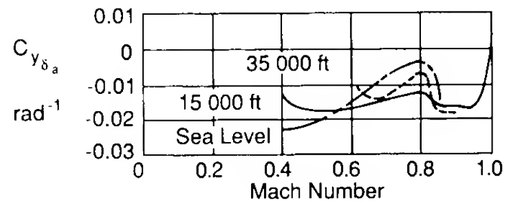

FIGURE B.22
$C_{y_{\delta_a}}$ versus Mach number.

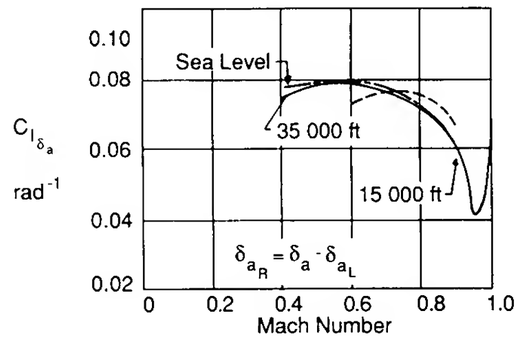

FIGURE B.23
$C_{l_{\delta_a}}$ versus Mach number.

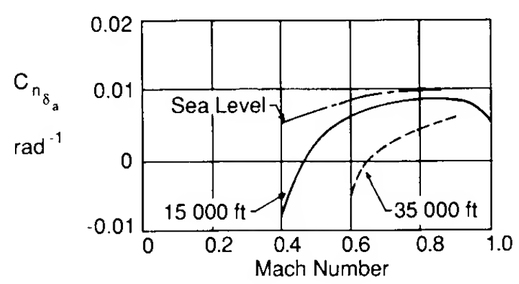

FIGURE B.24
$C_{n_{\delta_a}}$ versus Mach number.

Business Jet: Jetstar[a]

Longitudinal	C_L	C_D	C_{L_α}	C_{D_α}	C_{m_α}	$C_{L_{\dot\alpha}}$	$C_{m_{\dot\alpha}}$	C_{L_q}	C_{m_q}	C_{L_M}	C_{D_M}	C_{m_M}	$C_{L_{\delta e}}$	$C_{m_{\delta e}}$
M = 0.20														
Sea level	0.737	0.095	5.0	0.75	−0.80	0.0	−3.0	0.0	−8.0	0.0	0.0	−0.05	0.4	−0.81
M = 0.80														
40,000 ft	0.6	0.04	6.5	0.60	−0.72	0.0	−0.4	0.0	−0.92	0.0	−0.6	−0.60	0.44	−0.88

Lateral	C_{y_β}	C_{l_β}	C_{n_β}	C_{l_p}	C_{n_p}	C_{l_r}	C_{n_r}	$C_{l_{\delta a}}$	$C_{n_{\delta a}}$	$C_{y_{\delta r}}$	$C_{l_{\delta r}}$	$C_{n_{\delta r}}$
M = 0.20												
Sea level	−0.72	−0.103	0.137	−0.37	−0.14	0.11	−0.16	0.054	−0.0075	0.175	0.029	−0.063
M = 0.80												
40,000 ft	−0.75	−0.06	0.13	−0.42	−0.756	0.04	−0.16	0.060	−0.06	0.16	0.029	−0.057

[a] All derivatives are per radian.

Jetstar

Business Jet

Center of Gravity and Mass Characteristics

W = 38,200 lb
CG at 25% MAC
I_x = 118 773 Slug - ft^2
I_y = 135 869 Slug - ft^2
I_z = 243 504 Slug - ft^2
I_{xz} = 5 061 Slug - ft^2

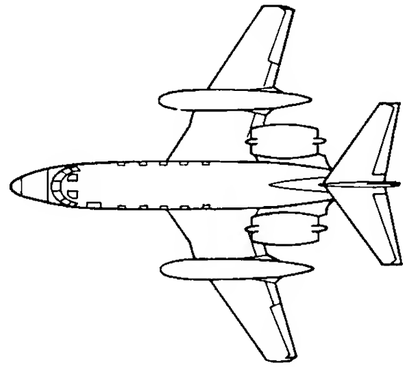

References Geometry

S = 542.5 ft^2
b = 53.75 ft
$\bar{c}$ = 10.93 ft

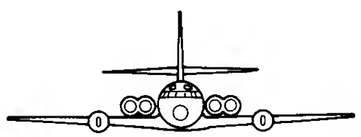

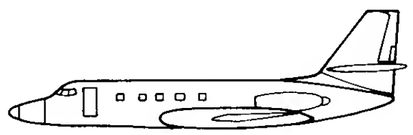

FIGURE B.25
Three-view sketch and stability data for an executive business jet.

Transport aircraft: Convair 880[a]

Longitudinal	C_L	C_D	C_{L_α}	C_{D_α}	C_{m_α}	$C_{L_{\dot\alpha}}$	$C_{m_{\dot\alpha}}$	C_{L_q}	C_{m_q}	C_{L_M}	C_{D_M}	C_{m_M}	$C_{L_{\delta e}}$	$C_{m_{\delta e}}$
M = 0.25														
Sea level	0.68	0.08	4.52	0.27	−0.903	2.7	−4.13	7.72	−12.1	0.0	0.0	0.0	0.213	−0.637
M = 0.8														
35,000 ft	0.247	0.024	4.8	0.15	−0.65	2.7	−4.5	7.5	−4.5	0.0	0.0	0.0	0.190	−0.57

Lateral	C_{y_β}	C_{l_β}	C_{n_β}	C_{l_p}	C_{n_p}	C_{l_r}	C_{n_r}	$C_{l_{\delta a}}$	$C_{n_{\delta a}}$	$C_{y_{\delta r}}$	$C_{l_{\delta r}}$	$C_{n_{\delta r}}$
M = 0.25												
Sea level	−0.877	−0.196	0.139	−0.381	−0.049	0.198	−0.185	−0.038	0.017	0.216	0.0226	−0.096
M = 0.8												
35,000 ft	−0.812	−0.177	0.129	−0.312	−0.011	0.153	−0.165	−0.050	0.008	0.184	0.019	−0.076

[a] All derivatives are per radian

Convair 880

Jet Transport

Center of Gravity and Mass Characteristics

W = 126 000 lb
CG at 25 % MAC
I_x = 115 000 Slug - ft^2
I_y = 2 450 000 Slug - ft^2
I_z = 4 070 000 Slug - ft^2
I_{xz} = 0

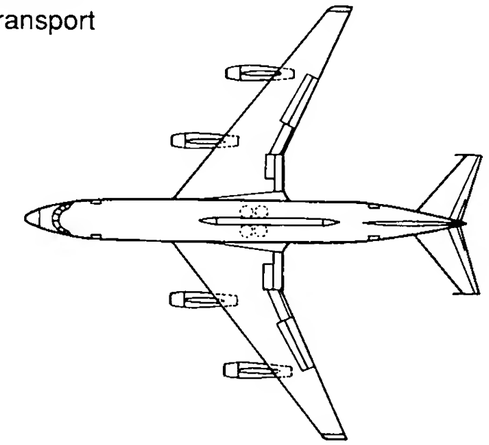

References Geometry

S = 2000 ft^2
b = 120 ft
$\bar{c}$ = 18.94 ft

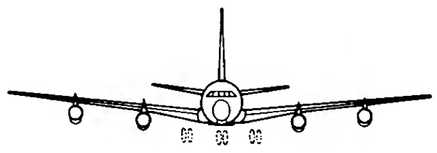

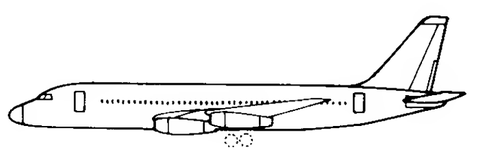

FIGURE B.26
Three-view sketch and stability data for a jet transport.

Transport aircraft: Boeing 747[a]

Longitudinal	C_L	C_D	C_{L_α}	C_{D_α}	C_{m_α}	$C_{L_{\dot\alpha}}$	$C_{m_{\dot\alpha}}$	C_{L_q}	C_{m_q}	C_{L_M}	C_{D_M}	C_{m_M}	$C_{L_{\delta e}}$	$C_{m_{\delta e}}$
M = 0.25														
Sea level	1.11	0.102	5.70	0.66	−1.26	6.7	−3.2	5.4	−20.8	−0.81	0.0	0.27	0.338	−1.34
M = 0.90														
40,000 ft	0.51	0.042	5.5	0.47	−1.6	0.006	−9.0	6.58	−25.0	0.2	0.25	−0.10	0.3	−1.2

Lateral	C_{y_β}	C_{l_β}	C_{n_β}	C_{l_p}	C_{n_p}	C_{l_r}	C_{n_r}	$C_{l_{\delta a}}$	$C_{n_{\delta a}}$	$C_{y_{\delta r}}$	$C_{l_{\delta r}}$	$C_{n_{\delta r}}$
M = 0.25												
Sea level	−0.96	−0.221	0.150	−0.45	−0.121	0.101	−0.30	0.0461	0.0064	0.175	0.007	−0.109
M = 0.90												
40,000 ft	−0.85	−0.10	0.20	−0.30	0.20	0.20	−0.325	0.014	0.003	0.075	0.005	−0.09

[a] All derivatives are per radian.

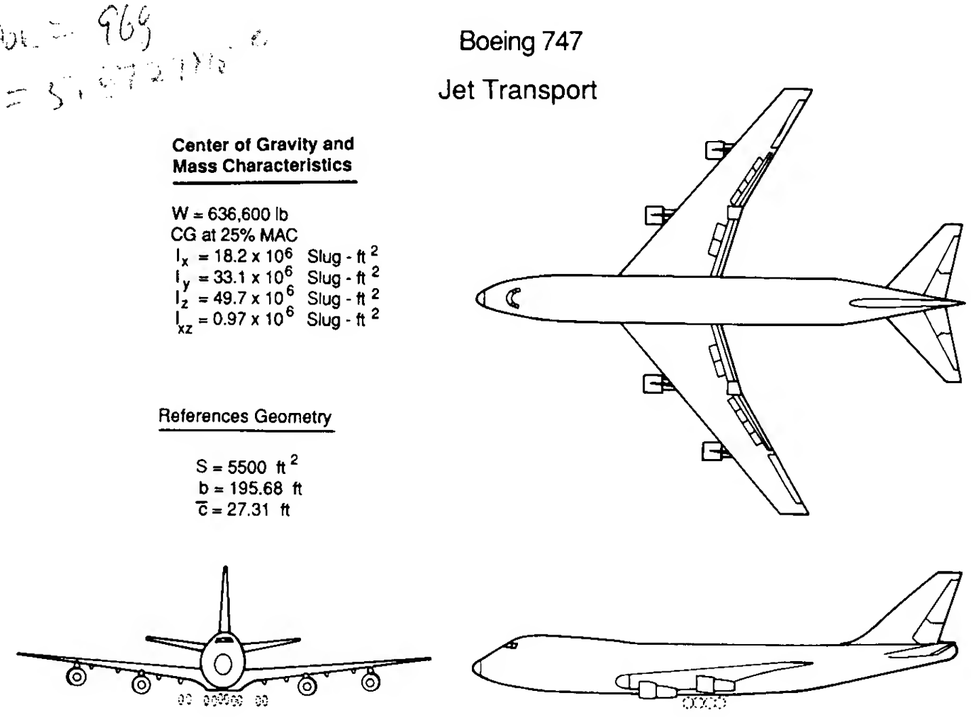

FIGURE B.27
Three-view sketch and stability data for a large jet transport.

APPENDIX C

MATHEMATICAL REVIEW LAPLACE TRANSFORMS MATRIX ALGEBRA

REVIEW OF MATHEMATICAL CONCEPTS

Laplace Transformation

The Laplace transform is a mathematical technique that has been used extensively in control system synthesis. It is a very powerful mathematical tool for solving differential equations. When the Laplace transformation Technique is applied to a differential equation it transforms the differential equation to an algebraic equation. The transformed algebraic equation can be solved for the quantity of interest and then inverted back into the time domain to provide the solution to the differential equation.

The Laplace transformation is a mathematical operation defined by

$$\mathscr{L}[f(t)] = \int_0^\infty f(t)\mathrm{e}^{-st}\,\mathrm{d}t = F(s) \tag{C.1}$$

where $f(t)$ is a function of time. The operator, $\mathscr{L}$, and the complex variable, s, are the Laplace operator and variable, respectively and $F(s)$ is the transform of $f(t)$. The Laplace transformation of various functions $f(t)$ can be obtained

by evaluating Eq. (C.1). The process of obtaining $f(t)$ from the Laplace transform $F(s)$ is called the inverse Laplace transformation and is given by

$$f(t) = \mathscr{L}^{-1}[F(s)] \tag{C.2}$$

where the inverse Laplace transformation is given by the following integral relationship.

$$f(t) = \frac{1}{2\pi i}\int_{c-\infty}^{c+\infty} F(s)e^{st}\,ds \tag{C.3}$$

Several examples of Laplace transformations are presented below.

Example Problem C.1. Consider the function $f(t) = e^{-at}$, then the Laplace transform of this expression yields

$$\mathscr{L}[f(t)] = \mathscr{L}[e^{-at}] = \int_0^\infty e^{-at}e^{st}\,dt = \int_0^\infty e^{-(a+s)t}\,dt$$

and the evaluation of the integral gives the transform $F(s)$

$$F(s) = -\frac{e^{-(a+s)t}}{a+s}\bigg|_0^\infty = \frac{1}{s+a}$$

As another example suppose that $f(t) = \sin \omega t$, then upon substituting into the definition of the Laplace transformation one obtains

$$F(s) = \mathscr{L}[\sin \omega t] = \int_0^\infty \sin \omega t e^{-st}\,dt = \frac{1}{2i}\int_0^\infty (e^{i\omega t} - e^{-i\omega t})e^{-st}dt$$

Evaluating this integral yields

$$F(s) = \frac{\omega}{s^2 + \omega^2}$$

Example Problem C.2. As another example consider the Laplace transformation of operations such as the derivative and definite integral. When $f(t)$ is a derivative, for example $f(t) = dy/dt$, then

$$\mathscr{L}[f(t)] = \int_0^\infty \frac{dy}{dt}e^{-st}dt$$

Solution of this integral can be obtained by applying the method of integration by parts. Mathematically integration by parts is given by the following expression.

$$\int_a^b u\,dv = uv\Big|_a^b - \int_a^b v\,du,$$

Letting u and dv be as follows

$$u = e^{-st}$$

$$dv = \frac{dy}{dt}dt$$

then

$$du = -se^{-st}\,dt$$

$$v = y(t)$$

Substituting and integrating by parts yields

$$\mathscr{L}[f(t)] = y(t)e^{-st}\Big|_0^\infty + s\int_0^\infty y(t)e^{-st}\,dt$$

but the integral

$$\int_0^\infty y(t)e^{-st}\,dt = Y(s)$$

$$\mathscr{L}\left[\frac{dy}{dt}\right] = -y(0) + sY(s)$$

In a similar manner the Laplace transformation of higher order derivatives can be shown to be

$$\mathscr{L}\left[\frac{d^n y}{dt^n}\right] = s^n Y(s) - s^{n-1}y(0) - s^{n-2}\frac{dy}{dt}\bigg|_{t=0} - \cdots - \frac{d^{n-1}y}{dt^{n-1}}\bigg|_{t=0}$$

When all initial conditions are zero the transform simplifies to the following expression.

$$\mathscr{L}\left[\frac{d^n y}{dt^n}\right] = s^n Y(s)$$

Now consider the Laplace transform of a definite integral:

$$\mathscr{L}\left[\int_0^t y(\tau)\,d\tau\right] = \int_0^\infty e^{-st}\,dt\int_0^t y(\tau)\,d\tau$$

This integral can also be evaluated by the method of integration by parts. Letting u and dv be as follows.

$$u = \int_0^t y(\tau)\,d\tau$$

$$dv = e^{-st}\,dt$$

then

$$du = y(t)$$

$$v = \frac{1}{s}e^{-st}$$

Substituting and integrating by parts yields

$$\mathscr{L}\left[\int_0^t y(\tau)\,d\tau\right] = \frac{1}{s}e^{-st}\int_0^t y(\tau)\,d\tau\Big|_0^\infty - \frac{1}{s}\int_0^\infty e^{-st}y(t)\,dt$$

or

$$\mathscr{L}\left[\int_0^t y(\tau)\,d\tau\right] = \frac{Y(s)}{s}$$

TABLE C1
Table of Laplace transform pairs

$f(t)$	$F(s)$	$f(t)$	$F(s)$
$u(t)$	$1/s$	$\sin \omega t$	$\omega/(s^2+\omega^2)$
t	$1/s^2$	$\cos \omega t$	$s/(s^2+\omega^2)$
t^n	$n!/s^{n+1}$	$\sinh \omega t$	$\dfrac{\omega}{s^2-\omega^2}$
$\delta(t)$ Unit impulse	1	$\cosh \omega t$	$\dfrac{s}{s^2-\omega^2}$
$\int_{-\varepsilon}^{+\varepsilon} \delta(t)\,dt = 1$		$e^{-at}\sin \omega t$	$\dfrac{\omega}{(s+a)^2+\omega^2}$
e^{-at}	$1/(s+a)$	$t\cos \omega t$	$\dfrac{s^2-\omega^2}{(s^2+\omega^2)^2}$
te^{-at}	$\dfrac{1}{(s+a)^2}$	$t\sin \omega t$	$\dfrac{2\omega s}{(s^2+\omega^2)^2}$
$t^n e^{-at}$	$n!/(s+a)^{n+1}$		

By applying the Laplace Transformation to various functions $f(t)$ one can develop a table of transform pairs as shown in Table C1. This table is a list of some of the most commonly used transform pairs that occur in control system analysis.

Solution of Ordinary Linear Differential Equations

In control system design, a linear differential equation of the form

$$a_n \frac{d^n y}{dt^n} + a_{n-1}\frac{d^{n-1}y}{dt^{n-1}} + \cdots + a_1 \frac{dy}{dt} + a_0 y = f(t) \qquad \text{(C.4)}$$

is common. This is a nonhomogeneous linear differential equation with constant coefficients. The Laplace-transformations of a differential equation results in an algebraic equation in terms of the transform of the derivatives and the Laplace variables. The resulting algebraic equation can be manipulated to solve for the unknown function $Y(s)$. The expression for $Y(s)$ can then be inverted back into the time domain to determine the solution $y(t)$.

Example Problem C.3. Given a second order differential equation

$$\frac{d^2y}{dt^2} + 2\zeta\omega_n \frac{dy}{dt} + \omega_n^2 y = \omega_n^2 u(t)$$

where $u(t)$ is a unit step function and the initial conditions are as follows

$$y(0) = 0$$
$$\frac{dy(0)}{dt} = 0$$

Taking the Laplace transformation of the differential equation yields

$$[s^2 + 2\zeta\omega_n s + \omega_n^2]Y(s) = \frac{\omega_n^2}{s}$$

Solving for $Y(s)$ yields

$$Y(s) = \frac{\omega_n^2}{s(s^2 + 2\zeta\omega_n s + \omega_n^2)}$$

$y(t)$ can now be obtained by inverting $Y(s)$ back into the time domain.

$$y(t) = 1 + \frac{1}{\sqrt{1-\zeta^2}} e^{-\zeta\omega_n t}\sin(\omega_n\sqrt{1-\zeta^2}t - \phi)$$

where

$$\phi = \tan^{-1}[\sqrt{1-\zeta^2}/-\zeta]$$

Partial Fractions Technique for Finding Inverse Transformations

When solving a differential equation using the Laplace transformation approach, the major difficulty is in inverting the transformation back into the time domain. The dependent variable is found as a rational function of the ratio of two polynomials in the Laplace variable, s. The inverse of this function can be obtained by the inverse Laplace transform defined by Eq. (C.3). However, in practice it is generally not necessary to evaluate the inverse in this manner. If this function can be found in a table of Laplace Transform pairs, the solution in the time domain is easily obtained. On the other hand, if the transform cannot be found in the table, then an alternate approach must be used. The method of partial fractions reduces the rational fraction to a sum of elementary terms which are available in the Laplace Tables.

The Laplace transform of a differential equation typically takes the form of a ratio of polynomials in the Laplace variable s.

$$F(s) = \frac{N(s)}{D(s)}$$

The denominator can be factored as follows.

$$D(s) = (s+p_1)(s+p_2)\cdots(s+p_n)$$

These roots can be either real or complex conjugate pairs and can be of multiple order. For the case when the roots are real and of order one the

Laplace transform can be expanded in the following manner

$$F(s)=\frac{N(s)}{D(s)}=\frac{N(s)}{(s+p_1)(s+p_2)\cdots(s+p_n)}$$
$$=\frac{C_{p_1}}{s+p_1}+\frac{C_{p_2}}{s+p_2}+\cdots+\frac{C_{p_n}}{s+p_n}$$

where the constants C_{p_i}'s are defined as

$$C_{p_1}=\left[(s+p_1)\frac{N(s)}{D(s)}\right]_{s=-p_1}$$
$$C_{p_2}=\left[(s+p_2)\frac{N(s)}{D(s)}\right]_{s=-p_2}$$
$$C_{p_i}=\left[(s+p_i)\frac{N(s)}{D(s)}\right]_{s=-p_i}$$

For the case where some of the roots are repeated, the Laplace transform can be represented as

$$F(s)=\frac{N(s)}{D(s)}=\frac{N(s)}{(s+p_1)(s+p_2)\cdots(s+p_i)^r(s+p_n)}$$

and in expanded form

$$F(s)=\frac{C_{p_1}}{s+p_1}+\frac{C_{p_2}}{s+p_2}+\cdots+\frac{k_1}{(s+p_i)}+\frac{k_2}{(s+p_i)^2}+\cdots+\frac{k_r}{(s+p_i)^r}$$

The coefficients for the nonrepeated roots are determined as shown previously and the coefficients for the repeated roots can be obtained from the following expression.

$$k_j=\frac{1}{(r-j)!}\frac{d^{r-j}}{ds^{r-j}}\left[(s+p_i)^r\frac{N(s)}{D(s)}\right]_{s=-p_i}$$

With the partial fraction technique the Laplace transform of the differential equation can be expressed as a sum of elementary transforms that can be easily inverted to the time domain.

Matrix Algebra

In this section we will review some of the properties of matrices. A matrix is a collection of numbers arranged in square or rectangular arrays. Matrices are used in the solution of simultaneous equations and are of great utility as a shorthand notation for large systems of equations. A brief review of some of the basic algebraic properties of matrices are presented in the following section.

A rectangular matrix is a collection of elements that can be arranged in rows and columns as shown below

$$\mathbf{A}=a_{ij}=\begin{bmatrix}a_{11} & a_{12} & \cdots & a_{1j}\\ a_{21} & & & \\ a_{31} & & & \\ a_{41} & & & \\ \vdots & & & \\ a_{i1} & a_{i2} & \cdots & a_{ij}\end{bmatrix}$$

where the index i and j represent the row and column respectively. The rectangular matrix reduces to a square matrix when $i=j$.

A unit matrix or identity matrix is a square matrix with the elements along the diagonal being unity and all other elements of the array are zero. The identity matrix is denoted in the following manner

$$\mathbf{I}=\begin{bmatrix}1 & 0 & \cdots & 0\\ 0 & 1 & \cdots & 0\\ \vdots & \vdots & & \vdots\\ 0 & 0 & \cdots & 1\end{bmatrix}$$

Addition and Subtraction

Two matrices are equal if they are of the same order, i.e., they have the same number of rows and columns and if the corresponding elements of the matrices are identical. Mathematically this can be stated as follows

$$\mathbf{A}=\mathbf{B}$$

if

$$a_{ij}=b_{ij}$$

Matrices can be added provided they are of the same order. Matrix addition is accomplished by adding corresponding elements together.

$$\mathbf{C}=\mathbf{A}+\mathbf{B}$$

or

$$c_{ij}=a_{ij}+b_{ij}$$

Subtraction of matrices is defined in a similar manner.

$$\mathbf{C}=\mathbf{A}-\mathbf{B}$$

or

$$c_{ij}=a_{ij}-b_{ij}$$

Multiplication of Two Matrices

Two matrices **A** and **B** can be multiplied provided that the number of columns of **A** is equal to the number of rows of **B**. For example, suppose the matrices **A** and **B** are defined as follows

$$\mathbf{A} = [a_{ij}]_{n,p}$$
$$\mathbf{B} = [b_{ij}]_{q,m}$$

These matrices can be multiplied if the number of columns of **A** is equal to the number of rows of **B**, i.e., $p = q$

$$\mathbf{C} = \mathbf{AB} = [a_{ij}]_{n,p}[b_{ij}]_{a,m} = [c_{ij}]_{n,m}$$

where

$$c_{ij} = \sum_{k=1}^{P} a_{ik}b_{kj} \qquad \begin{matrix} i = 1, 2, \ldots, n \\ j = 1, 2, \ldots, m \end{matrix}$$

Example Problem C.4. Given the matrices **A** and **B**, determine the product **AB**.

$$\mathbf{A} = \begin{bmatrix} a_{11} & a_{12} & a_{13} \\ a_{21} & a_{22} & a_{23} \\ a_{31} & a_{32} & a_{33} \end{bmatrix} \quad \text{and} \quad \mathbf{B} = \begin{bmatrix} b_{11} & b_{12} \\ b_{21} & b_{22} \\ b_{31} & b_{32} \end{bmatrix}$$

A and **B** can be multiplied together because the number of columns of **A** is equal to the number rows of **B**.

$$\mathbf{C} = \mathbf{AB}$$

$$\mathbf{C} = \begin{bmatrix} (a_{11}b_{11} + a_{12}b_{21} + a_{13}b_{31})(a_{11}b_{12} + a_{12}b_{22} + a_{13}b_{32}) \\ (a_{21}b_{11} + a_{22}b_{21} + a_{23}b_{31})(a_{21}b_{12} + a_{22}b_{22} + a_{23}b_{32}) \\ (a_{31}b_{11} + a_{32}b_{21} + a_{33}b_{31})(a_{31}b_{12} + a_{32}b_{22} + a_{33}b_{32}) \end{bmatrix}$$

Some additional properties of matrix multiplication are included in Table C2. Notice that in general matrix multiplication is not commutative. Multiplication of a matrix **A** by a scalar constant k is equivalent to multiplying each element of the matrix by the scalar k

$$k\mathbf{A} = \begin{bmatrix} ka_{11} & ka_{12} & ka_{13} \\ ka_{21} & ka_{22} & ka_{23} \\ ka_{31} & ka_{32} & ka_{33} \end{bmatrix}$$

TABLE C2
Properties of matrix multiplication

$\mathbf{(AB)C = A(BC)}$	Associative
$\mathbf{(A + B)C = AC + BC}$	Distributive
$\mathbf{A(B + C) = AB + AC}$	Distributive
$\mathbf{AB \neq BA}$	Commutative

TABLE C3
Properties of an inverse matrix

1) $\mathbf{AA^{-1} = A^{-1}A = I}$
2) $\mathbf{[A^{-1}]^{-1} = A}$
3) If **A** and **B** are nonsingular and square matrices then $\mathbf{(AB)^{-1} = B^{-1}A^{-1}}$

Matrix Division (Inverse of a Matrix)

The solution of a system of algebraic equations requires matrix inversion. For example, if a set of algebraic equations can be written in matrix form

$$\mathbf{Ax = y}$$

then the solution is given as

$$\mathbf{x = A^{-1}y}$$

where $\mathbf{A^{-1}}$ is the inverse of the matrix **A**. For the inverse of **A** to exist, the matrix **A** must be square and nonsingular. The condition that **A** be nonsingular means that the determinant of **A** must be a nonzero value. The inverse of a matrix, is defined as follows

$$\mathbf{A^{-1}} = \frac{Adj\,\mathbf{A}}{|\mathbf{A}|}$$

where *Adj* **A** is called the adjoint of **A**. The adjoint of a matrix is obtained by taking the transpose of the co-factors of the **A** matrix, where the cofactors are determined as follows

$$C_{ij} = (-1)^{i+j}D_{ij}$$

and D_{ij} is the determinant obtained by eliminating the ith row and jth column of **A**. Some additional properties of the inverse matrix are given in Table C3.

The transpose of a matrix is obtained by interchanging the rows and columns of the matrix. Given the matrix **A**

$$\mathbf{A} = \begin{bmatrix} a_{11} & a_{12} & a_{13} \\ a_{21} & a_{22} & a_{23} \\ a_{31} & a_{32} & a_{33} \end{bmatrix}$$

then the transpose of **A**

$$\mathbf{A}^T = \begin{bmatrix} a_{11} & a_{21} & a_{31} \\ a_{12} & a_{22} & a_{32} \\ a_{13} & a_{23} & a_{33} \end{bmatrix}$$

For additional properties of matrices the reader should consult his or her mathematics library.

APPENDIX D

REVIEW OF CONTROL SYSTEM ANALYSIS TECHNIQUES

BODE DIAGRAMS

The frequency response of a linear system is determined experimentally by applying a sinusoidal input signal and then measuring the sinusoidal response of the system. The frequency response data includes the measurement of the amplitude and phase shift of the sinusoidal output compared to the amplitude and phase of the input signal as the input frequency is varied. The relationship between the output and input to the system can be used by the designer to determine the performance of the system. Furthermore, frequency response data can be used to deduce the performance of a system to an arbitrary input that may or may not be periodic.

The magnitude of the amplitude ratio and phase angle can be presented graphically in a number of ways. However, one of the most useful presentations of the data is in the so called Bode diagram, named after H. W. Bode for his pioneering work in frequency response anlysis. In a Bode diagram the logarithm of the magnitude of the system transfer function, $|G(i\omega)|$, and the phase angle, ϕ, are plotted separately versus the frequency.

The frequency response, output/input amplitude ratio and phase with respect to the input can be determined analytically from the system transfer

function written in factored time constant form.

$$G(s) = \frac{k(1 + T_a s)(1 + T_b s) \cdots}{s^r(1 + T_1 s)(1 + T_2 s) \cdots \left(1 + \frac{2\zeta}{\omega_n} s + \frac{s^2}{\omega_n^2}\right)} \tag{D.1}$$

This transfer function has simple zeros at $-1/T_a$, $-1/T_b \ldots$, a pole at the origin of order r, simple poles at $-1/T_1$, $-1/T_2, \ldots$, and complex poles at $-\zeta\omega_n \pm i\omega_n\sqrt{1-\zeta^2}$. It can be shown that the steady state response can be determined by substituting $i\omega$ for the Laplace variable s, in the system transfer function. Upon substituting $i\omega$ for s, one can express the transfer function in terms of the magnitude of its amplitude ratio and phase angle as follows

$$\begin{aligned} 20 \log |G(i\omega)| = {} & 20 \log k + 20 \log |1 + i\omega T_a| + 20 \log |1 + i\omega T_b| + \cdots \\ & - 20\, r \log |i\omega| - 20 \log |1 + i\omega T_1| - 20 \log |1 + i\omega T_2| \\ & - 20 \log |1 + 2\zeta(\omega/\omega_n) - (\omega/\omega_n)^2| \cdots \end{aligned} \tag{D.2}$$

and the phase angle in degrees

$$\begin{aligned} \angle G(i\omega) = {} & \tan^{-1} \omega T_a + \tan^{-1} \omega T_b + \cdots - r(90°) - \tan^{-1} \omega T_1 \\ & - \tan^{-1} \omega T_2 \cdots - \tan^{-1}\left(\frac{2\zeta\omega\omega_n}{\omega_n^2 - \omega^2}\right) \end{aligned} \tag{D.3}$$

The magnitude has been expressed in terms of decibels. A magnitude in decibels is defined as follows

$$\text{Magnitude in db} = 20 \log \frac{|\text{Magnitude of Output}|}{|\text{Magnitude of Input}|} \tag{D.4}$$

where the logarithm is to the base 10.

The Bode diagram can now be constructed using a semi-log plot. The magnitude in decibels and phase angle are plotted separately on a linear ordinate versus the frequency on a logarithmic abscissa. Because the Bode diagram is obtained by adding the various factors of $G(i\omega)$ one can construct the Bode diagram quite rapidly.

In the general case the factors that will make up the transfer function are a constant term (system gain), poles at the origin, simple poles and zeros on the real axis and complex conjugate poles and zeros. The graphical representation of each of these individual factors are described in the following section.

System Gain

The log-magnitude of the system gain is given as follows

$$20 \log k = \text{constant db} \tag{D.5}$$

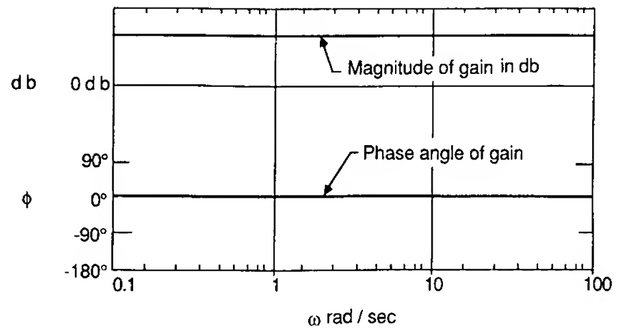

FIGURE D1
Bode representation of the magnitude and phase of the system gain k.

and the phase angle by

$$\angle k = \begin{matrix} 0° & k>0 \\ 180° & k<0 \end{matrix} \qquad \text{(D.5)}$$

Figure D1 shows the Bode plot for a positive system gain.

Poles or Zeros at the Origin $(i\omega)^{\pm r}$

The log-magnitude of a pole or zero at the origin of order r can be written as

$$20 \log |(i\omega)^{\pm r}| = \pm 20r \log \omega \text{ db} \qquad \text{(D.6)}$$

and the phase angle is given by

$$\angle (i\omega)^{\pm r} = \pm 90° r \qquad \text{(D.7)}$$

The log-magnitude is zero db at $\omega = 1.0$ rad/sec and has a slope of 20 db/decade, where a decade is a factor of 10 change in frequency. Figure D2 is a sketch of the log-magnitude and phase angle for a multiple zero or pole.

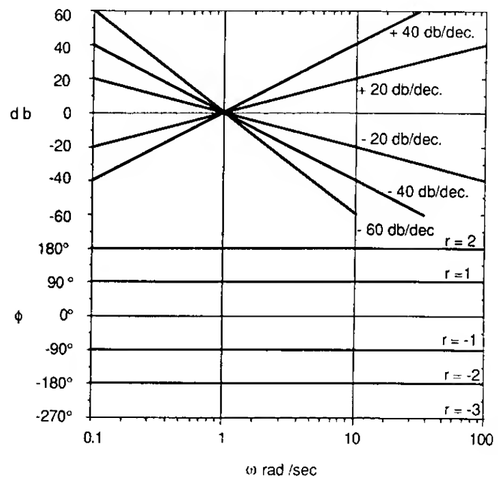

FIGURE D2
Bode representation of the magnitude and phase of a pole or zero at the origin.

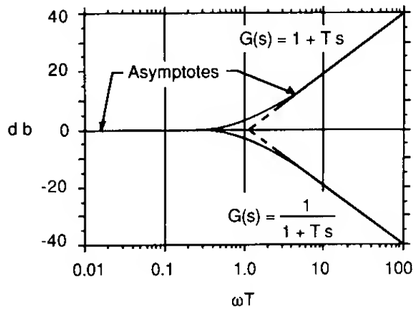

FIGURE D3
Bode representation of the magnitude of a simple pole or zero.

Simple Poles or Zeros $(1 + i\omega T)^{\pm 1}$

The log-magnitude of a simple pole or zero can be expressed as

$$\pm 20 \log |1 + i\omega T| = \pm 20 \log \sqrt{1 + (\omega T)^2} \qquad \text{(D.8)}$$

For very low values of ωT i.e., $\omega T \ll 1$, then

$$\pm 20 \log \sqrt{1 + (\omega T)^2} \cong 0 \qquad \text{(D.9)}$$

and for very large values of ωT i.e., $\omega T \gg 1$ then

$$\pm 20 \log \sqrt{1 + (\omega T)^2} \cong \pm 20 \log \omega T \qquad \text{(D.10)}$$

From this simple analysis one can approximate the log-magnitude plot of a simple pole or zero by two straight line segments as shown in Fig. D3. One of the asymptotic lines is the 0 db line and the second line segment has a slope of 20 db/decade that intersects the 0 db line at the frequency $\omega = 1/T$. The intersection frequency is called the corner frequency. The actual log-magnitude differs from the asymptotic approximation in the vicinity of the corner frequency.

The phase angle for a simple pole or zero is given by

$$\angle (1 + i\omega T)^{\pm 1} = \pm \tan^{-1} \omega T \qquad \text{(D.11)}$$

Figure D4 is a sketch of the phase angle.

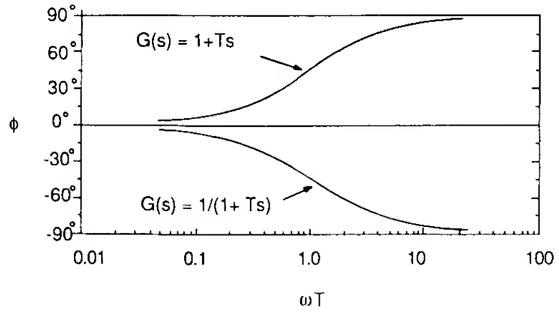

FIGURE D4
Bode representation of the phase angle of a simple pole or zero.

Complex Conjugate Pole or Zero $(1 + i2\zeta\omega/\omega_n - (\omega/\omega_n)^2)^{\pm 1}$

The log-magnitude of the complex pole can be written as

$$20 \log \left| \frac{1}{1 + i2\zeta\omega/\omega_n + (\omega/\omega_n)^2} \right| = -20 \log[(1 - (\omega/\omega_n)^2)^2 + (2\zeta\omega/\omega_n)^2]^{1/2}$$
$$= -10 \log[(1 - (\omega/\omega_n)^2)^2 + (2\zeta\omega/\omega_n)^2] \tag{D.13}$$

The log-magnitude can be approximated by two straight line segments. For example, when $\omega/\omega_n \ll 1$

$$20 \log \left| \frac{1}{1 + i2\zeta\omega/\omega_n - (\omega/\omega_n)^2} \right| \cong 0 \tag{D.14}$$

and when $\omega/\omega_n \gg 1$

$$20 \log \left| \frac{1}{1 + i2\zeta\omega/\omega_n - (\omega/\omega_n)^2} \right| \cong -40 \log \omega/\omega_n \tag{D.15}$$

The two straight line asymptotes consist of a straight line along the 0 db line for $\omega/\omega_n \ll 1$ and a line having a slope of -40 db/decade for $\omega/\omega_n \gg 1$. The asymptotes intersect at $\omega/\omega_n = 1$ or $\omega = \omega_n$, where ω_n is the corner frequency. Figure D5 shows the asymptotes as well as the actual magnitude plot for various damping ratios for a complex pole.

The phase angle for a complex pole is given by

$$\angle(1 + i2\zeta\omega/\omega_n - (\omega/\omega_n)^2)^{-1} = -\tan^{-1}\left[\frac{2\zeta\omega/\omega_n}{1 - (\omega/\omega_n)^2}\right] \tag{D.16}$$

Figure D6 shows the phase angle for a complex pole. Similar curves can be developed for a complex zero.

If the transfer function is expressed in time constant form, then the Bode diagram can be easily constructed from the simple expressions developed in this section.

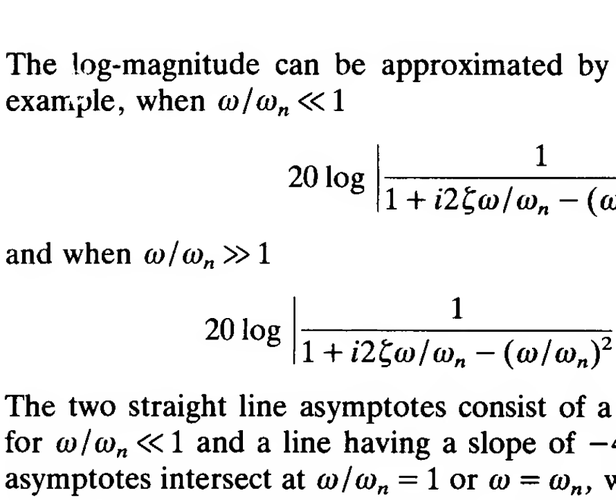

FIGURE D5
Bode representation of the magnitude of a complex conjugate pole.

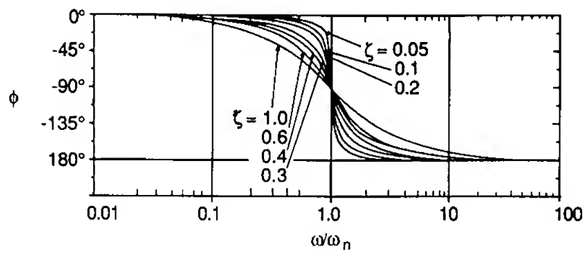

FIGURE D6
Bode representation of the phase angle of a complex conjugate pole.

Root Locus Technique

The transfer function was described earlier as the ratio of the output to the input. Upon examining a transfer function we note that the denominator is the characteristic equation of the system. The roots of the denominator are the eigenvalues that describe the free response of the system, where the free response is the solution of the homogeneous equation. In controls terminology the characteristic roots are called the poles of the transfer function. The numerator of the transfer function governs the particular solution and the roots of the numerator are called zeros.

As was noted earlier in Chapters 4 and 5 the roots of the characteristic equation (or poles) must have negative real parts if the system is to be stable. In control system design, the location of the poles of the closed loop transfer function allows the designer to predict the time domain performance of the system.

However, in designing a control system the designer will typically have a number of system parameters that are unspecified. The root locus technique permits the designer to view the movement of the poles of the closed loop transfer function as one or more unknown system parameters are varied.

Before describing the root locus technique it would be helpful to examine the significance of the root placement in the complex plane and the type of response that can be expected to occur. Figure D7 illustrates some of the

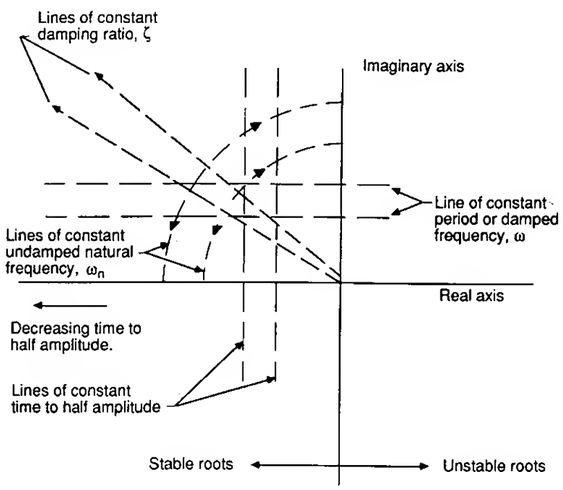

FIGURE D7
Graphical description of characteristic roots.

important features of pole location. First we note that any pole lying in the left half portion of the complex plane is stable, i.e., the response decays with time. Any pole in the right half plane leads to a response that grows with time which will result in an unstable system. The farther the root is to the left of the imaginary axis the faster the response decays. All poles lying along a particular vertical line will have the same time to half amplitude. Poles lying along the same horizontal line have the same damped frequency, ω, and period. The farther the pole is from the real axis the higher the frequency of the response will be. Poles lying along a radial line through the origin have the same damping ratio, and roots lying on the same circular arc around the origin will have the same undamped natural frequency. Finally some comments must be made about the poles lying on the imaginary axis. Poles of the order one on the imaginary axis lead to undamped oscillations, however, multiple order poles result in responses that grow with time.

The closed loop transfer function was shown earlier to be

$$M(s) = \frac{G(s)}{1 + G(s)H(s)} \tag{D17}$$

The characteristic equation of the closed loop system is given by the denominator of Eq. (D.17)

$$1 + G(s)H(s) = 0 \tag{D.18}$$

or

$$G(s)H(s) = -1 \tag{D.19}$$

The open loop transfer function $G(s)H(s)$ can be expressed in factored form as follows

$$G(s)H(s) = \frac{k(s+z_1)(s+z_2)\cdots(s+z_m)}{(s+p_1)(s+p_2)\cdots(s+p_n)} \tag{D.20}$$

where $n > m$ and k is an unknown system parameter. Substituting this equation into the characteristic equation yields

$$\frac{k(s+z_1)(s+z_2)\cdots(s+z_m)}{(s+p_1)(s+p_2)\cdots(s+p_n)} = -1 \tag{D.21}$$

The characteristic equation is complex and can be written in terms of a magnitude and angle as follows

$$\frac{|k|\,|s+z_1|\,|s+z_2|\cdots|s+z_m|}{|s+p_1|\,|s+p_2|\cdots|s+p_n|} = 1 \tag{D.22}$$

$$\sum_{i=1}^{m} \angle(s+z_i) - \sum_{i=1}^{n} \angle(s+p_i) = (2q+1)\pi \tag{D.23}$$

where $q = 0, 1, 2$ etc. Solution of the above equations yields the movement of the roots as a function of the unknown system parameter. These equations can be solved on the computer to determine the root locus contours. There is, however, a simple graphical technique developed by W. R. Evans that can be used to sketch a root locus plot. This graphical procedure is presented in the next section.

It can be easily shown that the root locus contours start at the open loop transfer function $G(s)H(s)$ poles and ends at the open loop zeros as k is varied

TABLE D1
Rules for graphical construction of the root locus plot

1. The root locus contours are symmetrical about the real axis.
2. The number of separate branches of the root locus plot is equal to the number of poles of the open loop transfer function $G(s)H(s)$. Branches of the root locus originate at the open loop poles of $G(s)H(s)$ for $k = 0$, and terminate at either the open loop zeros or at infinity for $k = \infty$. The number of branches that terminate at infinity is equal to the difference between the number of poles and zeros of the open loop transfer function.
3. Segments of the real axis that are part of the root locus can be found in the following manner. Points on the real axis that have an odd number of poles and zeros to their right are part of the real axis portion of the root locus.
4. The root locus branches that approach the open loop zeros at infinity do so along straight line asymptotes that intersect the real axis at the center of gravity of the finite poles and zeros. Mathematically this can be expressed as follows.

$$\sigma = \left[\sum \text{Real Parts of the Poles} - \sum \text{Real Parts of the Zeros}\right] \Big/ (n-m)$$

where n is the number of poles and m the number of finite zeros.

5. The angle that the asymptotes make with the real axis is given by

$$\phi_a = \frac{180°[2q+1]}{n-m}$$

for $q = 0, 1, 2, \ldots, (n-m-1)$.

6. The angle of departure of the root locus from an open loop pole can be found by the following expression.

$$\phi_p = \pm 180°(2q+1) + \phi \qquad q = 0, 1, 2, \ldots$$

where ϕ is the net angle contribution at the pole of interest due to all other open loop poles and zeros. The arrival angle at the open loop zero is given by a similar expression

$$\phi_z = \pm 180°(2q+1) - \phi \qquad q = 0, 1, 2, \ldots$$

The angle ϕ is determined by drawing straight lines from all the poles and zeros to the pole or zero of interest and then summing the angles made by these lines.

7. If a portion of the real axis is part of the root locus and branch is between two poles, the branch must break away from the real axis so that the locus ends on a zero as k approaches infinity. The break away points on the real axis are determined by solving

$$1 + kGH = 0$$

for k and then find the roots of the equation $dk/ds = 0$. Only roots that lie on a branch of the locus are of interest

from zero to infinity. For example, if we rearrange the magnitude criteria as

$$\frac{|s+z_1|\,|s+z_2|\cdots|s+z_m|}{|s+p_1|\,|s+p_2|\cdots|s+p_n|}=\frac{1}{|k|} \tag{D.24}$$

then as k goes to zero the function becomes infinite. This implies that the roots approach the poles as k goes to zero. On the other hand, as k goes to infinity the functon goes to zero which implies the roots are at the open loop zeros. Therefore, the root locus plot of the closed loop system starts with a plot of the poles and zeros of the open loop transfer function. Evans developed a series of rules based upon the magnitude and angle criteria for rapidly sketching the root locus branches on a pole zero map. A proof of these rules can be found in most control textbooks and will not be presented here. Table D1 is a summary of the rules for constructing a root locus contour.

INDEX

Active control technology, 147
Adverse yaw, 72
Aerodynamic force and moment coefficients, 20
Ailerons, 58
  effectiveness, 77
  positive deflection, 58
Airspeed, 23
  indicator, 23
  calibrated airspeed, CAS, 24
  equivalent airspeed, EAS, 25
  indicated airspeed, IAS, 23
  true airspeed, TAS, 25
Airspeed, automatic control of, 220
Altitude, 14
  density altitude, 26
  geometric and geopotential, 15
  pressure altitude, 26
  temperature altitude, 26
Angle of attack, 21
  definition, 21
  sensors, 29
Angular momentum, 84
Argand diagram, 136
Atmosphere, 12
  characteristics, 12
  standard atmosphere, 14, 246
Atmospheric turbulence, 189
  gusts, 183, 192
  wind shear, 198
Automatic flare control, 220
Autopilots
  (see logitudinal and lateral autopilots)
Axes system, 19
  body frame, 19, 84
  Eulerian frame, 88
  inertial frame, 19, 84
Axial force coefficient, 20
  definition, 20
  due to change in α, 107
  due to change in u, 102

Bairstow, L., 113
Bandwith, 208
Barometer, 9
Bernoulli's equation, 9
  incompressible flow, 9
  compressible flow, 11
Block diagrams, 200
Bode, H. W. 178, 270
Bode diagrams, 177
Body axes, 84
Bryan, G. H. 100, 111, 112

Calibrated airspeed, 24
Canard control, 49
  positive deflection, 58
Characteristic equation
  definition, 115
  first order, 154, 164, 185
  lateral, 161, 164
  longitudinal, 129, 130
  second order, 115
Chanute, O., 35, 38
Closed-loop control, 199
Closed-loop transfer function, 200
Coefficient of viscosity
  absolute, 5
  kinematic, 6, 247
Control surfaces, description of
  aileron, 58, 75
  canard, 36, 49, 58
  elevator, 58, 59

Control surfaces, description of—*contd.*
rudder, 58, 71
spoiler, 76
Control effectiveness, 59, 71, 77
Controllability, 231
Cycles for doubling, 124
or halving initial amplitude, 124

Damping ratio
definition, 117
Dutch roll, 165
long or phugoid motion, 129
short period motion, 131
Decibels, 177, 271
Delay time, 207
Density, 5
Density altitude, 26
Density ratio, 5
Dihedral, definition of, 73
Dihedral effect
fuselage contribution, 75
wing contribution, 74, 108, 109
Directional control
requirement for, 72
rudder sizing, 72
Directional divergence, 152
Directional static stability, 67
fuselage contribution, 68
vertical tail contribution, 70
Displacement autopilot, 211
pitch, 211
roll, 211
yaw, 211
Dominate poles, 210
Downwash
wing contribution, 46
effect on horizontal tail, 47
effect on fuselage, 49
Dutch roll motion, 162
approximate solution, 164
damping ratio, 165
flying qualities, 170
undamped natural frequency, 165
Dynamic stability, 40

Eigenvalues, 128
Eigenvectors, 128, 136
Elevator
angle for trim, 61
effectiveness, 59
floating characteristics, 63
positive deflection, 58
requirements for, 61
Equations of motion, 84
linearized three degree of freedom equations, 92
lateral, 95
longitudinal, 95
non-linear six degree of freedom equation, 88, 92
single degree of freedom equation
pitching motion, 120
plunging motion, 183
rolling motion, 153
yawing motion, 158
Equilibrium state, 39
Equivalent airspeed, 25
Euler angles, 88
definition, 88
Euler rates, 90
Evans, W. R., 204

Feedback control, 199
Flare, automatic control of, 220
Flight control system
(see lateral and longitudinal autopilots)
Flight measurement of neutral point, 61
Flight simulation, 144
Fluid, 2
Flying qualities, 113
definition, 139
lateral requirements, 169, 170
longitudinal requirements, 142
Forcing function, 115
Free elevator, 63
Frequency response, 176
of complete transfer function, 177, 271

of first order system, 189, 273
of longitudinal transfer function, 177
of second order system, 274

Gain, 208, 271
Gearing ratio, 65
Glide slope beam, 218
Gust, wind, 180
sharp-edged, 185
sinusoidal, 185

Harmonic analysis, 191
Hinge moments, 62
elevator, 59, 62
effect of trim tab on, 66
Horizontal tail, 45
contribution to static stability, 48
sizing, 49

Indicated airspeed, 24
Inertia
moments of, 87
products of, 87
Inertial axes, 84
Inertial cross-coupling, 172
Instrument landing system, 217
Ionosphere, 13

Jones, B. M., 113

Lanchester, F. W., 34, 112
Langley, S. P., 35, 36, 38
Laplace transforms, 261
Lapse rate, 17
Lateral autopilots
heading control autopilot, 211
wings leveling autopilot, 213
stability augmentation system, 215, 237
Lateral flying qualities
(see flying qualities)
Lateral motions, 160
Dutch roll motion, 162, 164
roll motion, 162, 164
spiral motion, 162, 163
Lateral transfer functions, 97
Lilienthal, O, 35, 38
Localizer, 217
Longitudinal autopilots
automatic flare, 220
automatic landing, 217
pitch displacement control, 211
speed control, 220
stability augmentation system, 215, 234
Longitudinal flying qualities
(see flying qualities)
Longitudinal motions, 124
long or phugoid motions, 128
short period motions, 130
Longitudinal eigenvectors, 136
Longitudinal transfer functions, 96

Mach number, 6
Mach meter, 28
Manely, C., 36
Mass moment of inertia, 87
(see inertia, moments of)
Matrix algebra, 266
Modern control theory, 225
Multhopp, H., 49
Munk, M., 49

Natural frequency, 117
Neutral point
stick fixed, 52, 61
stick free, 64
Nonuniform atmosphere, 181
influence on equations of motion, 182
also see atmospheric turbulence

Observability, 231
Open loop control, 199
Optimal control, 240
Overshoot, 207

Partial fractions, technique, 156
Penaud, A., 34
Performance index, 240
Period, 123
Phase margin, 208
Phugoid motion (long period), 128
  approximation, 128
  damping ratio, 129
  flying qualities, 142
  undamped natural frequency, 129
Pilot, human
  opinion, 141
  induced oscillations PIO, 42
Pitch damper, 212
Pitch damping, 103
Pitch displacement autopilot, 211
Pitching moment coefficient, 20
  definition, 20
  due to change in α, 52, 107
  due to change in $\dot{\alpha}$, 105, 107
  due to change in δ_e, 59, 107
  due to change in q, 103, 107
  due to change in u, 102, 107
Pitching motion
  single degree of freedom, 120
Pilot static probe, 23, 28
Plunging motion, 183
Poles, 204
Power effects
  on static stability, 51
  on trim, 51
Power spectral density, 192
Pressure, 4
Pressure altitude, 26

Resonance frequency, 208
Resonance peak, 208
Reynolds number, 6
Riccati equation, 240
Rigid body equations of motion, 84
  (see Equation of motion)
Rise time, 207
Roll angle control system, 214
Roll control, 75
  control effectiveness, 77
  reveral, 156
Roll motion, 153, 162
  approximation, 153, 164
  damping, 154
  flying qualities, 170
Roll stability, 73
Rolling moment coefficient, 20
  definition, 20
  due to change in β, 73, 108
  due to change in δ_a, 77, 108
  due to change in p, 108
  due to change in r, 108
Root locus, 204, 275
Routh's criteria, 201
Rudder, 77
  effectiveness, 72
  positive deflection, 58
  sizing, 72

Second order differential equation, 114
Servo, control surface, 212
Settling time, 207
Short period motion, 125
  approximate solution, 130
  damping ratio, 131
  flying qualities, 142
  undamped natural frequency, 131
Side force coefficient, 20
  definition, 20
  due to change in β, 108
  due to change in δ_a, 108
  due to change in δ_r, 108
  due to change in p, 108
  due to change in r, 108
sideslip angle, 21
  definition, 21
  sensor, 30

Sidewash, 70
  effect on fuselage, 70
  effect on vertical tail, 70
Small disturbance theory, 92
  applied to lateral equations, 95
  applied to longitudinal equation, 95
Speed of sound, 6
Speed stability, 66, 102
Sperry, L., 198
Spiral divergency, 152
Sprial motion, 162
  approximate solution, 163
  damping, 164
  flying qualities, 169
Spoiler, 58
Stability Augmentation (SAS), 39, 41, 170, 214, 233
Stability derivatives, 94
  definition, 100
  methods for estimating derivatives, 102–109
Standard atmospheric table, 246
State feedback design, 232
State transition matrix, 228
State observer, 238
State variables, 125, 225
Static longitudinal stability, 42
  definition, 42
  fuselage contribution 49
  power effects, 51
  stick fixed, 42
  stick free, 64
  tail contribution, 45
  wing contribution, 44
Static margin, 64
  stick fixed, 64
  stick free, 64
Stick fixed neutral point, 52
Stick forces, 64
  gradients, 66
Stick free neutral point, 64
Solution to equations of motion
  forced response
    pitching motion due to step change in elevator angle, 121
    plunging motion due to sharp edged gust, 183
    rolling motion due to step change in aileron angle, 153
    yawing motion due to step change in rudder angle, 156
  free response
    lateral equations of motion, 160
    longitudinal equations of motion, 123

Tab surface, 66
Tail efficiency, 47
Tail volume ratio, 47
Temperature, 4
Temperature altitude, 26
Time constant, 154
  plunging motion, 184
  rolling motion, 154
  spiral motion, 164
Time for doubling or halving of motion amplitude, 123
Transfer functions, 95
  control servos, 212
  definition, 96, 177
  lateral, 97
  longitudinal, 96
Transient response
  (see solution of equations of motion forced and free response)
Trim changes, 51
  due to power
Trim tabs, 66
Troposphere, 15
True airspeed, 25
Turbulence
  (see atmospheric turbulence)

U-tube manometer, 8
Upwash, 46
  due to wing, 46
  effect on fuselage, 49

Vertical tail, 70
Viscosity, coefficient of, 5
  absolute, 5
  kinematic, 6
Vortex, 46
  bound, 46
  trailing, 46, 49, 70

Weathercock stability, 159
  (see directional stability)
Wind shear, 193
Wright brothers, 38, 198
Wright, O, 34, 36, 83
Wright, W, 1, 36

Yaw angle, 89, 158
Yaw damper, 170
Yaw rate damping, 164
Yawing moment coefficient, 20
  definition, 20
  due to change in β, 67, 108
  due to change in δ_a, 108
  due to change in δ_r, 71, 108
  due to change in p, 108
  due to change in r, 108
Yawing motion, 158
  single degree of freedom, 158

Z force coefficient, 20
  definition, 20
  due to change in α, 107
  due to change in $\dot{\alpha}$, 105, 107
  due to change in δ_e, 107
  due to change in q, 103, 107
  due to change in u, 102, 107
Zahm, A, 34
Zeros, 204